CIENCE

JOURNAL OF RESEARCH

OF THE U.S. GEOLOGICAL SURVEY

JULY–AUGUST 1978
VOLUME 6, NUMBER 4

UICC LIBRARY
JUNE 30 1978
DOCUMENTS

Scientific notes and summaries of investigations in geology, hydrology, and related fields

U.S.
DEPOSITORY

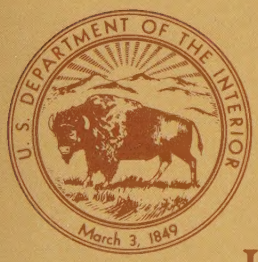

U.S. DEPARTMENT OF THE INTERIOR

UNITED STATES DEPARTMENT OF THE INTERIOR
CECIL D. ANDRUS, Secretary
GEOLOGICAL SURVEY
H. William Menard, Director

For sale by Superintendent of Documents, U.S. Government Printing Office, Washington, DC 20402. Annual subscription rate, $18.90 (plus $4.75 for foreign mailing). Make check or money order payable to Superintendent of Documents. Send all subscription inquiries and address changes to Superintendent of Documents at above address.

Purchase single copy ($3.15) from Branch of Distribution, U.S. Geological Survey, 1200 South Eads Street, Arlington, VA 22202. Make check or money order payable to U.S. Geological Survey.

Library of Congress Catalog-card No. 72-600241.

The Journal of Research is published every 2 months by the U.S. Geological Survey. It contains papers by members of the Geological Survey and their professional colleagues on geologic, hydrologic, topographic, and other scientific and technical subjects.

Correspondence and inquiries concerni
Journal (other than subscription inquiri
address changes) should be directed to A
Orellana, Managing Editor, Journal of Re
Publications Division, U.S. Geological S
321 National Center, Reston, VA 22092.

Papers for the Journal should be sub
through regular Division publication chan

The Secretary of the Interior has determined that the publication of this perio
cal is necessary in the transaction of the public business required by law of t
Department. Use of funds for printing this periodical has been approved by
Director of the Office of Management and Budget through June 30, 1980.

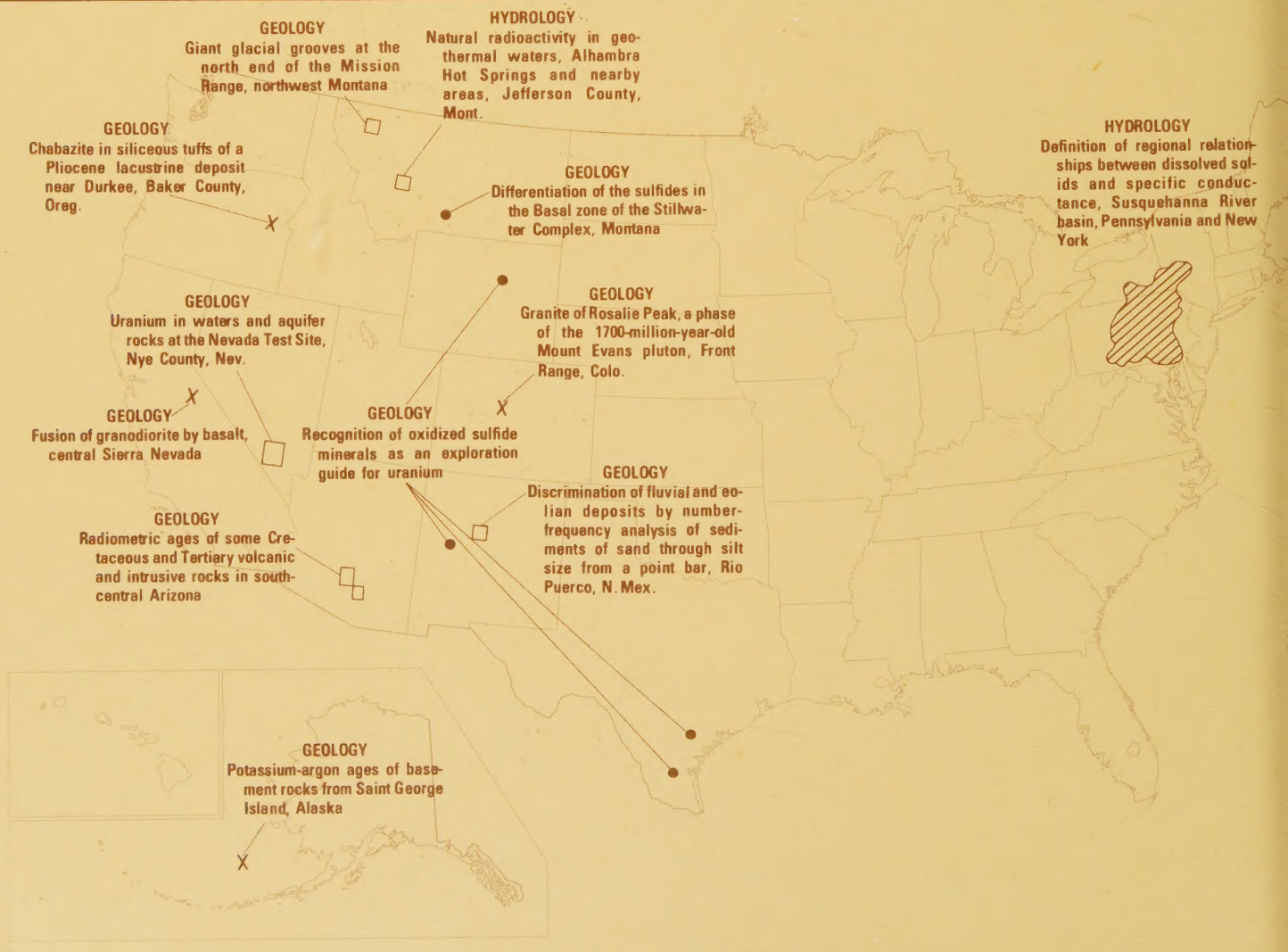
GEOLOGY
Giant glacial grooves at the north end of the Mission Range, northwest Montana
HYDROLOGY
Natural radioactivity in geothermal waters, Alhambra Hot Springs and nearby areas, Jefferson County, Mont.
GEOLOGY
Chabazite in siliceous tuffs of a Pliocene lacustrine deposit near Durkee, Baker County, Oreg.
GEOLOGY
Differentiation of the sulfides in the Basal zone of the Stillwater Complex, Montana
HYDROLOGY
Definition of regional relationships between dissolved solids and specific conductance, Susquehanna River basin, Pennsylvania and New York
GEOLOGY
Uranium in waters and aquifer rocks at the Nevada Test Site, Nye County, Nev.
GEOLOGY
Granite of Rosalie Peak, a phase of the 1700-million-year-old Mount Evans pluton, Front Range, Colo.
GEOLOGY
Fusion of granodiorite by basalt, central Sierra Nevada
GEOLOGY
Recognition of oxidized sulfide minerals as an exploration guide for uranium
GEOLOGY
Discrimination of fluvial and eolian deposits by number-frequency analysis of sediments of sand through silt size from a point bar, Rio Puerco, N. Mex.
GEOLOGY
Radiometric ages of some Cretaceous and Tertiary volcanic and intrusive rocks in south-central Arizona
GEOLOGY
Potassium-argon ages of basement rocks from Saint George Island, Alaska

GEOGRAPHIC INDEX TO ARTICLES

See "Contents" for articles concerning areas outside the United States and articles without geographic orientation.

JOURNAL OF RESEARCH

of the

U.S. Geological Survey

Vol. 6 No. 4 July–Aug. 1978

CONTENTS

SI units and U.S. customary equivalents ---------- II

GEOLOGIC STUDIES

Giant glacial grooves at the north end of the Mission Range, northwest Montana ---- *I. J. Witkind* 425

Potassium-argon ages of basement rocks from Saint George Island, Alaska ---------- *D. M. Hopkins and M. L. Silberman* 435

Radiometric ages of some Cretaceous and Tertiary volcanic and intrusive rocks in south-central Arizona --- *N. G. Banks, R. D. Dockter, M. L. Silberman, and C. W. Naeser* 439

Granite of Rosalie Peak, a phase of the 1700-million-year-old Mount Evans pluton, Front Range, Colo ---------- *Bruce Bryant and C. E. Hedge* 447

Comendite (peralkaline rhyolite) and basalt in the Mitu Group, Peru: Evidence for Permian-Triassic lithospheric extension in the central Andes ---------- *D. C. Noble, M. L. Silberman, François Mégard, and H. R. Bowman* 453

Fusion of granodiorite by basalt, central Sierra Nevada - *F. C. W. Dodge and L. C. Calk* 459

Chabazite in siliceous tuffs of a Pliocene lacustrine deposit near Durkee, Baker County, Oreg ---------- *A. J. Gude 3d and R. A. Sheppard* 467

Differentiation of the sulfides in the Basal zone of the Stillwater Complex, Montana ---- *N. J Page and F. O. Simon* 473

Recognition of oxidized sulfide minerals as an exploration guide for uranium -------- *R. L. Reynolds and M. B. Goldhaber* 483

Uranium in waters and aquifer rocks at the Nevada Test Site, Nye County, Nev ------ *R. A. Zielinski and J. N. Rosholt* 489

Discrimination of fluvial and eolian deposits by number-frequency analysis of sediments of sand through silt size from a point bar, Rio Puerco, N. Mex ---------- *R. G. Shepherd and D. L. Macke* 499

Spectral gradient of lunar radiobrightness—heat flow or volume scattering? ---------- *A. W. England and G. R. Johnson* 505

APPLICATIONS OF REMOTELY SENSED DATA

Use of a remote computer terminal during field checking of Landsat digital maps ------ *C. J. Robinove and C. F. Hutchinson* 511

HYDROLOGIC STUDIES

Accuracy of flood mapping ---------- *D. E. Burkham* 515

Natural radioactivity in geothermal waters, Alhambra Hot Springs and nearby areas, Jefferson County, Mont ---------- *R. B. Leonard and V. J. Janzer* 529

Definition of regional relationships between dissolved solids and specific conductance, Susquehanna River basin, Pennsylvania and New York ---------- *D. J. Lystrom, F. A. Rinella, and W. D. Knox* 541

Preliminary evaluation of the floating dome method of measuring reaeration rates ----- *D. W. Stephens* 547

Recent publications of the U.S. Geological Survey ---------- Inside of back cover

SI UNITS AND U.S. CUSTOMARY EQUIVALENTS

[SI, International System of Units, a modernized metric system of measurement. All values have been rounded to four significant digits except 0.01 bar, which is the exact equivalent of 1 kPa. Use of hectare (ha) as an alternative name for square hectometer (hm^2) is restricted to measurement of land or water areas. Use of liter (L) as a special name for cubic decimeter (dm^3) is restricted to the measurement of liquids and gases; no prefix other than milli should be used with liter. Metric ton (t) as a name for megagram (Mg) should be restricted to commercial usage, and no prefixes should be used with it. Note that the style of meter^2 rather than square meter has been used for convenience in finding units in this table. Where the units are spelled out in text, Survey style is to use square meter]

SI unit		U.S. customary equivalent	
Length			
millimeter (mm)	=	0.039 37	inch (in)
meter (m)	=	3.281	feet (ft)
	=	1.094	yards (yd)
kilometer (km)	=	0.621 4	mile (mi)
	=	0.540 0	mile, nautical (nmi)
Area			
centimeter^2 (cm^2)	=	0.155 0	inch^2 (in^2)
meter^2 (m^2)	=	10.76	feet^2 (ft^2)
	=	1.196	yards^2 (yd^2)
	=	0.000 247 1	acre
hectometer^2 (hm^2)	=	2.471	acres
	=	0.003 861	section (640 acres or 1 mi^2)
kilometer^2 (km^2)	=	0.386 1	mile^2 (mi^2)
Volume			
centimeter^3 (cm^3)	=	0.061 02	inch^3 (in^3)
decimeter^3 (dm^3)	=	61.02	inches^3 (in^3)
	=	2.113	pints (pt)
	=	1.057	quarts (qt)
	=	0.264 2	gallon (gal)
	=	0.035 31	foot^3 (ft^3)
meter^3 (m^3)	=	35.31	feet^3 (ft^3)
	=	1.308	yards^3 (yd^3)
	=	264.2	gallons (gal)
	=	6.290	barrels (bbl) (petroleum, 1 bbl=42 gal)
	=	0.000 810 7	acre-foot (acre-ft)
hectometer^3 (hm^3)	=	810.7	acre-feet (acre-ft)
kilometer^3 (km^3)	=	0.239 9	mile^3 (mi^3)
Volume per unit time (includes flow)			
decimeter^3 per second (dm^3/s)	=	0.035 31	foot^3 per second (ft^3/s)
	=	2.119	feet^3 per minute (ft^3/min)
Volume per unit time (includes flow)—Continued			
decimeter^3 per second (dm^3/s)	=	15.85	gallons per minute (gal/min)
	=	543.4	barrels per day (bbl/d) (petroleum, 1 bbl=42 gal)
meter^3 per second (m^3/s)	=	35.31	feet^3 per second (ft^3/s)
	=	15 850	gallons per minute (gal/min)
Mass			
gram (g)	=	0.035 27	ounce avoirdupois (oz avdp)
kilogram (kg)	=	2.205	pounds avoirdupois (lb avdp)
megagram (Mg)	=	1.102	tons, short (2 000 lb)
	=	0.984 2	ton, long (2 240 lb)
Mass per unit volume (includes density)			
kilogram per meter^3 (kg/m^3)	=	0.062 43	pound per foot^3 (lb/ft^3)
Pressure			
kilopascal (kPa)	=	0.145 0	pound-force per inch^2 (lbf/in^2)
	=	0.009 869	atmosphere, standard (atm)
	=	0.01	bar
	=	0.296 1	inch of mercury at 60°F (in Hg)
Temperature			
temp kelvin (K)	=	[temp deg Fahrenheit (°F)+459.67]/1.8	
temp deg Celsius (°C)	=	[temp deg Fahrenheit (°F)−32]/1.8	

The policy of the "Journal of Research of the U.S. Geological Survey" is to use SI metric units of measurement except for the following circumstance:

When a paper describes either field equipment or laboratory apparatus dimensioned or calibrated in U.S. customary units and provides information on the physical features of the components and operational characteristics of the equipment or apparatus, then dual units may be used. For example, if a pressure gage is calibrated and available only in U.S. customary units of measure, then the gage may be described using SI units in the dominant position with the equivalent U.S. customary unit immediately following in parentheses. This also applies to the description of tubing, piping, vessels, and other items of field and laboratory equipment that normally are described in catalogs in U.S. customary dimensions.

S. M. LANG, *Metrics Coordinator,*
U.S. Geological Survey

Any use of trade names and trademarks in this publication is for descriptive purposes only and does not constitute endorsement by the U.S. Geological Survey.

Jour. Research U.S. Geol. Survey
Vol. 6, No. 4, July–Aug. 1978, p. 425–433

GIANT GLACIAL GROOVES AT THE NORTH END OF THE MISSION RANGE, NORTHWEST MONTANA

By IRVING J. WITKIND, Denver, Colo.

Abstract.—Giant glacial grooves both cut across and wrap around the north end of the Mission Range. Some of these grooves are straight, others crescentic, but all appear to be independent of stratigraphic units and of the gross structure of the range. They were seemingly localized by preexisting stream valleys whose original trends were determined by joints. The grooves are cut in bedrock, U-shaped in cross section, thickly veneered with till, and roughly parallel. Most range in length from 0.5 km to 3.5 km. Each groove maintains a uniform width, but widths range from about 50 m to 275 m. Depths of individual grooves vary widely, ranging from about 10 m to about 60 m. The grooves are probably contemporaneous in age, but their time of formation is uncertain; it seems to have been prior to late Pinedale time but after the pre-Bull Lake glaciations. Of the various interpretations offered to explain their origin, the one that appears to fit most of the facts suggests that those grooves at the northern tip of the mountains were carved by a lobe of the south-flowing Cordilleran ice sheet, whereas those farther south were likely formed by the westward deflection of a north-flowing Swan valley glacier.

A series of giant grooves both cuts across and wraps around the north end of the Mission Range in northwest Montana (fig. 1). These grooves are large furrows whose lengths are measured in kilometers and whose widths extend to hundreds of meters. Because of the thick forest they are difficult to perceive from the ground but are easily recognized from the air and on aerial photographs (fig. 2). Although some are straight and resemble the giant linear grooves of glacial origin described by Smith (1948) from the Mackenzie Valley in northwest Canada, others are curved and are crescentic in plan view. They have been known for many years, but little has been written about them. This paper describes the grooves, presents evidence that stamps them clearly as being of glacial origin, and offers several alternative interpretations regarding the influence of the extent of glaciers and the direction of ice flow on the origin of the grooves.

PHYSIOGRAPHIC SETTING

The Mission Range is an imposing north-trending topographic barrier flanked by the irregular-shaped Mission valley on the west and the linear Swan and Clearwater valleys on the east. The Mission valley is shaped like a bulbous bottle. Near its southern end it is about 25 km wide, but at its northern end it narrows to about 10 km. Flathead Lake occupies the northern neck of the bottle. The Swan and Clearwater valleys, by contrast, are long, narrow, northwest-trending valleys which range in width from 8 to 13 km. Their east edges are sharply defined by the steep, straight face of the Swan Range. Major rivers, flowing in opposite directions, occupy the valleys. The Swan River, in the Swan valley, flows northwest into the southern end of the Kalispell valley, where it abruptly changes direction to flow south and finally west through a narrow gap cut into the north end of the Mission Range to empty into Flathead Lake at Big Fork. The Clearwater River, in the Clearwater valley, flows south and is tributary to the west-flowing Blackfoot River. Both the Swan and Clearwater Rivers originate near the Clearwater divide, a low rise about midway in the length of the trench (fig. 1).

The Mission Range gradually decreases in altitude toward the north, and near Big Fork the mountains finally disappear beneath outwash. Here, the Mission valley and the Swan and Clearwater valleys merge to form the broad, flat Kalispell valley, about 25 km wide.

STRATIGRAPHY AND STRUCTURE OF THE MISSION RANGE

The rocks that form the Mission Range consist mainly of slightly metamorphosed fine-grained rocks such as argillite, siltite, dolomite, and quartzite in vivid hues of purple, red, green, tan, and gray. They are part of the Precambrian Y Belt Supergroup. Locally these rocks are intruded by thin dikes and sills of a dark-gray speckled diorite.

Structurally the Mission Range is an eastward-tilted fault block bounded on the west by the great high-angle Mission normal fault. The metasedimentary beds that form the mountains trend north parallel to

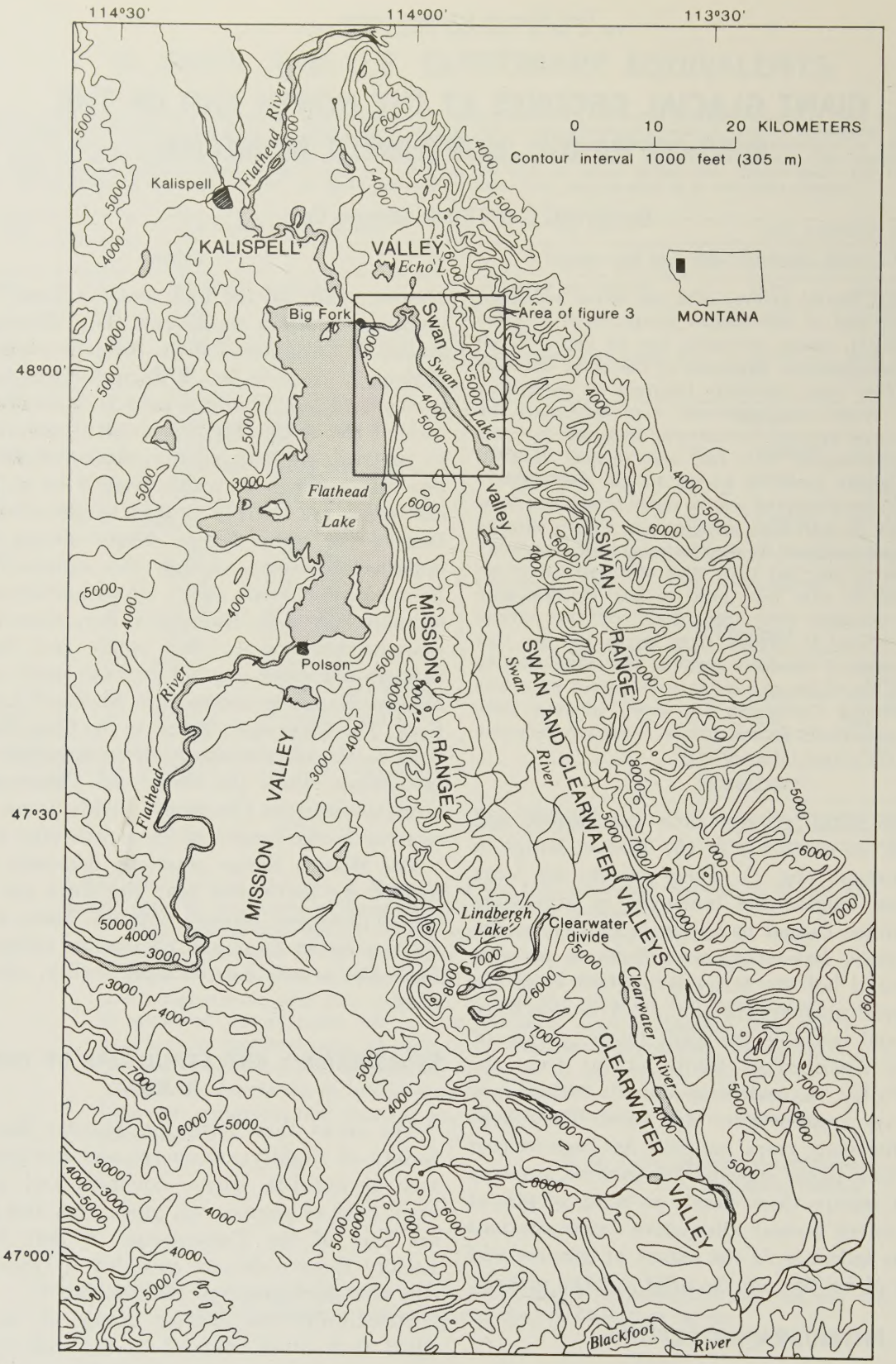

FIGURE 1.—Index map of part of northwest Montana showing major physiographic features. Topography modified from the Butte, Glacier Park, Kootenai, and Spokane sectional aeronautical charts compiled and printed by the U.S. Department of Commerce.

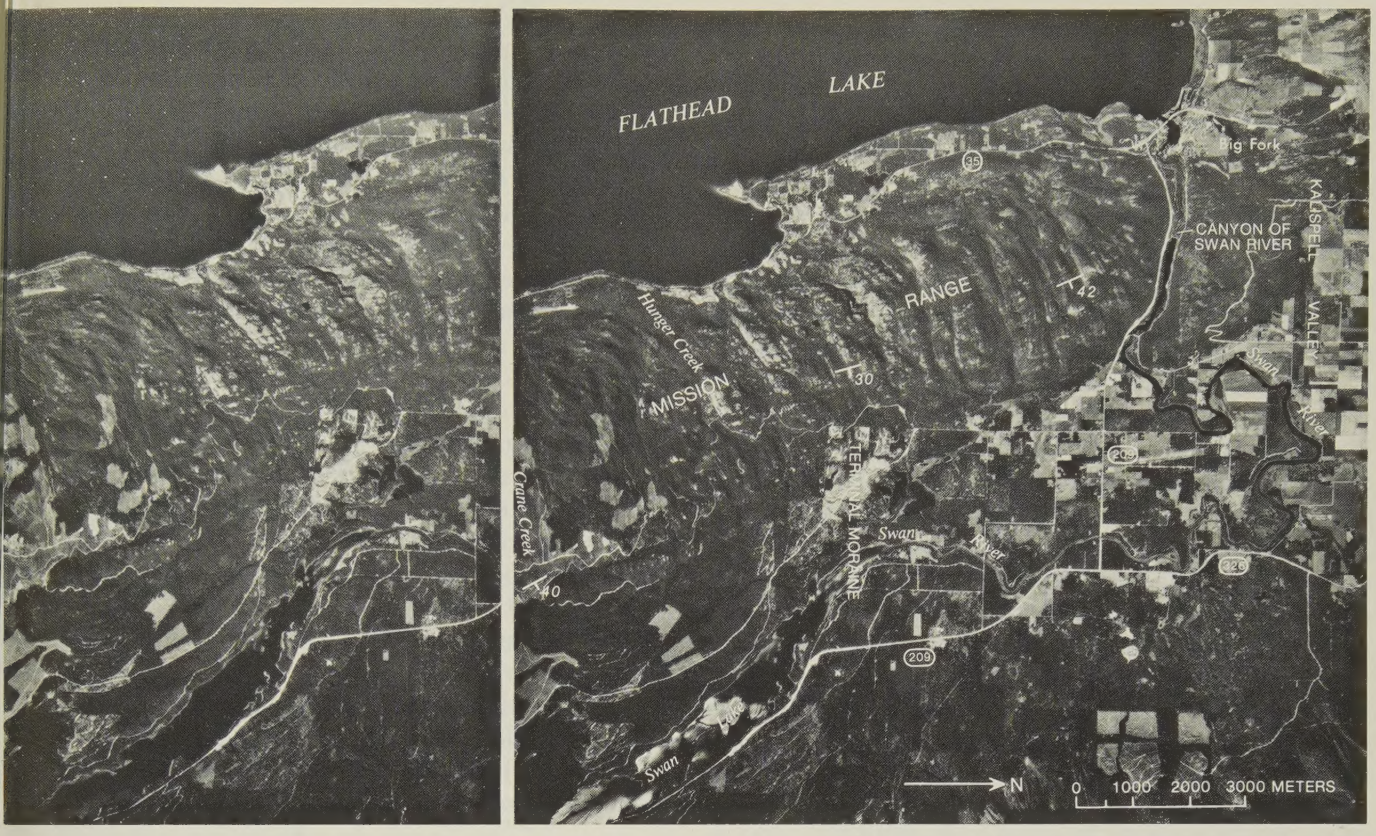

FIGURE 2.—Stereophotograph pair showing some giant grooves that cut across the north end of the Mission Range, northwest Montana.

the range and dip eastward toward the Swan and Clearwater valleys. These beds are broken here and there by both normal and right-lateral strike-slip faults, but these do not greatly disrupt the northward trend of the beds.

Three joint sets break the rocks. One set trends N. 12°–30° W., a second set trends N. 75° W. to west, and a third set trends about N. 80° E. All are either nearly vertical or dip very steeply at angles between 65° and 85°. Although the joints are mostly concealed beneath till in the area discussed here, they are well exposed farther south in the central part of the Mission Range, where they were studied by personnel of the U.S. Geological Survey during a geologic examination of the Mission Mountains Primitive Area (Harrison and others, 1969; M. W. Reynolds, written commun., 1977). Most of the streams and lakes appear to be controlled by one or another of these joint sets. Additional details about both the stratigraphy and structure of the Mission Range are given by Harrison and others (1969) and by Johns (1970).

GLACIAL DEPOSITS

The general area centered at Kalispell has been extensively glaciated, chiefly by a lobe of the Cordilleran ice sheet[1] that time and again has moved southward from Canada into this part of northwestern Montana and then withdrawn (Richmond and others, 1965). Glacial drift is widespread. Much of the Kalispell valley is floored by outwash, and thick till mantles the lower slopes of the west flank of the northern Mission Range. This till can be traced until it ends as a wide terminal moraine south of Polson. The Swan and Clearwater valleys are floored by extensive deposits of unmodified tills that are marked by striking knob-and-kettle topography; kettle lakes, swamps, and undrained depressions are common. Drumlinoid features extend for almost the entire lengths of the two valleys. Glacial erratics, some as much as 5 m on a side, are profuse; and they show virtually no evidence of weathering. Locally the tills

[1] The Flathead glacier of Alden (1953, p. 115).

in the Swan and Clearwater valleys are mantled by outwash that contains large lakes and undrained depressions, the result of the melt of former buried ice blocks. The general impression is that the drift, at least in the valleys, is almost unchanged, appearing much as it was when deposited.

Just how many times ice advanced into and withdrew from the area is uncertain. Most of the glacial deposits that now fill the valleys and mantle the mountain flanks are probably of Pinedale age. The youngest deposits, likely of late Pinedale age, are widespread in the Swan valley, in the northern half of the Mission valley, and in the Kalispell valley. They are best displayed in the upper reaches of the Swan valley where the till is dark brown, is very coarse, and consists of a heterogeneous mixture of unconsolidated gravel, cobbles, and boulders in a matrix of medium to coarse sand. Lithologically both the till and the accompanying outwash are dominated by clasts of green, gray, and purple argillite; tan quartzite and sandstone clasts are minor components. As this till is traced northward in the Swan valley, its matrix becomes silty and somewhat clayey, and it takes on a semiconsolidated appearance. The till ends in a low inconspicuous terminal moraine at the north end of Swan Lake, where it appears as a light-brown, silty to clayey till containing virtually similar lithologic types but in far less abundance. This silty till rests on a grayish-brown till that mantles the north end of the Mission Range.

Glacial deposits in the Clearwater valley were probably formed during early or middle Pinedale time. These deposits differ markedly from the younger glacial deposits. The till of these older deposits is light brown to brown, is semiconsolidated, and consists of an unsorted mixture of gravel, cobbles, and boulders in a silty to clayey matrix. The most striking difference is in lithologic content; this older till is strongly dominated by tan quartzite and sandstone clasts; the green, gray, and purple argillite clasts are minor components.

Another till, possibly comparable in age to the one in the Clearwater valley, mantles the very northern tip of the Mission Range. This till is grayish brown and ranges from semiconsolidated to unconsolidated; it consists of a heterogeneous mixture of gravel, cobbles, and boulders in a sandy to clayey matrix. Lithologically it appears to contain about as much tan quartzite and sandstone as various-colored argillite.

In addition to these deposits, which can be related either to large valley glaciers or to one or more of the recurrent advances and withdrawals of the Cordilleran ice sheet, there are also many signs of alpine glaciation. Most of the higher mountains are dominated by a landscape marked by sharp jagged peaks and ridges separated by cirques containing small glacial lakes. U-shaped valleys are common, and many have small moraines blocking their mouths.

The older till that mantles the north end of the Mission Range partly fills the grooves; consequently its age is of keen interest. Some hint about its relative age is given by tenuous stratigraphic relations. It can be traced to an altitude of 1615 m along the crest of the range; above that altitude the only evidence of glaciation consists of sparse glacial erratics scattered across a thick regolith. These relations suggest two ages of glaciation—one during which the thick till was deposited and an older episode during which another till was deposited, one that has since been eroded leaving only the glacial erratics as relicts. This older till was probably deposited in either Bull Lake or pre-Bull Lake time. If so, the thick till (below the 1615 m altitude) must have been formed during either the middle or early stades of the Pinedale, or during the Bull Lake Glaciation. The abundance of kettle lakes and undrained depressions favors an early or middle Pinedale, rather than a Bull Lake, age; but firm evidence to support this age assignment is lacking.

GLACIAL GROOVES

Most of the grooves are confined to the northernmost 15 km of the Mission Range; they have not been found elsewhere in the Missions. But a few comparable grooves, seemingly related to those in the Missions, are just across the Swan valley along the west face of the Swan Range. The description of the grooves given here stems from a study of those carved in the Mission Range, but the descriptions apply equally well to those in the Swan Range.

The grooves in the Mission Range can be traced as an uninterrupted band from the north tip of the mountains to Crane Creek (fig. 3). Most come to an abrupt end at Crane Creek, although a few faint grooves continue along the west flank of the mountains. Those along the east flank of the range persist for another 6 km to the south. They are paralleled by similar grooves along the west flank of the Swan Range. The implication is strong that the sets of grooves flanking the Swan valley were formed contemporaneously.

Although individual grooves are much alike, two types can be recognized. Those at the extreme northern end of the Mission Range appear as short linear features that bend sharply to the south to merge with similar grooves along the west flank of the mountains. By contrast, those that are farther south appear as

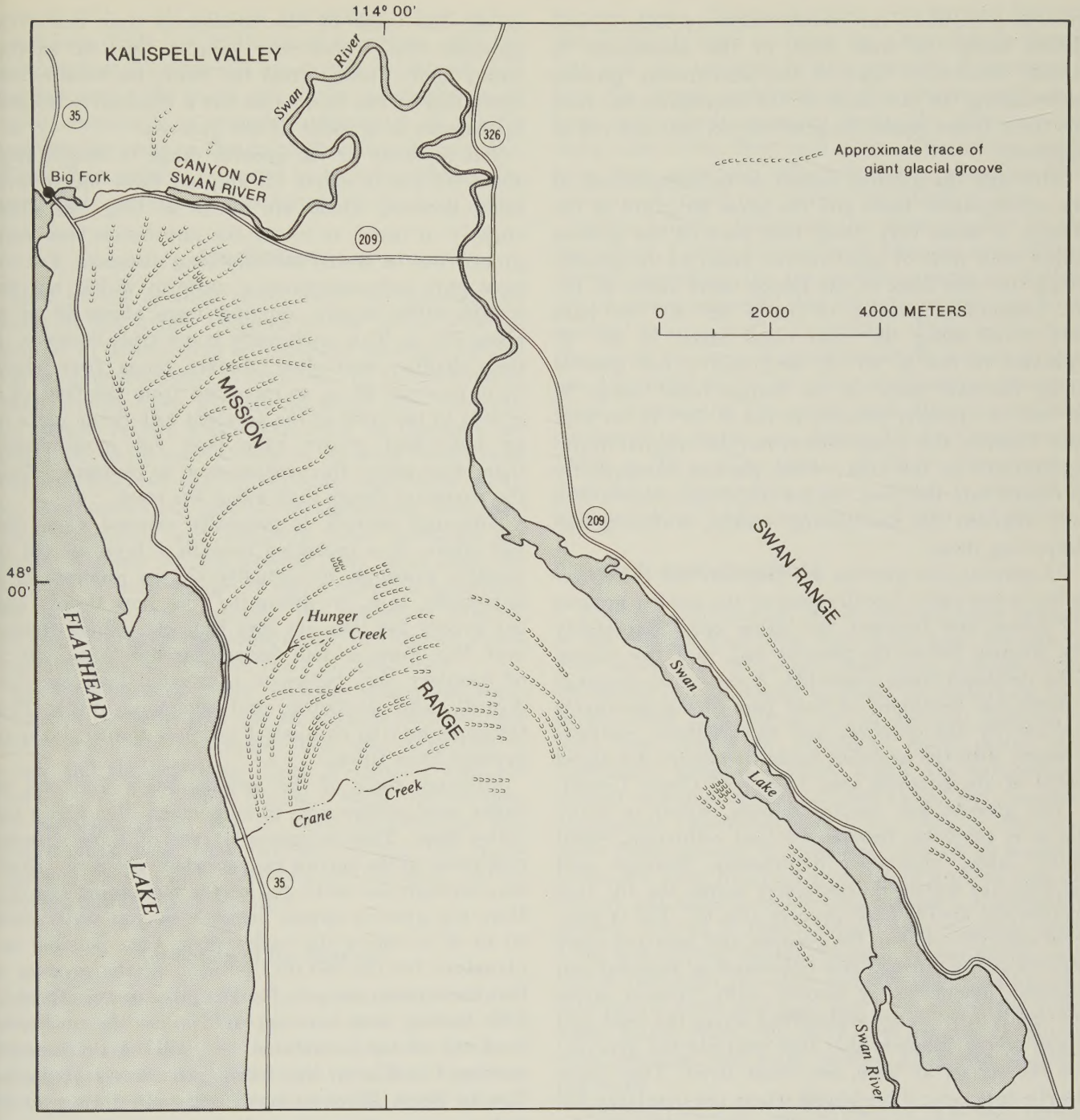

FIGURE 3.—Pattern of giant grooves at the north end of the Mission Range and along part of the west flank of the Swan Range, northwestern Montana.

semicircular furrows that form a crescentic pattern about the north end of the mountains. All grooves, thus, both parallel and transect the north-trending beds that form the mountains. This is very well shown on the aerial photographs; the north trend of the upturned beds can be seen as gray lines cut by the grooves (fig. 2). The linear grooves at the northern tip of the mountains (near Big Fork) trend either south, southwest, or west; and the eastern ends of several of the west-trending grooves curve to the north, giving them a sigmoid appearance. The abrupt southward bend of both the linear and semicircular

grooves parallel to the metasedimentary beds is well shown along the west flank of the mountains. A similar southward bend of the semicircular grooves occurs along the east flank of the mountains, but here the thick forest masks the grooves and they are not as apparent.

Although the grooves appear to be independent of the stratigraphic units and the gross structure of the Range, it seems very likely that most of the grooves reflect some form of joint control. Many of the grooves along the west flank of the Range trend about N. 15° W. (essentially parallel to the N. 12°–30° W. joint set), those along the crest trend about N. 80° E. (parallel to the N. 80° E. set), and a few grooves along the east flank of the Range trend about N. 75°–80° W. (nearly parallel to the N. 75° W. to west set). Possibly the joints determined the original drainage pattern in the area; when glaciers subsequently advanced into the area, the ice could have moved into and followed the pre-existing valleys, widening and deepening them.

In general, the grooves are parallel, but the parallelism is not exact. Locally some of the smaller grooves cut across and intersect the larger ones. Expectably the streams follow the grooves and, in a few places, have deepened them somewhat. A crescentic drainage pattern has developed on that part of the mountains marked by the grooves, and this pattern contrasts strongly with the modified dendritic pattern developed south of the grooved area (south of Crane Creek).

The grooves are cut in bedrock, which in many places is concealed beneath till and colluvium. Small kettle lakes, undrained depressions, swamps, and marshes are scattered irregularly across the till that mantles the floors of the grooves (fig. 2). Till is plastered onto the walls of the grooves, and here and there bedrock pokes through this till veneer as rounded and polished hummocks or smooth cliffs. Glacial striae and small grooves are widespread along the crest and flanks of the bedrock hills that separate the grooves; but the striae, at least, are short lived. They show clearly only near those places where the overlying till has recently been removed. The striae are collinear with the grooves, and in many places striae of several subparallel trends overlap. Possibly the different trends represent minor shifts in the direction of flow of the basal ice as a result of slight irregularities in the ice-buried surface or they may represent two ice advances widely separated in time—a concept that I consider unlikely in view of the delicate nature of the striae.

Virtually all the grooves are U-shaped in cross section. Most can be traced from a valley floor upward across the crest of the mountains and down the opposite side, where they seem to end at another valley floor. Viewed from the flank, the crest of the north end of the mountains has a distinctive notched appearance as a result of the grooves.

The majority of the grooves range in length from about 0.5 km to about 3.5 km, but these merge with other grooves, which are about as long but differ slightly in trend, to create the impression that some grooves can be traced for very long distances. For the most part each maintains a uniform width, but the widths differ widely, ranging from about 50 m to about 275 m. This uniformity is not true, however, of their depths; individual grooves range from about 10 m to about 60 m, as measured from the floor of a groove to the crest of the adjacent hill. Some parts of an individual groove have been cut more deeply than other parts: the grooves seem to be deeper along the mountain flanks than along the crest.

Although bedrock is generally exposed along the hill crests, it is concealed beneath a layer of till of variable thickness in virtually all the grooves. It is impossible, thus, to determine just how deeply any one groove has been cut into bedrock. In one groove, near Big Fork, a drill passed through some 120 m of bouldery clay before it penetrated bedrock (Les Averill, land developer, oral commun., 1976). This thickness may be unusual; I estimate the till layer to average 15 m thick.

Although some of the grooves begin and end at valley level, others seem to be perched high above the valley floor. This is especially true of those grooves that front on the narrow canyon where the Swan River cuts through the north end of the mountains (fig. 2). Here the grooves appear in both canyon walls some 60 to 90 m above the valley floor. One possible explanation for the elevated position of the grooves is that the canyon was cut after the grooves were formed. This cutting may have occurred when the northernmost tip of the mountains was still buried beneath wasting Cordilleran ice, forcing the ancestral north-flowing Swan River to turn south and then west to seek an escape route across the mountains.

Origin

It is hard to visualize what could have formed these grooves other than large glaciers, for the evidence of a glacial origin is overwhelming. The grooves are in a glaciated terrain, and virtually all are U-shaped in cross section and mantled with till. Only here and there does bedrock crop out through the till cover; and where exposed it is rounded, polished, and locally

covered with small grooves and striae. These minor scours invariably are collinear or nearly so with the giant grooves. The grooves are carved in bedrock, and they cut across the north end of the mountains at all angles, seemingly in complete disregard of specific stratigraphic units or the gross structure of the range. (There does appear, however, to be some relation between their trends and the trends of the joint sets.)

Localization

Most of the grooves reflect both the spacing and trends of the joints. Presumably the joints were influential in determining the original drainage pattern that developed across the north end of the mountains. Subsequently, when glaciers advanced into the area, the stream valleys must have acted as channels for small lobes of the encroaching ice. As these lobes flowed into and followed the valleys, they must have modified them somewhat, possibly straightening them, and surely deepening and widening them. Although the trends of many of the grooves may have been determined by such valleys, it seems plausible to assume that some grooves—possibly the shallower ones—do not reflect preexisting topography but rather alined concentrations of abrasive tools in basal ice.

Once the grooves were formed, subsequent readvances of the same lobe (or an advance of a younger lobe) very likely reoccupied them and continued to widen and deepen them. Thus, it may be that the grooves were not formed during a single ice advance, but represent rather two or more ice advances. The grooves may have been outlined during Bull Lake time and subsequently deepened and widened during early or middle Pinedale time.

Formation of the Grooves

At least two alternative interpretations are available to explain how the grooves were formed. The first, which I favor, is that they are the result of abrasion by rock fragments tightly held in basal ice. The second is that the grooves are the result of subglacial fluids, under high hydrostatic pressure and heavily charged with various sized rock and ice fragments. Glacial features formed by such processes are called "plastically moulded surfaces" (Embleton and King, 1975, p. 191).

Glacial scour

The polish, striae, and small grooves that mark the bedrock are all evidence that ice has passed over the area and, in so doing, has abraded and scoured the exposed rocks. These markings were formed by rock debris tightly held in basal ice. Once the ice flowed into and was localized by the preexisting stream valleys, the armed underside of the glacier acted as a huge rasp slowly grinding away the protuberances along the valley floor and sides. The action would have been especially effective if the abrading tools were concentrated in a narrow longitudinal zone.

Smith (1948), discussing the giant grooves in the Mackenzie Valley of northwest Canada, and Carney (1909), describing the far smaller grooves on Kelleys Island, Ohio, suggested that the grooves they described resulted from such a concentration. These tools armed the sole of the ice and concentrated the erosive processes. As quickly as the grinding and scouring formed a small groove, the ice spread and filled it and then continued to widen and deepen it. As Carney noted (1909, p. 645): "The weight of the ice mass keeps it moulded to the growing groove, which is enlarged so long as cutting tools, even grains of sand, are present."

Plastically molded surfaces

The crescentic nature of the grooves lends support to the concept that they may have been formed by fluid movement. Although plastically molded forms (p-forms) can be shaped by basal ice containing rock debris, most such forms are, in general, believed to have been eroded by subglacial fluids under high hydrostatic pressure. Typical media are water-soaked ground moraine, subglacial meltwater, and ice-water compounds (Embleton and King, 1975, p. 191–194). Such fluids, guided by subglacial tunnels or englacial tubes, are more likely to give rise to grooves that are curved and sinuous rather than straight. Presumably, grooves formed in this fashion might resemble somewhat meandering stream channels. These fluids, moving at very high velocities and consisting mainly of a solution of water and rock particles, attack the valley walls, scallop them, and carve such features as solution cups, potholes, and giant kettles. They also sandblast the rocks.

Although some of the grooves may have been formed by subglacial fluids, it seems likely that most, if not all, are the result of basal ice scour. Even though a few grooves are somewhat sinuous, most are straight or gently curved. Minor features such as potholes and scallops were not seen, though it is possible that they are buried beneath till. Where exposed, the striated bedrock lacks a sandblasted effect; indeed, rather than a pitted surface, most of the striated bedrock has a high polish and locally almost a glazed surface. This type surface, it would seem, can result only from

continuous polish by basal ice containing a high percentage of very fine grained rock flour.

Most of the evidence favors the concept that the grooves were formed by basal ice scour rather than by the attack of subglacial fluids.

DIRECTION OF ICE FLOW

Although the origin of the grooves is clearly related to differential glacial erosion, the direction of glacier movement that formed the grooves is open to question. Smith (1948) noted that the giant glacial grooves in the Mackenzie Valley clearly record the direction of ice flows—west and then northwest. Although many of the grooves at the very northern tip of the Mission Range do indicate the direction of ice movement—essentially south-flowing—other grooves, especially those flanking the Swan valley, are ambiguous in that one is unable to state conclusively whether they were formed by north- or south-flowing ice. In this area, then, only some of the grooves are reliable indicators of direction of ice flow.

In general, the trends of the grooves suggest three possible interpretations: the first assumes that the grooves were formed by a glacier that flowed north in the Swan valley and that was deflected westward across the northern end of the Mission Range by the Cordilleran ice sheet (Johns, 1970, fig. 3); the second alternative assumes that the Cordilleran ice sheet, flowing south, overrode the north end of the Mission Range, bifurcated, and in so doing formed both the linear and crescentric grooves; and the third alternative, which I favor, is that the grooves were formed by some combination of both movements.

Westward diversion of the north-flowing Swan valley glacier.—This interpretation is based on studies of glacial striae and other evidence of glacial movement by Willis Johns of the Montana Bureau of Mines and Geology. Johns, in his publication on the geology and mineral deposits of Lincoln and Flathead Counties, used a series of arrows to indicate his interpretation of the direction of ice flow (1970, fig. 3). The arrows imply that the north-flowing Swan valley glacier was deflected westward across the mountains. This interpretation is seemingly supported by the pattern of some grooves. Near the southern end of Swan Lake, the grooves trend about N. 30° W.; as they are traced northward they curve gradually (N. 40° W., N. 55° W., N. 75° W.), and finally trend west and then southwest (S. 65° W.) (fig. 3). Presumably this westward deflection occurred near the mouth of the Swan valley when the glacier encountered a southward-moving lobe of the Cordilleran ice. Then, either the glacier rode up onto the Cordilleran ice and was deflected westward across the mountains by the bulk of the lobe, or it piled up against the lobe until it became thick enough to flow across the north end of the mountains and empty into the Mission valley. In this interpretation the Swan valley glacier is literally forced to make a complete 180° reversal of direction—flowing north in the Swan valley and eventually south in the Mission valley. Although the concept fits much of the available data, my current mapping suggests that the last valley glacier to occupy the Swan valley never extended beyond the mouth of Swan Lake. (See section "Glacial Deposits.") Deposits interpreted as a late (?) Pinedale terminal moraine in that general area seemingly mark the farthest northern extent of the ice. But it is possible that an earlier glacier, also flowing north in the Swan valley, could have been diverted westward to form the grooves. Although glacial striae are of little assistance in determining direction of glacier flow (Flint, 1971, p. 95), other evidence, chiefly stoss-and-lee topography, does suggest that ice did flow westward at least over the southern part of the grooved area.

But the grooves that trend south and southwest across the northern tip of the mountains (see section "Glacial Grooves" and figs. 2 and 3) could not have been formed by the deflected Swan valley glacier. These grooves must have been carved by ice from the north that flowed south and southwestward.

Bifurcation of the south-flowing Cordilleran ice sheet.—This alternative assumes that the Cordilleran ice sheet, as it flowed southward, gradually overwhelmed the low northern tip of the Mission Range and eventually split into two lobes. One very broad lobe, west of the mountains, filled the north end of the Mission valley and extended south of Polson; the other lobe, a narrow, elongate mass, moved into the Swan valley, but how far south it reached is unknown. The striking south and southwesterly trends of those grooves at the northern end of the mountains imply strongly that all or part of this eastern lobe was deflected southwestward across the mountains into the Mission valley. But what deflected the ice? One possibility is that the feasible access route to the south—the Swan valley—was filled by a glacier. The lobe of ice piled up against this obstruction until it found an escape route into the Mission valley. Another possibility is that this eastern lobe did indeed flow southward in the Swan valley (possibly overriding the Swan valley glacier) until its thickness at the northern tip of the mountains was great enough to flow across the mountains.

Some combination of the two previous explana-

tions.—The third interpretation assumes that the grooves were formed by some combination of the two alternatives. Probably grooves at the north end of the mountains were indeed formed by the deflection of the eastern lobe of the Cordilleran ice to the southwest. Those grooves farther south, however (on the basis of stoss-and-lee topography), appear to have formed as a result of the westward deflection of the north-flowing Swan valley glacier. If this interpretation is valid, all the grooves between the north tip of the mountains and Hunger Creek were probably formed by the southwestward deflection of the eastern lobe, and all grooves between Hunger and Crane Creeks were probably formed by the deflected Swan valley glacier.

CONCLUSIONS

1. The grooves are clearly the result of differential glacial erosion. They are independent of stratigraphic units and of the gross structure of the mountains. Most apparently were localized by the preexisting stream valleys, whose original trends probably followed established joint sets.
2. The grooves are probably contemporaneous.
3. The grooves were likely formed prior to late Pinedale but after pre-Bull Lake time.
4. Some of the grooves are useful in recording the true direction of ice flow, but many are not.
5. It is uncertain which ice masses carved which grooves, but of the various interpretations, the one that fits most of the facts suggests that those grooves at the north end of the mountains were cut by the southwestward deflection of a lobe of the Cordilleran ice sheet, whereas other grooves farther south, which are crescentic about the mountains, were formed by the westward deflection of a north-flowing Swan valley glacier.

REFERENCES CITED

Alden, W. C., 1953, Physiography and glacial geology of western Montana and adjacent areas: U.S. Geol. Survey Prof. Paper 231, 200 p. [1954].

Carney, Frank, 1909, Glacial erosion on Kelleys Island, Ohio: Geol. Soc. America Bull., v. 20, p. 640–645.

Embleton, Clifford, and King, Cuchlaine A. M., 1975, Glacial geomorphology: New York, John Wiley and Sons, 573 p.

Flint, R. F., 1971, Glacial and Quaternary geology: New York, John Wiley and Sons, Inc., 892 p.

Harrison, J. E., Reynolds, M. W., Kleinkopf, M. D., and Pattee, E. C., 1969, Mineral resources of the Mission Mountains Primitive Area, Missoula and Lake Counties, Montana: U.S. Geol. Survey Bull. 1261–D, 48 p.

Johns, W. M., 1970, Geology and mineral deposits of Lincoln and Flathead Counties, Montana: Montana Bur. Mines and Geology Bull. 79, 182 p.

Richmond, G. M., Fryxell, Roald, Neff, G. E., and Weis, P. L., 1965, The Cordilleran ice sheet of the northern Rocky Mountains, and related Quaternary history of the Columbia Plateau, *in* The Quaternary of the United States, VII Congress, INQUA: Princeton, N.J., Princeton Univ. Press, p. 231–242.

Smith, H. T. U., 1948, Giant glacial grooves in northwest Canada: Am. Jour. Sci., v. 246, no. 8, p. 503–514.

Jour. Research U.S. Geol. Survey
Vol. 6, No. 4, July–Aug. 1978, p. 435–438

POTASSIUM-ARGON AGES OF BASEMENT ROCKS FROM SAINT GEORGE ISLAND, ALASKA

By D. M. HOPKINS and M. L. SILBERMAN, Menlo Park, Calif.

Abstract.—Potassium-argon ages from basement granitic rocks that intrude serpentinized peridotite on St. George Island, Alaska, range from 50 to 57 million years, with an initial argon isochron age, interpreted as a minimum figure, of 52 ± 2 m.y. The age of the granitic rocks and their association with serpentinized peridotite near the continental margin, which apparently marks the site of a Mesozoic subduction zone, suggest that the position of the subduction zone shifted southward to the Aleutian Trench in early Tertiary time.

St. George Island is one of the Pribilof Islands, which lie between lat 56°35′ and 57°11′ N. in the Bering Sea, 350 km (kilometers) north of the Aleutian chain. The islands are situated near the margin of the continental platform that underlies most of the north half of the Bering Sea (fig. 1). They are made up mostly of olivine basalt and basanite flows, pillow breccias, pyroclastic deposits, sills and dikes, most of which are nepheline normative (Barth, 1956). The volcanic rocks on St. George are Pliocene and early Pleistocene in age (Cox and others, 1966; D. M. Hopkins and M. L. Silberman, unpub. data, 1975) and are interbedded with marine sand and gravel, glacially derived sediments, frost breccia, and windblown sand and silt.

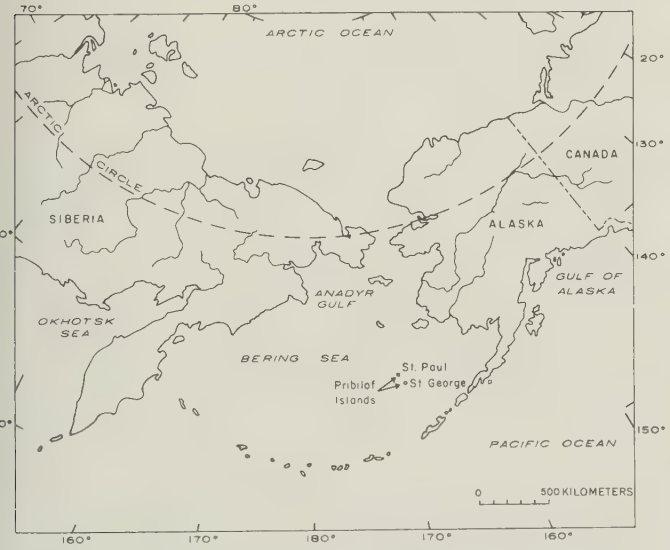

FIGURE 1.—Index map showing the location of the Pribilof Islands in the Bering Sea region.

Acknowledgments.—We benefited greatly from the helpful suggestions of W. W. Patton and M. A. Lanphere. J. L. Morton aided in the preparation of the figures.

BASEMENT

Serpentinized peridotite crops out for a distance of 5 km along the southeast shore of the island (fig. 2). In some places, the smoothly planed but warped upper surface is covered by marine sediments overlain by pillow breccia of Pliocene age (fig. 3); between Garden Cove and Sea Lion Point, the serpentinized peridotite underlies a glaciated marine terrace of middle Pleistocene age (Hopkins and Einarsson, 1966).

North of Garden Cove, the peridotite is intruded by a 400-m (meter)-wide composite granitic body referred to as "aplite" by Barth (1956). Its margin, about 3 m wide, is fine grained and contains alkali feldspar phenocrysts, some biotite, largely altered to sericite, and small amounts of garnet. The central part of the body, more mafic in composition, is a medium- to fine-grained granular rock consisting

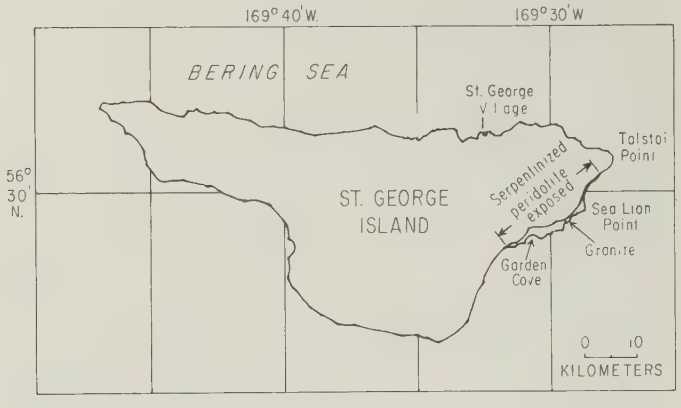

FIGURE 2.—Location of serpentinized peridotite and granite outcrops at base of cliffs on southeastern St. George Island.

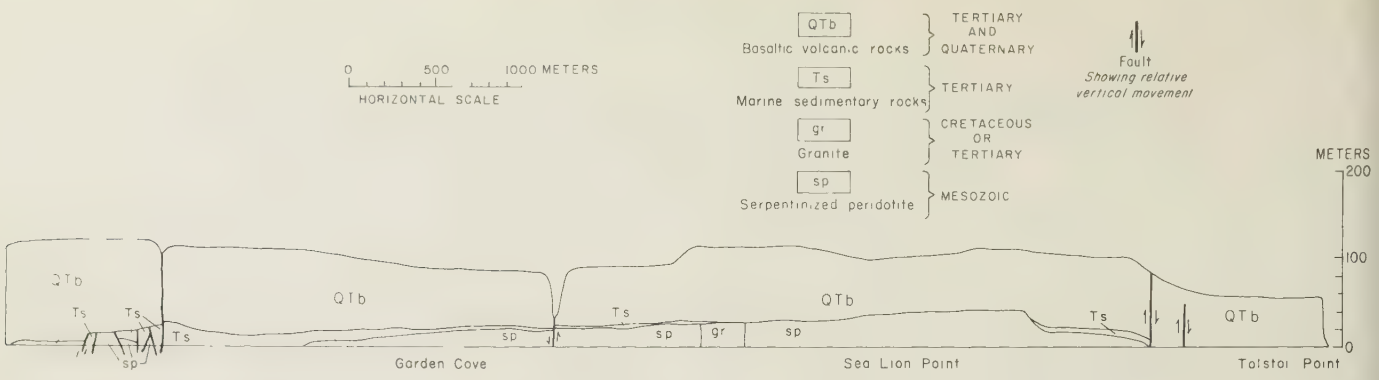

FIGURE 3.—Diagrammatic sketch of bluffs along southeast coast of St. George Island.

largely of plagioclase with interstitial quartz and potassium feldspar. Amphibole is present, largely altered to chlorite. In both rocks, the feldspars are heavily sericitized. Barth (1956) described these rocks in greater detail. The granite is younger than the serpentinized peridotite that it intrudes and older than the alkaline olivine basalts that unconformably overlie it. The peridotite and the granite are the only outcrops of pre-late Tertiary basement found in the Pribilof Islands.

POTASSIUM-ARGON AGES

Because of its alteration and lack of potassium-bearing minerals, the peridotite is not suitable for potassium-argon age determination. We collected one sample from the center of the granitic body and one from the margin. Both samples are altered; the fine-grained margin is sericitized, and mafic minerals in the coarser grained central part are altered to chlorite. Feldspars in both samples are at least partially sericitized.

Purified mineral concentrates were prepared by J. A. Peterson, using standard heavy-liquid and magnetic techniques. For sample G199, from the margin of the granitic body, she prepared an alkali feldspar and a sericite concentrate, and for sample G200, from the coarser grained center, a potassium feldspar concentrate and a concentrate consisting of chlorite and minor interleaved sericite that had replaced amphibole. Potassium-argon ages and analytical data are given in table 1.

The potassium-argon ages of the four minerals from the two samples range from 50 to 57 m.y. (million years). The determinations on the two minerals from each sample are not in agreement within the analytical precision. Two of the dated minerals, G199 sericite and G200 chlorite, are alteration minerals, and the feldspars are also partially sericitized, suggesting that the potassium-argon ages may represent minimum ages.

TABLE 1.—*Potassium-argon ages of mineral separates from the granitic body on St. George Island, Alaska*

[Analytical uncertainty of apparent age estimated at one standard deviation is a combined estimate made from uncertainties in the potassium and argon analytical techniques and is approximately 4 percent. Constants used in age calculation: $\lambda\varepsilon=0.572\times10^{-10}$/y, $\lambda\varepsilon'=8.78\times10^{-13}$/y, $\lambda\beta=4.963\times10^{-10}$/y, $K^{40}/K_{total}=1.167\times10^{-4}$ mole/mole]

Sample No.	Mineral	K_2O[1]	$^{40}Ar^*$ (moles/g)[2]	$^{40}Ar^*/^{40}Ar$	Apparent age (m.y.)
G199	Alkali feldspar	3.15	2.532×10^{-10}	0.57	55.0±2.2
G199	Sericite concentrate	3.35	2.419×10^{-10}	.78	49.5±2.0
G200	K-feldspar	7.21	5.546×10^{-10}	.49	52.7±2.1
G200	Chlorite	.407	$.3404\times10^{-10}$	.47	57.2±2.3

[1]Potassium was analyzed by flame photometry using a lithium metaborate fusion technique (Ingamells, 1970), the lithium serving as an internal standard. Mineral standards were used for calibration. Analysts: M. Cremer, J. H. Christie.

[2]Argon was analyzed by standard isotope dilution - mass spectrometry techniques described by Dalrymple and Lanphere (1969). Ar* represents radiogenic argon. Analyst: M. L. Silberman.

The data suggest an inverse relation between potassium-argon ages and potassium content of the mineral concentrates (table 1). A similar inverse relation has been noted in areas where small to moderate amounts of extraneous argon (argon-40 other than that generated by radioactive decay of potassium in place after crystallization) are present in a suite of rocks (MacDougall and others, 1969; Hayatsu and Carmichael, 1970; Shafiqullah and Damon, 1974). Extraneous argon-40 can produce anomalously old ages, the effect being greater in minerals of low potassium content because they produce less radiogenic argon over a given time period. The mineral containing the least potassium, chlorite sample G200 (table 1), yielded the oldest age among the St. George samples, as would be expected if extraneous argon-40 were present.

We note, however, that the sample having the youngest potassium-age (sample G199 sericite, 49.5 ± 2.0 m.y.) is not the sample having the highest potassium content.

The potassium and argon data from the granitic body on St. George Island are plotted on an initial argon diagram in figure 4. If the extraneous argon

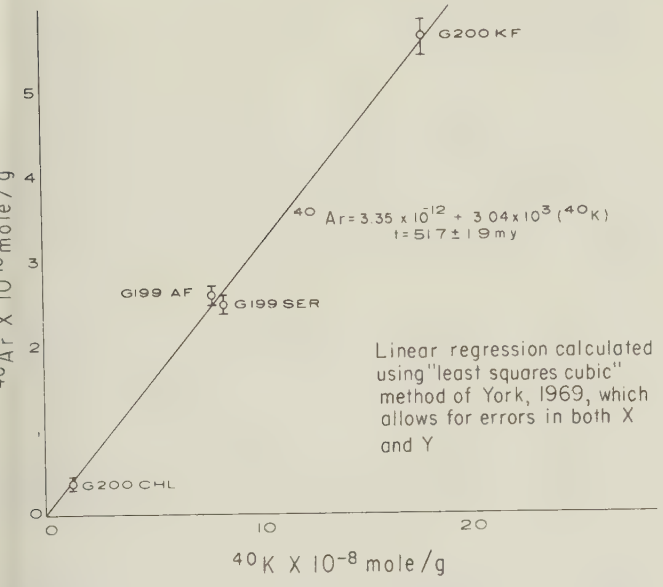

FIGURE 4.—Initial argon diagram for granitic body, St. George Island.

model applies, the intercept in this diagram would correspond to the amount of excess argon-40 present, and the slope would be proportional to the age at which the system became closed to gain or loss of argon. The age suggested by the slope of the initial argon plot (51.7 ± 1.9 m.y.) is not greatly different from the potassium-argon ages calculated conventionally on table 1, and the intercept suggests that the amount of excess argon-40 is small (3.3 x 10^{-12} mole/gram) and that any redistribution of argon-40 took place soon after emplacement of the granite and was not caused by the volcanic activity that emplaced the Pliocene and early Pleistocene basaltic lavas. Both methods of calculation point toward a latest Cretaceous or an earliest Tertiary age for the granitic body on St. George Island.

DISCUSSION AND CONCLUSIONS

Marine geologic and geophysical studies indicate that the Pribilof Islands lie near the southern margin of a belt of volcanic and plutonic rocks and minor interbedded continental sediments of Late Cretaceous

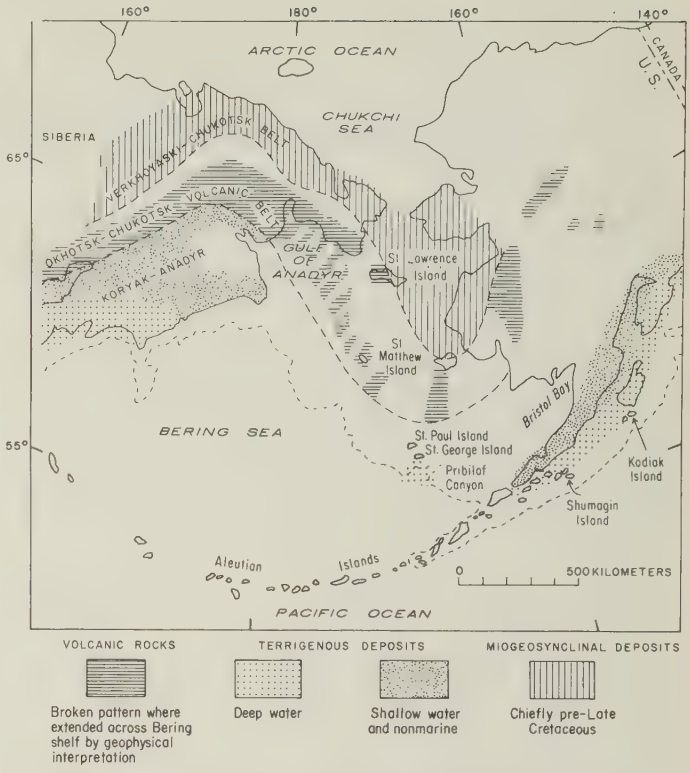

FIGURE 5.—Distribution of volcanic rocks and terrigenous deposits in the Bering Sea region during Late Cretaceous and earliest Tertiary time (≈ 80 to 55 m.y. ago). Outer margin of Bering Sea shelf at 200-m contour shown by short-dashed line. The pre-Late Cretaceous miogeosynclinal deposits are not discussed in this report. Modified from Patton and others (1976) and Marlow and others (1976).

and Paleocene age (the Okhotsk-Chukotsk volcanic belt of Russian geologists) and near the northern margin of a belt of deep-water flysch deposits of Late Cretaceous age (the Koryak-Anadyr flysch belt of Russian geologists) (Marlow and others, 1976; Patton and others, 1976) (fig. 5). The Alaskan continuation of the Okhotsk-Chukotsk volcanic belt probably extends inland from the north shore of Bristol Bay, and the Alaskan continuation of the Koryak-Anadyr flysch belt lies on the continental shelf of the Gulf of Alaska from the Shumagin Islands through Kodiak Island (Burk, 1965; Marlow and others, 1976). The two belts are separated in northeast Siberia and southwestern Alaska by a belt, 100 to 500 km wide, consisting of shallow-water and nonmarine sedimentary rocks of Cretaceous and Paleocene age (Patton and others 1976).

On St. Matthew Island, 500 km north of St. George Island, the Okhotsk-Chukotsk volcanic belt is represented by calc-alkaline volcanic rocks of basaltic to rhyolitic composition that are intruded and locally

metamorphosed by a small granodiorite pluton. The volcanic rocks have yielded potassium-argon ages of 65 to 77 m.y. (Late Cretaceous) and hornblende from the granodiorite has yielded a potassium-argon age of 61 m.y. (earliest Tertiary) (Patton and others, 1976).

Flysch deposits from the Pribilof Canyon that evidently represent the eastward extension of the Koryak-Anadyr flysch belt have yielded a microfauna originally diagnosed as Maestrichtian (Hopkins and others, 1969), but recent reexamination suggests that it is more likely of Campanian age (W. V. Sliter, written commun. to W. W. Patton, April 3, 1975). The Cretaceous flysch deposits in the Shumagin-Kodiak Island area are intruded by granodiorite and quartz diorite plutons having potassium-argon ages of 56 to 64 m.y. (Moore 1972).

Scholl, Buffington, and Marlow (1975) confirmed earlier inferences that during much of Mesozoic time the edge of the continental shelf in the Bering Sea formed the boundary between the North American–northeast Siberian continental plate and the Kula oceanic plate of Grow and Atwater (1970). After reviewing the alternatives, Scholl and his colleagues concluded that subduction probably shifted southward from the continental margin to the Aleutian trench-arc system during latest Cretaceous or earliest Tertiary time. These workers suggested that the serpentinized peridotite on St. George Island marks a subduction zone formed when the North American–Eurasian continental plate overrode the Kula volcanic plate during Mesozoic time.

The potassium-argon estimates, association with serpentinite, proximity to Late Cretaceous flysch deposits, and location near the continental margin all tend to ally the St. George granitic body with the small plutons that intrude the Alaskan extension of the Koryak-Anadyr flysch belt rather than those which invade the St. Matthew segment of the Okhotsk-Chukotsk volcanic belt. The age estimates of 50 to 57 m.y. for the St. George granitic body suggest that the shift in the position of the subduction zone from the southern margin of the Bering Shelf to the Aleutian trench-arc system took place in early Tertiary rather than in Late Cretaceous time.

REFERENCES CITED

Barth, T. F. W., 1956, Geology and petrology of the Pribilof Islands, Alaska: U.S. Geol. Survey Bull. 1028–F, p. 101–160.

Burk, C. A., 1965, Geology of the Alaska Peninsula-Aleutian Island Arc and continental margin: Geol. Soc. America Mem. 99, 250 p.

Cox, A. V., Hopkins, D. M., and Dalrymple, G. B., 1966, Geomagnetic polarity epochs; Pribilof Islands, Alaska: Geol. Soc. American Bull., v. 77, p. 883–910.

Dalrymple, G. B., and Lanphere, M. A., 1969, Potassium-argon dating: San Francisco, W. H. Freeman and Co., 258 p.

Grow, J. A., and Atwater, Tanya, 1970, Mid-Tertiary tectonic transition in the Aleutian Arc: Geol. Soc. America Bull., v. 81, p. 3715–3722.

Hayatsu, A., and Carmichael, C. M., 1970, K-Ar isochron method and initial argon ratios: Earth and Planetary Sci. Letters, v. 8, p. 71–76.

Hopkins, D. M., and Einarsson, Th., 1966, Pleistocene glaciation on St. George, Pribilof Islands: Science, v. 152, p. 343–345.

Hopkins, D. M., Scholl, D. W., and others, 1969, Cretaceous, Tertiary, and early Pleistocene rocks from the continental margin in the Bering Sea: Geol. Soc. America Bull., v. 80, p. 1471–1480.

Ingamells, C. O., 1970, Lithium metaborate flux in silicate analyses: Anal. Chim. Acta, v. 52, p. 323–334.

MacDougall, Ian, Polach, H. A., and Stipp, J. J., 1969, Excess radiogenic argon in young subaerial basalts from the Auckland volcanic field, New Zealand: Geochim. et Cosmochim. Acta, v. 33, p. 1485–1520.

Marlow, M. S., Scholl, D. W., Cooper, A. K., and Buffington, E. C., 1976, Structure and evolution of Bering Sea shelf south of St. Lawrence Island: Am. Assoc. Petroleum Geologists Bull., v. 60, p. 161–183.

Moore, J. C., 1972, Uplifted trench sediments—southwestern Alaska-Bering Shelf: Science, v. 175, p. 1103–1105.

Patton, W. W., Jr., Lanphere, M. A., Miller, T. P., and Scott, R. A., 1976, Age and tectonic significance of volcanic rocks on St. Matthew Island Bering Sea, Alaska: U.S. Geol. Survey Jour. Research, v. 4, no. 1, p. 67–73.

Scholl, D. W., Buffington, E. C., and Marlow, M. S., 1975, Plate tectonics and the structural evolution of the Aleutian-Bering Sea region, *in* Forbes, R. B., ed., The geophysics and geology of the Bering Sea region: Geol. Soc. America Spec. Paper 151, p. 1–32.

Shafiqullah, M., and Damon, P. E., 1974, Evaluation of K-Ar isochron methods: Geochim. et Cosmochim. Acta, v. 38, p. 1341–1358.

York, D., 1969, Least squares fitting of a straight line with correlated errors: Earth and Planetary Sci. Letters, v. 5, p. 320–324.

Jour. Research U.S. Geol. Survey
Vol. 6, No. 4, July–Aug. 1978, p. 439–445

RADIOMETRIC AGES OF SOME CRETACEOUS AND TERTIARY VOLCANIC AND INTRUSIVE ROCKS IN SOUTH-CENTRAL ARIZONA

By NORMAN G. BANKS, ROGER D. DOCKTER, MILES L. SILBERMAN;
and CHARLES W. NAESER, Menlo Park, Calif.; Denver, Colo.

Abstract.—Reconnaissance geologic mapping and radiometric ages provide the framework for correlation of Cretaceous and middle Tertiary volcanic and clastic rocks in the Vaca Hills and Eloy quadrangles, Arizona. The radiometric ages also record a middle Tertiary thermal event of much greater extent than suggested by the volume of middle Tertiary igneous rocks present in outcrop.

Four new K-Ar and five new fission-track ages are reported from five samples from the Vaca Hills and Eloy quadrangles, Arizona, about 70 km west of Tucson (fig. 1). The fission-track ages are from late Cretaceous or early Tertiary Laramide rocks which yielded K-Ar ages that are anomalous with respect to geologic relations. The K-Ar ages are from Cretaceous and Oligocene volcanic rocks. Modal, rapid-rock, and trace-element analyses are presented for four of the five samples dated (table 1).

ANALYTICAL METHODS

The K-Ar age determinations were made in the laboratories of the U.S. Geological Survey, Menlo Park, Calif. Argon content was determined by standard isotope-dilution methods (Dalrymple and Lanphere, 1969). Mass analyses were done with a Nier-type mass spectrometer operated in the static mode. Potassium was determined by a lithium metaborate fusion (Ingamells, 1962) flame photometer procedure with lithium as the internal standard. The fission-track ages for apatite, sphene, and zircon were determined by using the procedures outlined in Naeser and Dodge (1969), Naeser and Faul (1969), and Naeser (1976). J. L. Galey supplied sample VHNE–168N.

CRETACEOUS AND TERTIARY VOLCANIC ROCKS

Plagioclase from one specimen from a sequence of rhyodacite flows in the south-central part of the Eloy quadrangle (fig. 1) yielded a K-Ar age of 25.2±1.0 m.y. (million years) (sample E–2N, table 2). The flows now considered to be Oligocene on the basis of this age are isolated from other Tertiary rocks by Quaternary sedimentary deposits. Previously, the flows were considered to be of Pliocene or Pleistocene age. Plagioclase and whole-rock K-Ar ages of 22.2±1.1 and

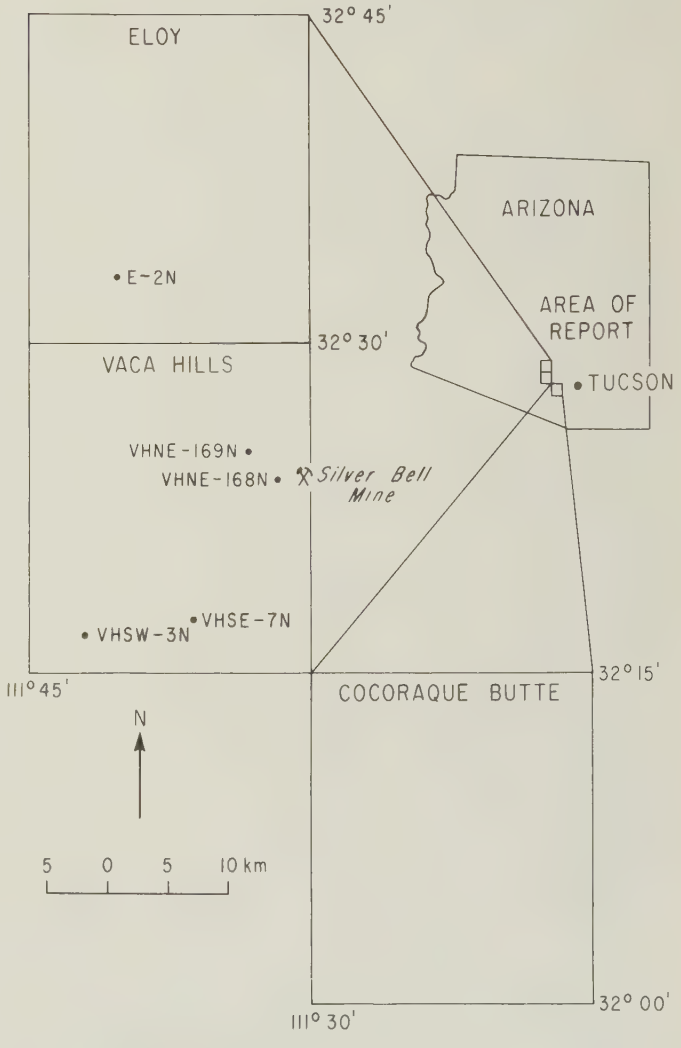

FIGURE 1.—Index showing location of study area and samples.

TABLE 1.—*Chemical analyses and norms of igneous rocks, Vaca Hills and Eloy quadrangles*

[Rapid-rock analyses (samples E-2N, VHSE-7N, and VHNE-168N) by H. Smith. X-ray fluorescence and special analyses (sample VHSW-3N) by Neil Elsheimer and M. Cremer. Fluorine analyses by R. Moore. Chlorine and sulphur analyses by L. F. Espos. Quantitative spectrographic determinations by Chris Heropoulos]

Sample no. ----	VHSW-3N	VHSE-7N	E-2N	VHNE-168N
Lab. no. -----	M126587W	M126586W	M126588W	M126589W
Chemical analyses				
SiO_2 ----------	54.88	67.0	66.6	70.1
Al_2O_3 ---------	16.98	16.0	16.0	15.7
Fe_2O_3 ---------	2.75	2.4	3.7	2.3
FeO ----------	4.73	.52	.06	.36
MgO ----------	3.98	.99	1.2	.92
CaO ----------	6.33	2.0	3.2	2.8
Na_2O ----------	3.97	3.6	4.1	4.0
K_2O ----------	3.17	3.7	4.1	3.6
H_2O+ ----------	.28	1.4	.59	.69
H_2O- ----------	.14	1.5	.46	.12
TiO_2 ----------	1.20	.42	.48	.41
P_2O_5 ----------	.68	.21	.32	.17
MnO ----------	.142	.08	.06	.04
CO_2 ----------	.15	.02	.05	.03
Cl ----------	.021	.006	.016	.003
F ----------	.048	.076	.036	.026
S ----------	<.001	<.001	.041	<.001
Total -------	99.45	99.9	101.0	101.3
Powder density-	2.72	2.54	2.53	2.60
Quantitative spectrographic determinations,[1] in parts per million				
Ti[2] ----------	0.82	0.22	0.30	0.19
Mn ----------1,100		760	600	380
Ba ----------1,300		940	1,800	620
Co ----------	25	6	12	8
Cr ----------	46	<2	22	7
Cu ----------	29	1.2	49	7
La ----------	120	72	82	<20
Ni ----------	66	<2	18	8
Pb ----------	26	24	25	22
Sc ----------	18	6	7	4
Sr ----------	520	250	510	310
V ----------	110	29	60	53
Y ----------	46	25	18	13
Zn ----------	290	150	140	94
Zr ----------	280	200	230	64
Ga ----------	29	27	27	24
Yb ----------	7	4	3	2
Norms				
Quartz --------	2.6	29.4	19.5	26.0
Orthoclase ----	18.8	22.1	24.1	21.0
Albite --------	33.5	30.7	34.4	33.5
Anorthite -----	19.3	3.0	13.2	12.3
Enstatite -----	9.9	2.5	3.0	2.3
Magnetite -----	4.0	.73	--	.10
Hematite ------	--	1.9	3.7	2.2
Ilmenite ------	2.3	.81	.25	.77
Corundum ------	--	5.0	--	.64
Apatite -------	1.6	.50	.75	.40
Other ---------	7.5	1.6	.58	.10
Total -------	99.5	98.2	99.5	99.3

[1]Results are reported to two significant figures and have an overall accuracy of ±15 percent except that they are less accurate near the limits of detection where only one digit is intended.

[2]Ti values in percent.

TABLE 1.—*Chemical analyses and norms of igneous rocks, Vaca Hills and Eloy quadrangles*—Continued

Sample descriptions:

VHSW-3N. Trachyandesite (32°16.7' N., 111°42.1' W.; NE¼NE¼SE¼ unsurveyed sec. 23, T. 13 S., R. 6 E.; Pima County, Ariz.). Dark-gray fine-grained vesicular rock composed of 7-8 percent euhedral to subhedral plagioclase ($An_{\sim 60}$), 2-3 percent subhedral olivine, 2 percent subhedral pigeonite, and <1.0 percent magnetite phenocrysts in a felty to pilotaxitic groundmass composed of 50-55 percent plagioclase laths, 20 percent olivine and pyroxene, 5-10 percent glass heavily dusted with opaque material, 5 percent magnetite, <1 percent accessory apatite. Vesicles, sometimes filled with calcite, compose 1-20 percent of the rock.

VHSE-7N. Quartz latite (32°17.7' N., 111°36.3' W.; SE¼SE¼NW¼ sec. 14, T. 13 S., R. 7 E.; Pima County, Ariz.). Grayish or yellowish-light-brown fine-grained platy-weathering flows composed of 7-12 percent euhedral plagioclase (An_{15}), 2-3 percent euhedral biotite, 1 percent anhedral to subhedral quartz and 1 percent magnetite phenocrysts in a devitrified glass groundmass with about 35 percent plagioclase microlites and 5 percent magnetite, 6.7 percent quartz recognizable in the glass. Accessory minerals are apatite and zircon.

E-2N. Rhyodacite (32°33' N., 111°40.3' W.; SW¼SW¼SW¼ sec. 17, T. 10 S., R. 7 E.; Pinal County, Ariz.). Dark-reddish-brown to gray, locally flow-banded porphyritic rock composed of 15-18 percent plagioclase (An_{52-55}) and 8-10 percent biotite phenocrysts in a pilotaxitic to hyalopilitic groundmass composed of about 10 percent plagioclase (An_{45-50}), 5 percent biotite, 50-55 percent glass, rare pyroxene, 1-2 percent hematite-magnetite. Accessory minerals are apatite and zircon. Vesicles comprise about 4 percent of the sample and are filled with unidentified isotropic and low-birefringent minerals.

VHNE-168N. Porphyritic granodiorite-quartz monzonite, locally called quartz monzonite or monzonite (32°23.87' N., 111°31.77' W.; NE¼SW¼NE¼ sec. 9, T. 12 S., R. 8 E.; Pima County, Ariz.). Light-gray to pale-flesh-colored porphyritic intrusive rock composed of 36-37 percent plagioclase (An_{35-40}), 7-10 percent potassium feldspar, 4-5 percent quartz, 2-3 percent biotite, as much as 1 percent hornblende, and 1-1½ percent magnetite phenocrysts in an aplitic groundmass (0.03-mm grain size) composed of 13-15 percent plagioclase, 15-18 percent potassium feldspar, 15-16 percent quartz, and about 1 percent combined biotite, hornblende, and magnetite. Accessory minerals are apatite (0.2 percent of rock), sphene (0.2 percent of rock), and zircon (trace).

VHNE-169N. (Not chemically analyzed. See tables 3 and 4). Leucocratic quartz monzonite, locally called alaskite (32°24.59' N., 110°33.0' W.; NW¼SW¼NE¼ sec. 5, T. 12 S., R. 8 E.; Pinal County, Ariz.). Pinkish-gray medium- to coarse-grained hypidiomorphic-granular to seriate porphyritic intrusive rock composed of 30 percent euhedral to resorbed oligoclase with albitized rims, 40 percent euhedral to anhedral orthoclase and microcline, 25 percent anhedral quartz, 2-3 percent subhedral to anhedral biotite, <1 percent subhedral to anhedral magnetite, and accessory apatite and zircon.

19.5±0.8 m.y., respectively (sample VHSW–3N, table 2), suggest that olivine-pigeonite trachyandesite flows in the Tertiary sequence exposed in the Vaca Hills in the southwest corner of the Vaca Hills quadrangle (figs. 1, 2) are late Oligocene or early Miocene in age. Shafiqullah, Lynch, and Damon (1976) obtained similar ages for trachyandesite flows in the Picacho Peak area, 50 km north-northeast of the Vaca Hills. At both of these localities the flows are underlain by red

TABLE 2.—*Potassium argon dates, sample locations and analytical data, Vaca Hills and Eloy quadrangles*

[^{40}K decay constants: $\lambda_e = 0.585 \times 10^{-10}$ year^{-1}, $\lambda_\beta = 4.72 \times 10^{-10}$ year^{-1}. Abundance ratio: $^{40}K/K = 1.19 \times 10^{-4}$ atom percent. K analyses by L. Schlocker, argon analyses by M. L. Silberman]

Rock type	Sample No.	Location	Mineral dated and size fraction	Purity[1] (percent)	Impurities (percent)	K_2O analyses (percent)	^{40}Ar (10^{-10} rad moles per gram)	^{40}Ar rad/ ^{40}Ar total	Apparent age (m.y.)
Trachy-andesite	VHSW-3N	32°16.7' N. 111°42.1' W.	Whole rock 60-100			3.17 3.19	0.923	0.51	19.5±0.8
Trachy-andesite	VHSW-3N	32°16.7' N. 111°42.1' W.	Plagioclase 60-100	98.9	0.7 glass .4 magnetite	.602 .603	.199	.29	22.2±1.1
Quartz latite	VHSE-7N	32°17.7' N. 111°36.3' W.	Biotite 60-100	99.8	.2 magnetite	8.86 8.87	9.36	.73	70.1±2.1
Quartz latite	E-2N	32°33.0' N. 111°40.3' W.	Plagioclase 60-100	99.6	.2 glass .2 magnetite	.788 .786	.295	.44	25.2±1.0

[1]Purity was determined by counting 100-500 mineral grains and estimating the percentage of impurities in binary grains.

and maroon sedimentary deposits that are probably equivalent in age to parts of the Whitetail Conglomerate, Pantano Formation, and San Manuel Formation (Bikerman and Damon, 1966; Finnell, 1968; Banks and others, 1972; Krieger, 1974; Krieger and others, 1974; Cornwall and Krieger, 1975). Trachyandesite flows that are petrographically similar to those in the Vaca Hills and Picacho Peak area occur between the two localities in and northeast of the northeastern part of Vaca Hills quadrangle (fig. 2). However, these flows are overlain by younger sedimentary deposits that are possible age equivalents of the Big Dome Formation and correlative clastic deposits (Bikerman and Damon, 1966; Banks and others, 1972; Krieger and others, 1974). Local alkali basalt flows of similar age (Jennison, 1976) are found in the same stratigraphic setting, 70 km to the northeast in the Tortolita Mountains quadrangle (Banks and others, 1977). In the Tortolita Mountains quadrangle, however, Tertiary volcanic rocks underlie the older Tertiary sedimentary deposits.

One of a sequence of quartz latite and rhyolite flows and tuffs in the south and southeastern parts of the Vaca Hills quadrangle (sample VHSE–7N, fig. 1) yielded a biotite K-Ar age of 70.1±2.1 m.y. (table 2). The flows and tuffs are petrographically very similar to flows in the upper unit of the Cretaceous Mount Lord Volcanics (fig. 3) in the north half of the quadrangle (Banks and Dockter, 1976; Dockter, 1977), and although separated by Quaternary sedimentary deposits from the Cretaceous Roskruge Volcanics to the south of the quadrangle (fig. 3)., they also are petrographically like the upper unit of the Roskruge Volcanics (Heindl, 1965; Bikerman, 1967) which have reported K-Ar ages of 66.3±3.0 to 72.6±1.5 m.y. (Bikerman, 1967). The lower units of both the Mount Lord Volcanics (Banks and Dockter, 1976; Dockter, 1977) and Roskruge Volcanics (Heindl, 1965; 74.1±1.5–74.2±1.2 m.y., Bikerman, 1967) are ash-flow tuffs that have been correlated on the basis of petrography by Hayes (1970). They also have been correlated with the Cat Mountain Rhyolite of Brown (1939) in the Tucson Mountains (65.6±2.8 and 70.3±2.3 m.y., Bikerman and Damon, 1966) by Richard and Courtright (1960), Watson (1964, 1968), Heindl (1965), and Bikerman and Damon (1966). Underlying the ash-flow tuffs of the Roskruge Volcanics is the Roadside Formation of Cretaceous age which is correlated by Heindl (1965) with the Claflin Ranch and Silver Bell Formations of Richard and Courtright (1960). The last-named formations underlie the lower ash-flow tuff unit of the Mount Lord Volcanics (fig. 3). Both the Roadside and Claflin Ranch

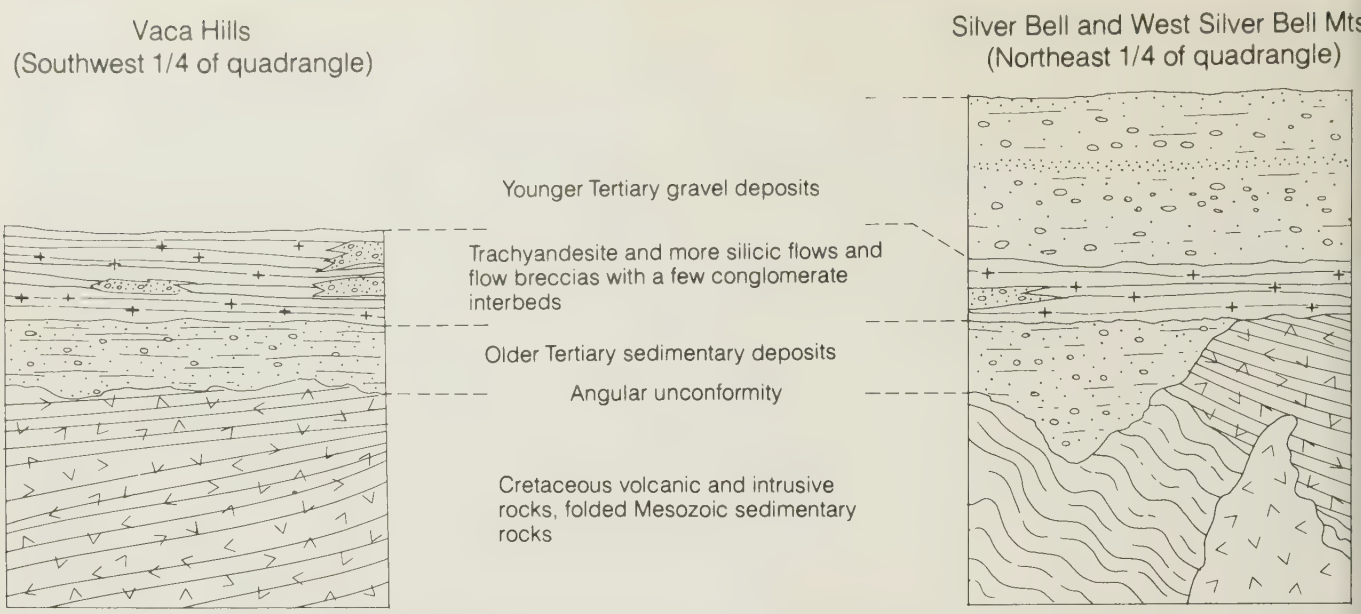
Vaca Hills
(Southwest 1/4 of quadrangle)
Silver Bell and West Silver Bell Mts
(Northeast 1/4 of quadrangle)
Younger Tertiary gravel deposits
Trachyandesite and more silicic flows and flow breccias with a few conglomerate interbeds
Older Tertiary sedimentary deposits
Angular unconformity
Cretaceous volcanic and intrusive rocks, folded Mesozoic sedimentary rocks

FIGURE 2.—Generalized stratigraphic sections of Tertiary rocks, Vaca Hills quadrangle.

Formations lie on folded Mesozoic sedimentary rocks (fig. 3). The quartz latite and rhyolite flows and tuffs represented by the sample dated here directly overlie folded Mesozoic sedimentary rocks (fig. 3). If the correlations outlined are correct, as much as 2 km of the Cretaceous section is missing in the southern part of the quadrangle compared with the Cretaceous sections 10 km to the southeast and 14 km to the north (fig. 3). The absence of these rocks is attributed to nondeposition rather than to uplift and erosion during deposition of the Cretaceous rocks because (1) the Roadside Formation and Roskruge Volcanics to the south and the Claflin Ranch and Silver Bell Formations and Mount Lord Volcanics to the north are apparently paraconformable; (2) lithologically similar tuffs, ash flows, flows, and clastic beds occur in the Claflin Ranch and Silver Bell Formations of Richard and Courtright (1960) and in the lower and upper units of the Mount Lord Volcanics (Banks and Dockter, 1976; Dockter, 1977) which suggests that the depositional environment and the volcanic and clastic source areas were similar during the deposition of all three formations; and (3) only local channel fills rather than thick clastic deposits are found between the lower and upper units of Mount Lord Volcanics (Banks and Dockter, 1976).

LARAMIDE IGNEOUS ROCKS

Mauger, Damon, and Giletti (1965) presented seven K-Ar ages for Laramide age rocks in and near the Vaca Hills quadrangle—six from intrusive rocks near the Silver Bell mine and one from the lower unit o the Mount Lord Volcanics. All their samples wer collected within 2 km of commercial ore bodies of th Silver Bell porphyry copper deposit near the easter edge of the Vaca Hills quadrangle (fig. 1). The age they reported are anomalous with respect to geologi relations (table 3), and each mineral separate had les potassium (in some, substantially less) than is possibl for the minerals dated. Mauger, Damon, and Gilett (1965) attribute the low potassium contents and dis crepancies between geologic relations and the radio metric ages to a combination of weathering, heatin by younger Laramide intrusions, and heating and al teration associated with mineralization.

Five fission-track ages were determined in an at tempt to clarify the problems raised by the age given by Mauger, Damon, and Giletti (1965). Fission track ages were determined for sphene, zircon, an apatite from the same sample site located in the por phyritic granodiorite-quartz monzonite by Mauge Damon, and Giletti (1965) and for zircon and apatit from a sample of the leucocratic quartz monzonit from a site with fresher appearing rock than the sit located by Mauger, Damon, and Giletti (1965). Th results were surprising in that, within analytical un certainty, the apatite ages from both units are identi cal and record a Miocene age (21.8 ± 4.3 and 19.2 ± 2.8 m.y., table 4). Likewise, the ages for zircon fro the two samples are analytically indistinguishabl (50.6 ± 3.2 and 54.0 ± 5.1 m.y., table 4), althoug older than the apatite ages, as expected by fission track annealing experiments and field observation

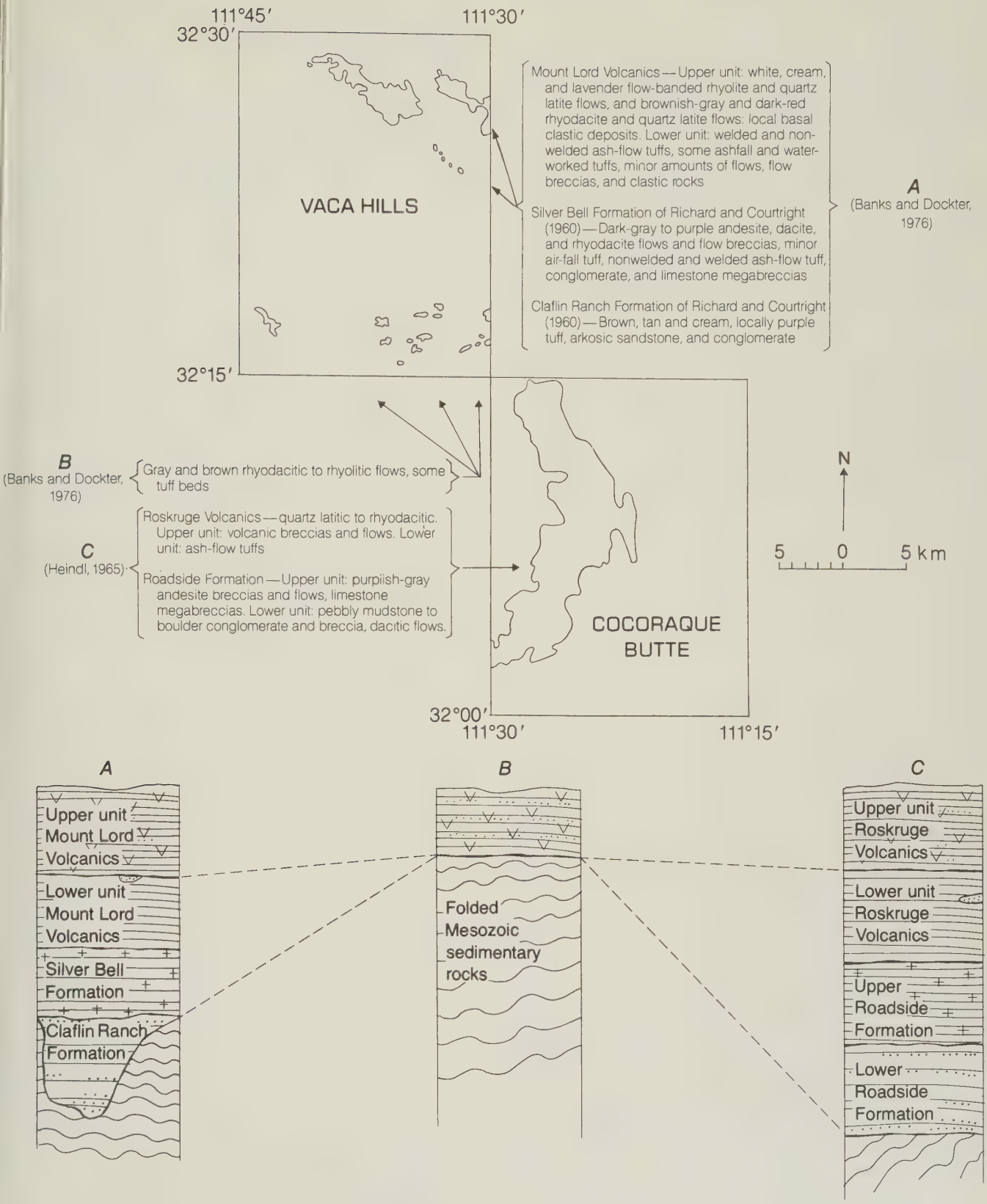
111°45′
111°30′
32°30′
VACA HILLS
Mount Lord Volcanics—Upper unit: white, cream, and lavender flow-banded rhyolite and quartz latite flows, and brownish-gray and dark-red rhyodacite and quartz latite flows: local basal clastic deposits. Lower unit: welded and non-welded ash-flow tuffs, some ashfall and water-worked tuffs, minor amounts of flows, flow breccias, and clastic rocks
Silver Bell Formation of Richard and Courtright (1960)—Dark-gray to purple andesite, dacite, and rhyodacite flows and flow breccias, minor air-fall tuff, nonwelded and welded ash-flow tuff, conglomerate, and limestone megabreccias
Claflin Ranch Formation of Richard and Courtright (1960)—Brown, tan and cream, locally purple tuff, arkosic sandstone, and conglomerate
A
(Banks and Dockter, 1976)
32°15′
B
(Banks and Dockter, 1976)
Gray and brown rhyodacitic to rhyolitic flows, some tuff beds
C
(Heindl, 1965)
Roskruge Volcanics—quartz latitic to rhyodacitic. Upper unit: volcanic breccias and flows. Lower unit: ash-flow tuffs
Roadside Formation—Upper unit: purpiish-gray andesite breccias and flows, limestone megabreccias. Lower unit: pebbly mudstone to boulder conglomerate and breccia, dacitic flows.
N
5 0 5 km
COCORAQUE BUTTE
32°00′
111°30′
111°15′
A
Upper unit
Mount Lord
Volcanics
Lower unit
Mount Lord
Volcanics
Silver Bell
Formation
Claflin Ranch
Formation
B
Folded
Mesozoic
sedimentary
rocks
C
Upper unit
Roskruge
Volcanics
Lower unit
Roskruge
Volcanics
Upper
Roadside
Formation
Lower
Roadside
Formation

FIGURE 3.—Distribution and generalized stratigraphic sections of Cretaceous volcanic and sedimentary rocks, Vaca Hills and Cocoraque Butte quadrangles.

TABLE 3.—*Simplified Laramide igneous sequence, Vaca Hills quadrangle*

Decreasing geologic age

Granodiorite and quartz monzonite porphyry (locally called monzonite or quartz monzonite porphyry). K-Ar age of 65.5±2.0 m.y. (Mauger and others, 1965)

Geologic relation unknown

Porphyritic granodiorite-quartz monzonite (locally called monzonite or quartz monzonite). K-Ar ages of 63.4±2.2 and 67.1±2.7 m.y. (Mauger and others, 1965)

Quartz latite porphyry (locally called dacite or dacite porphyry). K-Ar ages of 57.7±2.0 and 55.3±2.8 m.y. (Mauger and others, 1965)

Leucocratic quartz monzonite (locally called alaskite). K-Ar age of 64.6±2.5 m.y. (Mauger and others, 1965)

Mount Lord Volcanics. K-Ar age of 59.7±1.8 m.y. (Mauger and others, 1965)

TABLE 4.—*Fission-track analytical data*

[Fission-track determinations by C. W. Naeser. $\lambda F = 6.85 \times 10^{-17} yr^{-1}$. ( ) number of tracks counted]

Sample No.[1]	Lab No.	Mineral	P_s x10^6	P_i x10^6	ϕ x10^{15}	U (ppm)	Apparent age±2σ (m.y.)
VHNE-168N	DF-890	Apatite	0.0787 (164)	0.248 (516)	1.08	6.7	21.8±4.3
VHNE-168N	DF-891	Zircon	11.3 (2398)	15.5 (1650)	1.14	410	50.6±3.2
VHNE-168N	DF-892	Sphene	5.68 (644)	6.14 (697)	2.12	90	59.8±6.5
VHNE-169N	DF-1052	Apatite	.114 (238)	.500 (1042)	1.37	11	19.2±2.8
VHNE-169N	DF-1051	Zircon	6.39 (1331)	6.36 (662)	8.80	220	54.0±5.1

[1]See table 1 for sample descriptions.

(Fleischer and others, 1965; Naeser and Faul, 1969; Calk and Naeser, 1973; Naeser, 1976). The sphene age (59.8 ± 6.5 m.y., table 4) is older than the coexisting zircon age and younger than biotite age (PED–21–59, Mauger and others, 1965), from the same sample site (sample VHNE–168N, fig. 1), but the assigned analytical errors overlap for all three minerals. The samples yielding fission-track ages were collected a minimum of 350 m (sample VHNE–169N, fig. 1) and 500 m (sample VHNE–168N, fig. 1), respectively, from the nearest known Tertiary intrusive rocks (each a dike less than 3 m thick), and it seems unlikely that such small independent and relatively distant heat sources would have thermally affected the minerals, let alone reset the zircon and apatite in one sample to ages analytically indistinguishable from those of zircon and apatite in the second sample. It seems equally unlikely that approximately identical thermal regimes could be produced by overlying Tertiary volcanic rocks or hidden stock-size Tertiary intrusive bodies at the two fission-track sample sites, which are more than 2 km apart. It seems more likely that such thermal regimes resulted from a more regional event, perhaps directly or indirectly associated with the middle Ter tiary batholithic masses exposed to the north and eas of the area (Creasey and others, 1977; Banks, 1977) Whatever the source of the heat, the possibility that i was associated with a regional middle Tertiary ther mal event suggests that all radiometric ages for th pre-Tertiary rocks near the Silver Bell mine might b partially reset ages and offers another explanation i addition to those of Mauger, Damon, and Gilett (1965) for the discrepancies between geologic relation and the K-Ar ages.

REFERENCES CITED

Banks, N. G., 1977, A Tertiary igneous-metamorphic comple in southeastern Arizona: Geol. Soc. America Abs. wit Programs, v. 9, no. 4, p. 385.

Banks, N. G., Cornwall, H. R., Silberman, M. L., Creasey, S C., and Marvin, R. F., 1972, Chronology of intrusion an ore deposition at Ray, Arizona—Part I, K-Ar ages: Econ Geology, v. 67, p. 864–878.

Banks, N. G., and Dockter, R. D., 1976, Reconnaissance geo logic map of the Vaca Hills quadrangle, Arizona: U.S Geol. Survey Misc. Field Studies Map MF–793, scal 1:62,500.

Banks, N. G., Dockter, R. D., Briskey, J. A., Davis, G. H. Keith, S. B., Budden, R. T., Kiven, C. W., and Anderson Philip, 1977, Reconnaissance geologic map of the Tortolit Mountains quadrangle, Arizona: U.S. Geol. Survey Misc Field Studies Map MF–864, scale 1:62,500.

Bikerman, Michael, 1967, Isotopic studies in the Roskrug Mountains, Pima County, Arizona: Geol. Soc. Americ Bull., v. 78, p. 1029–1036.

Bikerman, Michael, and Damon, P. E., 1966, K/Ar chronolog of the Tucson Mountains, Pima County, Arizona: Geol Soc. America Bull., v. 77, p. 1225–1234.

Brown, W. H., 1939, Tucson Mountains, an Arizona basi range type: Geol. Soc. America Bull., v. 50, no. 5, p. 697 760.

Calk, L. C., and Naeser, C. W., 1973, The thermal effect of basalt intrusion on fission tracks in quartz monzonite Jour. Geology, v. 81, p. 189–198.

Cornwall, H. R., and Krieger, M. H., 1975, Geologic map o the Kearny quadrangle, Pinal County, Arizona: U.S Geol. Survey Geol. Quad. Map GQ–1188, scale 1:24,000.

Creasey, S. C., Banks, N. G., Ashley, R. P., and Theodore, T G., 1977, Middle Tertiary plutonism in the Santa Catalin and Tortolita Mountains, Arizona: U.S. Geol. Survey Jour. Research, v. 5, no. 6, p. 705–717.

Dalrymple, G. B., and Lanphere, M. A., 1969, Potassium-argo dating: San Francisco, Calif., W. H. Freeman and Co. 258 p.

Dockter, R. D., 1977, Mount Lord Volcanics, Pima County Arizona, *in* Changes in stratigraphic nomenclature b the U.S. Geological Survey: U.S. Geol. Survey Bull 1435–A. (In press.)

Finnell, T. L., 1968, Pantano Formation *in* Changes in strati graphic nomenclature by the U.S. Geological Survey: U.S Geol. Survey Bull. 1294–A, p. A35–A36.

Fleischer, R. L., Price, P. B., and Walker, R. M., 1965, Effect of temperature, pressure, and ionization on the formatio

and stability of fission tracks in minerals and glasses: Jour. Geophys. Research, v. 70, p. 1497–1502.

yes, P. T., 1970, Cretaceous paleogeography of southeastern Arizona and adjacent areas: U.S. Geol. Survey Prof. Paper 658–B, 42 p.

indl, L. A., 1965, Mesozoic formations in the Comobabi and Roskruge Mountains, Papago Indian Reservation, Arizona, *in* Contributions to stratigraphy: U.S. Geol. Survey Bull. 1194–H, p. H1–H15.

gamells, C. O., 1962, Determination of major and minor alkalies in silicates by differential flame spectrophotometry: Talanta, v. 9, p. 781–793.

nnison, Margo, 1976, Miocene basalt in the "Pantano Formation," Three Buttes area, Owl Head mining district, Pinal County, Arizona [abs.]: Tucson, Arizona Univ., 4th Ann. Geosci. Daze, p. 16.

ieger, M. H., 1974, Geologic map of the Crozier Peak quadrangle, Pinal County, Arizona: U.S. Geol. Survey Geol. Quad. Map GQ–1107, scale 1:24,000.

ieger, M. H., Cornwall, H. R., and Banks, N. G., 1974, Big Dome Formation and revised Tertiary stratigraphy in the Ray-San Manuel area, Arizona, *in* Changes in stratigraphic nomenclature by the U.S. Geological Survey: U.S. Geol. Survey Bull. 1394–A, p. A54–A62.

uger, R. L., Damon, P. E., and Giletti, B. J., 1965, Isotopic dating of Arizona ore deposits: Am. Inst. Mining, Metall., and Petroleum Engineers Trans., v. 232, p. 81–87.

Naeser, C. W., 1976, Fission-track dating: U.S. Geol. Survey Open-file Rept. 76–190.

Naeser, C. W., and Dodge, F. C. W., 1969, Fission-track ages of accessory minerals from granitic rocks of the central Sierra Nevada batholith, California: Geol. Soc. America Bull., v. 80, p. 2201–2212.

Naeser, C. W., and Faul, H. O., 1969, Fission-track annealing in apatite and sphene: Jour. Geophys. Research, v. 74, no. 2, p. 705–710.

Richard, K. E., and Courtright, J. H., 1960, Some Cretaceous-Tertiary relationships in southern Arizona and New Mexico: Arizona Geol. Soc. Digest, v. 3, p. 1–7.

Shafiqullah, M., Lynch, D. J., and Damon, P. E., 1976, Geology, geochronology, and geochemistry of the Picacho Peak area, Arizona: Arizona Geol. Soc. Digest, v. 10, p. 305–324.

Watson, B. N., 1964, Structure and petrology of the eastern portion of the Silver Bell Mountains, Pima County, Arizona: Tucson, Arizona Univ., Ph. D. thesis, 168 p.

——— 1968, Intrusive volcanic phenomena in southern and central Arizona, *in* Southern Arizona Guidebook III—Geol. Soc. America Cordilleran Sec., 64th Ann. Mtg., Tucson, 1968: Arizona Geol. Soc., p. 147–153.

Jour. Research U.S. Geol. Survey
Vol. 6, No. 4, July–Aug. 1978, p. 447–451

GRANITE OF ROSALIE PEAK, A PHASE OF THE 1700-MILLION-YEAR-OLD MOUNT EVANS PLUTON, FRONT RANGE, COLORADO

By BRUCE BRYANT and CARL E. HEDGE, Denver, Colo.

bstract.—The Rosalie Granite was a name applied by H. Ball in 1906 to a granite which forms a ridge between unt Evans and Mount Rosalie (renamed Rosalie Peak). The e locality originally designated for the Rosalie Granite s in a pluton (later called the Rosalie lobe) 10 kilometers theast of Rosalie Peak on Deer and Elk Creeks. The name osalie Granite" was abandoned by T. S. Lovering in 1929 ause the granite of the Rosalie lobe is actually the distinctly nger Pikes Peak Granite, only 1,030 m.y. (million years) , whereas the "Rosalie Granite" between Mount Evans l Rosalie Peak is a felsic phase of the 1,700-m.y.-old Mount ns pluton. In addition, the Rosalie Granite has more MgO l Sr and less Na_2O, F, and Rb than the Pikes Peak nite, and the two granites differ petrographically. In er to avoid confusion in correlation, the name Rosalie uld not be applied to rocks in this area. Therefore, we pose that the Rosalie lobe be renamed Lone Rock pluton l that the "Rosalie Granite" be informally referred to as granite of Rosalie Peak until it can be attached to a mal geologic rock unit.

Ball's (1906, 1908) work in the Georgetown 15-nute quadrangle about 50 km west of Denver in-ded the first detailed study of granites in the lorado Front Range (figs. 1 and 2). In that study, ll (1906) named the Rosalie Granite for exposures ween Mount Rosalie (renamed Rosalie Peak) and unt Evans, although the type locality he desig-ed for the Rosalie Granite was between Deer and k Creeks in the southeastern part of the George-n quadrangle, about 10 km from Rosalie Peak, in luton separate from the one on Rosalie Peak (fig. Lovering (1929) recognized that the granite at type locality of the Rosalie correlates with the es Peak Granite and is part of a satellitic pluton the Pikes Peak batholith. This satellitic pluton has ome known as the Rosalie lobe of the Pikes Peak holith. Consequently, the granite of the two small tons which Ball (1908) mapped as Rosalie Granite hin the Mount Evans batholith was also considered be Pikes Peak Granite. At that time Lovering 29) officially abandoned the name "Rosalie Gran-" although some workers have used it more recently

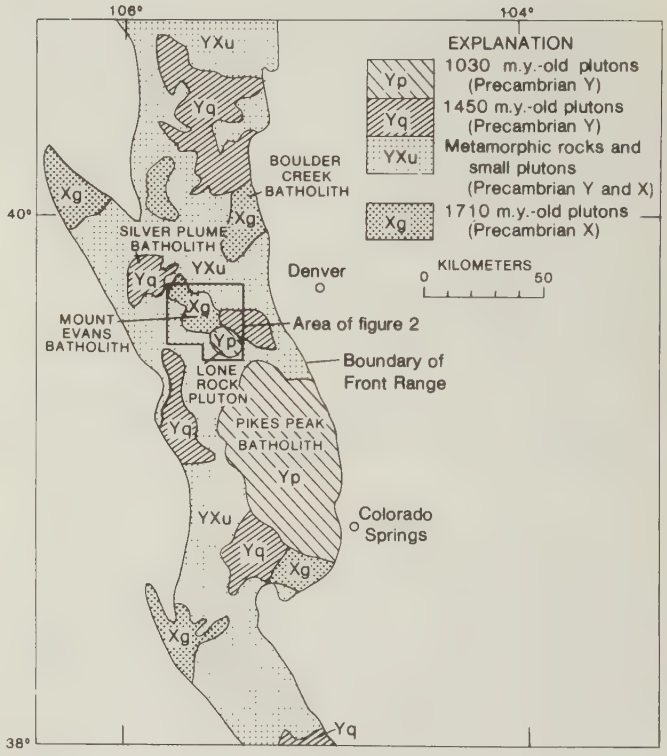

FIGURE 1.—Location of the Mount Evans area and major plutons in the Front Range, Colo.

(Puffer, 1972). In this report the informal name, granite of Rosalie Peak, will be used for the "Rosalie Granite" within the Mount Evans pluton.

Ball (1908) found several small bodies of granite that he correlated with the Silver Plume Granite cutting bodies of the granite of Rosalie Peak in the Mount Evans area, and he tentatively concluded that the Silver Plume was younger than the granite of Rosalie Peak. Because of the erroneous correlation of the granite of Rosalie Peak with the Pikes Peak Granite, it was thought for many years that the Silver Plume Granite was younger than the Pikes Peak

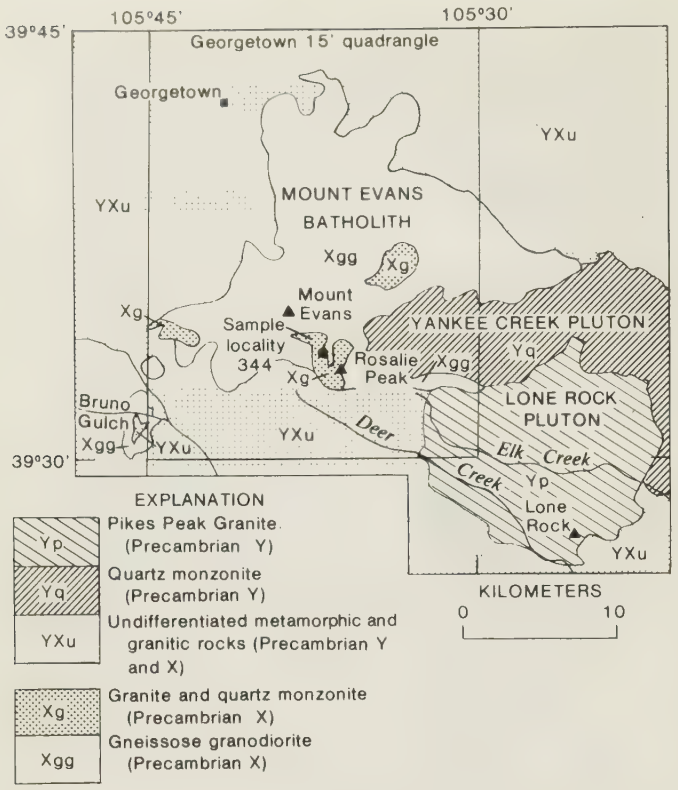

FIGURE 2.—Plutons in the Mount Evans area, outline of the Georgetown 15-minute quadrangle, and location of analyzed sample.

(Boos and Aberdeen, 1940; Lovering and Goddard, 1950; Chronic and Chronic, 1972). Adding to the confusion, Lovering (1929) observed gradations between granite in the Mount Evans area and a pluton he mapped as Pikes Peak Granite in Bruno Gulch to the southwest (Lovering, 1936). This observation led him to infer a close relationship in time of emplacement and origin. More recent work (Robinson and others, 1974) has shown that the pluton in Bruno Gulch is indeed related to the rocks on Mount Evans but is not Pikes Peak Granite. The idea that the older gneissose granitic rocks and the younger Pikes Peak Granite were genetically related led to the designation of many bodies of foliated granitic rocks in the Precambrian of central Colorado as Pikes Peak Granite (Stark and others, 1949; Stark and Barnes, 1935).

Confusion as to the relative age of the granitic rocks of the Front Range has been largely dispelled by isotopic dating during the past two decades. Three principal Precambrian intrusive suites with distinct ages are now recognized: foliated granodiorite and quartz monzonite about 1700 m.y. old (Boulder Creek Granodiorite), generally nonfoliated quartz monzoni and granite about 1430 m.y. old (Silver Plume Quar Monzonite), and a subalkalic granite 1030 m.y. o (Pikes Peak Granite). In the Georgetown qua rangle, Boulder Creek Granodiorite composes t Mount Evans batholith, Silver Plume Quartz Mo zonite composes the Yankee Creek pluton, and t Pikes Peak Granite composes the pluton (Rosa lobe) southeast of the Mount Evans batholith (fig 1 and 2; Peterman and Hedge, 1968; Hedge, 196 Stern and others, 1971; Barker and others, 1976 Yet the idea that the Silver Plume is younger th the Pikes Peak persists in some publications (Chron and Chronic, 1972). To dispel further confusi caused by the use of the name "Rosalie," we sugge that the term Rosalie lobe be abandoned and that t new name Lone Rock pluton be adopted for t satellitic pluton because it is composed of Pikes Pe Granite which is unrelated to the granite of Rosal Peak. Lone Rock is a prominent outcrop near t south margin of the pluton in NE¼ sec. 10, T. 7 R. 72 W., just north of U.S. Highway 285 in the Bail 7.5-minute quadrangle.

During reconnaissance mapping of the Denver 1° 2° quadrangle, Bryant reexamined the plutons in t Georgetown 15-minute quadrangle and noted textur differences between the granite of Rosalie Peak a the Pikes Peak Granite. The granite of Rosal Peak resembles rocks of Boulder Creek age elsewhe in the Front Range. To test this observation, Brya collected a sample of granite from one of the pluto within the Mount Evans batholith, from the headwa of a cirque northwest of Rosalie Peak, and Hed determined the Sr-isotope and Rb contents.

AGE OF THE GRANITE OF ROSALIE PEAK

The granite of Rosalie Peak has a Rb^{87}/Sr^{86} rat of 0.513 and a Sr^{87}/Sr^{86} ratio of 0.7144. Assuming initial Sr^{87}/Sr^{86} ratio of 0.7024 as given by the oth samples from the Mount Evans batholith, the grani of Rosalie Peak has an age of 1660±60 m.y. Figure shows the isochron for the Mount Evans batholit the solid dot is the sample of the granite of Rosal Peak. While the age of 1660±60 m.y. is not preci it does demonstrate that the granite of Rosalie Pe is in the same age group as other samples from t approximately 1700-m.y.-old Mount Evans batholi (fig. 3).

FIELD AND PETROGRAPHIC CHARACTERISTICS

Petrographically, as well as in age, the granite Rosalie Peak differs from the Pikes Peak Granite.

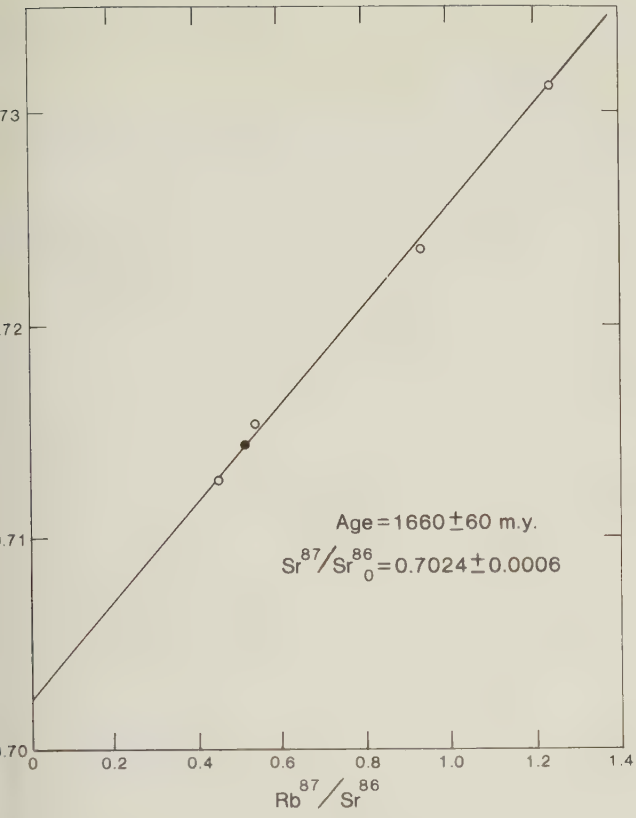

URE 3.—Isochron of Mount Evans pluton. Solid dot repre-ents sample of granite of Rosalie Peak. Open circles repre-ent other samples from the Mount Evans batholith.

BLE 1.—*Petrographic differences between granite of Rosalie Peak and the Pikes Peak Granite*

	Pikes Peak Granite	Granite of Rosalie Peak
ldspar----	Strongly perthitic--------	Weakly perthitic.
ioclase---	Albite or sodic oligoclase	Calcic oligoclase.
ite-------	Z=dark yellowish brown to dusky yellowish brown. X=dark yellowish orange, tends to occur in single subhedral grains.	Z=light to moderate brown; X=pale yellowish orange, occurs in aggregates of anhedral grains.
on--------	Euhedral----------	Euhedral to round; overgrowths.
ite-------	Rare----------	Common.
rite------	Present----------	Absent.

mmary of the petrographic differences is given in le 1.

The granite of Rosalie Peak consists of coarse-grained equigranular to porphyritic granite and quartz monzonite. The rock is gray to light pinkish gray. Microcline in this granite is pale pink to pinkish gray and imparts that color to the rock where it is especially abundant. In contrast the potassic feldspar in the Pikes Peak Granite is moderate pink in many places. Carlsbad-twinned microcline is commonly a centimeter long and is as much as 4 cm long in some phenocrysts.

Granite of Rosalie Peak, which forms a pluton northeast of Rosalie Peak, intrudes the Mount Evans batholith and contains rotated inclusions of coarse-grained granodiorite gneiss from that batholith. However, the granite also locally has a weak foliation suggesting that it was emplaced before the end of the deformation that produced the foliation in the Mount Evans batholith. The weak foliation of the granite of Rosalie Peak is formed by alined aggregates of biotite, whereas biotite in the Pikes Peak Granite commonly occurs as single grains rather than aggregates and is not alined.

In thin section the granite of Rosalie Peak consists of anhedral to subhedral, weakly perthitic microcline; anhedral to subhedral calcic oligoclase to sodic andesine with some normal zoning; anhedral quartz in large grains and aggregates interstitial to the feldspars; anhedral biotite in aggregates; and accessory myrmekite, zircon, sphene, allanite, apatite, and opaque mineral.

Some of the petrographic differences between the Pikes Peak Granite and the granite of Rosalie Peak are related to distinctive mineralogic features of the Pikes Peak in contrast to the older granitic rocks. Puffer (1972) studied the mineralogy of the Pikes Peak Granite at the north margin of the Lone Rock pluton,[1] adjacent parts of the Mount Evans pluton (Boulder Creek Granodiorite), and the Yankee Creek pluton (Silver Plume Quartz Monzonite). Chemical analyses (Puffer, 1972) of biotite from granitic rocks of the three plutons show that the biotite of the Pikes Peak Granite is very iron rich, compared to that of the older granitic rocks, and is similar to biotite from the main part of the Pikes Peak batholith (Barker and others, 1975). The high iron content accounts for the strong absorption of biotite observed in thin sections of Pikes Peak Granite. Puffer also found that potassic feldspar of the Pikes Peak Granite has a composition of Or_{60}, compared to Or_{90} for that of the older granitic rocks. The low Or content accounts for the highly perthitic nature of the potassic feldspar grains of the Pikes Peak Granite.

[1] Although he used the term "Rosalie Granite," his data are from the Pikes Peak Granite in the Lone Rock pluton.

CHEMICAL DIFFERENCES

Chemical analysis of a sample of the granite of Rosalie Peak shows that the rock is similar to the average fayalite-free granite of the Pikes Peak batholith in many respects (table 2). It also falls within the rather broad compositional range of the quartz monzonite of the Boulder Creek batholith and nearby dikes. The similarity to Pikes Peak Granite is probably fortuitous, for field observations indicate that the rocks composing the two plutons of granite of Rosalie Peak in the Mount Evans batholith vary considerably in proportions of plagioclase and potassic feldspar and, consequently, should have different contents of CaO and alkalis than the analyzed sample and the Pikes Peak Granite. The sample of granite of Rosalie Peak contained many components in quantities close to the average for fayalite-free Pikes Peak Granite, and the amounts of nearly all components fell within the ranges of values used to compute that average.

TABLE 2.—*Chemical analyses of granite of Rosalie Peak, average fayalite-free granite of the Pikes Peak batholith, and quartz monzonite of the Boulder Creek batholith and vicinity*

[Data are in percent]

	Quartz monzonite from Boulder Creek batholith[1]	Granite of Rosalie Peak[2]	Fayalite-free granite of Pikes Peak batholith[3]	
			Average	Range of values
SiO_2	62.0-75.1	72.5	72.59	
Al_2O_3	12.3-16.9	13.7	13.36	
Fe_2O_3	.34-3.2	1.2	.69	0.38-1.9
FeO	.88-2.7	2.4	1.88	1.17-2.8
MgO	.24-1.6	.74	.14	.03- .5
CaO	.92-3.2	1.4	1.18	
Na_2O	2.3 -4.4	2.6	3.31	3.08-3.7
K_2O	2.4 -6.6	5.6	5.60	
H_2O+	.0 - .80	.51	.35	
H_2O-	.02- .17	.03	.07	
TiO_2	.18- .96	.47	.28	
P_2O_5	.04- .34	.14	.05	
MnO	.04- .12	.03	.07	
CO_2	.02- .09	.09	.06	
F	.01- .12	.11	.35	.13- .67

[1] Range of analyses from 12 samples collected in and near Boulder Creek batholith (D. J. Gable, written commun., 1977).

[2] Field no. 344; lab. no. W-191-543. Rapid rock analysis by single solution method by Hezekiah Smith. Total 101.52 percent. Sample from outcrop 1,200 m N. 44° W. of summit of Rosalie Peak and 350 m south of Clear Creek-Park County line. Harris Park quadrangle, 39°34'02" N., 105°36'52" W. Rock is composed of anhedral, somewhat strained quartz as much as 6 mm in diameter; anhedral to subhedral, locally bent plagioclase (An_{30}) as much as 4 mm in diameter; anhedral weakly perthitic microcline as much as 7 mm in diameter; anhedral brown biotite as much as 2 mm long in aggregates; accessory myrmekite, zircon, allanite, sphene, apatite, and opaque minerals; and secondary chlorite from biotite.

[3] Data from Barker and others (1975, table 4). Ranges of values are reported only for components whose concentrations in the granite of Rosalie Peak differed significantly from the averages for Pikes Peak Granite.

However, the Pikes Peak Granite contains significantly more Na_2O and F and significantly less MgO than does the granite of Rosalie Peak. These differences are reflected mineralogically by the abundance of accessory fluorite, the iron-rich composition of the biotite, and the perthitic nature of the potassic feldspar in the Pikes Peak Granite.

The granite of Rosalie Peak has a lower Rb and higher Sr content than the Pikes Peak Granite, and its content of those elements is similar to that in the enclosing rocks of the Mount Evans batholith and in rocks of similar age of the Boulder Creek batholith (fig. 4).

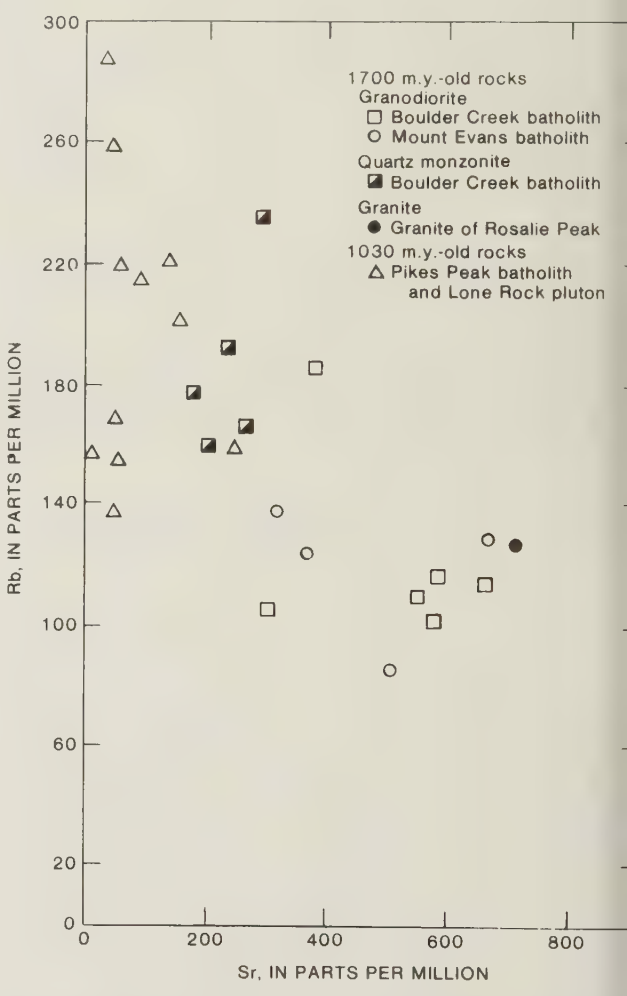

FIGURE 4.—Plot of Rb contents versus Sr contents of Pikes Peak Granite, rocks of the Mount Evans and Boulder Creek plutons, and the granite of Rosalie Peak. Data from Hedge (1969).

CONCLUSION

Field, petrographic, isotopic, and chemical data all show that the granite of Rosalie Peak (Rosal

ranite of former usage), which forms plutons with- the Mount Evans batholith, is a felsic phase of the 00-m.y.-old Mount Evans batholith and does not rrelate with the Pikes Peak Granite. In order to minate the nomenclatural confusion that has evolved er the years, the name "Rosalie" should be used ither for rocks of these plutons nor for the satellitic one Rock pluton of the 1030-m.y.-old Pikes Peak tholith southeast of the Mount Evans batholith.

REFERENCES CITED

ll, S. H., 1906, Pre-Cambrian rocks of the Georgetown quadrangle, Colorado: Am. Jour. Sci., ser. 4, v. 21, p. 371–389.

———1908, Part 1—General geology, *in* Spurr, J. E., Garrey, G. H., and Ball, S. H., Economic geology of the Georgetown quadrangle, Colorado: U.S. Geol. Survey Prof. Paper 63, p. 29–69.

arker, Fred, Wones, D. R., Sharp, W. N., and Desborough, G. A., 1975, The Pikes Peak batholith, Colorado Front Range and a model for the origin of the gabbro-anorthosite-syenite-potassic granite suite: Precambrian Research, v. 2, p. 97–160.

arker, Fred, Hedge, C. E., Millard, H. T., Jr., and O'Neill, J. R., 1976, Pikes Peak Batholith—Geochemistry of some minor elements and isotopes, and implications for magma genesis, *in* Epis, R. C., and Weimer, R. J., eds., Studies in Colorado field geology: Colorado School Mines Prof. Contr. 8, p. 44–56.

oos, M. F., and Aberdeen, E. J., 1940, Granites of the Front Range, Colorado—The Indian Creek plutons: Geol. Soc. American Bull., v. 51, no. 5, p. 695–730.

Chronic, John, and Chronic, Halka, 1972, Prairie, peak, and plateau—A guide to the geology of Colorado: Colorado Geol. Survey Bull. 32, 126 p.

Hedge, C. E., 1969, A petrogenetic and geochronologic study of migmatites in the central Front Range: Colorado School Mines, Ph. D. thesis, 158 p.

Lovering, T. S., 1929, Geologic history of the Front Range, Colorado: Colorado Sci. Soc. Proc., v. 12, no. 4, p. 59–111.

———1936, Geology and ore deposits of the Montezuma quadrangle, Colorado: U.S. Geol. Survey Prof. Paper 178, 119 p.

Lovering, T. S., and Goddard, E. N., 1950, Geology and ore deposits of the Front Range, Colorado: U.S. Geol. Survey Prof. Paper 233, 319 p.

Peterman, Z. E., and Hedge, C. E., 1968, Chronology of Precambrian events in the Front Range, Colorado: Canadian Jour. Earth Sci., v. 5, p. 749–756.

Puffer, J. H., 1972, Iron-bearing minerals as indicators of intensive variables pertaining to granitic rocks from the Pegmatite Points area, Colorado: Am. Jour. Sci., v. 272, p. 273–289.

Robinson, C. S., Warner, L. A., and Wahlstrom, E. E., 1974, General geology of the Harold D. Roberts tunnel, Colorado: U.S. Geol. Survey Prof. Paper 831–B, 48 p.

Stark, J. T., and Barnes, F. F., 1935, Geology of the Sawatch Range, Colorado: Colorado Sci. Soc. Proc., v. 13, no. 8, p. 467–479.

Stark, J. T., Johnson, J. H., Behre, C. H., Jr., Powers, W. E., Howland, A. L., Gould, D. B., and others, 1949, Geology and origin of South Park, Colorado: Geol. Soc. America Mem. 33, 188 p.

Stern, T. W., Phair, George, and Newell, M. F., 1971, Boulder Creek Batholith, Colorado—Part II, Isotopic age of emplacement and morphology of zircon: Geol. Soc. America Bull., v. 82, p. 1615–1634.

Jour. Research U.S. Geol. Survey
Vol. 6, No. 4, July–Aug. 1978, p. 453–457

COMENDITE (PERALKALINE RHYOLITE) AND BASALT IN THE MITU GROUP, PERU: EVIDENCE FOR PERMIAN-TRIASSIC LITHOSPHERIC EXTENSION IN THE CENTRAL ANDES

By DONALD C. NOBLE,[1] MILES L. SILBERMAN, FRANÇOIS MEGARD,[2] AND HARRY R. BOWMAN,[3]

Houghton, Mich., Menlo Park, Calif., Montpellier, France, and Berkeley, Calif.

Abstract.—The Mitu Group consists of generally coarse astic strata and volcanic rock of Permian and (or) Triassic ge filling elongate basins that parallel the general structural end of the Peruvian Andes. Volcanic rocks of the Mitu roup include peralkaline and nonperalkaline rhyolite and balkaline basalt. To our knowledge, the peralkaline rhyolites re the first of this rock type reported from South America. he presence of appreciable volumes of peralkaline rhyolite nd basalt supports the interpretation that the Mitu Group as deposited in major graben structures that resulted from thospheric extension produced by rifting or possible back-rc extension.

The central Andes have a long and involved tectonic istory. Mesozoic tectonism is relatively well known, nd the basic features of Cenozoic deformation and plift presently are being worked out. Western South merica also underwent major deformation prior to ne Mesozoic, a fact long known but not generally ppreciated.

Precambrian rocks are exposed in various places in eru and northern Argentina (Dalmayrac and others, 971). A major pulse of deformation affected virtually ne entire central Andes at the close of the Devonian Mégard and others, 1971; Helwig, 1972, 1973), and is not unreasonable to suspect the presence of one r more early Paleozoic episodes. Minor vertical move-ent appears to have taken place in Peru during the Iississippian (Mégard and others, 1971).

Southern Peru appears to have undergone compres-ve deformation during the early Permian (Mégard nd others, 1971; Audebaud and Laubacher, 1969). lsewhere, late Paleozoic tectonism appears to have een largely extensional, with the apparent formation f major graben structures oriented parallel to the eneral structural grain of the region (Mégard, 1973; ewell and others, 1953).

Redbeds, conglomerates, and volcanic rocks associated with the graben structures comprise the Mitu Group (fig. 1), which postdates Lower Permian marine strata of Late Triassic and locally Middle Triassic (Ladinian) age (Levin, 1974). Stewart, Evernden, and Snelling (1974) report a potassium-argon age of 251 million years obtained on a pluton that intrudes the Mitu Group in central Peru. A rubidium-strontium isochron age of 238 ± 16 m.y. has been obtained for the batholith of La Merced in central Peru (François Mégard, unpub. data, 1976). This pluton intrudes

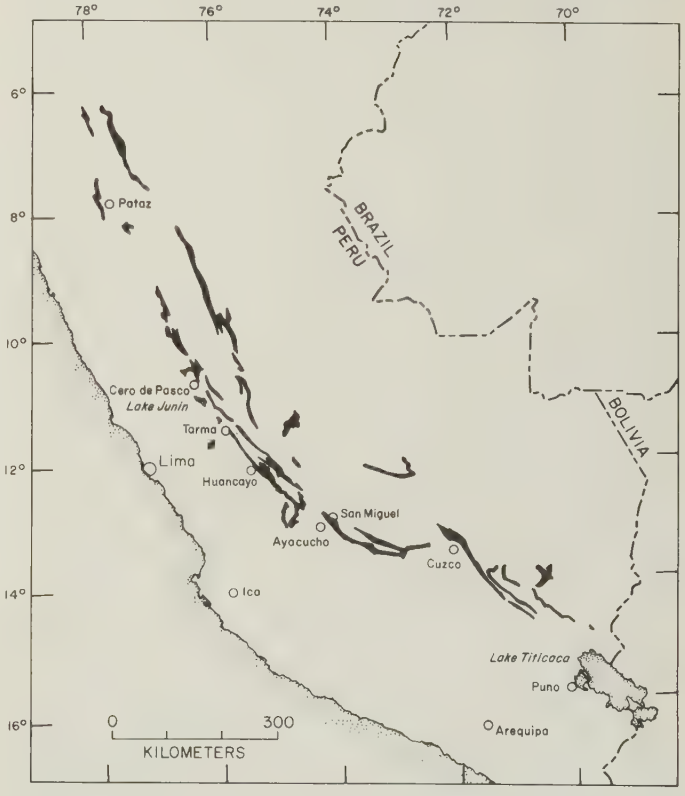

FIGURE 1.—Map of Peru showing distribution of rocks of Mitu Group and correlative units (from Dalmayrac and others, 1971) and locations referred to in text.

[1] Michigan Technological University.
[2] Université des Sciences et Techniques du Languedoc.
[3] Lawrence Berkeley Laboratory.

Lower Permian marine rocks and is unconformably overlain by rocks of the upper part of the Mitu Group and by Ladinian marine strata. Both radiometric ages suggest that an appreciable part of the Mitu Group is of Permian age.

Although the volcanic rocks of the Mitu Group are voluminous, areally extensive, and, in many places, remarkably well exposed and preserved, they are virtually unstudied. This paper reports on preliminary field, petrographic, and chemical studies which demonstrate that certain volcanic rocks of the Mitu Group are of the type commonly erupted in regions undergoing active extension.

Acknowledgments.—Noble was supported by National Science Foundation grant GS–40421 and by a grant from the Petroleum Research Fund administered by the American Chemical Society. Mégard was supported by the Centre National de la Recherche Scientifique, and his work greatly facilitated by the Servico Geologico del Peru and L'Institut Français d'Etudes Andines. The analytical work at the Lawrence Berkeley Laboratory was supported by the U.S. Atomic Energy Commission. We thank James Helwig, P. E. Isaacson, and E. M. Moores for helpful comments.

VOLCANIC ROCKS OF THE MITU GROUP

Volcanic rocks of the Mitu Group are well exposed in the mountain range northeast of Ayacucho, in central Peru (fig. 1), where they have been mapped by Mégard and Paredes (Mégard, 1973) and studied in the field by Noble. The volcanic rocks, which have a total preserved thickness of 1500 to 2000 m, consist of roughly equal amounts of silicic lava and tuff and olivine-bearing basalt. The volcanic rocks overlie clastic strata of the Mitu Group, which in turn unconformably overlie rocks of the Copacabana Group. The Mitu is subhorizontal in the central part of the range and dips moderately to the southwest along the western flank of the range (Mégard, 1973).

The volcanic rocks are well preserved. For this reason, a potassium-argon age determination was made on a dense, holocrystalline specimen of comendite lava to rule out the possibility that the rocks are of Tertiary age. The age of 131 m.y. (table 1) indicates that the rocks are definitely pre-Cenozoic. The age, however, represents a minimum age for the lava because the Mitu Group was affected by low-grade metamorphism during the Mesozoic (Mégard, 1968, 1973; Stewart and others, 1974; and petrologic evidence presented below).

Many outcrops of silicic lava show the coarse granophyric texture typical of crystallized peralkaline

TABLE 1.—*Analytical data for potassiumargon age determination on comendite sample AYA–PAN*

[Argon analyses by M. L. Silberman using standard isotope dilution procedures; potassium analyses by L. F. Espos using X-ray fluorescence methods. Constants: $^{40}K\lambda\varepsilon+^{40}K\lambda\varepsilon'=0.581\times10^{-10}$/yr; $^{40}K\lambda\beta=4.962\times10^{-10}$/yr. Atomic abundance $^{40}K=1.167\times10^{-4}$ mole/mole.]

K_2O (wt.%)	Radiogenic Ar (mole/gm x 10^{-10})	Radiogenic Ar (percent)	Age (m.y.)
3.80	7.079	98	
3.72	7.621	94	
3.76 (Average)	7.350 (Average)		131±5

12 outcrops, most along the road between Ayacucho and San Miguel (fig. 1), reveal micrographic intergrowths of quartz and alkali feldspar. The feldspar is clouded with fine-grained white mica probably formed during the low-grade metamorphism. Phenocrysts of quartz and alkali feldspar are present in some

TABLE 2.—*Major-element analyses of comendites and a basalt*

Specimen	AYA-PAN		Tower	AYA-10A
Type of analysis	A	B	C	D
SiO_2	76.7	--	75.3	49.8
Al_2O_3	11.6	11.1	12.2	16.3
Fe as FeO	2.68	2.52	3.8	11.6
MgO	0.13	--	0.21	4.92
CaO	0.125	--	0.31	9.8
Na_2O	3.5	3.28	4.5	2.62
K_2O	4.12	--	3.4	0.98
H_2O	--	--	--	1.0
TiO_2	0.13	0.10	0.23	2.0
MnO	0.050	0.063	--	0.19
Total	99.9		100.0	99.2

A. Average of three determinations by X-ray fluorescence methods (Hebert and Street, 1974).
B. By neutron activation methods similar to those described by Perlman and Asaro (1969).
C. By nondestructive X-ray fluorescence methods; W. Kemp, analyst.
D. By atomic absorption methods, D. Bowden, analyst. S = ≤0.005 weight percent.
Sample locations:
AYA-PAN, 13°00.4' S., 74°06.0' W.
Tower, 12°58.7' S., 74°06.2' W.
AYA-10A, 12°57.2' S., 74°01.4' W.

ABLE 3.—*Minor-element analyses, in parts per million, of peralkaline rhyolite AYA–PAN*

nalysis A by neutron activation methods similar to those of Perlman and Asaro (1969); analysis B by semiquantitative (six-step) optical emission spectrographic methods similar to those of Myers, Havens, and Dunton (1961), Chris Heropoulos, analyst, except values in parentheses by X-ray fluorescence methods, L. F. Espos, analyst;—, not determined; N, not detected.]

ement	A	B
----------	3.3	--
----------	167	(148)
----------	80	70
----------	--	20(48)
----------	--	30
----------	44.4	50
----------	116	150
----------	34	N
----------	7.5	N
----------	0.064	N
----------	2.2	N
----------	14.0	N
----------	9.8	10
----------	1.40	--
----------	--	100
----------	30	N
----------	6.0	N
----------	--	700
----------	17	N
----------	--	30
----------	2.64	N
----------	--	3
----------	0.40	N
----------	3	N
----------	1.78	N
----------	--	10
----------	2	2
----------	51	N
----------	--	15
----------	--	3
----------	19	--
----------	0.6	--

nyolite. Thin sections of peralkaline rhyolites from f the rocks. Aggregates of very fine grained iron xides are texturally akin to those that replace iginal poikilitic grains and granular aggregates of roundmass sodic amphibole in comendites and pantelrites that have cooled under oxidizing conditions.

Chemical analyses have been made on two specimens of comendite (samples AYA–PAN and Tower, tables 2 and 3). An original peralkaline chemistry is shown by a number of major- and minor-element characteristics. The most distinctive chemical feature of peralkaline silicic rocks is their unusually high iron content (Noble, 1968; Macdonald, 1975). The comendites from the Mitu Group are very highly differentiated, as shown by the very low contents of Ca, Mg, Sr, Ba, Eu, Co, Cr, and Ni. Nonperalkaline rhyolites with comparably high SiO_2 and depleted alkaline earth contents have total iron contents of less than 1.5 weight percent and typically less than 1 weight percent, whereas the rhyolites from the Mitu Group have total iron as FeO contents of 2.6 and 3.8 weight percent. Peralkaline rhyolites also have high to very high concentrations of zirconium, hafnium, yttrium, and the heavy rare earths (Ewart and others, 1968; Noble and others, 1969; Macdonald and Bailey, 1973), elements that are markedly depleted in very highly differentiated nonperalkaline rhyolites. The high contents of iron, zirconium, hafnium, yttrium, and the heavy rare earths result from the presence of excess alkali in the magma, which stabilizes iron and large highly charged cations within the melt (Dietrich, 1968; Noble, 1968; Noble and Haffty, 1969; Melchior-Larsen and Steenfelt, 1974). Peralkaline silicic melts have high Fe^{+2}/Fe^{+3} ratios and are characterized by low oxygen fugacities (Noble, 1968; Nicholls and Carmichael, 1969). Very extensive feldspar separation and low oxygen fugacity during intratelluric crystallization are demonstrated by the extreme europium depletion of specimen AYA–PAN (table 3); the rock possesses only 2 percent of the europium that would be present in an unfractionated specimen having identical contents of the other rare earth elements. Similar depletion of europium has been found for a number of peralkaline rhyolites from the Western United States (D. C. Noble, unpub. data, 1976). Appreciable, although not as extreme, depletion of europium also has been reported in peralkaline rhyolites from New Zealand (Ewart and others, 1968) and Pantelleria (Villari, 1975). Also highly suggestive of original peralkaline chemistry are the somewhat low Al_2O_3 and high TiO_2 contents of the rocks (see Noble, 1968; Macdonald and Bailey, 1973).

Despite the strong indications of peralkaline chemistry, the rocks do not presently have an atomic excess of alkali over aluminum, the chemical definition of peralkalinity. Loss of sodium during primary crystallization is a ubiquitous feature of peralkaline silicic igneous rocks (Noble, 1968; 1970; Macdonald and Bailey, 1973). Appreciable amounts of sodium thus almost certainly were lost during primary granophyric

crystallization. Potassium and perhaps additional sodium appear to have been lost later, probably during metamorphism (compare Anderson, 1968); deuteric alteration producing fine-grained white micas does not occur during natural primary crystallization of peralkaline silicic magmas. Experience with Cenozoic volcanic rocks suggests that small amounts of magnesium, calcium, and strontium may have been added by groundwater subsequent to eruption.

Peralkaline rhyolite is exposed over an area of at least 50 km^2 between Ayacucho and San Miguel, and reconnaissance observations strongly suggest that similar rocks are present over a much larger area. A belt of rocks of the Mitu Group extends for almost 200 km from north of Ayacucho southeastward towards Cuzco (fig. 1), and much of this belt may consist of originally peralkaline rhyolite.

Silicic tuffs of the Mitu Group exposed east of Lake Junin, near Tarma, and east of Huancayo (fig. 1) have been examined by Noble. These rocks contain appreciable amounts of phenocrystic biotite, a mineral that is rare in peralkaline rhyolite. It thus appears that part of the volcanic rocks of the Mitu Group consists of nonperalkaline rhyolite.

A chemical analysis of a specimen of olivine-bearing basalt (sample AYA–10A, table 2) is very similar to those of many moderately potassic, somewhat differentiated, subalkaline basalts commonly erupted in continental areas undergoing crustal extension, such as the Western United States (for example, Wright and others, 1973; Gunn and Watkins, 1970; Noble and others, 1973).

DISCUSSION

Peralkaline silicic volcanic rocks typically are erupted in regions undergoing crustal extension. These include spreading centers in oceanic regions and areas of continental rifting and back-arc extension (for example, Barth, 1945; LeBas, 1971; Baker and others, 1972; Noble and Parker, 1975). In such settings, peralkaline rhyolites are commonly associated with appreciable volumes of nonperalkaline silicic volcanic rock, and the presence of nonperalkaline rhyolite in the Mitu Group does not contradict the tectonic implications of the peralkaline types.

Available geologic and geochemical evidence strongly suggests that peralkaline silicic rocks are produced by the protracted fractionation of originally hypersthene-normative basaltic magma. The parental basaltic magma may have a considerable range in the contents of large-ion lithophile elements (for example, Korringa and Noble, 1972; Noble and Christiansen, 1974). The presence of peralkaline rhyolite thus implies the generation and presence at relatively shallow levels of large volumes of mafic magma, a conclusion supported by the voluminous basalts associated with the peralkaline rhyolites.

The tectonic regime responsible for crustal extension and basalt-related volcanism in Peru during latest Paleozoic and (or) earliest Mesozoic time is unclear. Scattered data (for example, Burgl, 1967; Radelli, 1962; Pushcharovskiy and Arkhipov, 1972) suggest that extension and silicic alkaline volcanism occurred elsewhere along the west coast of South America at about the same time. Thus, extension and related volcanism could be ascribed to rifting associated with the onset of major crustal fragmentation at the end of the Paleozoic. Both tectonic (Mégard and others, 1971; Miller, 1971) and paleogeographic (Isaacson, 1975) arguments favor the existence of a western extracontinental land mass during the Devonian. This inferred land mass perhaps may be explained by alternative reconstructions (Le Pichon and Fox, 1971; Walper and Rowett, 1972; Vine, 1973; Van der Voo and others, 1976) that place northwestern South America in contact with southeastern North America in the Permian. Such a land mass may have separated during the latest Paleozoic along a rift line approximately parallel to the present Peru-Chile trench.

The presence of a magmatic arc parallel to the axis of the Peru-Chile trench (Mégard, 1973; James, 1971) shows unquestionably that by late Triassic time subduction was occurring along the western coast of central South America. The onset of subduction probably followed an episode of rifting, as discussed above. However, if, as suggested by Helwig (1972, 1973), subduction occurred along the western coast of central South America during Mitu time, then the faulting and peralkaline volcanism could perhaps be interpreted as an intracontinental analog of back-arc extension.

REFERENCES CITED

Anderson, C. A., 1968, metamorphosed Precambrian silicic volcanic rocks in central Arizona, *in* Coats, R. R., Hay, R. L., and Anderson, C. A., eds., Studies in volcanology: Geol. Soc. America Mem. 116, p. 9–44.

Audebaud, E., and Laubacher, G., 1969, Sur une discordance tartihercynienne dans la Cordillère Orientale du Sud du Pérou: Comptes Rendus Acad. Sci., v. 269, p. 2163–2166.

Baker, B. H., Mohr, P. A., and Williams, L. A. J., 1972, Geology of the eastern rift system of Africa: Geol. Soc. America Spec. Paper 136, 67 p.

Barth, T. F. W., 1945, Studies on the igneous rock complex of the Oslo region, Volume 2.—Systematic petrography of

the plutonic rocks: Skr. norske Videnskap-Akad. Mat.-naturv. Kl. 1944, v. 2, no. 9, 104 p.

Irgl, Hans, 1967, The orogenesis in the Andean system of Columbia: Tectonophysics, v. 4, p. 429–443.

Almayrac, B., Laubacher, G., Marocco, R. Martinez, Cl., Mégard, F., Paredes, J., and Tomasi, P., 1971, Carte géologique des terrains Paléozoiques et Precambriens du Pérou et de Bolivie: Cahiers Organization de la Recherche Sci. des Terrares d'Outre-Mer, ser. Geol., v. 3, no. 1.

Betrich, R. V., 1968, Behaviour of zirconium in certain artificial magmas under diverse P-T conditions: Lithos, v. 1, p. 20–29.

Evart, Anthony, Taylor, S. R., and Capp, A. C., 1968, Geochemistry of the pantellerites of Mayor Island, New Zealand: Contr. Mineralogy and Petrology, v. 17, p. 116–140.

Hinn, B. M., and Watkins, N. D., 1970, Geochemistry of the Steens Mountain Basalts, Oregon: Geol. Soc. America Bull., v. 81, p. 1497–1516.

Hebert, A. J., and Street, Kenneth, Jr., 1974, Nondispersive soft X-ray fluorescence spectrometer for the quantitative analysis of the major elements in rocks and minerals: Anal. Chemistry, v. 46, p. 203–207.

Helwig, James, 1972, Late Paleozoic stratigraphy and tectonics of the central Andes, *in* International Symposium on the Carboniferous and Permain Systems in South America: Annales Academia Brasileria de Ciencias, v. 44 (supp.), p. 161–171.

——1973, Plate tectonic model for the evolution of the central Andes: Discussion: Geol. Soc. America Bull., v. 84, p. 1493–1496.

Isacson, P. E., 1975, Evidence for a western extracontinental land source during the Devonian Period in the central Andes: Geol. Soc. America Bull., v. 86, p. 39–46.

James, D. E., 1971, Plate tectonic model for the evolution of the central Andes: Geol. Soc. America Bull., v. 82, p. 3325–3346.

Korringa, M. K., and Noble, D. C., 1972, Genetic significance of chemical, isotopic, and petrographic features of some peralkaline salic rocks from the island of Pantelleria: Earth and Planetary Sci. Letters, v. 17, p. 258–262.

LeBas, M. J., 1971, Per-alkaline volcanism, crustal swelling, and rifting: Nature Phys. Sci., v. 230, p. 85–87.

Le Pichon, Xavier, and Fox, P. J., 1971, Marginal offsets, fracture zones, and the early opening of the North Atlantic: Jour. Geophys. Research, v. 76, p. 6294–6308.

Levin, P., 1974, Die Pucará-Sedimente im Chanchamayo-Gebiet in Ost-Peru: Geol. Rundschau, v. 63, 345–356.

Macdonald Ray, 1975, Nomenclature and petrochemistry of the peralkaline over-saturated extrusive rocks: Bull. Volcanologique, v. 38, p. 498–516.

Macdonald, Ray, and Bailey, D. K., 1973, The chemistry of peralkaline over-saturated obsidians: U.S. Geol. Survey Prof. Paper 440–N–1, p. N1–N37.

Mégard, François, 1968, Geología del cuadrangulo de Huancayo: Servicio Geologia y Mineria del Perú, Bol. 18, 123 p.

——1973, Étude géologique d'une transversale des Andes au niveau du Pérou central: Academie de Montpellier, Dr. Sci. Thèse, 263 p.

Mégard, François, Dalmayrac, B. Laubacher, G., Marocco, R., Martinez, C., Paredes, J., and Tomasi, P., 1971, La chaine Hercynienne au Pérou et en Bolivie premiers résultats: Cahiers Office de la Recherche Scientifique et Technique Outre-Mer, ser. Geol., v. 3, no. 1, p. 5–44.

Melchior-Larsen, L., and Steenfelt, A., 1974, Alkali loss and retention in an iron-rich peralkaline dyke from the Gardar province, South Greenland: Lithos, v. 7, p. 81–90.

Miller, H., 1971, Das problem des hypothetischen "Pazifischen Kontinentes" gesehen von der Chilenischen Pazifikkuste: Geol. Rundschau, v. 60, p. 927–938.

Myers, A. T., Havens, R. G., and Dunton, P. J., 1961, A spectrochemical method for the semiquantitative analysis of rocks, minerals, and ores: U.S. Geol. Survey Bull. 1084–I, p. I207–I229.

Newell, N. D., Chronic, J., and Roberts, T., 1953, Upper Paleozoic of Peru: Geol. Soc. America Mem. 58, 276 p.

Nicholls, John, and Carmichael, I. S. E., 1969, Peralkaline acid liquids—A petrological study: Contr. Mineralogy and Petrology, v. 20, p. 268–294.

Noble, D. C., 1968, Systematic variation of major elements in comendite and pantellerite glasses: Earth and Planetary Sci. Letters, v. 4, p. 167–172.

——1970, Loss of sodium from crystallized comendite welded tuffs of the Miocene Grouse Canyon Member of the Belted Range Tuff, Nevada: Geol. Soc. America Bull., v. 81, p. 2677–2687.

Noble, D. C., and Christiansen, R. L., 1974, Black Mountain volcanic center, *in* Guidebook to the geology of four Tertiary volcanic centers in central Nevada: Nevada Bur. Mines and Geol. Rept. 19, p. 27–34.

Noble, D. C., and Haffty, Joseph, 1969, Minor-element and revised major-element contents of some Mediterranean pantellerites and comendites: Jour. Petrology, v. 10, p. 502–509.

Noble, D. C. Haffty, Joseph, and Hedge, C. E., 1969, Strontium and magnesium contents of some natural peralkaline silicic glasses and their petrogenetic significance: Am. Jour. Sci., v. 267, p. 598–608.

Noble, D. C., Hedge, C. E., McKee, E. H., and Korringa, M. K., 1973, Reconnaissance study of the strontium isotopic composition of Cenozoic volcanic rocks in the northwestern Great Basin: Geol. Soc. America Bull., v. 84, p. 1393–1406.

Noble, D. C., and Parker, D. F., 1975, Peralkaline silicic volcanic rocks of the western United States: Bull. Volcanologique, v. 38, p. 803–827.

Perlman, I., and Asaro, F., 1969, Pottery analysis by neutron activation: Archaeometry, v. 11, p. 21–52.

Pushcharovskiy, Y. M., and Arkhipov, I. C., 1972, Tectonic aspects of the Chilean Andes: Geotectonics, 1972, p. 44–52.

Radelli, L., 1962, Les formations éruptives hercyniennes de las Cordillère Oriental de Columbia: Geol. Colombia, v. 3, p. 99–124.

Stewart, J. W., Evernden, J. F., and Snelling, N. J., 1974, Age determinations from Andean Peru—A reconnaissance survey: Geol. Soc. America Bull., v. 85, p. 1107–1116.

Van der Voo, R., Mauk, F. J., and French, R. B., 1976, Permian-Triassic continental configurations and the origin of the Gulf of Mexico: Geology, v. 4, p. 177–180.

Villari, L., 1975, The Island of Pantelleria: Bull. Volcanologique, v. 38, p. 680–724.

Vine, F. J., 1973, Organic diversity, paleomagnetism, and Permian paleogeography, *in* Hughes, N. F., ed., Organisms and continents through time: Spec. Papers Palaeontology, No. 12, p. 61–77.

Walper, J. L., and Rowett, C. L., 1972, Plate tectonics and the origin of the Caribbean and the Gulf of Mexico: Gulf Coast Assoc. Soc. Trans., 22nd Ann. Conf. Proc., p. 105–116.

Wright, T. L., Grolier, M. J., and Swanson, D. A., 1973, Chemical variations related to the stratigraphy of the Columbia River Basalt: Geol. Soc. America Bull., v. 84, p. 371–386.

Jour. Research U.S. Geol. Survey
Vol. 6, No. 4, July–Aug. 1978, p. 459–465

FUSION OF GRANODIORITE BY BASALT, CENTRAL SIERRA NEVADA

By F. C. W. DODGE and L. C. CALK, Menlo Park, Calif.

Abstract.—A trachybasalt plug, 100 m in diameter, has partially fused inclusions and wallrock of porphyritic granodiorite near Tuolumne Meadows, Yosemite National Park, Calif. Granodiorite surrounding the plug was altered within distances of about 3.5 m. Within this distance, (1) trace amounts of glass occur along fractures and grain boundaries, (2) biotite has been altered from dark olive to dark reddish brown and contains bands of fine reddish iron oxide grains, and (3) optic axial angles of potassium feldspar decrease toward the contact.

As much as 20 volume percent of glass occurs in the granodiorite in a reentrant and in inclusions within the plug. Detailed study of two partially fused samples shows that, relative to unfused granodiorite, SiO_2 is clearly depleted in both samples, whereas K_2O is depleted in one but not the other. Total iron, Al_2O_3, MgO, Na_2O, and H_2O show apparent increases in both samples; other constituents show no significant changes. Chemical analyses suggest that much original material was lost from the partially fused rocks, probably by mass migration of melt rather than by chemical diffusion. The composition of glasses now present in the partially fused rocks was dominated by melting of quartz and feldspars, whereas the composition of the early-formed "lost" melt was strongly influenced by subsolidus reaction and subsequent melting of biotite.

The effects of thermal metamorphism caused by intrusion of mafic magmas into surrounding quartzofeldspathic rocks have been documented by numerous investigations, summarized by Wyllie (1961). Two localities have been described where mafic magmas have intruded and partially fused granitic rocks of the Sierra Nevada batholith, one near Bishop, Calif. (Knopf, 1938; Bateman, 1965), the other north of Mono Lake, Calif. (Al-Rawi and Carmichael, 1967). We have studied a third locality in the batholith, near the northwestern edge of Tuolumne Meadows on the south side of the Tuolumne River (lat 37° 54.0′ N., long 119° 24.5′ W.) in Yosemite National Park, Calif. Prior to our study, Calk and Naeser (1973) determined maximum reheating temperatures in the granitic rocks surrounding the mafic intrusion at this locality by analyses of fission-track retention in accessory minerals.

GEOLOGIC SETTING AND REHEATING TEMPERATURES

The trachybasalt plug at the Tuolumne River locality is irregularly shaped and averages about 100 m across (fig. 1). The contact between the plug and enclosing granodiorite is poorly exposed except along the northeastern edge of the plug, but it can generally be located within 1 m. The angularity of the contact suggests that the configuration of the plug was controlled by joints in the granodiorite. The age of the trachybasalt intrusion, as determined from the average of fission-track ages of apatite and sphene from closely associated granodiorite samples, is 9.4 ± 0.2 million years (Calk and Naeser, 1973). A trachyandesite flow at Rancheria Mountain 18 km northwest of the plug has been dated at 8.9±0.2 m.y. by the potassium-argon technique (Dalrymple, 1963). The near concordance of these ages suggests that the plug may have been a feeder for the flow and that the present

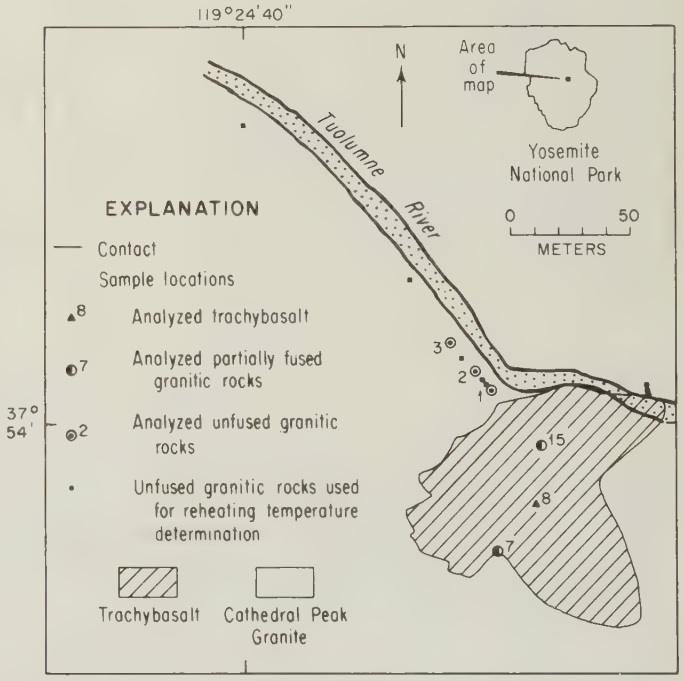

FIGURE 1.—Map of the trachybasalt plug on the Tuolumne River showing sample locations. Sample location 6, not shown, is 360 m N. 50° W. of location 1, and contact between Cathedral Peak Granite and older Half Dome Quartz Monzonite is exposed approximately 650 m N. 50° W. of location 1. Sample numbers from Calk and Naeser (1973).

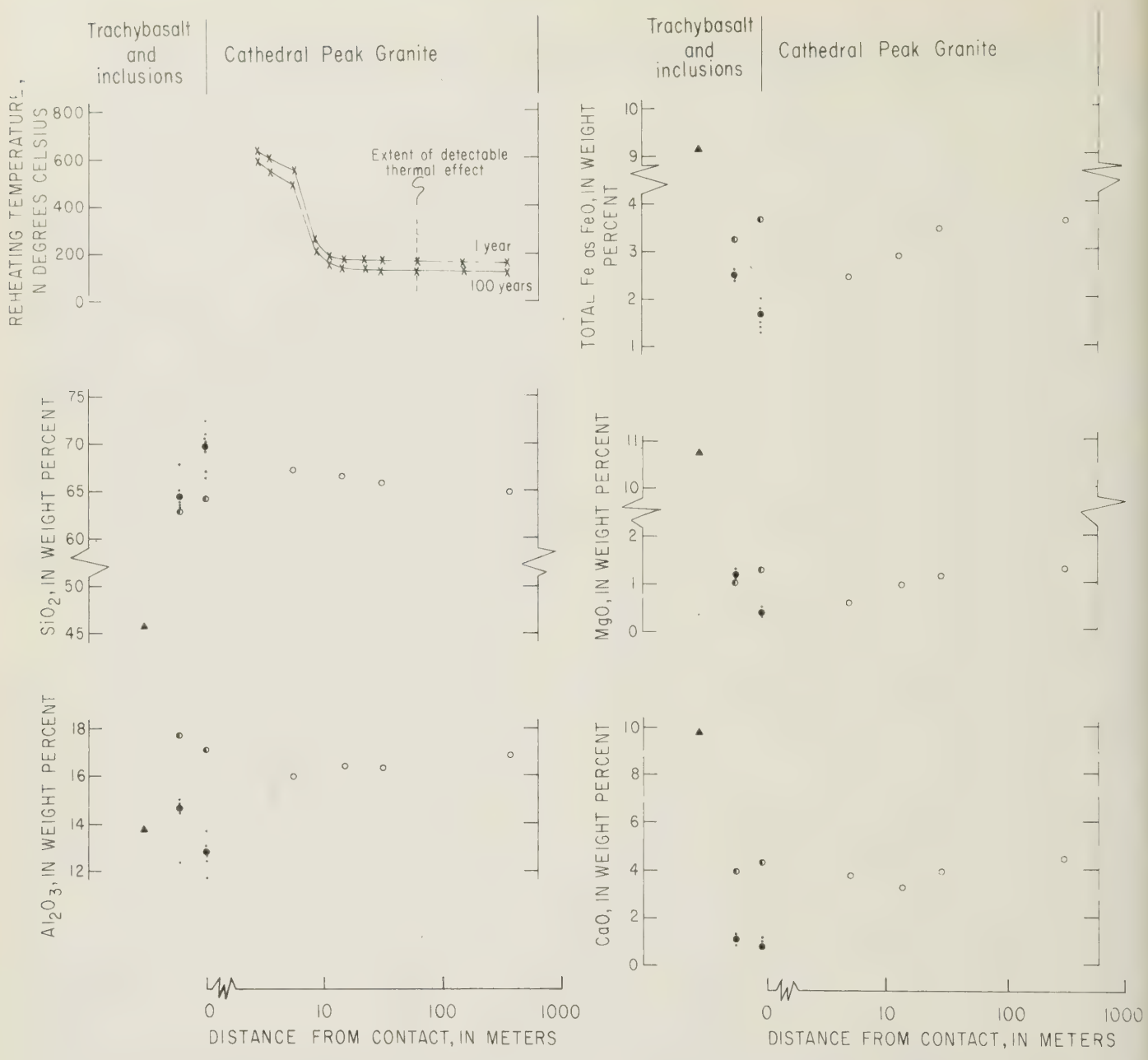

FIGURE 2.—Reheating temperatures (from Calk and Naeser, 1973), whole-rock major-element oxide contents, glass compositions, differentiation indices (weight percent Q+Or+Ab), and whole-rock powder densities plotted (above and on facing page) as a function of distance from contact of Cathedral Peak Granite and trachybasalt plug. Location of trachybasalt and inclusion samples arbitrarily plotted.

exposed level of the plug was not far below the surface at the time the plug was intruded.

The coarsely porphyritic granodiorite surrounding the plug, the Cathedral Peak Granite, originally described by Calkins (1930), crops out extensively in this part of the Sierra Nevada. This 80-m.y.-old intrusion (Evernden and Kistler, 1970; Calk and Naeser, 1973) cuts the older Half Dome Quartz Monzonite approximately 650 m northwest of the basalt plug.

Granodiorite at the contact and 60 m from the contact was reheated to more than 645°C and 165°C, respectively, assuming 1 year of heating time, or to more than 590°C and 125°C, respectively, assuming 100 years of heating time (fig. 2). The presence of

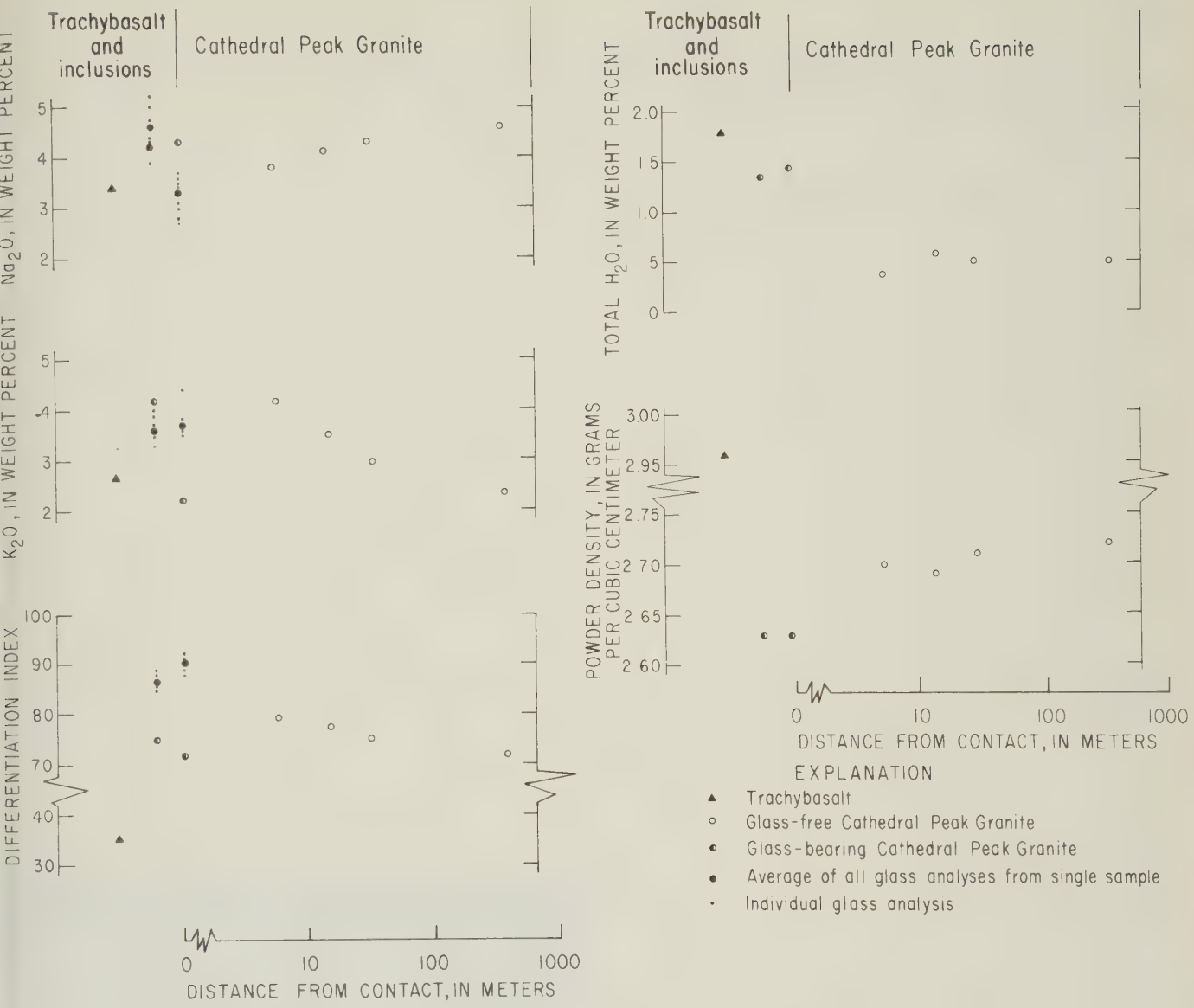

FIGURE 2.—Continued.

glass in the trachybasalt indicates that cooling was rapid, at least at higher temperatures, and 1 year rather than 100 years is the more probable duration of heating. Calk and Naeser (1973) found no reheating effect farther than about 60 m from the contact. Between 4 and 60 m, the only evidence of reheating is loss of fission tracks from apatite, and, at 60 m, the apatite fission-track age of the granodiorite has been reduced by only 10 percent.

PETROGRAPHY AND CHEMISTRY

The porphyritic trachybasalt consists of unaltered millimeter-sized phenocrysts of olivine, clinopyroxene, plagioclase, and opaque grains set in a brown glassy groundmass crowded with crystallites or in a completely cryptocrystalline groundmass. Feldspar ranges from sodic to calcic labradorite. The content of ferromagnesian minerals varies greatly; in some samples, olivine is dominant, whereas in others, augite is the sole ferromagnesian mineral. Textures range from intersertal to hyaloophitic.

A sample of an augite-rich trachybasalt (sample 8, table 1) is distinctly alkalic, as are many other analyzed volcanic rocks of Tertiary age in the central Sierra Nevada (see Hamilton and Neuerburg, 1956; Huber, 1968; Bateman and Lockwood, 1970; Kistler,

TABLE 1.—*Chemical analyses, CIPW norms, and powder densities of trachybasalt and glass-bearing and glass-free Cathedral Peak Granite*

[Analyst: G. O. Riddle, U.S. Geological Survey Denver Rock Analysis Laboratory. Sample numbers correspond to those used by Calk and Naeser (1973). Sample 8 is trachybasalt; 15 and 7 are glass-bearing Cathedral Peak Granite; 1, 2, 3, and 6 are glass-free Cathedral Peak Granite. -, not present]

Sample No.	8	15	7	1	2	3	6
Chemical analyses (weight percent)							
SiO_2	45.49	62.86	64.12	67.05	66.60	65.89	64.91
Al_2O_3	13.78	17.70	17.03	15.98	16.44	16.39	16.96
Fe_2O_3	2.37	2.01	2.46	1.62	1.69	2.15	2.00
FeO	7.01	1.44	1.44	1.01	1.37	1.53	1.82
MgO	10.75	1.09	1.14	.60	.96	1.12	1.29
CaO	9.80	3.84	4.29	3.71	3.46	3.85	4.41
Na_2O	3.40	4.25	4.28	3.80	4.12	4.32	4.59
K_2O	2.67	4.17	2.41	4.16	3.51	2.91	2.36
H_2O+	1.44	.96	1.06	.28	.45	.40	.45
H_2O-	.34	.38	.35	.09	.12	.10	.05
TiO_2	1.75	.57	.62	.66	.52	.61	.63
P_2O_5	.66	.21	.34	.33	.20	.23	.26
MnO	.16	.08	.09	.06	.06	.08	.09
CO_2	.02	.02	.01	.01	.01	.02	.01
Cl	.05	.01	.01	.00	.00	.01	.00
F	.09	.06	.07	.05	.05	.06	.07
Subtotal	99.78	99.65	99.72	99.41	99.56	99.67	99.90
O≡Cl,F	-.05	-.03	-.03	-.02	-.02	-.03	-.03
Total	99.73	99.62	99.69	99.39	99.54	99.64	99.87
CIPW norms (weight percent)							
Q	-	13.36	20.62	21.80	21.10	20.77	18.69
C	-	-	.55	-	.16	-	-
or	16.10	25.07	14.49	24.82	20.95	17.34	14.03
ab	6.76	36.51	36.76	32.47	35.22	36.79	39.07
an	14.95	17.23	19.03	14.40	15.72	16.92	18.82
ne	12.04	-	-	-	-	-	-
hl	.08	.02	.02	-	-	.02	-
wo	12.49	.13	-	.75	-	.17	.45
en	8.73	2.76	2.89	1.51	2.42	2.81	3.23
fs	2.71	.20	-	-	.38	.18	.82
fo	13.03	-	-	-	-	-	-
fa	4.46	-	-	-	-	-	-
mt	3.51	2.96	3.19	1.55	2.48	3.14	2.92
hm	-	-	.30	.57	-	-	-
il	3.39	1.10	1.20	1.27	1.00	1.17	1.20
ap	1.60	.51	.82	.79	.48	.55	.62
fr	.07	.09	.08	.04	.07	.08	.10
cc	.05	.05	.02	.02	.02	.05	.02
Powder density (g/cm^3)							
	2.96	2.63	2.63	2.70	2.69	2.71	2.72

1974). The silica content is the lowest yet reported for volcanic rocks in the Sierra Nevada.

The granodiorite surrounding the plug contains conspicuous microcline phenocrysts that are commonly 50 mm long, tabular, and euhedral. The phenocrysts are set in a medium-grained, hypidiomorphic-granular groundmass consisting of anhedral quartz; subhedral to euhedral polysynthetically twinned, generally zoned plagioclase (An_{20}-An_{35}); interstitial anhedral microline; subhedral to euhedral green biotite and hornblende; and accessory sphene and magnetite.

Trace amounts (less than 1 volume percent) of pale-yellow glass occur as thin films along fractures and grain boundaries in granodiorite samples taken 1 to 3.5 m from the basalt plug. There is no visible evidence of melting in these samples, but optic axial angles of potassium feldspar decrease toward the contact. Biotite tends to change progressively in its strongest absorption color from dark olive to dark reddish brown and becomes increasingly dusted with bands of fine reddish iron oxide grains at the expense of interlaminated chlorite. Other minerals appear to be unaffected by nearness to the contact.

Partially fused granodiorite samples collected at the contact in the reentrant on the southern side of the plug (sample 7) and from an inclusion in the basalt (sample 15) contain approximately 16.5 and 20.0 volume percent glass, respectively. The brown glass occurs in veinlike globular masses along grain boundaries and fractures (fig. 3). Locally microlites of orthopyroxene(?) and opaque minerals crowd the glass. Biotite and hornblende are both absent from the partially melted rocks. Potassium feldspar crystals are commonly riddled with fine glass inclusions, giving the

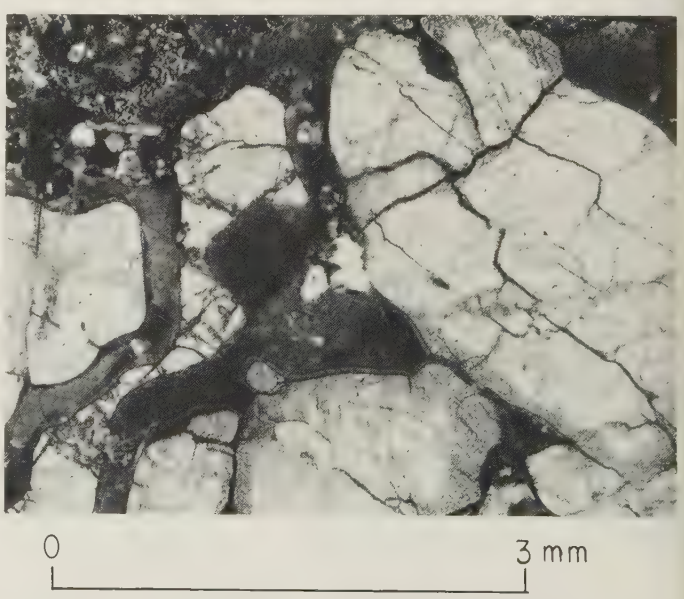

FIGURE 3.—Photomicrograph of partially fused granodiorite (sample 7). Brown glass separates grains of felsic minerals. Width of area shown is 3 mm.

TABLE 2.—*Electron microprobe analyses and CIPW norms of glass included in glass-bearing Cathedral Peak Granite*

[Instrument: Applied Research Laboratories EMX. Conditions: excitation potential, 15 kV; specimen current, 0.01 μA; standards, wet-chemically analyzed feldspars and kaersutite. Background, atomic number, absorption and fluorescence corrections applied using a computer program developed at the U. S. Geological Survey (Beeson, 1967; Beaman and Isasi, 1970). -, not present]

Sample No.	15								7								
	a	b	c	d	e	f	g	h	a	b	c	d	e	f	g	h	i
Microprobe analyses (weight percent)																	
SiO_2	63.3	63.4	63.6	63.8	64.1	64.5	65.0	67.7	66.3	67.0	69.1	70.0	70.1	70.4	71.0	71.0	72.4
Al_2O_3	14.8	14.6	15.0	14.6	14.5	14.5	14.3	12.3	13.7	13.1	12.9	12.4	13.1	12.7	13.1	12.6	11.7
[1]Fe_2O_3	1.5	1.6	1.5	1.6	1.6	1.5	1.5	1.6	1.2	1.3	1.2	1.0	.9	1.0	1.3	1.0	1.2
[1]FeO	1.0	1.1	1.0	1.1	1.2	1.0	1.0	1.1	.7	.8	.7	.6	.5	.6	.8	.6	.7
MgO	1.2	1.3	1.3	1.3	1.3	1.2	1.1	1.0	.5	.4	.4	.3	.3	.3	.5	.4	.3
CaO	1.1	1.2	1.1	1.1	1.3	1.0	1.0	.8	.8	1.1	.9	.7	.8	.7	.8	.7	.7
Na_2O	4.3	5.0	4.7	5.2	4.4	4.4	5.0	3.9	2.8	3.0	3.6	3.1	3.5	3.4	3.7	3.7	2.7
K_2O	4.0	3.5	3.9	3.3	3.7	3.7	3.5	3.5	4.4	3.6	3.8	3.6	3.7	3.5	3.7	3.6	3.8
TiO_2	1.0	1.0	1.0	.8	.8	.6	.8	.8	.4	.6	.1	.03	.2	.04	.4	.04	.4
Total	92.2	92.7	93.1	92.8	92.9	92.4	93.2	92.7	90.8	90.9	92.7	91.7	93.1	92.6	95.3	93.6	93.9
CIPW norms (weight percent)																	
Q	20.4	17.7	18.3	17.9	21.1	22.5	20.1	30.7	33.8	36.1	33.5	39.4	35.9	38.0	34.5	35.8	42.8
C	1.5	.4	1.1	.5	1.0	1.6	.5	.7	3.2	2.5	1.3	2.3	2.0	2.2	1.6	1.4	2.0
or	25.6	22.3	24.8	21.0	23.5	23.7	22.2	22.3	28.6	23.4	24.2	23.2	23.5	22.3	22.9	22.7	23.9
ab	39.5	45.6	42.7	47.4	40.1	40.3	45.4	35.6	26.1	27.9	32.9	28.6	31.8	31.1	32.9	33.4	24.3
an	5.9	6.4	5.9	5.9	6.9	5.4	5.3	4.3	4.4	6.0	4.8	3.8	4.3	3.7	4.2	3.7	3.7
en	3.2	3.5	3.5	3.5	3.5	3.2	2.9	2.7	1.4	1.1	1.1	.8	.8	.8	1.3	1.1	.8
fs	-	-	-	-	-	-	-	-	-	-	.1	.2	-	.2	-	.2	-
mt	.4	.7	.3	1.3	1.7	1.6	1.0	1.3	1.2	.9	1.9	1.6	1.1	1.6	1.5	1.5	1.2
hm	1.4	1.2	1.4	.8	.6	.5	.9	.8	.5	.8	-	-	.2	-	.3	-	.5
il	2.1	2.0	2.0	1.6	1.6	1.2	1.6	1.6	.8	1.3	.2	.1	.4	.1	.8	.1	.8

[1]Fe distributed between Fe_2O_3 and FeO in same proportions as in corresponding whole-rock analyses.

crystals a spongy appearance. Quartz and plagioclase grains are commonly rounded and appear to be partially melted immediately adjacent to glass, but zoning is retained in the plagioclase crystals. Sphene is surrounded with opaque material. Apatite and zircon are unaffected in the partially fused rocks.

The greatest differences in composition between partially fused and unfused granodiorite samples (table 1; fig. 2) are in contents of SiO_2, which is lower, and Al_2O_3 and H_2O, which are higher in the partially fused rocks. Other major-element oxides show less pronounced differences. Relative to the unfused granodiorite sample (no. 1) collected nearest the partially fused samples, the partially fused samples contain greater amounts of total iron, MgO, CaO, and Na_2O. Compared to the nearest unfused sample, K_2O is nearly the same in one partially fused sample but considerably less in the other. Powder densities are much lower in partially fused granodiorite, reflecting the low density of the included glass.

Systematic variations in major-element oxides are apparent within the group of unfused samples. SiO_2 and K_2O tend to decrease farther away from the basalt contact, whereas Al_2O_3, total iron, MgO, CaO, and Na_2O tend to increase, as does the powder density.

The low, but relatively consistent, totals of the electron microprobe analyses in table 2 reflect the hydrated nature of the glasses, as do the high water contents of the partially fused rock samples. Averages of the individual analyses of glasses from the two partially fused samples, as well as the individual analyses themselves, are depicted in figure 2. Relative to their host rocks, both glasses are higher in SiO_2 and lower in Al_2O_3, total iron, and CaO. Na_2O, K_2O,

and MgO show no consistent pattern.

In all analyzed granitic rocks and glasses, the sum of normative albite, anorthite, orthoclase, and quartz exceeds 90 percent; therefore the bulk of the normative variation is shown by these four constituents in figure 4. Differentiation indices (sum of normative quartz, orthoclase, and albite) are considerably higher in both analyzed glasses than in their hosts and tend to decrease in unfused granodiorite away from the basalt contact.

DISCUSSION

The trends of variations in chemical constituents in glass-free granodiorite are undoubtedly related to compositional patterns, described by Robinson (1977), that were produced during intrusive emplacement of the Cathedral Peak Granite magma. There is no evidence of chemical change in rocks reheated to 550°C or less, the reheating temperature obtained assuming a 1-year reheating time of the glass-free sample (no. 1) taken nearest the plug.

The source of the glass-bearing inclusion in the plug may have been considerably below the presently exposed level; thus, chemical differences between the inclusion and the wallrock may in part be related to different original compositions. The original composition of the glass-bearing sample from the wallrock (no. 7) likely was similar to the composition of the

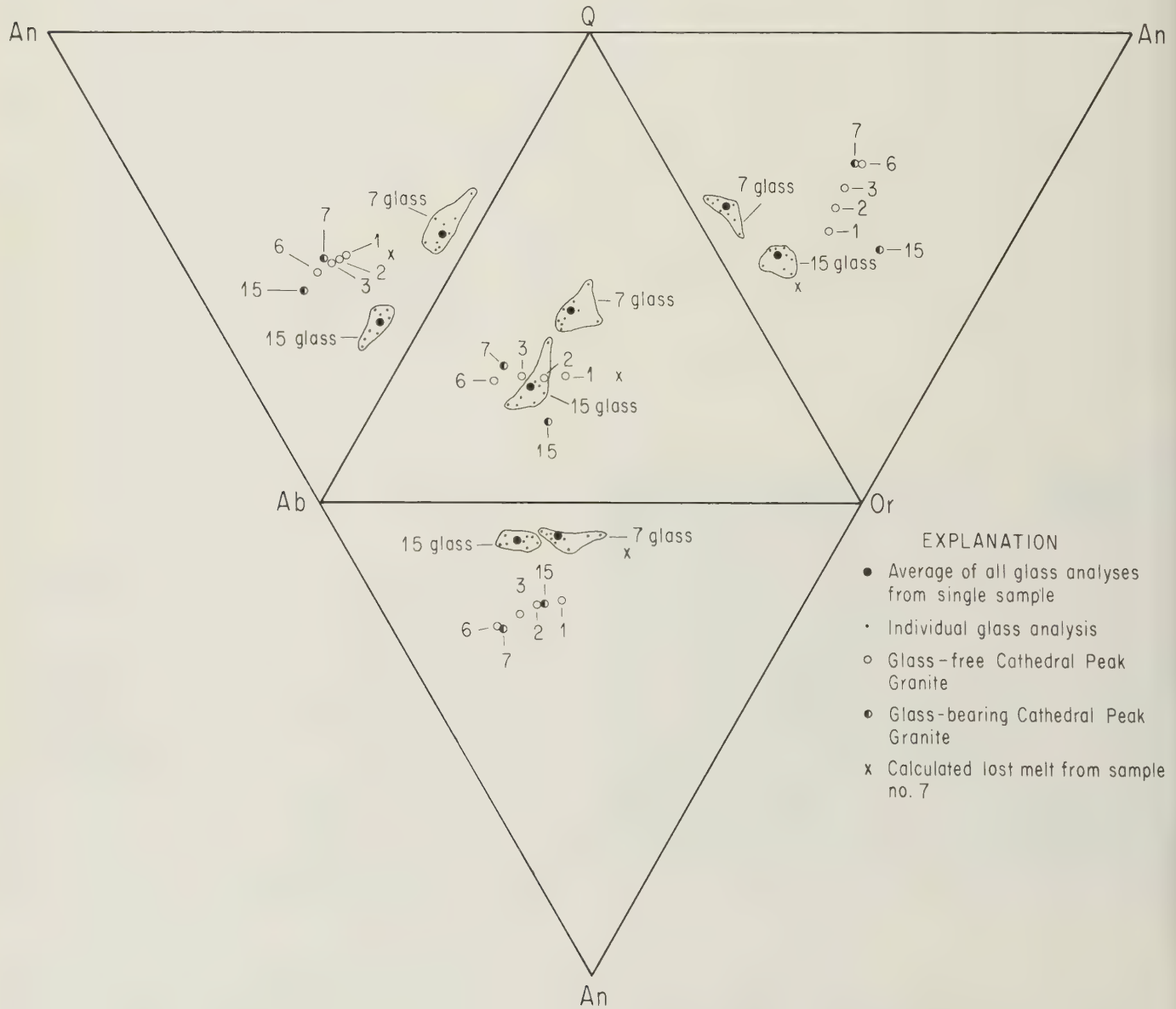

FIGURE 4.—Normative proportions of Q, Or, Ab, and An in glasses and glass-free and glass-bearing Cathedral Peak Granite.

nearest glass-free sample (no. 1). Compositional differences between these two rocks indicate a loss of material from the partially fused rock. This loss probably reflects mass migration of early-formed melt into surrounding wallrock, accounting for the thin films of glass in granodiorite within 3.5 m of the plug. In view of the chemical differences between the partially fused material and the trachybasalt, particularly with respect to Al_2O_3 and the alkali oxides, chemical diffusion was unlikely between the basalt magma and the granodiorite.

Of all the major-element oxides, MgO shows the greatest apparent enrichment in the glass-bearing rock relative to the nearby glass-free rock. Assuming that MgO did not enter the early melt and that prior to fusion the glass-bearing and glass-free rocks had the same composition, the calculated proportion of material missing from the partially fused sample is nearly 50 percent of the original rock; if MgO was incorporated in the melt, then an even greater portion was lost. Normative proportions of quartz, orthoclase, albite, and anorthite in the calculated melt are depicted in figure 4. In each of the ternary diagrams involving orthoclase, the early melt lies nearer the Or apex than do any of the other analyzed materials. The relative enrichment of normative orthoclase indicates that the composition of the early melt was strongly influenced by subsolidus reaction and subsequent melting of biotite, as well as fusion of quartz and feldspars. Both calculated stability curves for biotite (Wones and Eugster, 1965) and experimentally determined curves derived from melting of granitic rocks (Piwinskii and Wyllie, 1968; Piwinskii, 1968) show that the stability temperatures of biotite are substantially reduced in a low water-pressure environment. Water pressure at the time of fusion of the granodiorite cannot be quantitatively estimated but, because of the shallow depth of the exposed plug, could have been only hundreds of bars at the most.

After migration of the early melt phase, continued fusion, dominated by melting of feldspars and quartz, produced melt that was quenched to form the glass now present in the partially fused granodiorite. Judging from their positions within the quartz-orthoclase-albite-anorthite diagram relative to one another and to their respective hosts (fig. 4), glass in the granodiorite collected at the basalt contact represents less partial melting than does glass in the inclusion from within the plug.

REFERENCES CITED

Al-Rawi, Yehya, and Carmichael, I. S. E., 1967, A note on the natural fusion of granite: Am. Mineralogist, v. 52, p. 1806–1814.

Bateman, P. C., 1965, Geology and tungsten mineralization of the Bishop district, California: U.S. Geol. Survey Prof. Paper 470, 208 p.

Bateman, P. C., and Lockwood, J. P., 1970, Kaiser Peak quadrangle, central Sierra Nevada, California—Analytic data: U.S. Geol. Survey Prof. Paper 644–C, 15 p.

Beaman, D. R., and Isasi, J. A., 1970, A critical examination of computer programs used in quantitative electron microprobe analysis: Anal. Chemistry, v. 42, p. 1540–1568.

Beeson, M. H., 1967, A computer program for processing electron microprobe data: U.S. Geol. Survey open-file rept., 41 p.

Calk, L. C., and Naeser, C. W., 1973, The thermal effects of a basalt intrusion on fission tracks in quartz monzonite: Jour. Geology, v. 81, p. 189–198.

Calkins, F. C., 1930, The granitic rocks of the Yosemite region, *in* Matthes, F. E., Geologic history of the Yosemite Valley: U.S. Geol. Survey Prof. Paper 160, p. 120–129.

Dalrymple, G. B., 1963, Potassium-argon dates of some Cenozoic volcanic rocks of the Sierra Nevada, California: Geol. Soc. America Bull., v. 74, p. 379–390.

Evernden, J. R., and Kistler, R. W., 1970, Chronology of emplacement of Mesozoic batholithic complexes in California and western Nevada: U.S. Geol. Survey Prof. Paper 623, 42 p.

Hamilton, W. B., and Neurburg, G. J., 1956, Olivine-sanidine trachybasalt from the Sierra Nevada, California: Am. Mineralogist, v. 41, p. 851–873.

Huber, N. K., 1968, Geologic map of the Shuteye Peak quadrangle, Sierra Nevada, California: U.S. Geol. Survey Geol. Quad. Map GQ–728, scale 1:62 500.

Kistler, R. W., 1974, Hetch Hetchy Reservoir quadrangle, Yosemite National Park, California—Analytic data: U.S. Geol. Survey Prof. Paper 774–B, 15 p.

Knopf, Adolph, 1938, Partial fusion of granodiorite by intrusive basalt, Owens Valley, California: Am. Jour. Sci., 5th ser., v. 36, p. 373–376.

Piwinskii, A. J., 1968, Experimental studies of igneous rock series, central Sierra Nevada batholith, California: Jour. Geology, v. 76, p. 548–570.

Piwinskii, A. J., and Wyllie, P. J., 1968, Experimental studies of igneous rock series—A zoned pluton in the Wallowa batholith, Oregon: Jour. Geology, v. 76, no. 2, p. 205–234.

Robinson, C. A., 1977, Differentiation of the Tuolumne Intrusive Series, Yosemite National Park, California: Geol. Soc. America Abs. with Programs, v. 9, p. 487–488.

Wones, D. R., and Eugster, H. P., 1965, Stability of biotite—Experiment, theory, and application: Am. Mineralogist, v. 50, p. 1228–1272.

Wyllie, P. J., 1961, Fusion of Torridonian sandstone by a picrite sill in Soay (Hebrides): Jour. Petrology, v. 2, p. 1–37.

Jour. Research U.S. Geol. Survey
Vol. 6, No. 4, July–Aug. 1978, p. 467–472

CHABAZITE IN SILICEOUS TUFFS OF A PLIOCENE LACUSTRINE DEPOSIT NEAR DURKEE, BAKER COUNTY, OREGON

By ARTHUR J. GUDE 3d and RICHARD A. SHEPPARD,
Denver, Colo.

Abstract.—A relatively pure chabazite deposit of at least 5×10^6 metric tons occurs near the Durkee type locality of erionite. This erionite is in a welded tuff interbedded with lacustrine rocks of a closed Pliocene basin. The zeolites, chabazite, erionite, clinoptilolite, and other authigenic silicate minerals are confined to a 27-square-kilometer area of altered rocks enclosed in relatively freshwater lacustrine beds. About 135 meters of the lower part of the 350-m stratigraphic section at the southeastern part of the lake basin contain zeolitic tuff. The chabazite is an early product of the reaction between glass of rhyolitic or dacitic composition and alkaline (pH>9) saline lake waters. Erionite, clinoptilolite, analcime, and potassium feldspar follow chabazite in the paragenetic sequence. At the erionite type locality, chabazite and clinoptilolite form megascopic crystal clusters within fractures and cavities in unaltered welded tuff. Elsewhere in the basin, most zeolite crystals in the altered airfall or reworked tuffs are less than 30 micrometers long. Chemical analyses, unit-cell determinations, and mean indices of refraction show that fine-grained chabazite varies in composition and physical parameters.

Chabazite in thick, nearly monomineralic beds occurs in a Pliocene lacustrine deposit near Durkee, Baker County, in eastern Oregon. An irregularly shaped, northwesterly elongate basin, with Durkee near its center, is covered by 118 square kilometers of Pliocene lacustrine rocks and younger fluviatile deposits. About 27 km² in a crudely crescent-shaped area in the southeasternmost part of the basin contains the authigenic silicate minerals derived from siliceous tuffs. The best exposures of the chabazite are 4–5 kilometers east of Durkee in an amphitheater cut by erosion nearly 100 meters into the lower part of the lacustrine sequence (fig. 1).

HISTORY

Durkee has been known in zeolite literature since 1898 when Eakle (1898) described a new mineral, erionite, from an opal quarry in a "rhyolite" (welded ash-flow tuff) 6 km southeast of the townsite. In 1953, Staples (1957) rediscovered the locality, and later, Staples and Gard (1959) reexamined the type material. Sheppard and Gude (1975) first reported the existence of other authigenic zeolites at Durkee in the lacustrine rocks that surround and include the type locality for erionite. This Durkee chabazite study is part of a larger U.S. Geological Survey program on zeolites in sedimentary deposits that the authors started in 1963.

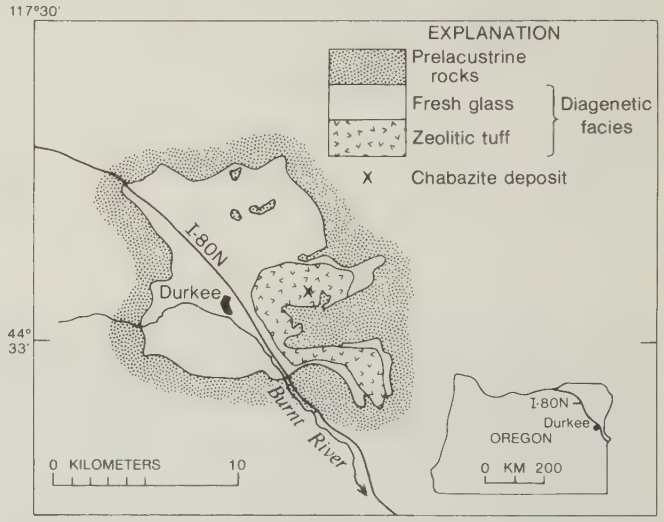

FIGURE 1.—Location and geologic sketch map of Durkee zeolite deposit.

GEOLOGIC SETTING

A closed saline, alkaline lake occupied the Pliocene Durkee basin during the early part of its geologic history. Rhyolitic and dacitic tuffs—in part directly deposited, but mostly reworked airfall ash—are referred to in this report as "tuffs." These, as well as a thick welded ash-flow tuff that was deposited in the lake, reacted with the water to form zeolites and other authigenic minerals. This process was limited to tuffs

in the southeastern part of the basin and in the stratigraphically lower part of the lacustrine sequence. Mudstone, siltstone, and sandstone are intercalated with the tuffs. The surrounding and overlying younger lacustrine rocks were deposited in fresh water and thus contain unaltered tuffs, thick diatomite beds, and other sediments that were mostly unaffected by reaction with marginal and dilute lake waters. At least two series of fluviatile gravels cap the lacustrine rocks. Remnants of Mazama ash are in channels of the Holocene alluvium in the basin. Thin detached irregular basalt flows are scattered throughout the area but are older than any of the lake deposits.

Many closely spaced normal faults trending nearly east-west displace the beds as much as 10 m. Associated parallel faults having smaller displacements are common. These features make coherent mapping of individual beds nearly impossible. Correlation of individual tuffs across the basin is difficult unless the welded ash-flow tuff is present in an undisturbed sequence. Except where faults and slump have disturbed the rock, the bedding has slight dips due to differential deposition or compaction.

STRATIGRAPHY

Approximately 350 m of stratigraphic section (fig. 2) can be measured in the deepest part of the lake. Diagenesis during the closed-basin period is recorded by zeolites and other authigenic minerals in the middle and bottom 135 m of lacustrine sediments.

The welded ash-flow tuff, which is the only reliable marker bed, is at least 15 m thick. It can be found throughout the basin at or near the lowest part of the section. Mudstone containing tuffaceous particles fills the next 15 m of the section, up to the base of the lower of two prominent airfall tuffs. These are each 10–12 m thick and are separated by 3 m of mudstone. Nearly two dozen thin, less than 10-cm-thick, airfall tuffs are interspersed in the mudstones, siltstones, sandstones, and diatomites in the overlying rocks. All the tuffs (eight or nine) in the lower closed-basin rocks have altered to zeolites. Those in the top part are fresh and difficult to find in the diatomites, which occupy more than 100 m in the upper freshwater facies.

OCCURRENCE AND PROPERTIES OF CHABAZITE

Chabazite, other zeolites, potassium feldspar, clay minerals, and silica minerals derived from the rhyolitic and dacitic tuffs are in the lowest lacustrine rocks near the center and southeastern part of the lacustrine deposit. Airfall tuffs in this part of the lake beds are

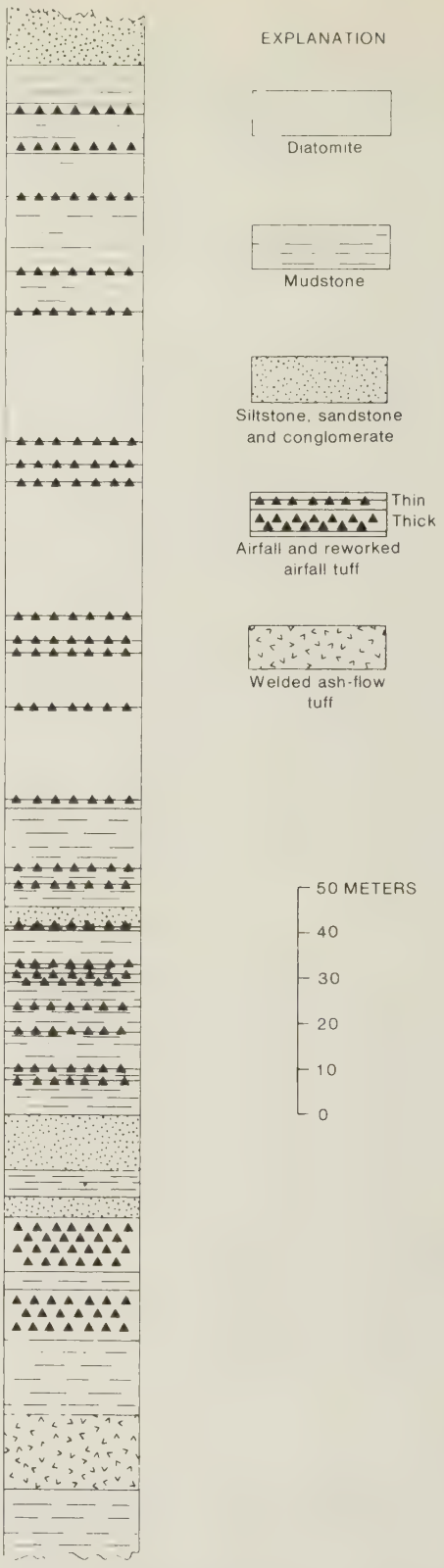

FIGURE 2.—Stratigraphic section of lacustrine sediments in Pliocene Durkee basin.

mpletely altered to zeolites. The lowest 1–2 m of e welded tuff is partly altered to chabazite. Fractures at extend several centimeters into the top of this ff have chabazite bands a few millimeters wide deloped along the cracks.

Chabazite formed midway during diagenesis of olcanic glass in the Pliocene saline, alkaline lake. areful studies of the altered rocks using thin sections, canning electron micrographs, and evidence from eld relationships are the bases for the generalized equence: glass → montmorillonite → phillipsite → habazite → erionite → clinoptilolite and then any f the preceding zeolites → analcime → K-feldspar. Details of the observed zeolite paragenesis at Durkee, rom early to late, are as follows:

Glass, then:

phillipsite → clinoptilolite and erionite
phillipsite → erionite
montmorillonite → clinoptilolite
montmorillonite → chabazite → clinoptilolite
montmorillonite → phillipsite → clinoptilolite
montmorillonite → erionite → clinoptilolite
montmorillonite → chabazite → erionite
phillipsite → clinoptilolite
phillipsite → erionite and chabazite
any of the above zeolites → analcime → K-feldspar

The morphology of the hexagonal ($R\bar{3}m$) chabazite rystals is seen best in SEM (scanning electron microcope) images (fig. 3). Euhedral, unmodified rhombohedra are most abundant and range in size from few tenths of a micrometer to as much as 15–20 m. Interpenetrating twins on (0001) of otherwise nmodified rhombohedra are common. Negative rhomb aces which truncate the corners of the common form re visible in a few specimens.

Elongate prisms and fiber bundles of erionite are resent with chabazite in nearly all samples. Even here X-ray diffractometer records do not show a attern of erionite, it is commonly seen in SEM images parsely scattered on chabazite rhombs or in openings etween clusters of the earlier formed chabazite.

SPECIAL OCCURRENCE

A special chabazite occurrence, different from the ne-grained material found in the altered tuffs, was oted in rubble of the quarry at the erionite type ocality. Clear crystal rhombs, as much as 1 mm in ze (fig. 4), coat cavities and fractures in the welded sh-flow tuff that contains the fibrous erionite on ractures, as described by Eakle (1898). No twinned

FIGURE 3.—Scanning electron micrograph showing the morphology of chabazite in a tuff. Note the (0001) twinning.

chabazite crystals have been seen in any of the specimens examined by the SEM. An energy-dispersive X-ray-spectrograph focused-beam analysis shows that these crystals are rich in calcium. The relationship here of chabazite to the erionite is not known because no rocks can now be found in place. The two minerals were not observed together here in any of the material studied by the authors.

FIGURE 4.—Scanning electron micrograph showing the morphology of chabazite in the welded ash-flow tuff.

COMPOSITION OF CHABAZITE

Two conventional rock analyses of Durkee chabazites are plotted in figure 5 (an updated version of

one presented earlier by Sheppard and Gude, 1970), which shows the variable compositions of chabazites from many localities and geologic environments. The two Durkee chabazites (D–1, D–10) plot in the middle of the field of the seven analyzed samples from the sedimentary environments. Table 1 gives the complete analytical data for these two samples.

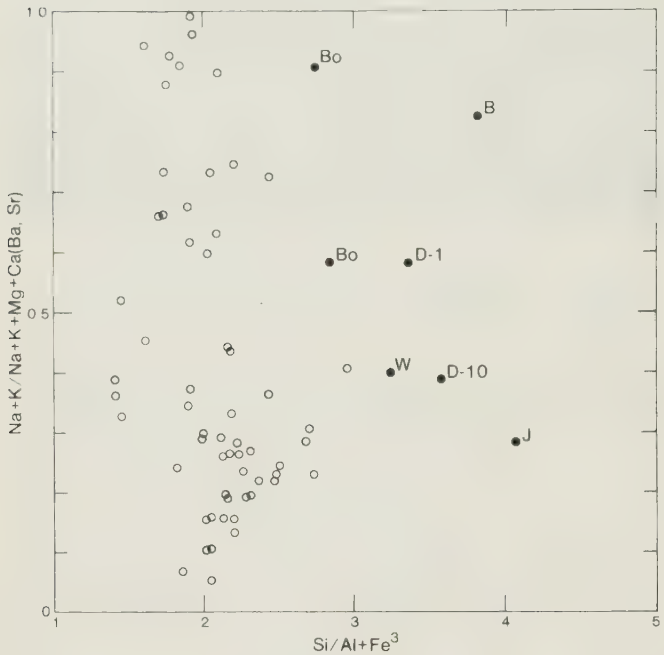

FIGURE 5.—Compositional variation of chabazites (modified from Sheppard and Gude, 1970). Open circles, chabazite from igneous rocks; filled circles with letters, chabazite from tuffs in sedimentary rocks from the following locations: B, Barstow, Calif. (Gude and Sheppard, 1966); Bo, Bowie, Ariz. (Sheppard and others, 1976); D, Durkee, Oreg. (this report); J, John Day, Oreg. (Sheppard and Gude, 1970); W, Wikieup, Ariz. (Sheppard and Gude, 1973).

TABLE 1.—*Chemical analyses of chabazite from Durkee*

[Analyst: Vertie C. Smith, U.S. Geological Survey, Denver]

Analyses in weight percent			Composition in atoms per unit cell		
Oxides	D-1	D-10	Elements	D-1	D-10
SiO_2	57.91	58.65	Si	27.90	28.31
Al_2O_3	14.25	13.51	Al	8.09	7.66
Fe_2O_3	.42	.61	Fe^{+3}	.15	.22
FeO	.02	.00	Mg	.28	.91
MgO	.40	1.27	Ca	1.98	1.92
CaO	3.85	3.78	Na	2.30	.72
Na_2O	2.46	.77	K	.82	1.08
K_2O	1.33	1.76	H_2O^+	17.00	18.88
H_2O^+	10.58	11.77	H_2O^-	12.54	11.54
H_2O^-	7.80	7.19	O	72.00	72.00
TiO_2	.15	.02	Si:Al+Fe^{+3}	3.38	3.58
P_2O_5	.03	.01			
MnO	.01	.00			
CO_2	.04	.02			
BaO	.01	.00			
Total	99.26	99.36			

The Durkee chabazite is more calcic than all othe reported samples except for the material from th John Day, Oreg., locality (Sheppard and Gud 1970). Although the atomic ratios of sodium an potassium are reversed between samples D–1 an D–10, it is clear (fig. 5) that all chabazites, regardles of origin, may have any cation ratio. However, the Si Al+Fe^{+3} ratios plot a distinct field for silica-ric chabazites from sedimentary rocks.

PHYSICAL PROPERTIES OF CHABAZITE

Cell parameters.—Table 2 gives the hexagonal unit cell parameters, the mean indices of refraction, and th associated mineralogy of 26 chabazite-rich sample The Durkee chabazites span the range of values tha have been published (Passaglia, 1970; Shepparc 1971) for chabazites from other sedimentary enviror ments.

TABLE 2.—*Chabazite unit cell*[1]*, optics*[2]*, and associated mine alogy*

[Ch, chabazite; Er, erionite; Cl, clinoptilolite; Cy, clay; *, particl too small to measure; ---, not measured; Tr., trace; R.I., index refraction]

Sample No.	a hex (A)	c hex (A)	V (A^3)	Mean R.I. (±0.001)	Ch	Er	Cl	Cy
1	13.703±.003	14.870±.006	2418±1	1.466	10	---	---	---
2	13.716±.004	14.882±.009	2424±2	-----	9	1	---	---
3	13.717±.005	14.883±.009	2425±2	1.466	10	Tr.	---	---
4	13.714±.005	14.90±.01	2427±2	1.468	10	---	---	---
5	13.752±.003	14.932±.006	2446±1	*	9	1/2	1/2	---
6	13.714±.005	14.93±.01	2431±2	*	7	1	1	1
7	13.736±.004	14.893±.008	2433±2	*	8	1	Tr.	1
8	13.738±.004	14.857±.006	2428±1	1.468	6	1	---	2
9	13.730±.005	14.876±.009	2429±2	1.467	10	Tr.	---	---
10	13.721±.003	14.843±.007	2420±1	1.468	10	---	---	---
11	13.730±.003	14.983±.009	2442±2	1.470	5	2	1	2
12	13.723±.004	14.917±.008	2432±2	1.470	8	2	---	---
13	13.738±.003	14.875±.006	2431±1	1.467	9	1	---	---
14	13.738±.002	14.887±.004	2433±1	1.469	10	Tr.	---	---
15	13.754±.005	14.936±.009	2447±2	1.469	8	2	---	---
16	13.717±.005	14.865±.008	2422±2	1.467	9	1	---	---
17	13.738±.004	14.866±.007	2430±1	1.470	9	1	---	---
18	13.729±.005	14.893±.009	2431±1	1.468	10	---	Tr.	---
19	13.726±.005	14.890±.004	2430±2	1.468	10	---	---	---
20	13.716±.007	14.87±.01	2423±3	1.469	8	1	Tr.	1
21	13.733±.005	14.89±.01	2432±2	*	8	1	1	---
22	13.707±.005	14.93±.01	2429±2	*	9	---	1	---
23	13.735±.001	14.872±.003	2430±1	1.468	10	Tr.	---	---
24	13.710±.004	14.86±.01	2419±2	-----	10	---	---	---
25	13.723±.006	14.85±.01	2422±3	-----	10	---	---	---
26	13.719±.006	14.85±.01	2420±2	-----	10	Tr.	---	---

[1]Computer-derived by least-squares program W9214. Powder data from CaF_2 internal-standard patterns, Cu $K\alpha_1$ radiation, LiF diffracted-beam monochromator.
[2]Indices of refraction measured using white light in calibrated immersion oils and corrected for temperature.

A plot (fig. 6) of unit-cell parameters indicate that chabazite from cavities in igneous rocks (Pas saglia, 1970) differs from the silica-rich variety fro sediments (Gude and Sheppard, 1966; this report) Four specimens described by Passaglia (1970) tha apparently contain strontium and potassium in th crystal structure occupy a distinct and separate fiel The single John Day specimen is rich in calciu and is the most siliceous. All the data presented i

this diagram clearly show that chabazite from siliceous rocks differs from chabazite from mafic rocks. Herschellite, the so-called sodic variety of chabazite, does not have a unique unit-cell position.

Indices of refraction.—The measured mean indices of refraction for these lacustrine chabazites are consistently lower than those reported for chabazites from basalts. This result is consistent with the higher silica content for analyzed zeolite specimens collected from silicic tuffs subjected to diagenesis in closed saline, alkaline basins.

ECONOMIC POTENTIAL

Economic factors may encourage the addition of this deposit to the growing list of producing zeolite localities; these factors include its estimated quantity (75 million metric tons of chabazite) and also the occurrence of erionite in large amounts; its near-surface, flat-lying zeolitic beds; and its short road distance (6 km) to the railroad at Durkee.

Chabazite, erionite, and these minerals in certain mixed proportions are used in various processes in which their molecular-sieve properties are needed. The means for adsorption of specific gases, such as methane, by these zeolites is currently being developed. Although the quantity and quality of the deposit are imperfectly known, this deposit appears to be as good as or better than other described sites. Physical exploration and commercial tests are needed to define the worth of the Durkee chabazite.

REFERENCES CITED

Eakle, A. S., 1898, Erionite, a new zeolite: Am. Jour. Sci., v. 155, p. 66–68.

Gude, A. J., 3d, and Sheppard, R. A., 1966, Silica-rich chabazite from the Barstow Formation, San Bernadino County, southern California: Am. Mineralogist, v. 51, p. 909–915.

Passaglia, Elio, 1970, The crystal chemistry of chabazites: Am. Mineralogist, v. 55, p. 1278–1301.

Sheppard, R. A., 1971, Zeolites in sedimentary deposits of the United States—A review, *in* Gould, R. F., ed., Molecular sieve zeolites—I: Am. Chem. Soc. Advances in Chemistry Ser. 101, p. 279-310.

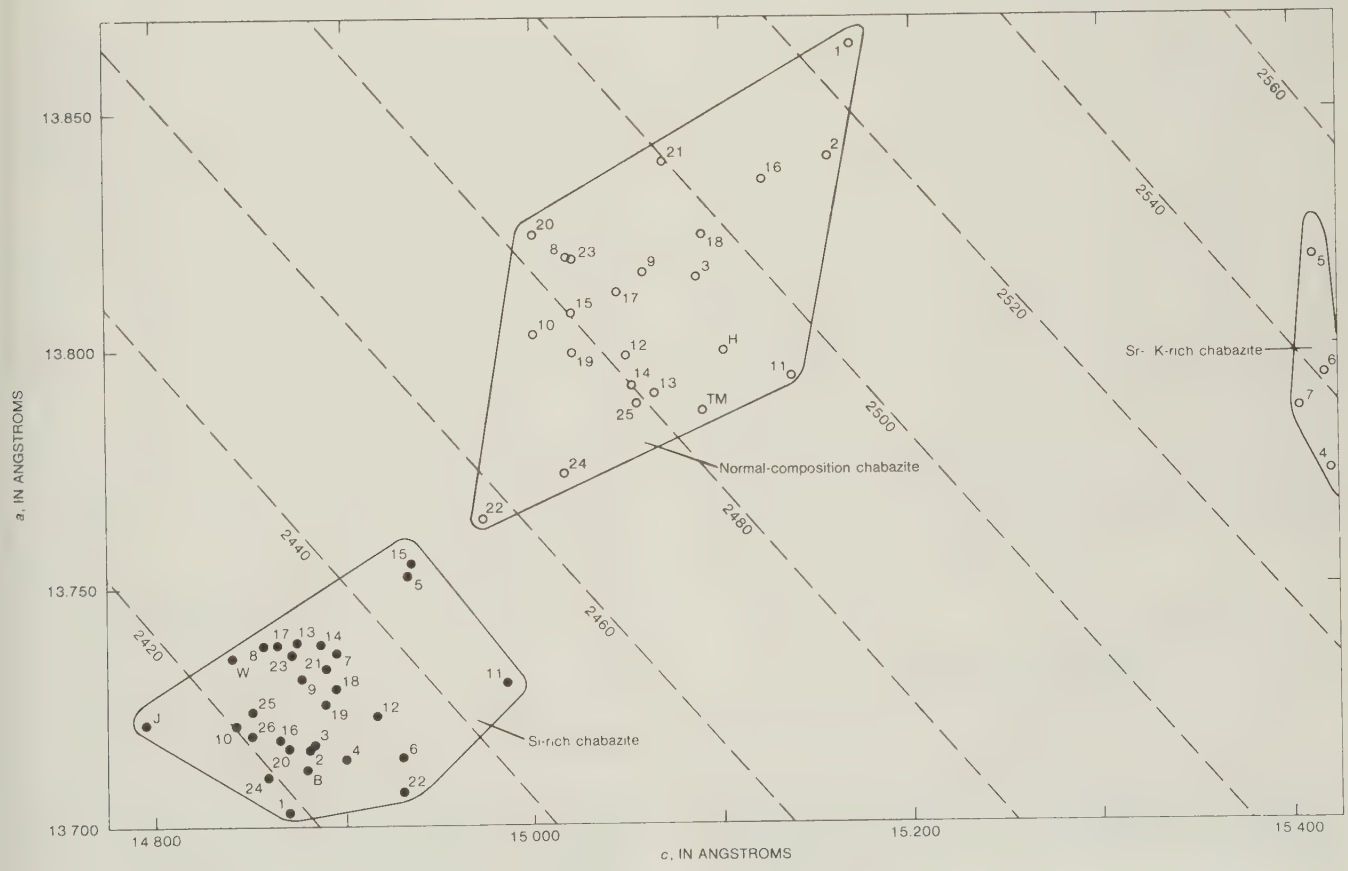

FIGURE 6.—Chabazite unit-cell variations related to differences in origin and composition. Open circles, chabazite from igneous rocks (numbers refer to Passaglia, 1970); TM, Table Mountain, Colo., and H, herschellite (from Gude and Sheppard, 1966). Filled circles, chabazite from tuffs in sedimentary rocks (numbers are from table 2); B, Barstow, Calif. (Gude and Sheppard, 1966); J, John Day, Oreg. (Sheppard and Gude, 1970); W, Wikieup, Ariz. (Sheppard and Gude, 1973). Dashed slanting lines (contours) represent volume in A^3.

Sheppard, R. A., and Gude, A. J., 3d, 1970, Calcic siliceous chabazite from the John Day Formation, Grant County, Oregon, *in* Geological Survey research 1970: U.S. Geol. Survey Prof. Paper 700–D, p. D176–D180.

———1973, Zeolites and associated authigenic silicate minerals in tuffaceous rocks of the Big Sandy Formation, Mohave County, Arizona: U.S. Geol. Survey Prof. Paper 830, 36 p.

———1975, Distribution of zeolites in Pliocene lacustrine rocks, Durkee basin, Baker County, Oregon: Geol. Soc. America Abs. with Programs, v. 7, no. 3, p. 374.

Sheppard, R. A., Gude, A. J., 3d, and Edson, G. M., 197 Bowie zeolite deposit, Cochise and Graham Countie Arizona, *in* Zeolite '76, Internat. Conf. on the Occu rence, Properties, and Utilization of Natural Zeolite Tucson, June 6–14, 1976, Programs and abs.: p. 73–9

Staples, L. W., 1957, X-ray study of erionite, a fibrou zeolite [abs.]: Geol. Soc. America Bull., v. 68, no. 2 p. 1847.

Staples, L. W., and Gard, J. A., 1959, The fibrous zeolit erionite; its occurrence, unit cell, and structure: Min eralog. Mag., no. 32, p. 261–281.

Jour. Research U.S. Geol. Survey
Vol. 6, No. 4, July–Aug. 1978, p. 473–482

DIFFERENTIATION OF THE SULFIDES IN THE BASAL ZONE OF THE STILLWATER COMPLEX, MONTANA

By NORMAN J PAGE and F. O. SIMON,
Menlo Park, Calif.

Abstract.—Chemical leaching and analysis of the sulfide portion of rocks from a section of the Basal zone of the Stillwater Complex demonstrate that mole fractions of nickel, copper, cobalt, and sulfur in the sulfides show trends and repeating patterns when plotted against stratigraphic position. These patterns are attributed to differentiation of immiscible sulfide liquids probably in response to differentiation of basaltic magma. Changes in composition of the immiscible sulfide liquids could most readily take place during the collection of the sulfide from the basaltic magma or during the crystallization of the sulfide liquid to the present assemblages of minerals.

Concentrations of monoclinic and hexagonal pyrrhotite, pentlandite, and chalcopyrite occur in the Basal zone of the Stillwater Complex, a stratiform mafic and ultramafic complex in southwestern Montana. The sulfide mineralization is comagmatic with the deposition of the silicates, and the sulfides were derived by settling, coalescence, and concentration of immiscible sulfide liquids from the basaltic parent magmas of the complex (Page, 1977a, b; unpub. data, 1971). The presence of immiscible sulfide liquids within a differentiating basaltic magma suggests that the sulfide liquids should also differentiate in response to the changing chemical and physical parameters of the basaltic magma if equilibrium is approached between the two liquids. Moreover, MacLean (1974) has shown that metallic elements enter the sulfide liquid in the following order: nickel, copper, cobalt, lead, and zinc. This report explores possible differentiation of sulfide liquids in the Basal zone through the study of a complete drill core section from the Mountain View area along the Stillwater River.

A meaningful study of differentiation in the sulfide liquid requires (1) a method for isolating and determining the bulk chemical composition of the sulfide portion and (2) an adequate sample of the sulfide portion of silicate rock that represents the composition of the immiscible sulfide liquids. Descriptions of mineralization and mapping by Howland (1933), Howland, Peoples, and Sampson (1936), Roby (1949), Peoples, Howland, Jones, and Flint (1954), Dayton (1971), Page, Simons, and Dohrenwend (1973a, b), Page and Dohrenwend (1973), Page and Nokleberg (1974), and Page (1977a, b) show that the sulfide concentrations occur as (1) disseminated blebs in silicate rock with no electrical continuity between blebs, (2) a dispersed sulfide network with electrical continuity that forms a matrix for silicate minerals, and (3) massive sulfide rocks with more than 65 percent sulfide. Although all three categories may represent different sulfide liquid compositions, network and massive sulfide rocks are difficult to sample because of their variable lateral and vertical extent and because the local bulk composition within any single continuous sulfide mass may have been changed by diffusion or differentiation by removal of crystalline solids. Disseminated sulfide blebs may more nearly represent initial sulfide liquid compositions, and samples of them are easy to obtain from the Basal zone. Because of the stratigraphic control given by the stratiform complex, such samples may be placed in an inferred relative time sequence and related to the overall geologic framework. This framework, including rock succession, petrology, metamorphism, structure, and geologic history of the complex and adjacent rocks, is based on Jackson (1961, 1967, 1968, 1969, 1970, 1971), Jones, Peoples, and Howland (1960), Hess (1960), and Page (1977a, b).

DESCRIPTION OF A MINERALIZED SECTION OF THE BASAL ZONE

Geologic context and silicate petrology

The Basal zone, which lies conformably below the Peridotite member of the Ultramafic zone, consists of two members, the Basal bronzite cumulate member and the Basal norite member (Page and Nokleberg, 1974). A columnar section based on core logging from drill

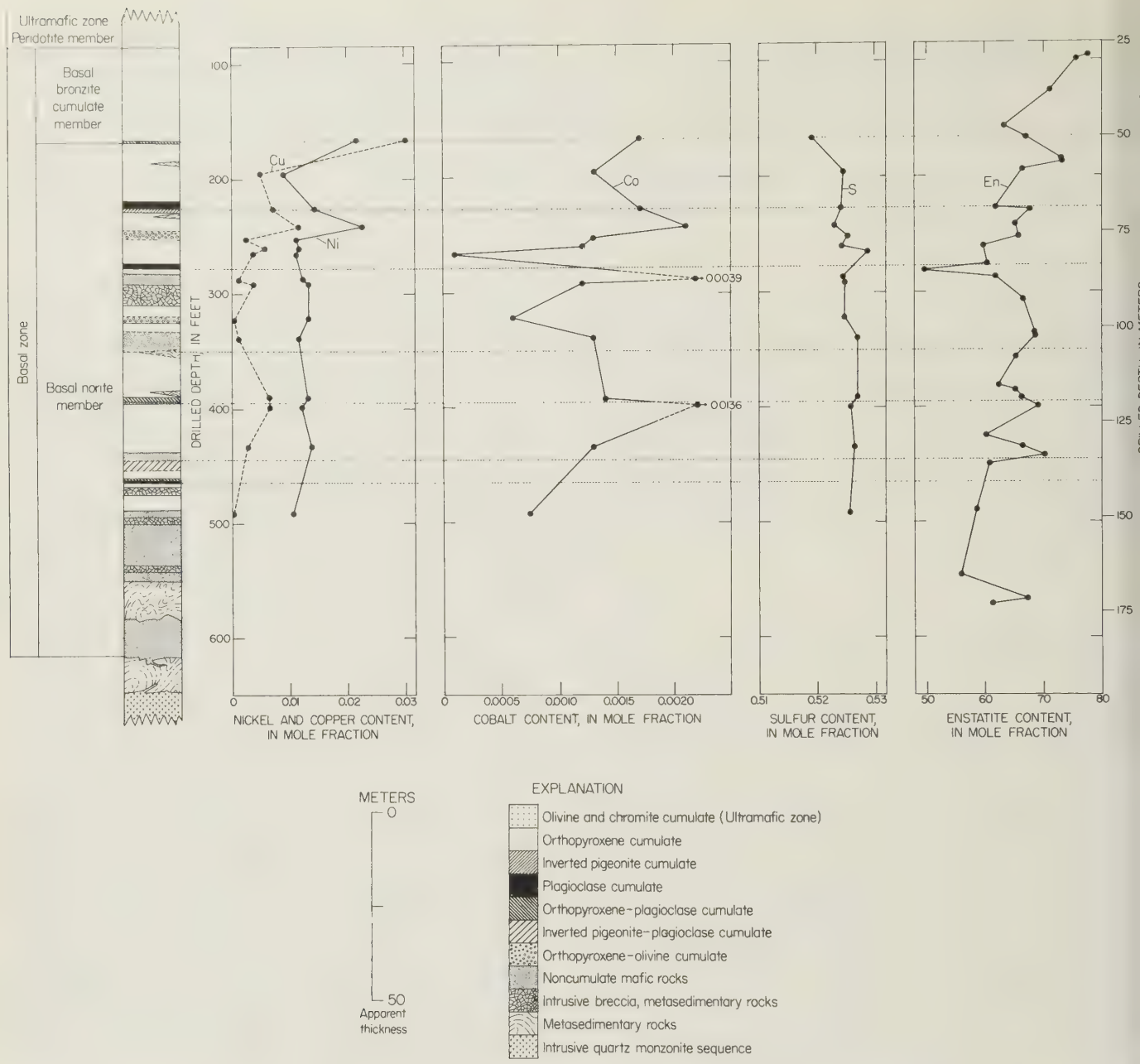

FIGURE 1.—Columnar section of rock types from drill hole M14 showing mole fractions of nickel, copper, cobalt, and sulfur and enstatite content of orthopyroxenes in Basal zone of Stillwater Complex in the Mountain View area. Dotted lines represent possible subdivision of Basal zone on basis of repeating patterns of orthopyroxene compositions and cumulate units.

hole M14 in the Mountain View area[1] shows this subdivision (fig. 1). The Basal zone rocks intruded metasedimentary rocks that are now cordierite+orthopyroxene+plagioclase+biotite±quartz hornfels and were in turn intruded by a sequence of quartz monzonites (Page and Nokleberg, 1972).

There are two main textural types of igneous rock in the Basal zone, and the compositional and physical properties of the two types form repeating patterns when correlated with stratigraphic position. One type consists of ophitic, subophitic, and ragged-textured (refers to the shape of interlocking crystals) rocks. These are considered to be of noncumulate origin—probably the result of rapid inplace crystallization of basaltic magma. The other textural type consists of

[1] The drill hole is vertical and located at coordinates 499 010 N., 1 917 015 E. (in feet) of the Montana (south) Rectangular Grid, which appears on the Mount Wood 15-minute quadrangle and on the maps of Page and Nokleberg (1974).

mulate rocks (see Jackson, 1967, for terminology) at are subdivided on the basis of the cumulus inerals orthopyroxene, plagioclase, olivine, inverted geonite, and clinopyroxene.

Orthopyroxene is by far the most abundant widely stributed cumulus mineral in the Basal zone; X-ray terminations of orthopyroxene compositions (Himelberg and Jackson, 1967) may be compared with ie cumulus stratigraphy (fig. 1). From this comarison and on the basis of repeating patterns of thopyroxene compositions and the cumulate units, rther subdivision of the Basal zone is possible. See fig. 1.) Similar techniques (Page and others, 972) were used to subdivide units in an olivine umulate in the Peridotite member of the Ultramafic one in which abrupt changes in olivine grain size orrelated with variations in olivine composition, hromite grain size, proportions of cumulus and ostcumulus minerals, and concentrations of trace lements.

ulfide mineralogy

The proportion of visible sulfide minerals ranges rom almost 100 percent in some rocks to zero in thers. Pyrrhotite (both monoclinic and hexagonal), entlandite, and chalcopyrite are the major opaque inerals. Magnetite, ilmenite, and trace amounts of ersdorffite are also present. Hexagonal pyrrhotite is ie dominant sulfide, but it everywhere contains 0–20 percent by volume of fine lamellae of monolinic pyrrhotite (see Page, 1977a, b). Modes in 15 olished sections of the specimens analyzed in this tudy are 5.8 to 88.6 percent pyrrhotite, 0.3 to 11.4 ercent pentlandite, trace to 5.2 percent chalcopyrite, races of gersdorffite, trace to 1.2 percent magnetite nd ilmenite, and 26.8 to 93.1 percent silicate. Such alues do not represent the true range or the average ompositional variation of the Basal zone because ther samples have much greater variation in composiion, but the modes do give an indication of the ariation present.

Modes normalized to pyrrhotite, pentlandite, and halcopyrite show a fairly narrow range of ratios fig. 2A). Calculated molecular modes based on hemical analyses of the sulfides in the core are also lotted for comparison and show a similar distribution f ratios (fig. 2*B*). The agreement between the two atterns shows that either a modal or an analytical echnique may be used to find the proportions of the ulfide minerals present. Pyrrhotite appears in domiant proportions, and chalcopyrite and pentlandite re present in roughly equal proportions (fig. 2).

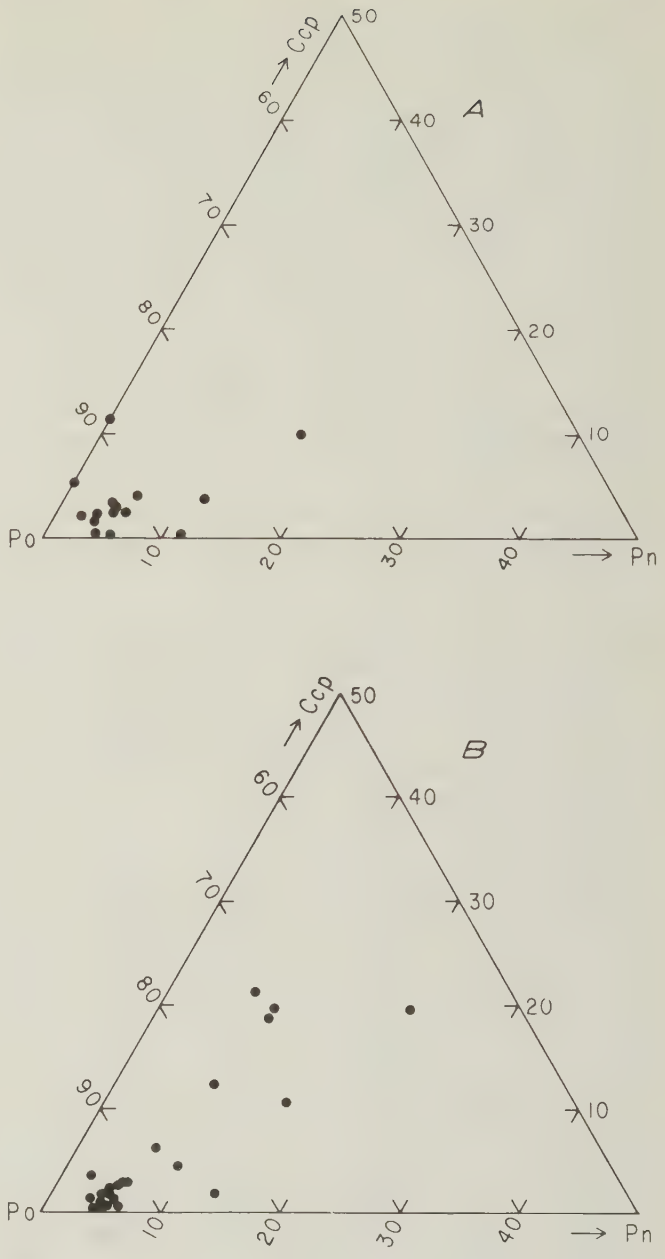

FIGURE 2.—Proportions of pyrrhotite (Po), pentlandite (Pn), and chalcopyrite (Ccp). *A*, Modes, volume percent. *B*, Mole percent calculated from chemical analyses.

Chemical data given by Roby (1949) and Dayton (1971) suggest similar proportions of chalcopyrite to pentlandite.

CHEMICAL COMPOSITION OF THE SULFIDE PORTION

Techniques

Two suites of samples were selected for study, one that covered the range of sulfide and silicate com-

positions in the Basal zone and could be used to develop a method to recover and analyze the sulfide portion, and the other from one cross section of the Basal zone in the Mountain View area (labeled M14) for studying the differentiation of the sulfide liquids. The samples in both suites consisted of 5 to 130 millimeters of a split half of a 50-mm-diameter core. Logging of the core and study of thin and polished sections were done before the crushing and chemical analysis.

Modal data are based on counting more than 1000 points in polished sections. Compositions of orthopyroxene were determined by using the X-ray method of Himmelberg and Jackson (1967) as developed specifically for Stillwater orthopyroxenes; the precision ranges from ± 0.05 to ± 3.0 mole percent and averages ± 0.51 mole percent enstatite ($Mg \times 100/\Sigma$ octahedral cations).

A chemical leach technique was chosen to extract the sulfide portion of the silicate rock because of the existence of fine-grained inclusions (Page, 1971) within silicate and oxide minerals and because fine projections of sulfide in silicate precluded mechanical separation of the silicate and sulfide fractions. Methods employing bromine and hydrochloric acid to leach the sulfide portion of silicate rocks have been used by Czamanske and Ingamells (1970) and Davis (1972). As a test of the application of these techniques to the sulfide portion of Basal zone rocks, a suite of 10 rocks covering a wide variation in silicate and sulfide proportions and compositions was selected and leached under the following conditions: a 1-gram sample was digested for 16 hours with 50 milliliters of 0.12 N hydrochloric acid and 1 ML liquid bromine at room temperature, and the excess bromine was extracted with carbon tetrachloride (method 1, table 1). The residues were removed by filtration before analyzing the solutions for iron, copper, nickel, cobalt, and in some samples manganese, lead, and zinc by atomic absorption spectroscopy. Sulfur content was determined by precipitation and weighing as barium sulfate (method 16, table 1).

Calculations using mineral compositions and these data yielded unsatisfactory results; therefore, various approaches were used to identify problems in the leaching technique. Sulfur was determined by X-ray fluorescence on the whole-rock sample by H. N. Elsheimer and L. F. Espos (method 5, table 1). Comparison of the barium-sulfate and X-ray techniques showed that either set of the sulfur values is acceptable. Conditions of the leaching experiments were varied in order to examine possible errors in leaching of iron, particularly leaching iron only from the sulfide fraction. Analyses for nickel and copper were made o some samples at the same time. The results are liste in table 1.

Analytical data for iron, nickel, copper, and sulfu (table 1) allow the leaching techniques to be evaluated Where duplicate analyses by methods 1 and 4 ar available, nickel and copper are within 14 percent o each other, suggesting that most of the nickel an copper sulfides were leached. Methods 2 and 3 indi cate that a small part of the nickel is acid soluble Methods 5 and 6, when combined with results fron 1 and 4, demonstrate that the nickel component of th sulfide rock is leached by methods 1 and 4.

As shown in table 1, the determination of iron i the sulfide portion is more difficult, and a variety o values is obtained dependent upon the specific sampl and the leaching technique. However, combining th copper, nickel, and sulfur to form chalcopyrite an pentlandite and using the excess sulfur to mak pyrrhotite with 47.6 atomic percent iron (compositio based on X-ray determinations of pyrrhotite) allow the calculation of iron in the sulfide fraction (metho 14). A comparison of calculated iron and leached iro determined by method 1 is shown in figure 3. Dat also are included from the second suite of samples Measured iron content in the sulfide portion may b either high or low when compared to calculated iro content. Data from methods 2, 3, 9, 10, 11, 12, and 1 demonstrate that in some of the samples part of th iron in the silicate rock is acid soluble, which ma account for high iron readings by using method 1 The two analyses showing less iron by method 1 ma result from the coprecipitation of iron with the bariu sulfate thus leading to a high value for sulfur. Thi precipitation would be a greater problem for thos samples with large amounts of iron. Small amount of both native sulfur and sulfate sulfur were de tected qualitatively although probably not in amount sufficient to explain the differences. These forms o sulfur are probably products of sample preparatio or possibly weathering. Inhomogeneous samples woul also explain the differences, but there were no othe indications throughout this study that inhomogeneit might be a problem.

Analytical data based on method 1 provide good representation of the composition of the sulfid portion of the rocks from the Basal zone, except fo the iron values. Because no satisfactory analytical wa to determine sulfide iron was found, in the followin discussions and calculations for the miscellaneou sample suite and for the suite labeled M14, analytica data from method 1 are used along with iron calculate by distribution of the other elements.

BLE 1.—*Comparison of analytical methods for iron, nickel, copper and sulfur for a variety of samples from the Basal zone*

alysts: Methods 1-5, 8-14, 16; F. O. Simon. Method 6; Harry Bastron. Method 7; R. E. Mays and Chris Heropoulos. Method 15; H. N. Elsheimer and L. F. Espos. -- = not determined]

mple mber	BB-7/ 850	BB-7/ 618	BB-3/ 317	BB-3/ 204.3	BB-3/ 259	BB-3/ 215	387-339/ 228	BB-3/ 352	387-336/ 385	M14/ 491.5
thod[1]	Fe determinations in weight percent									
1	3.02	0.24	1.60	2.63	2.22	1.17	11.6	26.8	34.4	34.8
2	2.30	--	.74	.39	.40	.36	.67	--	--	--
3	2.28	--		--	--	--	.71	--	--	--
4	--	--	--	--	--	--	--	26.6	43.2	41.2
5	--	--	--	--	--	--	--	6.16	4.50	3.35
8	--	--	--	--	--	--	--	43.52	52.02	52.72
9	5.47	--	--	--	--	--	--	--	--	--
10	2.11	--	--	--	--	--	--	--	--	--
11	2.39	--	--	--	--	--	--	--	--	--
12	2.21	--	--	--	--	--	--	--	--	--
13	3.07	--	--	--	--	--	--	--	--	--
14	1.60	.15	1.01	2.76	2.33	.94	11.04	32.7	53.8	53.8
	Ni determinations in weight percent									
1	0.060	0.0095	0.12	0.13	0.18	0.057	1.12	0.87	1.01	1.17
2	.0042	--	.0063	.0098	.0021	.0025	.013	--	--	--
3	.0060	--	--	--	--	--	.014	--	--	--
4	--	--	--	--	--	--	--	.83	1.15	1.21
5	--	--	--	--	--	--	--	.029	.12	.18
6	.03	.05	.05	.05	.07	.05	.05	.03	1.5	1.5
7	.10	.15	.15	.10	.15	.10	1.0	.50	1.0	1.5
	Cu determinations in weight percent									
1	0.056	0.019	0.135	0.370	0.270	0.109	0.717	0.232	0.346	0.17
4	--	--	--	--	--	--	--	.20	.36	.15
5	--	--	--	--	--	--	--	.0080	.015	.0080
6	.0007	.00015	.0050	.0005	.0030	.0010	.0030	.0100	.15	.070
7	.05	.02	.15	.30	.20	.07	.70	.13	.50	.15
	S determinations in weight percent									
15	1.06	0.82	0.78	2.06	--	0.69	--	19.58	30.1	31.18
16	.97	.10	.71	1.84	1.43	.62	7.48	19.28	31.50	31.43

[1]Method 1: 1 g sample, digested 16 h with 50 mL of 0.12 *N* HCl + 1mL Br_2 (liq) at room temperature; excess $_2$ extracted with CCl_4.
Method 2: 1 g sample, digested 16 h with 50 mL of 0.12 *N* HCl at room temperature.
Method 3: 1 g sample, digested 16 h with 50 mL of 0.12 *N* HCl at room temperature in purged Ar solution d in Ar atmosphere.
Method 4: 1 g sample, digested 16 h with 50 mL of 0.12 *N* HCl + 1 mL Br_2 (liq) on a water bath, excess $_2$ removed by heating.
Method 5: Undissolved residue from method 4 digested 16 h with concentrated HNO_3 on a water bath.
Method 6: Semiquantitative six-step spectrographic analysis of residue from method 1.
Method 7: Semiquantitative six-step spectrographic analysis of whole-rock sample.
Method 8: Sample fused with Na_2O_2, leached with H_2O, and total Fe determined volumetrically with $K_2Cr_2O_7$.
Method 9: 1 g sample, digested 16 h with 50 mL of 0.24 *N* HCl + 1 mL Br_2 (liq) at room temperature.
Method 10: 1 g sample, digested 16 h in 50 mL of H_2O + 1 mL Br_2 (liq) at room temperature. No HCl added.
Method 11: 1 g sample treated as in method 10, except 1 mL of concentrated HCl added just before filtering sidue.
Method 12: 1 g sample, digested 16 h with 50 mL of 0.012 *N* HCl + 1mL Br_2 (liq).
Method 13: 1 g sample, digested 16 h with 50 mL of 0.12 *N* HCl.
Method 14: Calculated Fe to satisfy balance with S, Ni, Cu, and Co.
Method 15: Sulfur determined by X-ray fluorescence on whole sample.
Method 16: Sulfur determined by precipitation and weighing as $BaSO_4$.

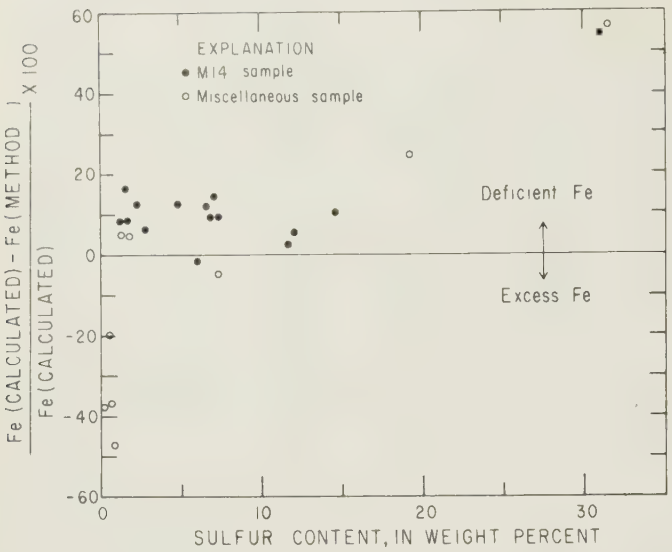

FIGURE 3.—Percentage difference between calculated iron content and iron content determined by method 1 of table 1 plotted against sulfur content.

Analytical results

Chemical data for the sulfide portion of the two suites of samples are given in table 2. The selected samples range in sulfur content from 0.10 to 31.5 percent. Samples of the sulfide portion vary in metal-to-sulfur ratios as well as in nickel-to-iron and nickel-to-copper ratios, as would be expected from the modal data. Lead, zinc, and manganese occur in minor amounts in the sulfide portion; cobalt is the only other metal present in significant amounts besides copper, nickel, and iron.

Variation in proportions of copper, nickel, and iron in the sulfide fraction is illustrated in terms of mole percent chalcopyrite, pentlandite, and pyrrhotite (fig. 2*B*). Except for a suggested 1:1 ratio of chalcopyrite to pentlandite, no trends are apparent. Cobalt contents of the sulfide fraction are related to the copper-nickel ratio; samples with more nickel contain more cobalt (fig. 4). Modes counted on polished sections show that gersdorffite is present (less than 1 percent) and could account for most of the cobalt in the richer samples. Where gersdorffite is not present, cobalt is inferred to occur in the pentlandite because of the correlation with nickel (fig. 4). The lead content of the sulfide fraction (table 2) is below the limit of determination, except in the samples with the most sulfides, for which values ranged from 22 to 76 ppm (parts per million). Zinc was found in most samples and ranged from less than 10 to 73 ppm. Both lead and zinc content tend to increase with sulfur content of the samples, whereas manganese has a more i regular distribution pattern.

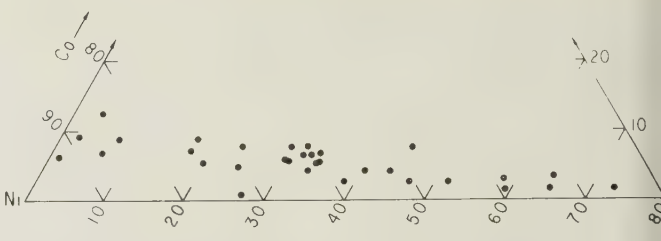

FIGURE 4.—Proportions of cobalt, copper, and nickel in sulfi fraction plotted in terms of normalized weight percent.

INTERPRETATION OF SULFIDE GENESIS IN THE BASAL ZONE

Immiscibility, coalescence, and collection

Sulfide-oxide immiscible liquids were present in th Stillwater magma very early in the intrusive histor of the Basal zone and throughout most of the depos tion of the lower part of the complex. Geologi evidence given by Page (1977a) for the early presenc of sulfide-oxide liquids includes (1) massive sulfid rocks with irregular and tabular shapes intruded b and into ophitic-textured noncumulate rocks, (2) in trusive breccias consisting of hornfels fragments i a massive sulfide rock matrix, and (3) fine polymine alic inclusions of sulfide minerals in the centers o some of the cumulus silicate and oxide phases from th lower part of the Basal zone.

Calculations of sulfide capacity (Haughton an others, 1974), which is (1) an empirical property o silicate melt, (2) a function of the fugacity of oxyge and sulfur, and (3) the weight percent sulfur dissolve in the melt, suggest that under the inferred geologi conditions the Stillwater magma could not dissolv the amounts of sulfur present and, therefore, som sulfur was present as an immiscible liquid. Suc calculations assume that the bulk compositions o noncumulate igneous-textured rocks (Page, 1977a represent the magma composition and that the equa tions given by Haughton, Roeder, and Skinner (1974 apply to natural magmas. The geologic (Page, 1977a and experimental (Haughton and others, 1974) evi dence suggests that the most likely mechanisms fo the development of immiscible sulfide melts involv decreases in the FeO activity of the basaltic magma

Immiscible sulfide liquid, once formed, must hav accumulated in the magma chamber by gravitationa settling. Moreover, the geologic evidence suggests tha this was an extremely rapid process and that initiall small immiscible droplets collected into droplets larg

BLE 2.—*Chemical analyses of the sulfide portions, pyrrhotite compositions, calculated mole percentages of sulfide minerals, and modes in volume percent of samples from the Basal zone of the Stillwater Complex*

alyst: F. O. Simon; hpo = hexagonal pyrrhotite, atomic percent determined by X-ray diffraction (Arnold and Reichen, 1962); Tr. = trace; -- = not determined. Weight percent data determined by method 1]

	BB-3/ 204.3	BB-3/ 215	BB-3/ 259	BB-3/ 317	BB-3/ 352	BB-7/ 618	BB-7/ 850	387-339 228	387-336 385	M14/ 166	M14/ 194	M14/ 226
Weight percent												
----------	2.63	1.17	2.22	1.60	26.8	0.24	3.02	11.6	34.4	2.94	4.31	2.36
----------	.13	.057	.18	.12	.87	.0095	.06	1.10	1.01	.18	.12	.088
----------	.370	.109	.270	.135	.232	.019	.056	.717	.346	.27	.057	.046
----------	.0082	.0029	.0064	.0069	.0615	<.0010	.0090	.0518	.0710	.0139	.0139	.0103
----------	0016	.0011	<.0010	.0013	.0073	<.0010	.0016	.0031	.0061	--	--	--
----------	<.0020	<.0020	<.0020	<.0020	.0076	<.0020	.0022	.0032	.0052	--	--	--
----------	.0064	.0048	.0079	.0072	.0096	.0026	.0265	.0079	.0079	--	--	--
----------	1.84	.62	1.43	.71	19.28	.10	.97	7.48	31.50	2.34	3.01	1.71
ole-rock Fe --------	--	--	--	--	43.52	--	--	--	52.02	10.8	16.8	13.5
omic percent	--	--	--	--		--	--	--	--	--	--	--
metals hpo ---------	--	--	47.38	--	47.25	--	--	--	--	--	--	47.61
Normalized mole percent of mineral phase												
alcopyrite ---------	21.1	18.4	2.0	19.7	1.3	19.6	6.1	10.0	1.2	12.1	2.0	2.9
ntlandite ----------	7.6	9.8	13.5	21.3	4.9	10.0	6.7	15.7	3.5	8.3	3.6	5.5
rrhotite (47.63%Fe)-	71.4	71.8	84.5	58.9	93.8	70.4	87.3	74.3	95.3	79.6	94.4	91.6
Normalized mode in volume percent												
alcopyrite ---------	--	--	--	--	--	--	--	--	--	2.5	Tr.	4.1
ntlandite ----------	--	--	--	--	--	--	--	--	--	4.8	11.4	5.9
rrhotite -----------	--	--	--	--	--	--	--	--	--	92.7	88.6	90.0

	M14/ 214.5	M14/ 253.5	M14/ 260	M14/ 265.5	M14/ 287.5	M14/ 292.5	M14/ 322.3	M14/ 339.5	M14/ 391	M14/ 398	M14/ 434.5	M14/ 491.5
Weight percent												
----------	1.87	8.96	17.5	9.22	6.43	17.4	9.42	9.86	9.01	2.06	19.8	34.8
----------	.11	.26	.48	.27	.21	.56	.28	.43	.33	.072	.70	1.17
----------	.061	.062	.26	.10	.071	.057	.013	.031	.17	.041	.16	.017
----------	.0100	.0312	.0485	.0028	.0235	.0530	.0410	.0340	.0335	.0080	.0650	.810
----------	--	--	--	--	--	--	--	--	--	--	--	.0046
----------	--	--	--	--	--	--	--	--	--	--	--	.0041
----------	--	--	--	--	--	--	--	--	--	--	--	.0046
----------	1.39	6.68	11.82	6.81	4.85	12.12	6.10	7.28	7.09	1.68	14.71	31.43
ole-rock Fe --------	14.9	21.9	29.8	21.1	17.7	27.4	20.6	20.0	21.1	14.1	33.2	52.72
omic percent												
metals hpo ---------	--	47.59	47.51	47.60	47.64	47.58	--	47.67	47.67	--	47.66	47.66
Normalized mole percent of mineral phase												
alcopyrite ---------	4.6	1.0	2.3	1.6	1.6	0.5	0.2	0.5	2.7	2.8	1.2	0.1
ntlandite ----------	8.6	4.2	4.4	4.3	4.7	5.0	5.0	6.4	5.4	5.1	5.4	4.0
rrhotite (47.63%Fe)-	86.8	94.8	93.3	94.1	93.7	94.5	94.8	93.1	91.8	92.9	93.4	95.9
Normalized mode in volume percent												
alcopyrite ---------	3.6	3.0	3.3	0.6	1.4	16.8	Tr.	0.4	2.5	0.3	2.2	--
ntlandite ----------	11.6	4.8	4.1	4.2	3.6	10.0	5.0	11.4	5.6	5.5	3.6	--
rrhotite -----------	84.7	92.2	92.6	95.2	95.0	73.2	95.0	88.1	91.9	94.1	94.1	--

ough to settle rapidly. Under the prevailing vis-ity and temperature conditions, the sulfide droplets uld have collected before silicates settled and ac-nulated or before some of the noncumulate igneous rocks crystallized. One attractive model involving growth, collision, and coalescence in a manner similar to that of raindrops can account adequately for the concentration of sulfide-oxide immiscible liquids (Page,

1977b). Disseminated sulfide would represent immiscible liquid droplets that were trapped in place. The disseminated sulfides should therefore approximate the compositions of sulfide liquids in equilibrium with the basaltic melt at the time they were trapped.

Differentiation of sulfide liquids

Examination of the chemical analyses (table 2) and data given by Roby (1949) and Page (1971) suggests that the variations in metal and sulfur content may correlate with stratigraphic position. In addition, Roby's data suggest repetitive or cyclic patterns of copper and nickel contents correlative with stratigraphic positions. One way to normalize each analysis of the sulfide portion of the rock is to calculate mole fractions. Variation in the mole fractions of nickel, copper, cobalt, and sulfur in the sulfide portion of the data shows that the mole fraction of sulfur decreases from the bottom to the top of the Basal zone section whereas the mole fractions of copper, nickel, and cobalt tend to increase upward in the section; closer examination of the trends shows a more complex pattern (fig. 1). This pattern, best illustrated by cobalt, consists of increases and decreases superimposed on a general trend. Trends of changes in orthopyroxene compositions (fig. 1) in the Basal zone rocks show repetitive patterns when compared with stratigraphic position. In general, orthopyroxenes are richer in iron at the base and richer in magnesium toward the top of the Basal zone. Superimposed on this general trend are six repetitive smaller scale units in which the orthopyroxene compositions also change in the same sense (fig. 1). Comparing the patterns of cobalt, copper, nickel, and sulfur mole fractions with orthopyroxene compositional cycles suggests a correlation.

The distribution patterns of metals in the Basal zone could be due either to partitioning of metals at liquidus temperatures between basaltic magma and immiscible sulfide liquid or to subsolidus partitioning between sulfide phases and silicate phases as suggested by Clark and Naldrett (1972), or to a combination of both processes. To evaluate the partitioning problem completely, it is necessary to know the basaltic magma composition associated with each sulfide mass and to know the partitioning factors of the magma-silicate minerals. Individual magma compositions are not and may not be known with sufficient accuracy to evaluate this problem, but limited information is available on the silicate compositions. Unpublished pyroxene compositions (E. D. Jackson, oral commun., 1969) show that NiO, CuO, and CoO occur in proportions of between 0.001 and 0.01 percent. Of the other min als in the Basal zone samples examined, only t iron-titanium-chromium oxides are present in amou large enough effectively to control the metal distrib tion of the sulfides. However, the close correlation metal and sulfur mole fractions with other propert that are primarily controlled by magmatic ever suggests that the repeating patterns of the sulf portion may have the same controls. Therefore, t analytical data given for the sulfide portion of t Basal zone probably represent the effects of basal magma differentiation on the differentiation of sulf metal.

Application of phase equilibria to the lower tempe ture equilibration of the sulfide minerals

The immiscible sulfide-oxide liquids began to cryst lize after they collected in the Basal zone rocks a temperatures fell below about 1150°C. Experimen studies by Kullerud, Clark, Craig, Sherman, a Naldrett on the iron-nickel-sulfur system, summariz and reexamined by Misra and Fleet (1973), and Naldrett (1969) on part of the iron-sulfur-oxi system form the basis for modeling the crystallizati history. The liquidus surface in the pyrrhotite porti of the iron-sulfur-oxide system (Naldrett, 1969) su gests that the immiscible sulfide-oxide liquids beg to crystallize at about 1150°C, given the amount magnetite associated with the sulfide concentratio The first solid to separate would contain little or oxides, but as crystallization proceeded, the residu liquid would become enriched in oxides. As pointed o by Naldrett's (1969) analysis, this model depends up the sulfide-oxide liquid reaching and maintaini equilibrium with respect to oxygen during crystalli tion with the basaltic magma. The sparsity of magn tite and variable magnetite content of the sulfide co centrations suggest, however, that equilibrium betwe the two liquids with respect to oxygen may not ha been reached and maintained throughout crystalli tion.

The first solid to crystallize from the immiscib sulfide melt would have been a nickel-copper-cob pyrrhotite solid solution. From about 1150°C to as l as 1050°C, a nickel-copper-cobalt pyrrhotite so solution and liquid would be present. The range sulfide analyses was plotted on an iron-nickel-sulf graph at 1100°C with the phase boundaries determin by Kullerud, Yund, and Moh (1969) and Naldrett a Gasparrini (1971) (fig. 5*A*). Solidification of the s fide-oxide liquid would continue, and if the sulf mass were isolated with respect to oxygen diffusi

om the basaltic magma and pyrrhotite, the solid ution would contain magnetite. Alternately, if not lated from diffused oxygen, the solidification oduct would contain no magnetite. After solidifica-n, exsolution of pentlandite and chalcopyrite from e nickel-copper-cobalt pyrrhotite solid solution uld take place below 600°C depending primarily on e nickel, copper, and sulfur content (Craig and llerud, 1969). The sulfide analyses were plotted on iron-nickel-sulfur graph with the pentlandite solvi termined by Naldrett, Craig, and Kullerud (1967) perimposed (fig. 5*B*). From this plot, one would spect that pentlandite exsolution began at about 0°C or lower. We believe from the textural evidence d from comparison with other similar deposits that e blocky pentlandite necklaces and flame textures in rticular are most likely the product of exsolution. According to Misra and Fleet's (1973) study, the mpositions of the phases would continue to adjust temperature decreased. The low nickel content of e pyrrhotite (Page, 1972) suggests that equilibra-on continued below 230°C (see Misra and Fleet, 73, p. 531). Both hexagonal and monoclinic pyrrho-e are considered stable phases below about 230°C Misra and Fleet, 1973), and it appears that the esent mineral assemblages and compositions reflect w-temperature subsolidus approaches to equilibri-n. The sulfide bulk compositions, however, may re-ct the compositions of the immiscible sulfide liquids.

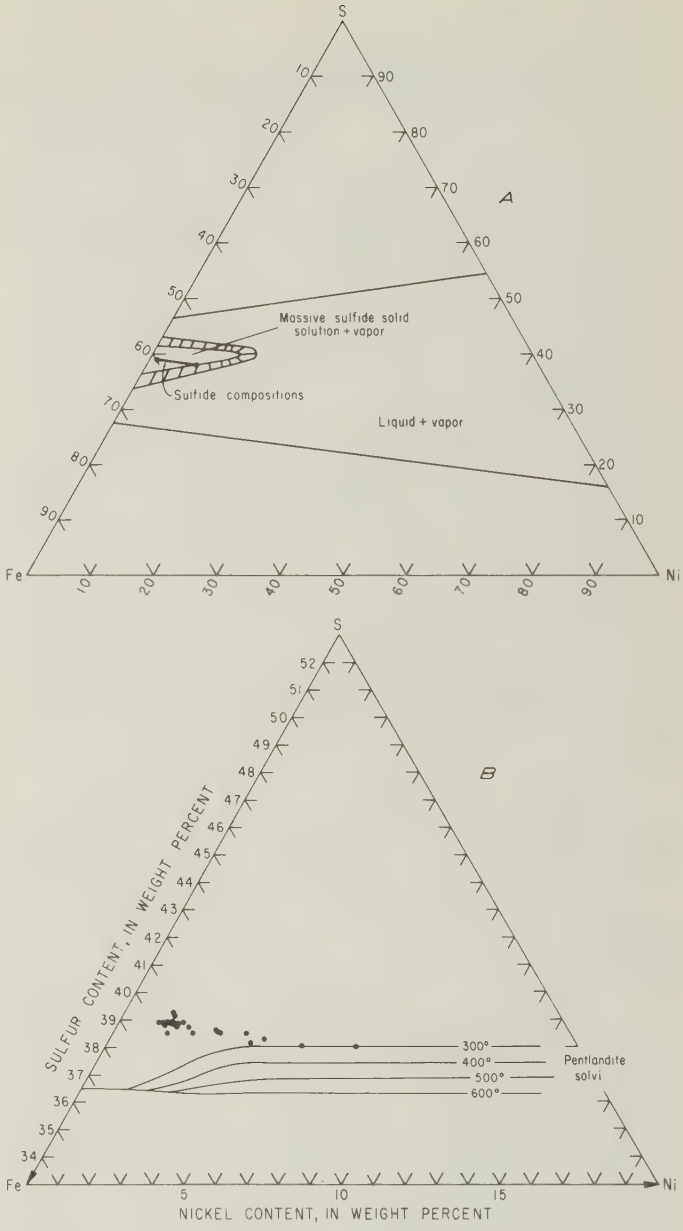

FIGURE 5.—Iron, nickel, and sulfur compositions of sulfide fraction. *A*, Weight percent iron, nickel, and sulfur at 1,100°C with phase relations from Kullerud, Yund, and Moh (1969) and Naldrett and Gasparrini (1971) superimposed. *B*, Part of the iron, nickel, and sulfur triangular diagram with pentlandite solvi from Naldrett, Craig, and Kullerud (1967) superimposed showing compositions of the sulfide fraction in weight percent.

REFERENCES CITED

hold, R. G., and Reichen, L. E., 1962, Measurement of the metal content of naturally occurring, metal-deficient, hexagonal pyrrhotite by an X-ray spacing method: Am. Mineralogist, v. 47, p. 105–111.

rk, T., and Naldrett, A. J., 1972, The distribution of Fe and Ni between synthetic olivine and sulfide at 900°C: Econ. Geology, v. 67, no. 7, p. 939–952.

ig, J. R., and Kullerud, Gunnar, 1969, Phase relations in the Cu-Fe-Ni-S system and their application to magmatic ore deposits, *in* Wilson, H. D. B., ed., Magmatic ore deposits, a symposium: Econ. Geology Mon. 4, p. 344–358.

manske, G. K., and Ingamells, C. O., 1970, Selective chemical dissolution of sulfide minerals—A method of mineral separation: Am. Mineralogist, v. 55, p. 2131–2134.

vis, C. E. S., 1972, Appendix—Analytical methods used in study of an ore intersection from Lunnon Shoot, Kambalda: Econ. Geology, v. 67, no. 8, p. 1091–1092.

yton, Stan, 1971, Hot air over Stillwater, profile of a hearing on mineral entry: Eng. and Mining Jour., v. 172, no. 10, p. 75–84.

ughton, D. R., Roeder, P. L., and Skinner, B. J., 1974, Solubility of sulfur in mafic magmas: Econ. Geology, v. 69, no. 4, p. 451–467.

Hess, H. H., 1960, Stillwater igneous complex, Montana—A quantitative mineralogical study: Geol. Soc. America Mem. 80, 230 p.

Himmelberg, G. R., and Jackson, E. D., 1967, X-ray determinative curve for some orthopyroxenes of composition Mg_{48-85} from the Stillwater Complex, Montana, *in* Geo-

logical Survey research 1967: U.S. Geol. Survey Prof. Paper 575–B, p. B101–B102.

Howland, A. L., 1933, Sulphides and metamorphic rocks at the base of the Stillwater Complex, Montana: Princeton, N.J., Princeton Univ., Ph. D. thesis, 76 p.

Howland, A. L., Peoples, J. W., and Sampson, Edward, 1936, The Stillwater igneous complex and associated occurrences of nickel and platinum metals: Montana Bur. Mines and Geology Misc. Contr., v. 7, 15 p.

Jackson, E. D., 1961, Primary textures and mineral associations in the ultramafic zone of the Stillwater Complex, Montana: U.S. Geol. Survey Prof. Paper 358, 106 p.

———1967, Ultramafic cumulates in the Stillwater, Great Dyke, and Bushveld intrusives, *in* Wyllie, P. J., ed., Ultramafic and related rocks: New York, John Wiley & Sons, p. 20–38.

———1968, The chromite deposits of the Stillwater Complex, Montana, *in* Ore deposits of the United States, 1933–1967 (Graton-Sales Volume), V. 2: New York, Am. Inst. Mining, Metall., and Petroleum Engineers, p. 1495–1510.

———1969, Chemical variation in coexisting chromite and olivine in chromite zones of the Stillwater Complex, *in* Wilson, H. D. B., ed., Magmatic ore deposits, a symposium: Econ. Geology Mon. 4, p. 41–71.

———1970, The cyclic unit in layered intrusions—A comparison of repetitive stratigraphy in the ultramafic parts of the Stillwater, Muskox, Great Dyke, and Bushveld complexes: Geol. Soc. South Africa Spec. Pub. 1, p. 391–424.

———1971, The origin of ultramafic rocks by cumulus processes: Fortschr. Mineralogie, v. 48, p. 128–174.

Jones, W. R., Peoples, J. W., and Howland, A. L., 1960, Igneous and tectonic structures of the Stillwater Complex, Montana: U.S. Geol. Survey Bull. 1071–H, p. 281–335.

Kullerud, Gunnar, Yund, R. A., and Moh, G. H., 1969, Phase relations in the Cu-Fe-S, Cu-Ni-S, and Fe-Ni-S systems, *in* Wilson, H. D. B., ed., Magmatic ore deposits, a symposium: Econ. Geology Mon. 4, p. 323–343.

MacLean, W. H., 1974, Base metal partitioning in sulfide-silicate melt: Geol. Soc. America Abs. with Programs, v. 6, no. 7, p. 854.

Misra, K. C., and Fleet, M. E., 1973, The chemical compositions of synthetic and natural pentlandite assemblages: Econ. Geology, v. 68, no. 4, p. 518–539.

Naldrett, A. J., 1969, A portion of the system Fe-S-O between 900 and 1080°C and its application to sulfide ore magmas: Jour. Petrology, v. 10, p. 171–201.

Naldrett, A. J., Craig, J. R., and Kullerud, Gunnar, 1967, The central portion of the Fe-Ni-S system and its bearing on pentlandite exsolution in iron-nickel sulfide ores: Econ. Geology, v. 62, no. 6, p. 826–847.

Naldrett, A. J., and Gasparrini, E. L., 1971, Archaean nick sulfide deposits in Canada—Their classification, geolog setting and genesis with some suggestions as to explor tion: Geol. Soc. Australia Spec. Pub. 4, p. 201–226.

Page, N. J, 1971, Sulfide minerals in the G and H chron tite zone of the Stillwater Complex, Montana: U. Geol. Survey Prof. Paper 694, 20 p.

———1972, Pentlandite and pyrrhotite from the Stillwat Complex Montana—Iron-nickel ratios as a function associated minerals: Econ. Geology, v. 67, p. 814–820.

———1977a, Stillwater Complex, Montana—Structure, mi eralogy, and petrology of the Basal zone with emphasis the occurrence of sulfides: U.S. Geol. Survey Prof. Pap 1038. [In press]

———1977b, Stillwater Complex, Montana—Rock successio metamorphism, and structure of the complex and adjace rocks: U.S. Geol. Survey Prof. Paper 999, 79 p.

Page, N. J, and Dohrenwend, J. C., 1973, Mineral resour potential of the Stillwater Complex and adjacent roc in the northern part of the Mt. Wood and Mt. Dougl quadrangles, southwestern Montana: U.S. Geol. Surv Circ. 684, 9 p.

Page, N. J, and Nokleberg, W. J., 1972, Genesis of mesozon granitic rocks below the base of the Stillwater Compl in the Beartooth Mountains, Montana, *in* Geological Surv research 1972: U.S. Geol. Survey Prof. Paper 800–I p. D127–D141.

———1974, Geologic map of the Stillwater Complex, Montan U.S. Geol. Survey Misc. Geol. Inv. Map I–797, sca 1:12 000, 5 sheets.

Page, N. J, Shimek, Richard, and Huffman, Claude, J 1972, Grain-size variations within an olivine cumulat Stillwater Complex, Montana, *in* Geological Survey search 1972: U.S. Geol. Survey Prof. Paper 800–C, C29–C37.

Page, N. J, Simons, F. S., and Dohrenwend, John, 1973 Reconnaissance geologic map of the Mt. Wood qua rangle, Montana: U.S. Geol. Survey Misc. Field Studi Map MF–491, scale 1:62 500.

———1973b, Reconnaissance geologic map of the Mt. Dougla quadrangle, Montana: U.S. Geol. Survey Misc. Fie Studies Map MF–488, scale 1:62 500.

Peoples, J. W., Howland, A. L., Jones, W. R., and Flin Delos, 1954, Geologic map, sections, and map of unde ground workings of the Mountain View Lake area, Sti water County, Montana: U.S. Geol. Survey open-fi report.

Roby, R. N., 1949, Investigations of copper-nickel deposits the Stillwater Complex, Stillwater and Sweetgra Counties, Montana: U.S. Bur. Mines Rept. Inv. RI–443 10 p.

Jour. Research U.S. Geol. Survey
Vol. 6, No. 4, July–Aug. 1978, p. 483–488

RECOGNITION OF OXIDIZED SULFIDE MINERALS AS AN EXPLORATION GUIDE FOR URANIUM

By RICHARD L. REYNOLDS and MARTIN B. GOLDHABER

Denver, Colo.

Abstract.—The difference in color between tan to red xidized sandstone and gray reduced sandstone on either ide of the reduction-oxidation (redox) interface, which is the ocus of uranium concentration in roll-type deposits, has een noted and used locally as an exploration guide within nown uranium districts. Reduced sandstone is characterized n many deposits by the presence of iron sulfide minerals particularly marcasite and pyrite) that occur as replacelents of and overgrowths on iron-titanium oxide minerals and lant debris and as cement of detrital grains. Oxidation of ne sulfides by oxygenated ground water forms yellow to red erric oxide and ferric hydroxide phases ("limonite") that eplace the FeS_2 minerals. Processes other than the oxidation f sulfides, however, can cause reddening of clastic sediments ithout the creation of a redox boundary, and so color alone s not a sufficient condition by which to judge the potential or uranium ore in frontier areas. Ferric oxides that form y the oxidation of iron sulfide minerals can be distinguished rom other forms of ferric oxide by reflection microscopic xamination of polished grain mounts and polished thin ections. Diagnostic features of oxidized sulfides are limonite seudomorphs of sulfides and limonite containing internal extures that mimic characteristic textures of previously sulidized detrital phases. Recognition of oxidized sulfides by eflection microscopy, then, can distinguish oxidized sandtones, which might have a redox boundary downdip and vhich would therefore be favorable hosts for uranium oncentration, from those without such potential.

Uranium associated with roll-type deposits is localed within the host beds near a reduction-oxidation redox) interface or roll front (for example, Klohn nd Pickens, 1970; Bailey, 1965; Melin, 1964; King nd Austin, 1966; Shawe and Granger, 1965; Granger nd Warren, 1969; Fischer, 1970; Rackley and others, 968; Harshman, 1968a; Adler, 1970). Sandstone ontaining oxidized iron phases bound within the ltered tongue behind the roll front is commonly drab, an, or orange to red in contrast to the gray color of reduced" sandstone ahead of the roll front. The ifference in color between the sediments of the diferent geochemical settings has been observed and uggested as an exploration guide locally within some uranium districts (Sharp and others, 1964; Davis, 1969; Bailey, 1965, 1969; Melin, 1969; Mrak, 1968; Rackley and Johnson, 1971; Harshman, 1962, 1968b; Fischer, 1970). The gray zones of reduced sandstone commonly contain iron sulfide minerals, particularly pyrite and marcasite. These sulfides form as individual anhedral to euhedral crysals and crystal aggregates, as interstitial cement, and as replacements of and overgrowths on detrital iron-titanium (Fe-Ti) oxide minerals (titanomagnetite and titanohematite) and fossil vegetal matter. Oxidation of iron sulfides to ferric oxides and hydroxide phases ("limonite") by oxygenated ground waters during the ore-forming episode imparts a drab yellow or orange to red coloration to the sediment. The concept that color differences reflect the disparite geochemical environments associated with uranium roll-type deposits and the chemistry of sulfide oxidation have been reviewed by Adler (1970, 1973), who further suggested that color differences might be used as an exploration guide for uranium in frontier areas.

Processes other than the oxidation of iron sulfides, however, can also cause reddening of clastic sediments. Walker (1967), for example, demonstrated that intrastratal alteration of detrital iron-bearing silicates and oxides is largely responsible for the red ferric oxide pigment in many red clastic sediments. Clay-sized ferric oxides deposited together with the larger grains is another potential source of red pigment in some sedimentary rocks (Van Houten, 1961, 1964). Obviously, color alone is not a sufficient criterion by which to judge the likelihood of finding uranium ore in sandstones.

It is important, then, as pointed out by Adler (1973), to develop criteria by which ferric oxides and hydroxides formed by the oxidation of iron sulfides can be distinguished from those having other origins. In this way, it should be possible in frontier areas to discriminate oxidized sediments with a redox boundary downdip, which, therefore, would be favorable for

uranium concentration, from those without such potential.

AREAS AND METHOD OF STUDY

We have examined mineralized formations of different ages from four uranium-producing districts. These are (1) the Morrison Formation (Upper Jurassic) in the Grants mineral belt, New Mexico, (2) the Wasatch Formation (Eocene) in the Powder River Basin, Wyo., (3) the Whitsett Formation (Eocene), Karnes County, Tex., and (4) the Catahoula Tuff (mid-Tertiary), Webb County, Tex. Each of these formations contains a roll-type ore body except the Morrison Formation, in which originally tabular ore has been redistributed into a roll by oxygenated ground waters. Samples were obtained adjacent to uranium deposits that are currently being mined or being considered for development. Although the completeness of the sample suite varied among the different deposits, each suite contains samples from oxidized rock behind the ore bodies and from reduced rock in front of the ore.

Ferric oxides formed by the oxidation of iron sulfides can best be recognized by viewing polished grain mounts and polished thin sections under reflected light. In this study, grains for polished sections were concentrated by heavy liquid, magnetic, or hand-picking techniques or by a combination of these. Polished thin sections of the whole rock are useful because they enable textural evaluation of limonite in relation to the framework grains but are disadvantageous because they do not represent a concentrated portion of limonitic phases. These methods are inexpensive and produce rapid analyses; however, they might be most advantageously used in combination with the exploration techniques already available.

IDENTIFICATION OF OXIDIZED IRON SULFIDE MINERALS

Limonite formed by the oxidation of sulfides can be distinguished from that formed by other processes by four especially diagnostic features. These are (1) limonite pseudomorphs after iron sulfide, (2) limonite formed from sulfidized Fe-Ti oxide minerals with the retention of characteristic textures of the original detrital grain, (3) characteristic internal textures in limonite indicative of oxidized sulfide cement, and (4) limonite formed by the oxidation of sulfidized plant debris. Not all of these distinguishing criteria are invariably present in any one deposit; nevertheless, in each of the deposits studied, oxidized iron sulfides have been recognized by at least two of these diagnostic features.

Unequivocal evidence of limonite formed by the oxidation of iron sulfide is seen in three of the four deposits examined: ferric oxide grains containing relicts of the precursor sulfide occur commonly in the host sandstone near the redox boundary. Although it is unlikely that these relationships are preserved in oxidized sandstone remote from the oxidation-reduction interface over a long period of time, observation of these grains near the redox boundary has been helpful in determining the genesis and textural significance of certain types of limonite.

The first criterion is best illustrated by the simple case in which a pyrite cube has been replaced by ferric oxide with preservation of the original shape. Pyrite in reduced rock of the Morrison Formation in the Grants mineral belt commonly occurs as cubes; limonite pseudomorphs of pyrite cubes are common in oxidized rock several kilometers behind the redistributed uranium ore (fig. 1*A*). Limonite "cubes" have been observed in the Morrison Formation not only in subsurface samples but also in the outcrop. It is not clear, however, whether the oxidized sulfide grains in the outcrop resulted from oxidative processes associated with the ore-forming episode or whether they are related to weathering. Pyrite cubes also occur in reduced rock of the Catahoula Tuff and the Wasatch Formation but are not the most abundant form of iron sulfide in these rocks.

In the reduced rocks of the Wasatch Formation sulfide occurs commonly as rounded aggregates forming partial rims around Fe-Ti oxides and as individual framboids (fig. 1*B*). These textures are preserved by the ferric oxides that replace the sulfides during oxidation (fig. 1*C*). Framboids of pyrite in reduced sandstone and limonite of similar shape and size in oxidized sandstone also have been identified in the Whitsett Formation of south Texas.

In the deposits studied, iron sulfide minerals also occur as a replacement of Fe-Ti oxide minerals (see Reynolds, 1975). Titanomagnetite is especially affected and may be partly to completely replaced by sulfide. Most of the titanomagnetite grains have undergone high-temperature oxidation in the source rocks under initial conditions of cooling that has resulted in the development of ilmenite along the (111) crystallographic planes. Because magnetite is more readily replaced by sulfide than is ilmenite (Reynolds, 1975), sulfidized magnetites commonly contain remnants of ilmenite lamellae showing the characteristic (111) orientation. During subsequent low-temperature oxida

FIGURE 1.—Ferric oxides formed from oxidized iron sulfides. *A*, Cube-shaped ferric oxide formed by the oxidation of pyrite cube. *B*, Pyrite (white) occurring as a partial overgrowth rim on detrital titanohematite (gray). *C*, Ferric oxide (colloform, mottled dark-gray phase) formed by the oxidation of an incomplete iron sulfide rim on detrital titanohematite (light-gray). Length of field 158 micrometers in *A*, *B*, and *C*.

tion, these textures are retained in the limonite that replaced the sulfidized titanomagnetite (fig. 2). The ilmenite may later be replaced by a TiO_2 phase leaving a network of TiO_2 lamellae along the original (111) planes.

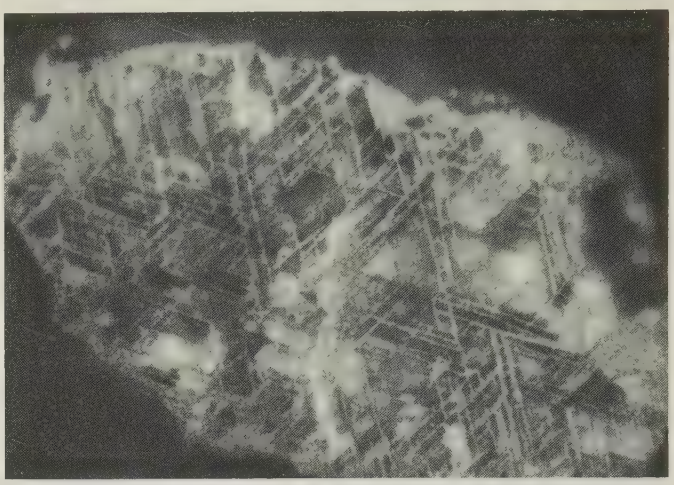

FIGURE 2.—Ferric oxide formed by the oxidation of a previously sulfidized titanomagnetite. Neither iron sulfide nor magnetite remain, but original grain is recognizable by relict lamellae of ilmenite (now TiO_2) and ferric oxide along the characteristic (111) planes of the detrital titanomagnetite. Length of field 158 μm.

Detrital grains of titanohematite, generally less susceptible to sulfidization than magnetite, are most commonly replaced by sulfide along grain margins and fractures. Ferric oxides formed by later oxidation of sulfidized titanohematite mimic the pattern of sulfidization. Oxidation of sulfidized titanomagnetite and titanohematite results in ferric oxides that by color and texture differ greatly from alteration products of these detrital phases formed by oxidation without an earlier episode of sulifidization (Reynolds, 1975).

Authigenic iron sulfide minerals occur in each of the deposits studied as an interstitial cement so that later oxidation results in the concentration of ferric oxides between detrital grains. Authigenic ferric oxides, however, can also be concentrated between framework grains by processes of oxidation in sandstones that have not undergone earlier sulfidization (Walker, 1967; Walker and others, 1967). It is important, then, to distinguish between the two types of ferric oxide occurring as interstitial matrix. Limonite formed by the replacement of iron sulfide cement is characterized texturally by convolute patterns. When viewed by reflected light under oil-immersion conditions, these convolute textures appear as complex intergrowths of different iron oxide and hydroxide

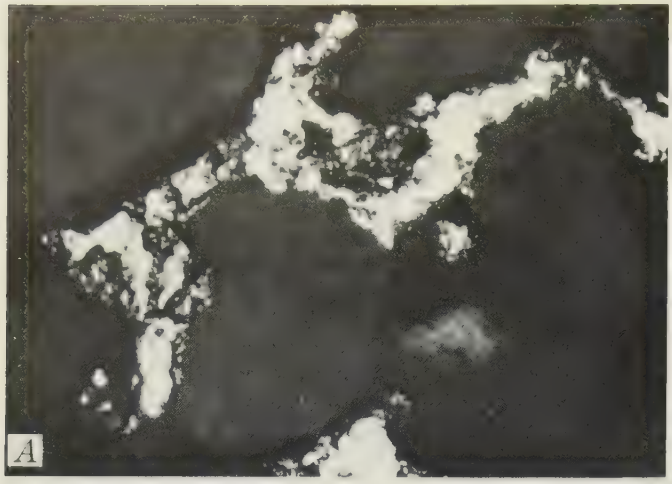

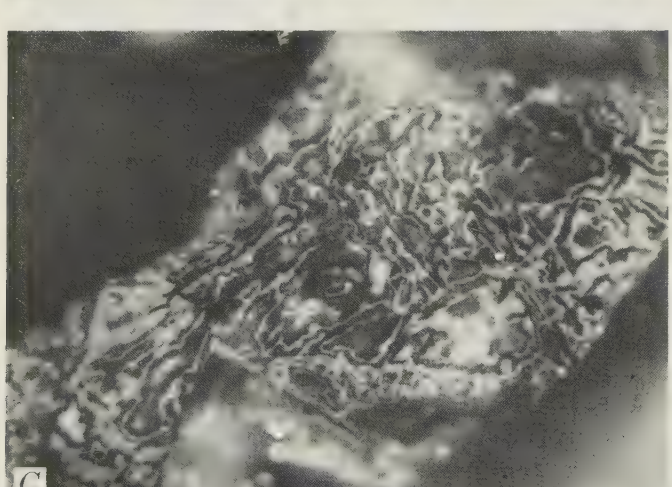

FIGURE 3.—Oxidation of iron sulfide cement. *A*, Interstitial iron sulfide (pyrite) cement. Length of field 158 μm. *B*, Interstitial ferric oxide formed by the oxidation of iron sulfide cement. Convolute pattern faint. Length of field 390 μm. *C*, Ferric oxide formed by the oxidation of interstitial iron sulfide; convolute pattern shown distinctly. Length of field 158 μm.

phases of slightly different reflectivity and colo (fig. 3). In samples of incompletely oxidized sandston at the redox interface, the texture is seen in partia stages of development, because limonite has only partl replaced the iron sulfide phases. This texture ha been observed in three of the four formations studied the exception being the Whitsett Formation, for whic our sampling is sparse. The reasons for the convolut pattern and the origins of the different phases ar presently unknown and are the objectives of our cur rent experimental studies on the oxidation of iron sul fide minerals.

We have examined many polished thin section from three unmineralized sandstones (of Triassic Miocene, and Pliocene age), which have been red dened by intrastratal alterations under oxidizing con ditions and have never been subjected to sulfidization and we have not found similar convolute texture within the interstitial ferric oxides. Much of the re matrix in the unmineralized sandstones is associate with clays in interstitial voids and in voids left b dissolution of metastable iron-bearing silicates suc as hornblende and biotite (Walker and others, 1967 Walker and Larson, 1976). We suggest, then, tha the convolute pattern described might be useful fo identifying ferric oxide phases that have formed b the oxidation of iron sulfides.

In some of the uranium-bearing sandstones ex amined, organic matter plays an important role as source of reductant by contributing to the develop ment of bacteriogenic H_2S. In these sands, under re ducing conditions, sulfides commonly form partia replacements of and overgrowths on plant debri Later oxidation results in the development of ferri oxides with retention of the original sulfide texture Relicts of sulfide minerals may also be present in th organic matter. These relationships are especially wel developed in the deposit of the Powder River Basi (fig. 4).

DISCUSSION

Many of the petrographic features described abov indicate the preservation of sulfide textures as pseudo morphic iron oxides during sulfide oxidation, sug gesting that iron was not extensively solubilized b the oxidation process. At first glance, this resul seems surprising because pyrite oxidation produce strong acids and the solubility of iron increase markedly at low pH (Garrels and Christ, 1965, p 220). Production of acids by pyrite oxidation can b illustrated by the reaction

$$4FeS_2 + 15O_2 + 14H_2O \rightarrow 16H^+ + 8SO_4^{2-} + 4Fe(OH)_3. \quad (1$$

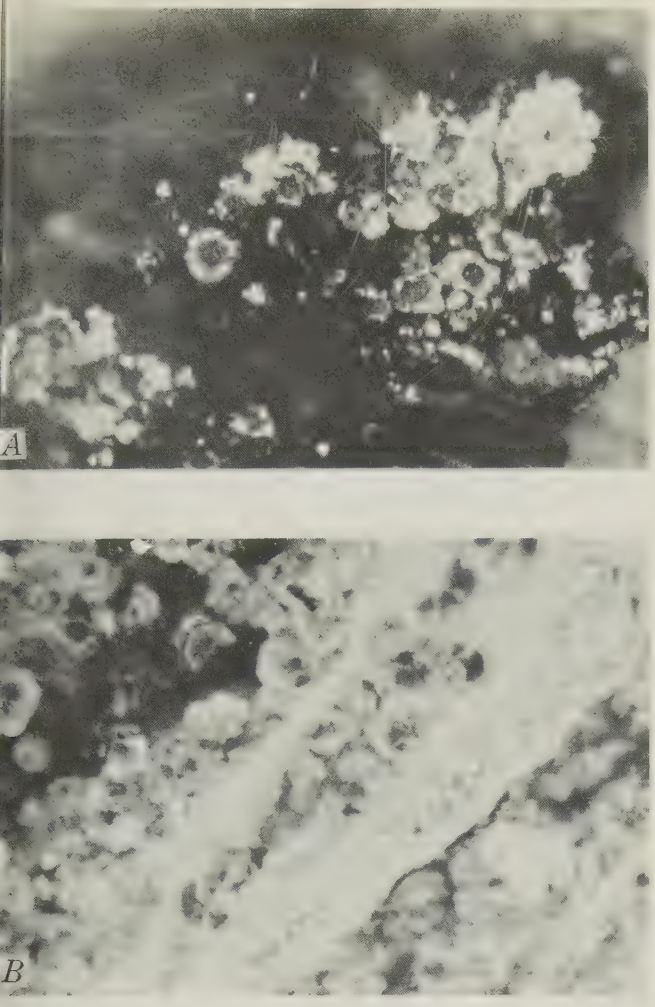

IGURE 4.—Ironsulfides and iron oxides associated with plant debris. *A*, Iron sulfide occurring as small crystals and framboidal aggregates that replace plant debris. Length of field 390 μm. *B*, Colloform concentrations and stringers of ferric oxide that formed by oxidation of iron sulfide associated with plant debris. Length of field 158 μm.

n fact, pyrite oxidation in high-sulfur coals is respon-ible for acidic mine drainage waters and extensive ron mobilization (Singer and Strumm, 1970; and Barnes and Romberger, 1968). However, pyrite oxida-on attending the formation of uranium roll-type de-osits occurs under conditions in which a significant art of the acidity is neutralized. Many of the de-osits occur in compositionally immature, relatively oorly sorted sandstones (arkoses). The hydrogen ion known to react quickly with several of the phases ommon to such rocks, notably feldspars, clay minerals, nd carbonates. Furthermore, the rate of pyrite oxi-ation in a ground-water system is limited by the ow input of oxidant caused by the relatively low olubility of oxygen in ground waters and by slow ground-water flow rates (C. G. Warren, oral commun., 1977). The absolute rate of pyrite oxidation, and thus of hydrogen-ion generation, may be slow compared to the rate of hydrogen-ion reaction with sedimentary components.

Clearly, however, some redistribution of iron has occurred in at least one of the deposits considered herein (that in the Catahoula Tuff) as attested by accumulations of iron as iron sulfide in reduced rock near the redox boundary. Enrichment of iron at the roll front and a short distance ahead of it in other deposits, which is apparently related to processes of ore formation, has also been noted by Harshman (1974) and King and Austin (1966). It may be possible to reconcile the presence of limonite pseudomorphs with evidence of iron mobility during ore genesis if the processes forming the pseudomorphs are not conservative with respect to iron. Or perhaps iron may be selectively mobilized from extremely fine-grained materials and not from the coarser fraction that we have studied. More work on a variety of deposits is required to answer these questions.

CONCLUSION

Oxidized sulfides have been suggested as exploration guides within known uranium-producing districts. In the past, however, these minerals have been recognized either by the color of sandstone or by low-magnification binocular microscopy—methods that cannot reliably identify the various modes of genesis of limonite. Reflection microscopy under high magnification is a method that is capable of distinguishing limonite formed by the oxidation of iron sulfides from that having other origins. Recognition of oxidized sulfides can distinguish oxidized sandstones that might have a redox boundary downdip, and which would be favorable hosts for uranium ore, from sandstones without such potential. This method, therefore, should be useful in guiding exploration for uranium in frontier areas.

REFERENCES CITED

Adler, H. H., 1970, Interpretation of colour relations in sandstone as a guide to uranium exploration and ore genesis, *in* Uranium Exploration Geology: Vienna, Internat. Atomic Energy Agency, p. 331–342.

———1973, Exploration for uranium in sandstones—geochemical, remanent magnetic and sulphur-isotope applications, *in* Uranium Exploration Methods: Vienna, Internat. Atomic Energy Agency, p. 155–166.

Bailey, R. V., 1965, Applied geology in the Shirley Basin uranium district, Wyoming: Wyoming Univ. Contr. Geology, v. 4, no. 1, p. 27–35.

———1969, Uranium deposits in the Great Divide Basin—Crooks Gap area, Fremont and Sweetwater Counties, Wyoming: Wyoming Univ. Contr. Geology, v. 8, no. 2, p. 105–120.

Barnes, H. L., and Romberger, S. B., 1968, Chemical aspects of acid mine drainage: Water Pollution Control Federation Jour., v. 40, p. 371–384.

Davis, J. F., 1969, Uranium deposits of the Powder River Basin: Wyoming Univ. Contr. Geology, v. 8, no. 2, p. 131–141.

Fischer, R. P., 1970, Similarities, differences, and some genetic problems of the Wyoming and Colorado Plateau types of uranium deposits in sandstone: Econ. Geology, v. 65, p. 778–784.

Garrells, R. M., and Christ, C. L., 1965, Solutions, minerals, and equilibria: New York, Harper and Row, 450 p.

Granger, H. C., and Warren, C. G., 1969, Unstable sulfur compounds and the origin of roll-type uranium deposits: Econ. Geology, v. 64, no. 2, p. 160–171.

Harshman, E. N., 1962, Alteration as a guide to uranium ore, Shirley Basin, Wyoming: U.S. Geol. Survey Prof. Paper 450–D, p. 8–10.

———1968a, Uranium deposits of Wyoming and South Dakota, *in* Ore deposits of the United States, 1933–1967 (Graton-Sales Volume): New York, Am. Inst. Mining, Metall., and Petroleum Engineers, v. 1, p. 815–831.

———1968b, Uranium deposits of the Shirley Basin, Wyoming, *in* Ore deposits of the United States, 1933–1967 (Graton-Sales Volume): New York, Am. Inst. Mining, Metall., and Petroleum Engineers, v. 1, p. 849–856.

———1974, Distribution of elements in some roll-type uranium deposits, *in* Formation of uranium ore deposits: Vienna, Internat. Atomic Energy Agency, p. 169–183.

King, J. W., and Austin, S. R., 1966, Some characteristics of roll-type uranium deposits at Gas Hills, Wyoming: Mining Eng., v. 18, no. 5, p. 73–80.

Klohn, M. L., and Pickens, W. R., 1970, Geology of the Felder uranium deposit, Live Oak County, Texas: Soc. Mining Engineers, preprint 70–1–38, 19 p.

Melin, R. E., 1964, Description and origin of uranium deposits in Shirley Basin, Wyoming: Econ. Geology, v. 59, no. 5, p. 835–849.

———1969, Uranium deposits in Shirley Basin, Wyoming: Wyoming Univ. Contr. Geology, v. 8, no. 2, p. 143–149.

Mrak, V. A., 1968, Uranium deposits in the Eocene sandstones of the Powder River basin, Wyoming, *in* Ore deposits of the United States, 1933–1967 (The Graton-Sales Volume) New York, Am. Inst. Mining, Metall., and Petroleum Engineers, v. 1, p. 838–848.

Rackley, R. I., and Johnson, R. L., 1971, The geochemistry of uranium roll-front deposits with a case history from the Powder River Basin: Econ. Geology, v. 66, no. 1, p. 202–203.

Rackley, R. I., Shockey, P. N., and Dahill, M. P., 1968, Concepts and methods of uranium exploration: Earth Sci. Bull., v. 1, no. 3, p. 23–34.

Reynolds, R. L., 1975, Alteration of iron-titanium oxide minerals associated with uranium deposits in sandstone, *in* Craig, L. C., Brooks, R. A., and Patton, P. L., eds. Abstracts of the 1975 Uranium and Thorium Research and Resources Conference: U.S. Geol. Survey Open-File Rept. 75–595, p. 38–39.

Sharp, W. N., McKay, E. J., McKeown, F. A., and White, A. M., 1964, Geology and uranium deposits of the Pumpkin Buttes area of the Powder River Basin, Wyoming: U.S. Geol. Survey Bull. 1107–H, p. 541–638.

Shawe, D. R., and Granger, H. C., 1965, Uranium ore rolls—an analysis: Econ. Geology, v. 60, p. 240–250.

Singer, P. C., and Stumm, Werner, 1970, Acidic mine drainage—The rate determining step: Science, v. 167, p. 1121–1123.

Van Houten, F. B., 1961, Climatic significance of red beds *in* Nairn, A. E. M., ed., Descriptive paleoclimatology New York, Interscience Publishers, Inc., p. 89–139.

———1964, Origin of red beds—Some unsolved problems, *in* Nairn, A. E. M., ed., Problems in paleoclimatology, Proceedings of NATO Paleoclimates Conference, 1963: New York, Interscience Publishers, Inc., p. 647–661.

Walker, T. R., 1967, Formation of red beds in modern and ancient deserts: Geol. Soc. America Bull., v. 78, p. 353–368.

Walker, T. R., and Larson, E. E., 1976, Hematite authigenesis in the Moenkopi Formation (Triassic age) Colorado Plateau: A contribution to the origin of magnetism in red beds: Geol. Soc. America Abs. with Programs, v. 8, no. 6, p. 1158.

Walker, T. R., Ribbe, P. H., and Honea, R. M., 1967, Geochemistry of hornblende alteration in Pliocene red beds Baja California, Mexico: Geol. Soc. America Bull., v. 98, p. 1055–1060.

Jour. Research U.S. Geol. Survey
Vol. 6, No. 4, July–Aug. 1978, p. 489–498

URANIUM IN WATERS AND AQUIFER ROCKS AT THE NEVADA TEST SITE, NYE COUNTY, NEVADA

By ROBERT A. ZIELINSKI and JOHN N. ROSHOLT, Denver, Colo.

Abstract.—Previous chemical, geological, and hydrological information describing the physical and chemical environment of the Nevada Test Site (a Federal reserve for the testing of nuclear explosive devices) has been combined with new radiochemical and isotope data for water and rock samples in order to explain the behavior of uranium during alteration of thick sequences of rhyolitic volcanic rocks and associated volcaniclastic sediments. A model is proposed in which uranium mobility is controlled by two competing processes. Uranium is liberated from the volcanic rocks through dissolution of the glassy constituents and is carried in solution as a uranyl carbonate complex. Uranium is subsequently removed from solution by adsorption on secondary oxides of iron, titanium, and manganese, as observed in fission-track maps of aquifer rocks. The model explains the poor correlation of dissolved uranium with depth within tuffaceous sequences in which percolation of ground water is predominantly downward. Good positive correlation of dissolved uranium with dissolved Na, total dissolved solids, and total carbonate supports the glass dissolution model, while inverse correlation of dissolved uranium with U^{234}/U^{238} ratios of waters implies uranium is being absorbed by a relatively insoluble, surficial phase. Alpha radioactivity of Test Site water is primarily caused by high U^{234} contents, and beta activity is highly correlated with dissolved K (K^{40}). Small amounts of dissolved radium, Pb^{210}, and Po^{210} are present but no evidence was found for alpha activity sources related to nuclear testing (Pu, U^{235}). A filtered but unacidified carbonate solution of uranium was found to be stable (±10 percent of original U concentration) for years when stored in acid-washed polyethylene bottles.

This study presents data on the uranium and radium abundances, alpha- and beta-particle emission rates and U isotopic compositions of surface and ground water sampled at the Nevada Test Site, Nye County, Nev. (a Federal reserve for the testing of nuclear explosive devices). Uranium abundances and distributions in some rhyolitic aquifer rocks are also presented. These data are integrated with geologic, chemical, and hydrologic data in an attempt to model the mobility of uranium in thick sequences of rhyolitic host rocks. Specifically, the study (1) evaluates changes in the uranium content and (or) isotopic composition of water as a function of residence time in rhyolites, (2) identifies changes of the uranium abundance and distribution in rhyolitic aquifer rocks as a function of degree of alteration, and (3) identifies sources of anomalously high alpha radioactivity in Test Site waters.

An extensive treatment of the geology and hydrology of the Nevada Test Site area is available in previously published reports (Eckel, 1968; Winograd and Thordarson, 1975; Blankennagel and Weir, 1973; Schoff and Moore, 1964). A generalized stratigraphic section of the Nevada Test Site area shows the area to be underlain by thick sequences (<11 000 m) of Precambrian and Paleozoic miogeosynclinal sediments. Mesozoic rocks are limited to a few small granitic stocks. A thick sequence (<4000 m) of Cenozoic volcanic and associated sedimentary rocks was deposited on a previously folded and faulted paleotopographic surface of moderate relief. Cenozoic volcanic rocks originated from at least two developing calderas, and they are predominantly calc-alkalic to peralkaline rhyolitic to quartz latitic ash and lava flows with subordinate air-fall tuff and tuffaceous sandstones. During Miocene to Quaternary time, the previously deformed miogeosynclinal rocks and overlying Cenozoic volcanics were subjected to normal block faulting and subsequent erosion to yield the present basin-and-range topography.

Because the structural and erosional history of the area was complex, the thickness and areal extent of individual units vary greatly, and this variation results in a complex hydrologic regime. Previous investigations of the local hydrology indicated that the major aquifer controlling regional movement of ground water occurs in Paleozoic carbonate rocks. Water enters the carbonate aquifer through recharge from precipitation on highland areas or from downward percolation within intermontane basins. Lateral movement of ground water within the carbonate aquifer allows integration of drainage from a number of nearby basins prior to ultimate discharge along a fault-controlled spring line at Ash Meadows in the Amargosa Desert (Winograd and Thordarson, 1975). Shallower aquifers occur in valley-fill sequences and

in bedded, fractured, and devitrified tuffs in the Cenozoic volcanics. Intrabasin movement of ground water is predominantly downward from these aquifers into the underlying carbonate aquifer although rates of communication between aquifers are controlled by intervening poorly fractured, zeolitized or argillitized rocks which act as aquitards of varying efficiency.

The chemical composition of ground water circulating in rhyolitic volcanic rocks is dominated by sodium, potassium, and bicarbonate ions. In contrast, waters of the carbonate aquifers or carbonate-rich valley-fill sequences are composed primarily of calcium, magnesium, and bicarbonate ions (Schoff and Moore, 1964). The contrasting chemistries of the two waters allow crude estimates of the degree of mixing for waters of mixed chemical types.

Release of sodium during alteration of rhyolitic glass and felsite is well documented (Lipman, 1965; Truesdell, 1966; Hoover, 1968; Noble, 1970). Both the sodium and sulfate content of ground water increase as a function of depth in a test well in the Cenozoic volcanic sequence (Winograd and Thordarson, 1975). This study was initiated in order to test for a similar behavior for uranium. Uranium dissolved in oxidizing, carbonate-bicarbonate waters of neutral to mildly alkaline pH should be stabilized by the formation of uranyl carbonate complexes (Garrels and Christ, 1965).

Several springs and water-supply wells tapping various aquifers within the Nevada Test Site were monitored during the period of 1957–72 for radioactivity (total alpha and beta activity) and uranium and radium content (Clebsch and Barker, 1960; Claassen, 1973). Most water analyses presented in this paper are taken from the earlier reports. Tritium and carbon-14 age dates were determined for waters from some of the sampling sites (Clebsch, 1961; Grove and others, 1969) and are utilized at appropriate points in the discussion.

Acknowledgments.—Water samples and much original sample data were graciously provided by H. C. Claassen. Help in obtaining background information about the Nevada Test Site was provided by G. L. Dixon, S. G. Steele, K. A. Sargent, and F. M. Byers. Special thanks goes to S. G. Steele for help in collecting core samples. Statistical analyses were aided by D. A. Lindsey and J. G. Boerngen.

SAMPLE DESCRIPTION

Water samples were collected during the period of 1957–72 by various members of the U.S. Geological Survey. Field treatment of samples varied (Claassen, 1973), but most samples collected after 1965 were

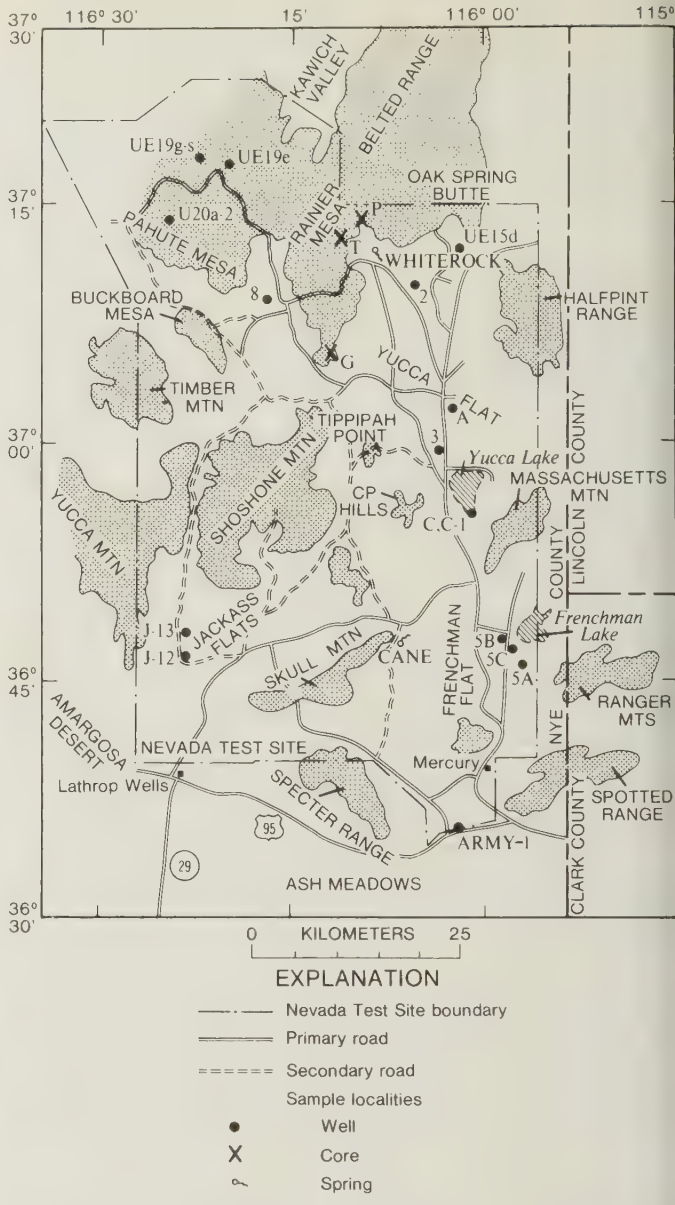

FIGURE 1.—Sample localities, Nevada Test Site (modified from Claassen, 1973).

filtered at the time of collection through filters having 0.45-μm openings and stored in acid-washed polyethylene bottles. Splits of samples submitted for cation and radiometric measurements were acidified to pH <1 with HCl or HNO_3. Most sample locations discussed in this paper (fig. 1) have been discussed in greater detail elsewhere (Claassen, 1973).

Rock samples were obtained as 100-g chips from 7.6-cm-diameter cores previously obtained at three exploratory sites on Rainier Mesa, Nevada Test Site

fig. 1). The holes penetrate some 600 m of Cenozoic rhyolite ash and lava flows, air-fall tuffs, and tuffaceous sandstones to bottom in Paleozoic carbonate rocks (Walter Danilchik, written commun., 1968). Samples reported in this study were taken from 30- to 60-m sections through the Grouse Canyon Member of the Belted Range Tuff—a peralkaline rhyolite of late Miocene age reported to be a major aquifer in the Cenozoic rhyolite sequence (Winograd and Thordarson, 1975). Samples exhibit a variety of degrees of devitrification, welding, and zeolitization. Thin sections were made of representative samples, and splits of all samples were ground to -100 mesh (< 150 μm) by ceramic plates prior to submission for U and Th analysis.

ANALYTICAL TECHNIQUES

Uranium and thorium concentrations in rock powders were determined by a delayed neutron technique (Millard, 1976). Eight-gram splits of samples and a standard of U-doped dunite were packaged in polyethylene vials, irradiated at the U.S. Geological Survey TRIGA[1] reactor for 1 min in a neutron flux of $6x10^{11}n \cdot cm^{-2} \cdot s^{-1}$, and transferred by pneumatic tube to an array of BF_3 neutron counters. After a decay period of 20 s, the samples and standard were counted for 1 min. The procedure was repeated for thorium except thorium standards were used and the irradiations were performed in a Cd-lined terminus. Sample transfers, data collections, and reduction were performed by computer. Reported coefficients of variation were less than 10 percent for uranium concentrations >2 ppm (parts per million) and thorium concentrations ≥10 ppm.

The uranium concentrations in waters reported here were determined by a fluorimetric technique (Barker and others, 1965). Solid residues produced by evaporation of a known aliquot of solution were fused with a flux of $NaF–Na_2CO_3–K_2CO_3$ mixture, and the resultant pellet was measured for fluorescence at the 5546-angstrom wavelength. After the samples were checked for the presence of elements which quench U fluorescence, their values were compared to those obtained from standards. Reported accuracy and precision is ±15 percent (1σ) for U concentrations >1 μg/L (Barker and others, 1965).

Uranium distribution in rock and water samples was determined by a fission-track technique similar in concept to alpha-particle autoradiography except that the presence of uranium was detected by reactor-induced production of fission-fragment traces in an appropriate detector material. Thin sections were covered by a strip of low-U muscovite and irradiated in a neutron flux of $2.5x10^{12}n \cdot cm^{-2} \cdot s^{-1}$ for 4 hours. During irradiation, U^{235} absorbed thermal neutrons and fissioned. Some recoiling fission fragments entered the muscovite detector and caused disruptions of the structure along their paths. These paths were made visible under high magnification by subsequent etching of the muscovite in 48 percent HF for 10 min. Uranium sites in the thin section could then be identified by reproducing the orientation of the muscovite "fission-track map" on the original slide using a series of previously produced reference marks. Uranium distribution in solutions was measured using a detector platelet of low-uranium silica glass immersed in solution. Irradiation conditions were the same and the recovered glass was etched in 48 percent HF for 2 min to develop distinctive fission-track pits.

Radium concentrations in water were determined by two techniques. In both techniques, radium is separated from other elements through coprecipitation with barium sulfate. The precipitate is then either (1) allowed to reach equilibrium with short-lived daughters, mounted on a planchet, and counted on an alpha scintillation detector along with equilibrated standards of Ra^{226}; or (2) sealed in a container for about 2 weeks to allow for equilibration with radon daughters, which are then flushed to a new container and counted for alpha activity with appropriate standards (Barker and Johnson, 1964). Reported precision is ±10 percent (1σ) for samples with more than 0.5 pCi/L (picocurie per liter) of radium.

Total alpha and beta ($\alpha+\beta$) activities were determined by evaporating an aliquot of solution, transferring the residue to a planchet, and counting the residue in a thin-window gas-flow proportional counter. Separate count data for α and β were compared with calibration curves obtained from appropriate standard solutions of uranyl acetate (for α), Sr^{90}, or Cs^{137}. The precision of the results is a function of the dissolved solids content and U content (sample aliquots were chosen to give constant dissolved solid contents), as well as reproducibility of counting geometry and detector efficiency. Estimated precisions are as poor as ±30 percent (1σ). (O. J. Feist, Jr., oral commun., 1975).

Polonium analyses were performed according to the method of Flynn (1968) in which Po is collected from solution onto silver disks which are counted for Po^{210} alpha activity.

Uranium and plutonium concentrations and uranium isotopic compositions were determined on a number of selected water samples using a radioisotope dilution-

[1] Training Research, Isotope General Atomic.

alpha spectrometric technique modified from Rosholt, Doe, and Tatsumoto (1966). Pure concentrates of uranium and plutonium were obtained using solvent extraction, ion exchange, and electrodeposition and were counted for 2–3 weeks in an alpha spectrometer.

RESULTS AND DISCUSSION

Water Analysis

Water analyses (U, Ra, α, β) generated in this investigation using stored samples, and other analyses taken from the literature (Claassen, 1973), have been grouped according to host rock and arranged in order of increasing sample depth (table 1).

Estimated depths of sampling represent the median depth of the potential "producing zone" defined as the depth from the water-table surface to the well bottom. Such estimates may be in gross error if wells penetrate large thicknesses of rock of low and variable permeability in which most actual production may be from a few narrow horizons of high permeability. The above situation is true for most wells in tuffaceous rocks. Some wells penetrating tuffs (UE15d, UE19e, UE19g–s) have hypothetical "producing zones" in excess of 1000 m. One well (UE19g–s) produces from tuffaceous and carbonate rocks but is assigned to the carbonate aquifer on the basis of the generally higher transmissivity of carbonate rocks.

Age data (Clebsch, 1961; Grove and others, 1969) were also included to document aging of waters at depth. Of particular interest are data taken from closely-spaced localities in areas of documented downward percolation of ground water such as Yucca and Frenchman Flats (fig. 1). The following discussion attempts to explain these data using knowledge of the regional hydrology and geology as well as the chemistry of uranium, radium, and related daughter products.

Uranium concentrations

Two springs at the Nevada Test Site (table 1) and 14 springs sampled just to the south (Robinson and Beetem, 1975) contain uranium in concentrations of 0.6–6.8 μg/L with an average value of 2.5 μg/L. Uranium concentrations in perched water encountered during drilling and tunneling of Rainier Mesa (fig. 1) range in concentration from 0.2–5.7 μg/L with an average of 2.2 μg/L (Clebsch and Barker, 1960), which is close to the value of 1.9 μg/L shown in table 1 for uranium in the U 12 T main tunnel. In comparison, surface waters in the United States contain uranium in

TABLE 1.—*Radiochemical data for Nevada Test Site waters*

[Ages are uncorrected C-14 ages from Grove and others (1969), except as indicated. Other data are from Claasen (1971), except as indicated. Numbers in parentheses indicate how many values were used in determining the data range. Leaders (---) indicate no data available]

Sample locality (see fig. 1)	Collection date(s)	Median depth of "producing zone" (m)	Host rock	Age of water[1] (yrs)	U content (μg/L)	Ra^{226} equivalent (pCi/L)	Alpha (U^{238} equivalent) (μg/L)	Beta (Sr^{90} equivalent) (pCi/L)	Ra^{226}/U^{238} (alpha activity ratios)
Cane Springs------	3/25/71	---	Tuff ------	---	[3]1.1	---	---	---	---
Whiterock Springs-	3/24/71	---	--- do ----	[2]<6	[3]1.3	---	---	---	---
U12T main tunnel, Rainier Mesa (near Core T)---	9/22/71	~280	Perched H_2O	[2]<6	[3]1.9	---	---	---	---
Well 5B----------	1957-1971	241	Valley fill	14,800	4.2-6.7 (5)	≤0.2 (5)	3.8-13 (7)	11-13 (4)	≤0.15
Well 5C----------	1957-1971	288	--- do ----	---	4.3-7.4 (6)	≤0.2 (6)	3.5-17 (7)	8.9-21 (4)	< .14
Well A----------	1960-1971	531	--- do ----	---	4.2-6.6 (8)	<0.1-<0.5 (8)	3.7-39 (14)	9.1-17 (14)	< .32
Well 5A----------	1957-1964	238	Tuff ------	---	1.7-21.0 (6)	<0.1-1.9 (6)	6.4-17 (5)	4.5-11 (3)	≤ .32
Well J-12--------	1958-1971	286	--- do ----	---	0.2-0.6 (4)	≤0.1 (4)	2- 9.6 (7)	4.7-13 (7)	≤1.5
Well 3----------	1957-1969	523	--- do ----	---	2.3-7.1 (7)	<0.1-0.5 (7)	4-17 (8)	6.7-14 (5)	≤ .42
Well J-13--------	1963-1971	672	--- do ----	---	0.7 (2)	0.1-0.2 (2)	2-6.1 (4)	4.9- 9.2 (4)	≤ .87
Well U20a-2-------	1964-1971	1005	--- do ----	15,100	2.9 (1)	<0.1 (1)	5.3-13 (4)	2.8-5.9 (4)	< .10
Well 8----------	1963-1971	1253	--- do ----	10,200	0.4-0.8 (3)	0.1-0.2 (3)	2.3-4.7 (3)	4.6-5.2 (4)	≤ .77
Well UE19e-------	1966-1971	1253	--- do ----	---	[3]0.6-0.7 (2)	---	1.5-4.0 (4)	0.9-2.7 (4)	---
Well UE19g-s-----	1971	1455	--- do ----	---	[3]12	---	24-67 (2)	3.9-9.7 (2)	---
Well Army-1------	1962-1971	351	Carbonate---	22,000	2.2-2.5 (3)	0.3-0.5 (3)	4-7.9 (6)	5.6-8.7 (6)	≤ .69
Well C----------	1962-1971	485	--- do ----	---	6.3-7.5 (5)	1.0-1.4 (5)	12-55 (14)	14-21 (14)	≤ .62
Well C-1---------	1961-1971	493	--- do ----	28,000	6.3-8.0 (4)	0.1-1.3 (4)	13-62 (6)	11-30 (7)	≤ .56
Well 2----------	1961-1971	835	--- do ----	15,200	0.5-2.5 (4)	0.1-0.5 (4)	3.0-13 (5)	5.9-50 (7)	≤1.5
Well UE15d-------	1961-1971	1007	--- do ----	---	2.7-2.8 (2)	0.3-1.5 (2)	12-48 (6)	16-25 (6)	≤1.7

[1] Time since water entered the ground.
[2] Tritium age from Clebsch (1961).
[3] Data determined in this study.

amounts ranging from 0.1–0.5 μg/L in nonuraniferous regions and 1–10 μg/L in uraniferous regions (Fix, 1956). The data on the uranium content of springs at the Nevada Test Site is limited and has not been collected in a systematic manner. Uranium content of spring waters is likely related to lithology of host rocks and local precipitation patterns.

Water from the shallow valley-fill aquifer is much older (one determination) and generally contains more uranium than the spring waters (table 1). The consistent ranges of U, Ra, and α and β activity values also suggest relatively uniform attack of U sources by ground water within the aquifer. Efficient mixing of ground waters is not supported by chemical analyses (Claassen, 1973).

In contrast to the waters from the valley-fill aquifer, uranium concentrations in waters of the tuffaceous aquifers sampled from numerous wells (table 1) show much greater interwell and intrawell variation.

The variability of uranium concentrations in waters from tuffaceous aquifers undoubtedly indicates inhomogeneous flow patterns imposed by intervention of structural and (or) lithologic barriers in the Cenozoic volcanic sequence which cause differing flow patterns. In particular, a major enrichment of uranium in waters tapped at the level of well 5A is indicated.

Such local enrichments may be due to ponding of ground waters causing excessive leaching of host rocks, or to the presence of a uraniferous host. Uranium concentrations in tuffaceous aquifer waters are generally lower than concentrations in waters of the valley-fill aquifer, indicating that uranium is being removed from solution by an absorbent and (or) that water from the valley-fill aquifer is not a major source of recharge to the tuff. Evidence for the former hypothesis will be presented below.

The uranium content of waters drawn from the carbonate aquifer is controlled by variable rates of input through overlying aquitards as well as by mixture with water recharged to and transported within the carbonate aquifer from areas in and around the Test Site. The transported water is considered to be the most likely uranium source because carbonate aquifer wells with the highest uranium content (C, C–1) are *not* in areas where the carbonate is overlain by water-saturated tuffaceous rocks (Claassen, 1973).

The existing chemical analyses (Claassen, 1973) of the well waters of this study were examined statistically to provide more rigorous estimates of possible correlations with U. The data set consisted of 107 partial or complete analyses for 17 chemical and radiometric parameters and 3 physical parameters (depth, specific conductance, and temperature). Some of the data were put into a logarithmic format to produce more nearly Gaussian sample distributions. Linear correlation coefficients were calculated for the entire data set and for subsets from each aquifer. The results (table 2) indicate a strong positive correlation of U with Na, carbonate ($HCO_3 + CO_3$), and dissolved solid content in waters draining tuffs. The results suggest a model in which U is mobilized during volcanic glass dissolution as an alkali complex with uranyl-carbonate anions. Similar correlations are obtained in the carbonate aquifer and may reflect some input of sodium species from the tuffaceous rocks. Small positive or negative correlation of U and most other chemical parameters with depth or with temperature (which is depth-related) is true of all aquifers. Predominant downward percolation of ground waters does not consistently produce a downward increase in concentrations of dissolved constituents, because water compositions are affected differently by competing processes such a (1) supersaturation and precipitation, (2) absorption, and (3) dilution with juvenile recharged waters (valley-fill aquifer) or drainage from neighboring basins (carbonate aquifer).

TABLE 2.—*Correlation coefficients between uranium and various parameters: Nevada Test Site aquifer water*

[Underlined coefficients are significant at the 95-percent confidence interval calculated on the basis of number of paired values]

Data set	SiO_2	Al	Fe	Mg	Ca	Na	K	Total carbonate	F	Cl	SO_4	NO_3	T(°C)	Dissolved solids	Specific conductance	β	α	Ra	Depth
All aquifers	0.14*	0.25	-0.17	0.13	0.02	0.74	0.40*	0.72	0.04	0.40	0.46	-0.01	0.17*	0.77	0.75	0.39	0.61	0.55	-0.39
Valley fill aquifer	-.23	-.05	.14	-.15	-.32	.37*	.02	.05	.33*	.31	.39	.21	-.62*	.30*	.43*	.35	.11	.46	-.52
Tuff aquifer	.38*	.19	-.45	.10	-.10	.72	.25*	.81	.20	.30	.47	-.02*	-.58	.81	.82	.07	.75	.89	-.32
Carbonate aquifer	.02	.30	.48	.82*	.68*	.90	.75*	.93*	.36	.96*	.80*	-.68	.78*	.94	.95*	.61*	.34*	.82*	-.43

*Log transformation did not improve the sample distribution: raw data for the element labeling the column was used.

Radium concentrations

Radium concentrations in waters of the Nevada Test Site range from <0.1–1.9 PCi/L. In comparison, surface and ground waters of the United States generally contain <1 pCi/L radium although some limestone aquifers in the north-central United States commonly contain >3 pCi/L (Barker and Johnson, 1964). Association of uranium and radium in ground water (table 2) is expected because radium is produced through decay of uranium (and thorium) and is soluble in carbonate- bicarbonate solutions. Dissolved concentrations of radium isotopes adjust to values in equilibrium with longer lived parents, the rate of adjustment depending upon the half-life ($T_{½}$) of the isotope. If Ra^{226} ($T_{½}$= 1622 yr) is in equilibrium with its parent U^{238}, alpha activity ratios for the two isotopes should equal 1.0. Conversion of U^{238} abundances to equivalent alpha activity allows comparison with measured alpha activity of radium expressed as equivalent Ra^{226}, which shows that most waters at the Test Site contain less radium than could be supported by the dissolved uranium (table 1). A factor affecting the dissolved lifetime of radium is its coprecipitation with barium sulfate. Well waters of this study contain 5–500 ppb (parts per billion) Ba and 7–100 ppm SO_4, resulting in solutions which are nearly saturated (valley-fill and tuff aquifer) to supersaturated (carbonate aquifer) with $BaSO_4$.

Alpha particle emission

All measured activities reported here are in excess of that which may be explained by assuming alpha activity is due to dissolved uranium and radium of normal isotopic composition (table 1). Claassen (1973) speculated that additional alpha activity was caused by unusual uranium isotopic compositions and (or) the presence of soluble daughter products.

The former hypothesis is suggested by the correlation of dissolved uranium and alpha activity (table 2). Results of measurements of U^{234}/U^{238} alpha activity ratios of selected samples give values of 2.8–4.88 (table 3). Samples were chosen to represent a range of uranium concentrations in different aquifers and to represent a time-related sampling of a well (C) whose waters contained high and variable amounts of alpha activity. Excesses of U^{234} are well documented for most natural waters (Kaufman and others, 1969; Kronfeld, 1972) and are believed to be caused by preferential oxidation and dissolution of U^{234} or preferential recoil into solution of U^{234} atoms from mineral surfaces (Rosholt and others, 1963; Chalov, 1959; Chalov and Merkulova, 1966). Once established, disequilibrium amounts of unsupported U^{234} readjust to equilibrium values at a rate determined by the half-life ($T_{½}$ = 2.27 × 10^5 yr). Variable efficiency of fractionation in waters of similar age probably reflects differences in the rate of solution of uranium hosts compared to the amount of recoil of U^{234} from grain surfaces and the degree of mixing of solutions at different locations. A comparison of the uranium contents and isotopic ratios of waters at well C (table 3) with the same values from the Ash Meadows discharge site (U = 2.3 μg/L; U^{234}/U^{238} = 2–3) suggests that water leaving the Test Site area (well C) is diluted with less fractionated waters from other areas (I. J. Winograd, written commun., 1976).

Although the amount of excess U^{234} is an insignificant atom fraction of the total dissolved U, its contribution to the net alpha activity results in calculated "equilibrium" U^{238} abundances (table 3, table 1) 3–5 times the dissolved U^{238} abundance. Correction for alpha activity produced by excess U^{234} and dissolved radium successfully (within the precision of α counting) accounts for most alpha activity excesses (table 3). Other possible sources of alpha activity, such as plutonium or U^{235} excesses related to nuclear testing, were not found (table 3).

Radioactive daughters of uranium and radium may also be sources of alpha activity although establishment of equilibrium concentrations in solutions is hindered by the escape of daughters through gaseous diffusion (Rn) or precipitation as relatively insoluble elements or compounds (Th, Pa, Ac). An attempt was made to detect the presence of Po^{210} ($T_{½}$ = 0.38) yr) and, by inference, its long-lived parent Pb^{210} ($T_{½}$ = 22 yr). Evidence was found for a small Pb^{210} — Po^{210} contribution to alpha activity (table 3).

TABLE 3.—*Isotopic abundances of Nevada Test Site water*

[Leaders (---) not determined]

Sample locality (see fig. 1)	Collection date	U content (μg/L)	U^{234}/U^{238} (activity ratio)	Apparent[1] equivalent U^{238} (μg/L)	Pu^{239} +Pu^{240} (pCi/L	Po^{210} (pCi/L)
Well C---------	4/11/69	7.04±.07	3.69±.04	36	<0.002	---
---do----------	4/11/69	7.06±.07	3.69±.04	36	<.007	---
---do[2]---------	4/11/69	---	3.72±.04	---	<.005	0.17
---do----------	3/29/71	6.28±.06	3.71±.04	33	<.005	---
---do----------	5/28/71	6.79±.07	3.66±.04	36	<.005	.41
Well UE15d-----	11/15/71	3.98±.05	3.85±.04	22	<.003	.04
Well J-12------	3/26/71	0.56±.01	4.88±.06	3.6	<.007	---
Well UE19g-s---	10/06/71	[3]12	[4]2.8	49	---	---
Well C (rinse)[5]	3/29/71	0.64±.03	3.61±.07	---	<.013	.15

[1] The sum of alpha activity from dissolved U^{238}, U^{235}, U^{234}, and Ra^{226} converted to μg/L of equivalent U^{238}.

[2] A U^{238}/U^{235} atom ratio of 138±4 was determined for this sample.

[3] U analysis by fluorimetry.

[4] Analysis performed by Rocky Flats Division, Dow Chemical Company.

[5] Analysis of 8 *N* HNO_3 solution used to rinse one of the polyethylene storage bottles—a test for adsorbed materials.

Beta particle emission

The beta particle emission rate of evaporated water samples is not as great or as variable as the associated alpha activity (table 1). Correlation of beta activity with uranium or radium is very poor, but correlation with potassium is 0.76 in tuff and 0.90 in carbonate aquifers, indicating that the source of beta activity in evaporated residues of these waters is the naturally occurring, beta-emitting isotope K^{40}. Other possible beta emitters include Rb^{87} as well as isotopes of the uranium and thorium decay series.

Sources of beta activity resulting from nuclear fission products (Sr^{90}, Cs^{137}) are a concern at the Nevada Test Site, but the total beta activity of water samples was not anomalous compared to regional background values and no specific identification of isotopes was attempted. Detailed investigation of beta-emitting sources is best performed using γ spectrometry or radiochemical procedures followed by beta energy and half-life determinations. Such investigations were not attempted in this report.

Variations of measured quantities related to sample aging

In order to evaluate the validity of data obtained from stored water samples (table 1, table 3), a number of waters originally collected and analyzed in 1969–71 were resubmitted for analysis (U and Ra) in 1976. An acid rinse (8 *N* HNO_3) of one of the polyethylene storage bottles was also performed to provide a measure of adsorbed material. All the water samples had been filtered at the time of collection, but not all the stored samples had been acidified.

The stability of uranium in carbonate-bicarbonate waters (Thatcher and others, 1977) was verified (table 4) for most samples, and acid-rinse data indicated that <10 percent of the original uranium was adsorbed on container walls. The comparison is limited by the precision of the fluorimetric technique as well as by the lack of specific data for many early samples. Fission-track measurements of the distribution of uranium in solution revealed generally homogenous distribution with a few uraniferous particles. Particulate matter may have been present in the original samples or may have grown during storage but most apparently remained in suspension. Uranium concentrations of unacidified solutions determined by a fission-track technique gave anomalously high values indicating that uranium was adsorbed on the glass fission-track detectors. An original suspicion that fission-track clusters were caused by particulates of plutonium was not verified by subsequent bulk sample analysis (table 3).

Four of five redetermined radium values are lower than the original values. However, these lower values could not indicate significant decay of excess radium during the 5-yr interval because of the long half-life (1622 yr) of Ra^{226}. Adsorption of radium on container walls is apparently the cause of the decrease. (See footnote 3 on table 4.)

Redeterminations of alpha and beta particle emission rates provide little definitive information because of the poor precision of the technique. Nevertheless,

TABLE 4.—*Comparison of radiochemical data obtained shortly after sample collection and data redetermined in 1976*

[If the original data did not report a value for the specific sample remeasured, a range of values is given, and the number of samples represented by that range is shown in parentheses. Leaders (---) indicate no data available]

Sample locality (see fig. 1)	Original collection date	U content (µg/L)		Ra^{226} equivalent (pCi/L)		Alpha (U^{238} equivalent) (µg/L)		Beta (Sr^{90} equivalent) (pCi/L)	
		Original	1976	Original	1976	Original	1976	Original	1976
Well 5C	[1]3/23/71	4.3-7.4(6)	5.0	<0.1	0.05	17	14	9	9
Well J-12	3/26/71	0.2-0.6(4)	[2].56	---	---	---	---	---	---
Well J-13	3/26/71	0.7(2)	.5	---	---	---	---	---	---
Well UE15d	11/15/71	2.7-2.8(2)	[2]3.98	---	---	---	---	---	---
Well U20A-2	10/06/71	2.9	3.0	---	---	---	---	---	---
Well C-1	3/29/71	6.3-8.0(4)	5.1	1.3	.9	34	49	16	15
Well C	[1]4/11/69	6.3-7.5(5)	[2]7.05	1.0-1.4(5)	1.1	54	85	19	28
Well C	3/29/71	6.3	[2,3]6.28	1.0	[3].6	28	32	14	19
Well C	5/28/71	6.3-7.5(5)	[2]6.79	1.0-1.4(5)	.6	33	42	15	28
Well C	[1]11/15/71	6.3-7.5(5)	4.7	1.0-1.4(5)	1.4	55	34	18	11

[1] Sample acidified prior to storage.

[2] Data obtained by isotope dilution alpha spectrometry.

[3] An 8 *N* HNO_3 acid solution used to rinse this sample's storage bottle contained 0.64 µg/L U and 0.4 pCi/L Ra^{226} equivalent.

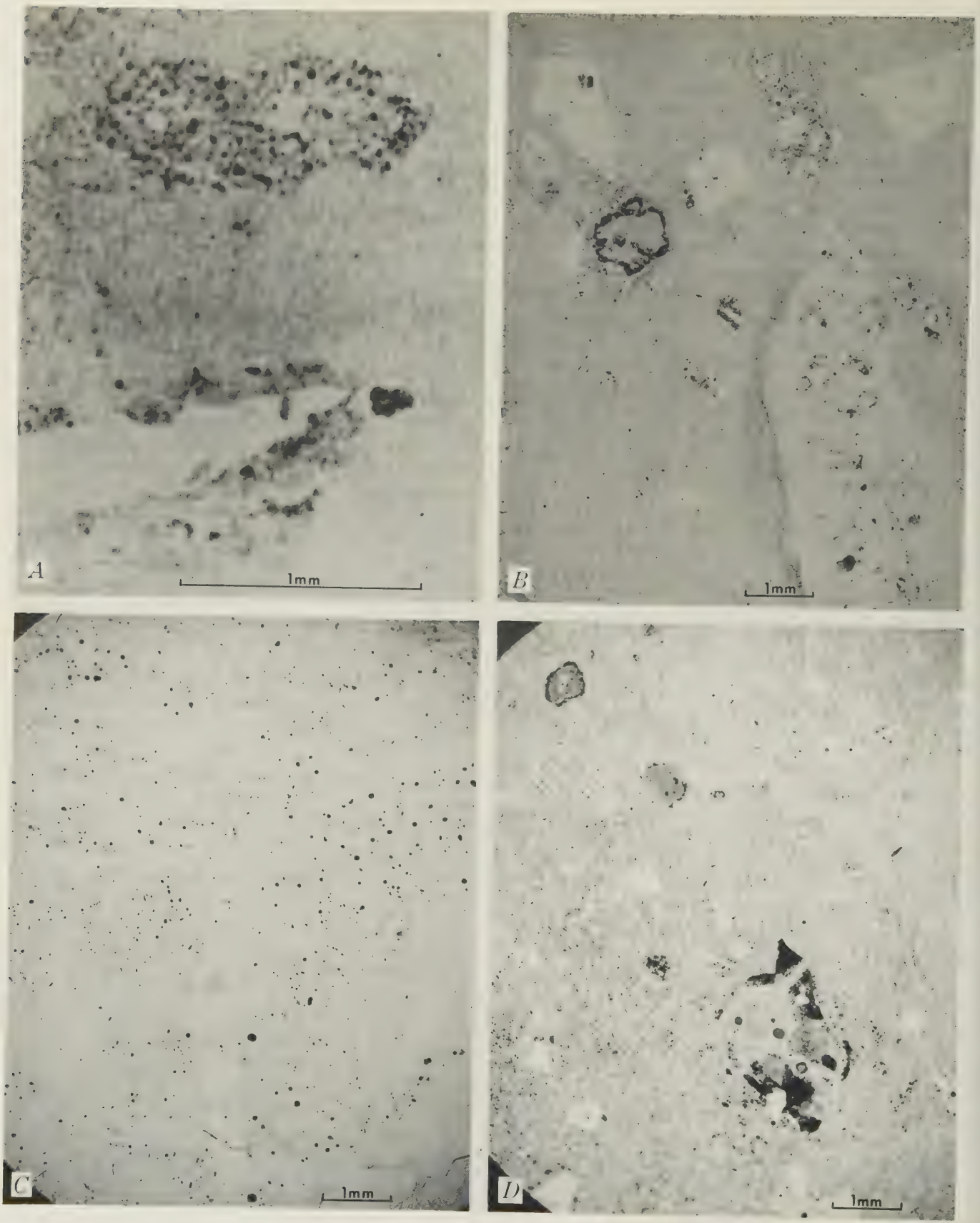

FIGURE 2

he absence of systematically lower values in rede-ermined samples indicated the emitting species are ong-lived.

Uranium Distribution and Abundance in Tuffaceous Aquifer Rocks

Uranium and thorium abundances in tuffaceous quifer rocks were determined by the delayed neutron echnique (table 5). Uranium abundances range from .6–9.0 ppm, while thorium abundances range from .7–27.4 ppm. Detailed sampling within a number of nits revealed generally homogenous uranium and horium contents which were independent of quali-ative estimates of the degree of welding or alteration. A fresh glassy zone within a densely welded unit could ot be distinguished from neighboring devitrified elded tuffs on the basis of uranium or thorium con-ent. The sharp gradients of uranium concentration etween some neighboring units and the constant ranium content within units argues against major obilization and (or) redistribution of uranium. Fis-ion-track maps of uranium distribution in thin ections indicated that some minor redistribution of ranium had occurred in altered samples. Uranium obility is evidenced through concentration of uranium n secondary oxides of iron, manganese, and titanium, hich form as alteration rims or collect in areas most ccessible to water such as microfissures or pumices fig. 2). Uptake of uranium by surficial alteration roducts of rhyolite explains the lower uranium con-

TABLE 5.—*Uranium and thorium abundances in core samples of the Grouse Canyon Member of the Belted Range Tuff, Rainier Mesa, Nevada Test Site*

Surface depth (meters)	U (ppm)	Th (ppm)	Th/U	Lithology[1]
				Core number UE12T#1
219.3	5.0	13.9	2.8	Ash flow, moderately welded.
220.3	4.1	21.0	5.1	Ash fall, zeolitized, welded.
221.7	5.3	14.7	2.8	Ash flow, zeolitized, densely welded.
224.0	5.8	20.8	3.6	Vitrophyre, black, vitreous.
224.9	5.7	22.7	4.0	Vitrophyre, black, zeolite present.
225.2	5.5	27.1	4.9	Ash fall, moderately welded.
225.8	5.4	24.8	4.6	Do.
226.4	5.3	26.5	5.1	Ash fall, moderately welded; abundant pumice and vitrophyre.
227.6	5.7	22.4	4.0	Do.
235.9	5.3	21.8	4.2	Ash fall; coarseness and alteration of pumice fragments increases with depth.
236.8	5.4	20.3	3.8	Do.
237.7	5.1	21.9	4.3	Do.
239.5	5.4	20.4	3.8	Do.
				Core number UE12P#1
367.5	2.6	9.2	3.5	Ash fall, slightly welded, zeolitized.
368.0	2.9	9.3	3.2	Do.
370.6	4.5	11.9	2.6	Ash fall, moderately welded.
383.7	4.5	20.0	4.4	Ash fall, highly zeolitized.
385.2	3.8	16.8	4.4	Ash flow, densely welded.
385.5	3.8	16.1	4.3	Do.
386.1	4.1	18.1	4.4	Do.
387.1	6.8	21.7	3.2	Do.
387.8	4.7	13.6	2.9	Do.
390.1	6.4	19.1	3.0	Do.
396.8	4.7	21.0	4.4	Do.
403.1	4.8	19.9	4.2	Ash flow, poorly welded, strongly zeolitized.
404.0	4.9	19.2	3.9	Do.
404.4	4.6	19.6	4.2	Do.
408.5	4.1	21.3	5.2	Ash fall, poorly welded, zeolitized.
411.4	4.9	21.6	4.4	Do.
416.0	5.1	18.0	3.6	Do.
422.7	4.5	19.3	4.3	Tuffaceous sand.
425.8	5.7	18.6	3.3	Ash fall, fine, zeolitized.
430.0	4.4	20.1	4.6	Do.
432.0	4.3	27.4	6.3	Tuffaceous sand.
				Core number UE12G10#1
401.2	4.4	16.6	3.7	Ash-flow tuff, moderately to densely welded.
405.3	4.2	16.7	4.0	Do.
409.3	4.3	18.3	4.3	Do.
412.3	4.2	20.7	4.9	Do.
414.8	5.0	19.8	4.0	Do.
416.2	5.0	24.6	5.0	Do.
417.2	4.4	16.7	3.8	Do.
421.0	7.5	20.6	2.8	Ash-fall tuff, zeolitized.
421.2	6.9	25.3	3.7	Do.
421.7	7.0	20.7	3.0	Do.
422.0	8.1	20.9	2.6	Do.
422.3	7.7	20.4	2.6	Do.
422.4	8.3	20.0	2.4	Do.
423.0	8.2	22.5	2.7	Do.
423.2	9.0	18.9	2.1	Do.
423.3	8.2	20.9	2.6	Do.
423.6	8.5	16.7	2.0	Do.
423.8	7.1	14.4	2.0	Do.
424.1	8.3	19.4	2.3	Do.

[1]Lithological units and descriptions provided by Walter Danilchik (written commun., 1968).

FIGURE 2.—Fission-track maps (photographs) of uranium distribution in the Grouse Canyon Member of the Belted Range Tuff. *A*, Surface sample of densely welded tuff. Uranium distribution is homogeneous in glassy matrix but inhomogeneous in pumice (upper) and in manganese oxides surrounding a plagioclase lath (lower). *B*, Core UE12P#1 sampled at 389.2 m in densely welded tuff. The glassy matrix shows uniform uranium distribution but heterogeneous uranium distribution occurs in pumice (upper right), magnetite rims (upper left) and along borders of matrix and pumice (lower right). *C*, Core UE12P#1 sampled at 380.8 m in zeolitized tuff. Uranuim distribution is in many tiny point sources which correspond to iron oxide concentrations. Some uranium in this sample was remobilized during epoxy impregnation. Uraniferous debris collected in airbubble pits which were transected during production of the thin section. Resultant pits also appear as uranium hotspots. *D*, Core UE12G10#1 sampled at 420.2 m in devitrified tuff. Groundmass uranium is distributed in many very small point sources. Major uranium concentrations occur as rims of rutile grains (upper left) and aong boundaries of groundmass and a glassy spherulite (lower right).

tent and the greater U^{234} enrichment of tuffaceous aquifer water compared to carbonate aquifer water. Preferential recoil of U^{234} into solution is enhanced by coating grains with relatively insoluble, uraniferous phases (Osmond and Cowart, 1976). In order to contrast with Rainier Mesa samples, future samples of tuffaceous aquifer rocks should concentrate on areas which presently experience high rates of ground water flow (Pahute Mesa wells; Blankennagel and Weir, 1973).

REFERENCES CITED

Barker, F. B., and Johnson, J. O., 1964, Determination of radium in water: U.S. Geol. Survey Water-Supply Paper 1696–B, 29 p.

Barker, F. B., Johnson, J. O., Edwards, K. W., and Robinson, B. P., 1965, Determination of uranium in natural waters: U.S. Geol. Survey Water-Supply Paper 1696–C, 25 p.

Blankennagel, R. K., and Weir, J. E., Jr., 1973, Geohydrology of the eastern part of Pahute Mesa, Nevada Test Site, Nye County, Nevada: U.S. Geol. Survey Prof. Paper 712–B, 35 p.

Chalov, P .I., 1959, The $^{234}U/^{238}U$ ratio in some secondary minerals: Geochemistry (a translation of Geokhimiya), 1959, p. 203–210.

Chalov, P. I., and Merkulova, K. I., 1966, Comparative rate of oxidation of U-234 and U-238 atoms in certain minerals: Acad. Sci. USSR Doklady, Earth Sci. Sec., v. 167, p. 146–148.

Claassen, H. C., 1973, Water quality and physical characteristics of Nevada Test Site water-supply wells: Available only from U.S. Dept. Commerce, Natl. Tech. Inf. Service, Springfield, VA 22161 as U.S. Geol. Survey Rept. USGS–474–158, 145 p.

Clebsch, Alfred, Jr., 1961, Tritium age of ground water at the Nevada Test Site, Nye County, Nevada, *in* Short papers in the geologic and hydrologic sciences: U.S. Geol. Survey Prof. Paper 424-C, p. C122–C125.

Clebsch, Alfred, Jr., and Barker, F. B., 1960, Analyses of ground water from Rainier Mesa, Nevada Test Site, Nye County, Nevada: U.S. Geol. Survey Trace Elements Inv. Rept. 763, 22 p.

Eckel, E. B. ed., 1968, Nevada Test Site: Geol. Soc. America Mem. 110, 350 p.

Fix, P. F., 1956, Hydrogeochemical exploration for uranium: U.S. Geol. Survey Prof. Paper 300, p. 667–671.

Flynn, W. W., 1968, The determination of low levels of polonium-210 in environmental materials: Anal. Chim. Acta, v. 43, p. 221–227.

Garrels, R. M., and Christ, C. L., 1965, Solutions, minerals, and equilibria, New York, Harper and Row, 450 p.

Grove, D. B., Rubin, Meyer, Hanshaw, B. B., and Beetem, W. A., 1969, Carbon-14 dates of ground water from a Paleozoic carbonate aquifer, south-central Nevada, *in* Geological Survey research 1969: U.S. Geol. Survey Prof. Paper 650–C, p. C215–C218.

Hoover, D. L., 1968, Genesis of zeolites, Nevada Test Site, *in* Eckel, E. B., ed., Nevada Test Site: Geol. Soc. America Mem. 110, p. 275–284.

Kaufman, M. I., Rydell, H. S., and Osmond, J. K., 1969, $^{234}U/^{238}U$ disequilibrium as an aid to hydrologic study of the Floridan aquifer: Jour. Hydrology, v. 9, p. 374–386.

Kronfeld, J., 1972, Hydrologic investigations and the significance of $^{234}U/^{238}U$ disequilibrium in the ground water of central Texas: Houston, Tex., Rice Univ., Ph. D. dissert., 78 p.

Lipman, P. W., 1965, Chemical comparison of glassy and crystalline volcanic rocks: U.S. Geol. Survey Bull. 1201–D, 24 p.

Millard, H. T., Jr., 1976, Determination of uranium and thorium in USGS standard rocks by the delayed neutron technique: U.S. Geol. Survey Prof. Paper 840, p. 61–65.

Noble, D. C., 1970, Loss of sodium from crystallized comendite welded tuffs of the Miocene Grouse Canyon Member of the Belted Range Tuff, Nevada: Geol. Soc. America Bull., v. 81, p. 2677–2688.

Osmond, J. K., and Cowart, J. B., 1976, The theory and uses of natural uranium isotopic variations in hydrology: Atomic Energy Review, I.A.E.A., Vienna, v. 14, no. 4.

Robinson, B. P., and Beetem, W. A., 1975, Quality of water in aquifers of the Armagosa desert and vicinity, Nevada: U.S. Dept. Commerce, Natl. Tech. Inf. Service, USGS–474–215, 64 p.

Rosholt, J. N., Shields, W. R., and Garner, E. L., 1963, Isotopic fractionation of uranium in sandstone: Science, v. 139, p. 224–226.

Rosholt, J. N., Doe, B. R., and Tatsumoto, M., 1966, Evolution of the isotopic composition of uranium and thorium in soil profiles: Geol. Soc. America Bull., v. 77, p. 987–1003.

Schoff, S. L., and Moore, J. E., 1964, Chemistry and movement of ground water, Nevada Test Site: U.S. Geol. Survey Trace Elements Inv. Rept. 838, 75 p.

Thatcher, L. L., Janzer, V. J., and Edwards, K. W., 1977, Methods for determination of radioactive substances in water and fluvial sediments: U.S. Geol. Survey Techniques Water-Resources Inv., book 5, chap. A5, 94 p.

Truesdell, A. H., 1966, Ion-exchange constants of natural glasses by the electrode method: Am. Mineralogist, v. 51, p. 110–121.

Winograd, I. J., and Thordarson, William, 1975, Hydrogeologic and hydrochemical framework, south-central Great Basin, Nevada-California, with special reference to the Nevada Test Site: U.S. Geol. Survey Prof. Paper 712–C, 126 p.

Jour. Research U.S. Geol. Survey
Vol. 6, No. 4, July–Aug. 1978, p. 499–504

DISCRIMINATION OF FLUVIAL AND EOLIAN DEPOSITS BY NUMBER-FREQUENCY ANALYSIS OF SEDIMENTS OF SAND THROUGH SILT SIZE FROM A POINT BAR, RIO PUERCO, NEW MEXICO

By R. G. SHEPHERD,[1] and D. L. MACKE,
Wheat Ridge, Colo., Golden, Colo.

Abstract.—Fluvial and eolian deposits are interbedded in phemeral-stream, arid-region point bars in the channel of ne Rio Puerco, west of Albuquerque, N. Mex. Number-requency distributions of grain size for both types of de-osits were obtained using an electronic automatic image nalyzer for a suite of 10 samples. The number-frequency esults were superior to weight-frequency (sieve) results in iscriminating between eolian units and fluvial units in a ertical point-bar sequence. The image-analysis technique lso identified those fluvial deposits whose size distributions ave been altered significantly by winds, as well as fluvial eposits that do not show a prominent eolian-process com-onent.

Can interbedded eolian and fluvial deposits of arid-egion point bars be differentiated through mechanical nalysis? Previous attempts to unequivocally discrimi-nate between these two types of deposits on the basis f texture constitute a considerable literature. (See ettijohn, 1975, chap. 3, and Folk, 1966, for refer-nces.) Probably most sedimentologists would agree hat an inordinate number of these attempts have ailed to satisfactorily attain this goal (Bigarella, 972; Ahlbrandt, 1975, Moiola and Weiser, 1968, p. 9). We met this classic problem of environmental iscrimination during an investigation of depositional rocesses and structures in a potential modern analog f some ancient uranium-bearing sandstone forma-ions in the Rio Puerco alluvial valley west of Albu-uerque, N. Mex. (fig. 1). In this arid fluvial environ-nent, wind ripples and dunes are common features, oth along the thalweg (which may be dry more than hree-fourths of the year), and higher up on the point ars of the sinuous entrenched channel. Such wind eposits are commonly preserved within point-bar equences as they are inundated by floods that rapidly eposit large amounts of fine sand and silt from sus-ension. In places the deposits have practically un-

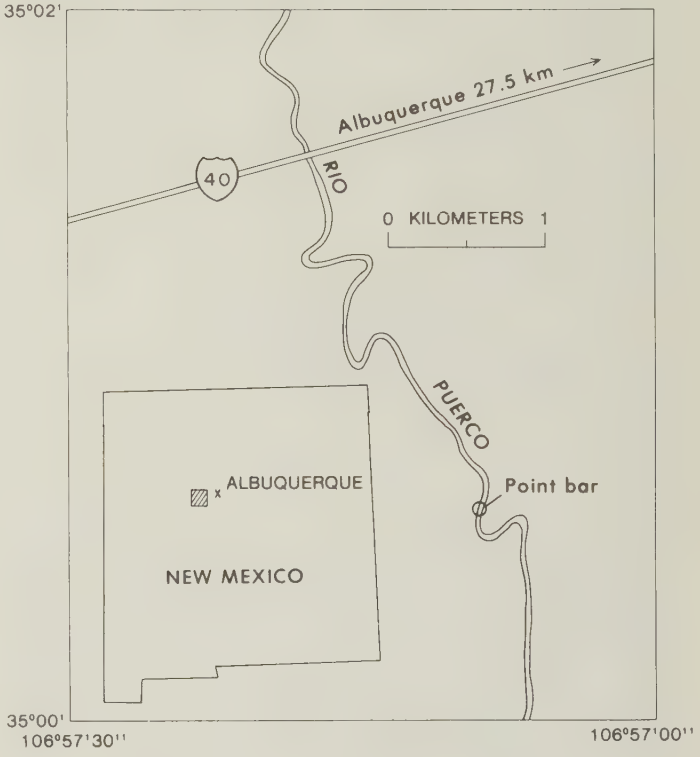

FIGURE 1.—Rio Puerco channel and point bar sampled for this study.

altered textures and structures. The channel pattern changes rapidly as bends migrate, causing preservation of complete point-bar sequences. Layers of wind-deposited sediment exist in some point bars that have been constructed almost entirely within the past 20 years as well as in valley alluvium deposited hundreds of years ago and now exposed in the entrenched-channel walls. Most wind deposits are easily recognized because, as compared to fluvial units, they are more friable, contain less clay, are more evenly laminated

[1] Willard Owens Associates, Inc., 7391 W. 38th Ave., Wheat Ridge, O 80033.

(commonly having inversely graded laminae) and are, consequently, more easily eroded. Sharp ledges form at their lower contacts. In addition, almost all fluvial units show sedimentary structures, textures, and sequences indicative of floods in dry regions (McKee and others, 1967; Denny, 1965, p. 12; Picard and High, 1973). For some units, however, it is difficult to ascertain the depositional agent because eolian deposits may be completely reworked by floods; between floods, high winds frequently alter the texture and distribution of fluvial detritus. Consequently, as an adjunct to interpreting the depositional agent, we used an uncommon method of grain size analysis. Our methods of determination of size distributions were different from those of previous investigators and produced noteworthy, if preliminary, results.

Acknowledgments.—Robert F. Gantnier performed sieve and hydrometer analyses. Carla Potter computed the weight-frequency data from the automatic-image-analyzer data.

NUMBER-FREQENCY ANALYSIS OF SAND- THROUGH SILT-SIZE SEDIMENTS

We used number-frequency data, through the silt range, to characterize size distributions. The phi-mean size of clast was almost always in the coarse- or medium-silt range (60–16 μm). The lengths of four diameters measured at 45° rotations were averaged for each of approximately 500 grains in a sample. Manually, this procedure would be impracticable, but we used an electronic automatic image analyzer (AIA) to do this rote work. Basically, the uncemented grains in the field of view of a microscope were measured by an image-reproducing electronic process, and the data were analyzed directly by computer (Textoris, 1971; Peach and Perrie, 1975; Cole, 1971, has an extensive bibliography). The AIA method does not produce results equivalent to counting in thin section. The AIA dimensions are measured from the projected outline of an entire grain lying on a glass plate, whereas for a thin-sectioned grain, commonly only some smaller section of a grain is observed.

One reason the numerical method of size analysis was attempted is that the statistical parameters used to describe sediments were originally developed for and should theoretically be applied only to number-frequency data, not weight-frequency data as is obtained with sieves (Blatt and others, 1972, p. 44). Another more important reason is that, especially for silt-size sediment, a significant disparity exists between the results of weight-frequency and number-frequency analysis for the same sample. This disparity is well illustrated by a comparison of the number- and weight-frequency distributions of a grab sample of sandy mud (fig. 2) collected from ripples on the surface of

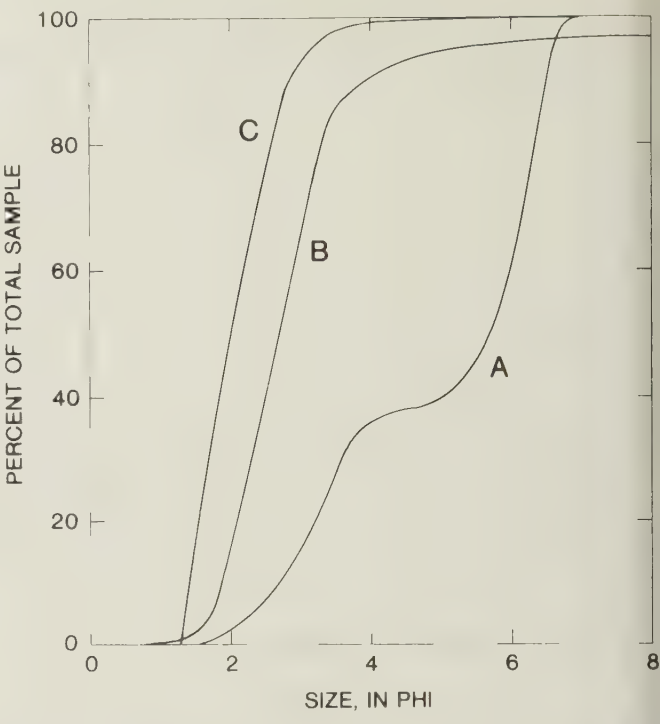

FIGURE 2.—Cumulative size-frequency distribution curves for a grab sample of eolian ripples, collected when the wind was not blowing. Curve A, number-frequency curve obtained by the automatic image analyzer; curve B, the direct weight-frequency curve obtained by sieving (one-quarter-phi intervals) and hydrometer analysis; and curve C, data of curve A converted to weight frequency.

an eolian deposit in the channel of the Rio Puerco. Curve A represents the AIA number-frequency distribution. Notice the prominent plateau, principally occupying the coarse-silt range and the 35th-percentile to 45th-percentile range of the cumulative distribution. This plateau is not apparent in the weight-frequency distribution from the sieve data in curve B, or in curve C, which represents number-frequency data of curve A converted to weight frequency.

To illustrate why this plateau is not apparent for weight-frequency data, the simple procedure of converting the AIA number-frequency data to weight-frequency data was performed. That is, grains of quartz (specific gravity=2.65) of spherical shape were assumed. The weight of each grain was calculated using the average of the four measured diameters to calculate volume. The resulting weight-frequency curve (C in fig. 2) has almost exactly the same shape as the

ve curve B. The reason the plateau of curve A is t shown by curve C is that grain weight is proportional to the cube of the diameter. Because the silt and ay grains constitute little of the total weight, they e not prominent in weight-frequency analysis. This why only 40 percent (the coarsest fraction) of the ains of the sample constitute 95 percent of the eight.

AN EOLIAN DISCRIMINANT?

The dearth of coarse-silt grains in eolian ripples was ocumented long ago by Udden (1898), who discussed is paucity in relation to the common abundance of ry fine sand and coarse silt in loess. Udden (1898, p.) also obtained number-frequency distributions of e smallest sizes by using counts of loose grains under e microscope. Since Udden's classic paper, hundreds analyses of textural attributes of eolian sediments ave been made, but texture has not been as valuable most sedimentologists would like in unequivocally entifying the eolian depositional environment Bigarella, 1972; Ahlbrandt, 1975). Furthermore, the nspicuous paucity of certain size ranges of clasts comes obscured if enough sample distributions are mped together for consideration (Shea, 1974). Even , Udden's (1898; 1914) data and conclusions alone ovide sufficient reason to attempt to ascertain hether the paucity of coarse silt shown in the wind-pple sample (fig. 2) is indicative of depositional rocess.

The wind-ripple sample having the distributions of gure 2 was collected the day after a brisk wind had used rapid ripple migration. To determine the effect wind entrainment of particles, a sample was later llected from identical ripples that were migrating hile the wind was blowing. Size-frequency distributions were obtained for this sample (fig. 3) in the me manner as those for the nonmigrating-ripple mple (fig. 2). The curves in figures 2 and 3 have sentially the same properties, except that the moving-pple sample has a sharper and flatter plateau at a gher percentile range of measured and accrued grains curve A). Indeed, only 8 of 497 grains measured were the coarse-silt range.

COMPARISON WITH ADJACENT FLUVIAL DISTRIBUTIONS

If the number-frequency method of identifying the ind-induced dearth of coarse silt was to have merit the Rio Puerco study, it had to provide distinctive stributions for samples taken from adjacent eolian d fluvial deposits. This requirement was essential be-

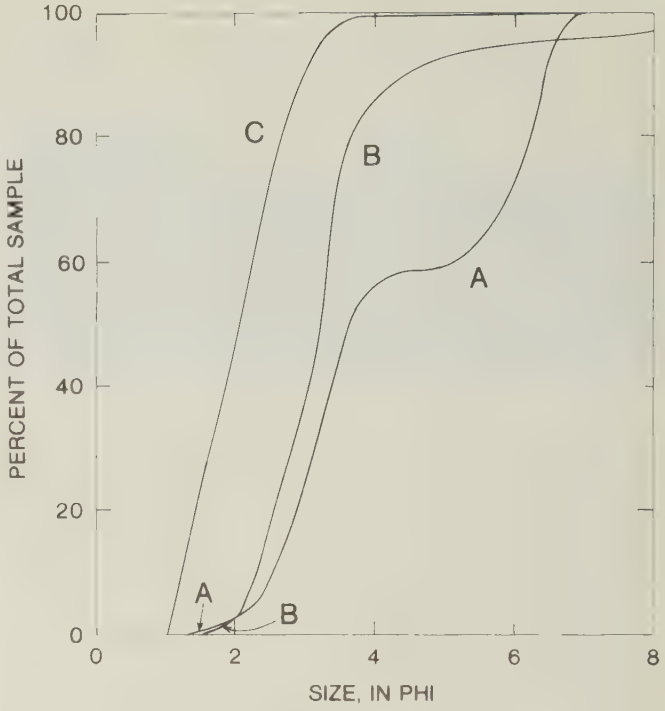

FIGURE 3.—Cumulative size-frequency distribution curves for a grab sample of migrating eolian ripples, collected when the wind was blowing briskly.

cause in Rio Puerco point-bar deposits, sheets and wedges of eolian sediment are preserved between units deposited by floods. In order to determine the effect of these processes on channel-sediment sizes, a vertical suite of samples was collected from a Rio Puerco point bar (fig. 1) south of where U.S. Interstate Route 40 crosses the channel (sec. 15, T. 9 N., R. 1 W., Bernalillo County). Our basic purpose in sampling was to determine the vertical change in grain size. At this location the modern point-bar deposit is being removed by bank erosion as the meander migrates. Consequently, a 5-m wall containing a complete point-bar depositional sequence is exposed (fig. 4*A*). The central part of this wall contains one wedge-shaped unit of sand (unit W1–6, fig. 5) which is texturally and structurally different from its overlying and underlying neighbors. It is poorly cohesive, evenly bedded, and apparently has less clay. The unit is truncated where it adjoins a scarp formed in rippled fluvial sediment, and it contains small angular slumped clasts of the scarp-forming material. These are textural and structural factors that exactly correspond to active eolian sand drifts in the lee of small scarps on the active point-bar surface just downstream, a fact indicating

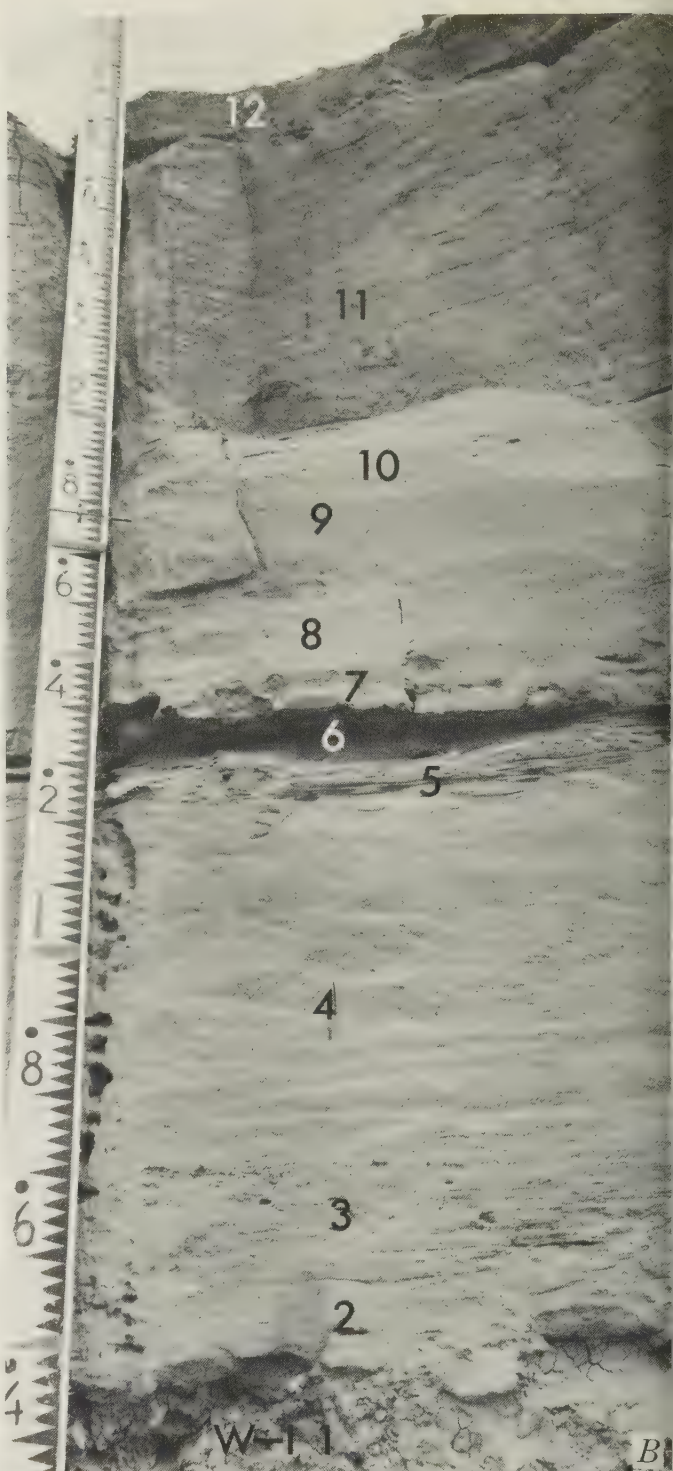

FIGURE 4.—Rio Puerco point-bar wall. *A*, Site where the vertical suite of eolian and fluvial samples (designated by numbers 1–12) was collected at the 4-m stadia rod (graduated in meters and tenths of meters). *B*, The number 6 designates the eolian unit in the sequence for which size curves are given in figure 5. Note that the interesting lateral-accretion surfaces, one of which the eolian bed rests on, slope to the right in the direction of point-bar construction and meander migration.

that this unit is eolian. A suite of 10 samples was used to characterize this wedge-shaped unit and those above and below it in the point-bar sequence (fig. 4*B*).

Both weight-frequency (sieve) and number-frequency (AIA) analyses were performed for the suite of samples (fig. 5). The mean sizes are notably different for the two methods of analysis, as expected. However, the AIA data indicate that, using number-frequency analysis, there is less variability between samples and that the unit hypothesized as eolian has a mean size significantly different from the other units. The textural similarities of the samples from the eolian ripples (figs. 2, 3) and this unit are striking.

Considering all the samples, three families of number-frequency size-distribution curves can be recognized (fig. 5). The eolian sediments (figs. 2, 3, and 5) all have size distribution curves showing marked plateaus in conjunction with a notable paucity of grains in and around the size of coarse silt. In addition, eolian curves show the highest proportion of sand (numerically at least 40–50 percent). In contrast, the fluvial group of distribution curves shows a commonly low percentage of sand (less than 10 percent) and no plateau. The paucity of sand in this group of samples is also reflected in the sieve-analysis curves, which singularly all cross the AIA curves (fig. 5). The third group of size-distribution curves shows intermediate characteristics and is designated fluvioeolian (fig. 5). Sedimentary structures and other criteria affirm that the fluvioeolian units were deposited by floods, but all the size-distribution curves have prominent plateaus in the lower cumulative percentages (but generally less than 25 percent). Fluvioeolian sieve-analysis curves do not cross AIA curves like the fluvial curves do. Apparently coarse silt grains were removed from fluvioeolian sediment by wind erosion and were not com-

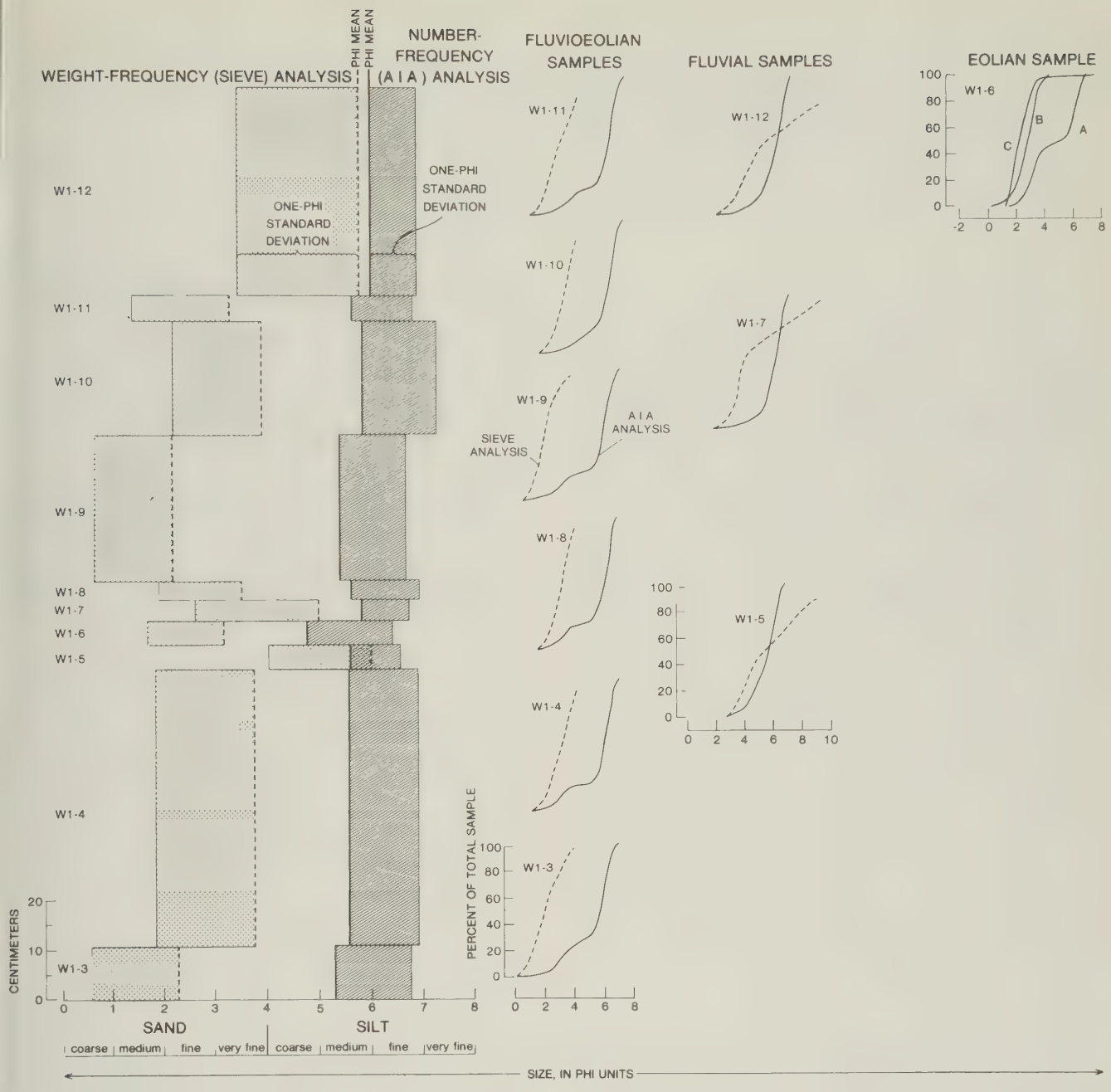

FIGURE 5.—Grain-size properties of samples taken from units W1–3 through W1–12 in the vertical sequence of the Rio Puerco point bar. Dotted pattern shows sieve results. The phi mean is plotted on the right of the column and the width represents one phi standard deviation. Hatched pattern shows automatic image analyzer (AIA) results. The phi mean is plotted on the left and the width represents one phi standard deviation. Size-distribution curves for the eolian sample have the same designations as those in figures 2 and 3. The other cumulative size distributions have dashed curves for sieve analysis (one-half phi intervals and hydrometer analysis for fines) and solid curves for AIA analysis.

etely replaced during flooding. Using the AIA num-er-frequency method, the majority of size-distribution urves for Rio Puerco sediments were identified as of ie fluvioeolian type.

Unfortunately, we cannot yet unequivocally predict depositional-agent distinctions for all units of Rio Puerco point bars. Absolute grain size, postdepositional infiltration of mud into both wind and flood deposits,

and the stage of development of point bars are only some of the additional factors not yet adequately investigated. Furthermore, the calibration and standardization of AIA procedures and the statistical evaluation of AIA results for textural analysis have yet to be satisfactorily determined. Nevertheless, the three groups of curves—fluvial, eolian, and fluvioeolian—are notably distinctive, despite the close proximity of samples from the point-bar exposure discussed here.

REFERENCES CITED

Ahlbrandt, T. S., 1975, Comparison of textures and structures to distinguish eolian environments, Killpecker dune field, Wyoming: Mountain Geologist, v. 12, no. 2, p. 61–73.

Bigarella, J. J., 1972, Eolian environments; their characteristics, recognition, and importance, *in* J. K. Rigby, and W. K. Hamblin, Recognition of ancient sedimentary environments: Soc. Econ. Paleontologists and Mineralogists Spec. Pub. 16, p. 12–62.

Blatt, Harvey, Middleton, Gerard, and Murray, Raymond, 1972, Origin of sedimentary rocks: Englewood Cliffs, N.J., Prentice-Hall, 634 p.

Cole, M., 1971, Instrument errors in quantitative image analysis: The Microscope, v. 19, no. 1, p. 87–103.

Denny, C. S., 1965, Alluvial fans in the Death Valley region, California and Nevada: U.S. Geol. Survey Prof. Paper 466, 62 p.

Folk, R. L., 1966, A review of grain-size parameters: Sedimentology, v. 6, no. 2 p. 73–93.

McKee, E. D., Crosby, E. J., and Berryhill, H. L., 1967, Flood deposits, Bijou Creek, Colorado, June, 1965: Jour. Sed. Petrology, v. 37, p. 829–851.

Moiola, R. J., and Weiser, D., 1968, Textural parameters—an evaluation: Jour. Sed. Petrology, v. 38, no. 1, p. 45–53.

Peach, P. A., and Perrie, L. A., 1975, Grain-size distribution within glacial varves: Geology, v. 3, no. 1, p. 43–46.

Pettijohn, F. J., 1975, Sedimentary rocks [3d ed.]: New York, Harper and Row, 628 p.

Picard, M. D., and High, R. L., Jr., 1973, Sedimentary structures of ephemeral streams, No. 17 *of* Developments in sedimentology: Amsterdam, Elsevier Publishing Co., 222 p.

Shea, J. H., 1974, Deficiencies of clastic particles of certain sizes: Jour. Sed. Petrology, v. 44, p. 985–1003.

Textoris, D. A., 1971, Grain-size measurement in thin-section, Chap. 5 *in* Carver, R. E., Procedures in sedimentary petrology: New York, Wiley-Interscience, p. 95–107.

Udden, J. A., 1898, The mechanical composition of wind deposits: Augustana Library Pub. 1, 69 p.

——— 1914, Mechanical composition of clastic sediments: Geol. Soc. America Bull., v. 25, p. 655–744.

Jour. Research U.S. Geol. Survey
Vol. 6, No. 4, July–Aug. 1978, p. 505–509

SPECTRAL GRADIENT OF LUNAR RADIOBRIGHTNESS—HEAT FLOW OR VOLUME SCATTERING?

By A. W. ENGLAND and G. R. JOHNSON,
Reston, Va., Denver, Colo.

Abstract.—Lunar heat flow cannot be derived unambiguously from the spectral gradient of the radiobrightness. Volume scattering of microwaves by rock clasts within the lunar regolith results in a spectral component in the 5- to 30-centimeter range of wavelengths that is a significant fraction of that resulting from lunar heat flow.

Lunar heat flow has been inferred from Earth-based measurements of the Moon's radiobrightness (Baldwin, 1961; Tikhonova and Troitskii, 1969; Keihm and Langseth, 1975a). A heat-flow-sensing, polychromatic radiometer has been proposed as one of the primary experiments for NASA's Lunar Polar Orbiting Satellite (U.S. Goddard Space Flight Center, 1975, p. 40–41). The principle employed is that longer wavelength, radio-thermal emission originates deeper within the lunar regolith than does shorter wavelength emission; thus, an increase in radiobrightness with wavelength implies an increase in thermal temperature with depth. Many of the problems of deriving heat flow from the spectral gradient of radiobrightness have been reviewed elsewhere (Troitskii and Tikhonova, 1970; Hagfors, 1970; Muhleman, 1972; Linsky, 1966). A problem that has not been considered is that of scattering of microwaves by rock clasts within the regolith. Because of this scattering, the proposed Lunar Polar Orbiting experiment may yield unacceptably ambiguous heat flows.

Keihm and Langseth (1975b) showed that only the spectral range between 5 and 30 cm is useful for determining heat flow. Shorter wavelength emission originates at shallow depths where the thermal temperature follows the diurnal insolation. Longer wavelength thermal emission originates near the base of the homogeneous regolith. Boulders and incoherent rock strata deep in the regolith scatter the microwaves and produce the apparently negative spectral gradient observed at wavelengths between 50 and 500 cm (Salisbury and Hernald, 1971).

In the spectral range of 5 to 30 cm, the spectral gradient yields heat flow only if there are no competing phenomena. England (1975) used radiative transfer scattering theory to show that the ubiquitous, 1-cm-size rock clasts found throughout the lunar regolith would darken radiobrightness at centimeter and decimeter wavelengths. Grain size distributions obtained from Apollo soil samples and from Surveyor images are used in this report to derive the spectral characteristics of scatter-induced lunar darkening. England's scattering theory is modified to include a thermal gradient, Q/k, where Q is heat flow and k is thermal conductivity.

The lunar surface can be approximated by 10 to 30 m of regolith lying upon a basaltic halfspace, even though the interface between regolith and basalt is probably indistinct (Keihm and Langseth, 1975b, Kovach and Watkins, 1973). The radiobrightness at wavelengths shorter than 30 cm is relatively insensitive to the characteristics of the interface. The regolith itself can be modeled as a homogeneous powder containing a distribution of spherical rock clasts. The assumption of sphericity is necessary for the problem to be mathematically tractable.

The radiobrightness of the two-layer medium depends upon the scattering albedo, ω,

$$\omega = \frac{\psi}{\psi + \lambda^3}, \qquad (1)$$

where λ is free-space wavelength and the scattering parameter, ψ, is

$$\psi = 2\pi^3 \left(\frac{\varepsilon_1^{3/2}}{\tan \delta_1} \right) \left(\frac{\varepsilon_s/\varepsilon_1 - 1}{\varepsilon_s/\varepsilon_1 + 2} \right)^2 \sum_j \ell_j^3 v_j. \qquad (2)$$

The physical properties are relative permittivity, ϵ_1, and loss tangent, $\tan \delta_1$, of the layer; relative per-

mittivity, ϵ_s, of the rock clasts; and volume fraction, $\bar{v}_j$, of rock clasts having diameter l_j. R. M. Fruland and D. S. McKay (written commun., 1975) have provided us a list of mass fractions for grains in the 1–2 mm, 2–4 mm, and 4–10 mm ranges of diameter for 60 lunar soil samples. The particle and bulk densities in table 1

TABLE 1.—*Physical properties of the two-layer model of the lunar surface*

[ρ is density, k is thermal conductivity, and $\ell_\lambda = \lambda/(2\pi\sqrt{\epsilon}\tan\delta)$ is dielectric absorption length where ϵ is relative permittivity and tan δ is dielectric loss tangent]

Material	ρ (g/cm^3)	k (W/m- K)	ϵ	ℓ_λ
Soil	[1]2.0	[2]0.023	[3]3.0 (<10cm) [4]4.0 (>10cm)	[3]50λ
Rock clasts	[4]2.8		[4]6.5	
Bedrock	[4]2.8	[2]1.1	[4]6.5	[4]10λ

[1] Carrier and others, 1973.
[2] Keihm and Langseth, 1975b.
[3] Gold and others, 1973.
[4] Bassett and Shackelford, 1972.

were used to convert mass fractions to the Apollo volume fractions shown in table 2. The average scat-

TABLE 2.—*Grain-size distribution for Apollo and Surveyor soils*

[The Apollo $\bar{v}_j\,\Delta\ell$ are derived from the mass fractions, χ_j, listed by Fruland and McKay, written communication. That is, $\bar{v}_j\,\Delta\ell = (\rho_{soil}/\rho_{rock})\,\chi_j$ where ρ_{soil} = 2.0 g/cm^3 and ρ_{rock} = 2.8 g/cm^3. The Surveyor volume fractions are integrations of Equation 5]

Mission	K (mm$^{-\gamma}$)	γ	$\int_{1mm}^{2mm} \bar{v}\,d\ell$	$\int_{2mm}^{4mm} \bar{v}\,d\ell$	$\int_{4mm}^{10mm} \bar{v}\,d\ell$
Apollo 14	---	---	0.0490	0.0449	0.0595
Apollo 15	---	---	.0456	.0580	.0751
Apollo 16	---	---	.0743	.0543	.0429
Apollo 17	---	---	.0392	.0313	.0356
Apollo Average	---	---	.0520	.0471	.0533
Surveyor I	5.0 x 10^5	-2.11	.0055	.0050	.0063
Surveyor III	3.3 x 10^6	-2.56	.0382	.0258	.0219
Surveyor V	1.25 x 10^6	-2.65	.0145	.0092	.0073
Surveyor VI	1.91 x 10^6	-2.51	.0220	.0154	.0136
Surveyor VII	7.9 x 10^5	-1.82	.0083	.0094	.0145

tering albedo as a function of wavelength for four Apollo sites appears as a solid in figure 1, and the high extreme (Apollo 15) and low extreme (Apollo 17) appear as dashed lines.

Equation 2 for the scattering parameter, ψ, is valid only if the diameter of the scatterer is small when compared to the microwave wavelength. That is, the Rayleigh scattering law is the small particle approximation to Mie scattering (Stratton, 1941, p. 563–573). As particle size approaches and becomes greater than the wavelength, the scattering efficiency, $\bar{s}$ (the ratio of scattering cross section to physical cross section), becomes and remains nearly unity, and so an approximation to Mie scattering is to use the Rayleigh law for $\bar{s} < 1$ and to use $\bar{s} = 1$ for larger particles. That is,

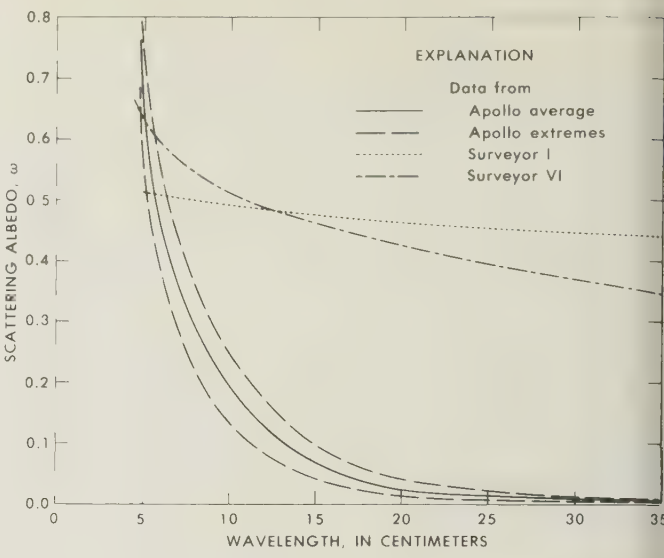

FIGURE 1.—Scattering albedos based upon Apollo and Surveyor soil models. The Apollo data, though more reliable only report on particles smaller than 1 cm. The Surveyor data are derived from samples including decimeter-sized boulders.

$$\psi = 2\pi^3 \left(\frac{\varepsilon_1^{3/2}}{\tan\delta_1}\right)\left(\frac{\varepsilon_s/\varepsilon_1 - 1}{\varepsilon_s/\varepsilon_1 + 2}\right)^2 \left\{\int_0^{f\lambda} \ell^3\,\bar{v}\,d\ell + (f\lambda)^4 \int_{f\lambda}^{K^{-1/\gamma}} \frac{\bar{v}}{\ell}\,d\ell\right\} \quad (3$$

where $\bar{v} = 0$ when $l = K^{-1/\gamma}$ and f is the ratio of particle diameter to wavelength at the lower limit of $\bar{s} = 1$. For the physical properties at depth in the lunar regolith (table 1), f = 0.23. Shoemaker and Morris (1969) obtained grain-size distributions from Surveyor TV images. Their data, fitted to functions of the form

$$N = K\ell^{\gamma}\ , \quad (4$$

yield the volume fraction, $\bar{v}dl$, in size range dl. That is

$$\bar{v}\,d\ell = \left(\frac{\pi}{4A_r}\right)\left(-\gamma K\ell^{\gamma+1}\right)\,d\ell \quad (5$$

where N is the number of particles larger than diameter l within an area (A_r) of 100 m^2. An integration of equation 5 yields the Surveyor size distribution

own in table 2. Equations 3 and 5 yield the repre-
tative Surveyor scattering albedos shown in figure 1.
The concentrations of pebbles observed in the Sur-
yor TV images are systematically lower than con-
ntrations measured in the Apollo soil samples. The
rveyor VI distribution is intermediate among the
rveyor data and, because the Surveyor VI site lies
the center of the lunar disk, might justifiably be
ed to reduce Earth-based observations. The Surveyor
distribution exhibits the most extreme slope (γ =
2.58). The striking differences between the Surveyor-
sed and Apollo-based curves occur because the Apollo
e distributions do not include clasts larger than 1 cm.
The microwave radiation within the lunar regolith
nsists of direct, I_p, (τ, μ), and diffuse, $\mathscr{L}_p$ (τ, μ), inten-
ies where p denotes either vertical, V, or horizontal,
, polarization, τ is optical depth, and μ is direction
sine of the ray's direction with respect to vertical.
e direct component arises from thermal emission
thin the media and satisfies the differential equation

$$\frac{I_p(\tau,\mu)}{\partial\tau'} = (1-\omega)\,\frac{\varepsilon_1 C_\lambda}{\mu} T(\tau')\; e^{-(\tau'-\tau)/\mu} \qquad (6)$$

here C_λ is the Rayleigh-Jeans ratio of free-space,
ack-body intensity to thermal temperature, $T(\tau)$.
e diffuse intensity arises from singly and multiply
attered radiation and satisfies the radiative transfer
uation

$$\frac{\mathscr{L}_p(\tau,\mu)}{\partial\tau} = \mathscr{L}_p(\tau,\mu) - \frac{\omega}{2}\sum_{q=V,H}\int_{-1}^{+1} P_{pq}(\mu,\mu')\,[\mathscr{L}_q(\tau,\mu') + I_q(\tau,\mu')]\,d\mu' \qquad (7)$$

here $P_{pq}(\mu, \mu')$ is the rotationally symmetric, Ray-
gh scattering phase matrix which relates incoming
diation of polarization q in conical anulus $d\mu'$ to
attered radiation of polarization p in any direction
μ. Solutions of equations 6 and 7, subject to the
undary conditions of specular reflection at the sur-
ce of the layer and at the interface between the
yer and halfspace, are discussed by England
975). The solutions for nonzero heat flow are readily
tained for $I_p(\tau, \mu)$ by replacing $T(\tau)$ with
+ (Q/k) (τ/α) where the extinction coefficient, α,
$2\pi\sqrt{\epsilon_1}\tan\delta_1/(\lambda(1-\omega))$. The solution for the dif-
se component is

$$\mathscr{L}_p(\tau,\mu)_{iso} + \omega\varepsilon_1 C_\lambda (Q/k)\;(\tau+\mu)/\alpha \qquad (8)$$

where $\mathscr{L}_p(\tau, \mu)_{iso}$ is the general solution for an isothermal medium.

The physical parameters in table 1 and an intermediate regolith thickness of 20 m were used to compute radiobrightness models for a heat flow of 0.03 W/m^2, the heat flow measured at the Apollo 15 and 17 sites (Langseth and others, 1972, 1974), and for a heat flow of 0.045 W/m^2, 50 percent greater than the Apollo values. Both models employed an effective, steady-state surface temperature of 251.2 K. This temperature is the Apollo 15 equilibrium temperature at 1.38 m depth (Langseth and others, 1972) extrapolated to the surface by subtracting 1.38(Q/k).

The effective relative permittivity of the lunar surface varies with wavelength (Hagfors, 1970). This occurs because the density of the regolith increases from about 1.3 g/cm^3 at the surface to a nearly steady value of 1.9 g/cm^3 at depths greater than 15 cm (Carrier and others, 1973). Over that 15-cm epilith, the relative permittivity increases from about 2.0 (Gold and others, 1973) to 4.0 (Bassett and Shackelford, 1972). Most radar measurements at longer wavelengths yield an $\epsilon \approx 3$ (Hagfors, 1970). Therefore, the computed emissivity of the surface is based upon ϵ=3.0 while the scattering albedo is based upon rock clasts embedded in a matrix whose relative permittivity is 4.0. The spectral gradient of radiobrightness is insensitive to changes in relative permittivity of ± 1.

The radiobrightness models yield temperatures equivalent to those at the center of the lunar disk. These disk center temperatures were reduced by 6 percent to correspond to average lunar disk temperatures (Krotikov, 1965). The uniformly calibrated set of disk brightnesses observed by the Soviets are included in figure 2 (Keihm and Langseth, 1975b).

Figure 2 shows disk brightness temperatures of an Apollo and two Surveyor scattering regoliths (Q = 0.03 W/m^2) and disk brightnesses of two scatterer-free regoliths (Q=0.03 and Q=0.045 W/m^2). Scatterers generally increase the spectral gradient. Except at short wavelengths, where the Rayleigh approximation overestimates the scattering, the Apollo scattering model fits the radio telescopic observations. The scatterer-free model for Q=0.045 W/m^2 provides the correct spectral gradient. The brightness curve must, however, be displaced downward by increasing the effective relative permittivity of the surface from 3.0 to 4.0, an increase that is probably unrealistic. The Surveyor VI scattering model predicts temperatures which are uniformly 6 K low. Although the curve

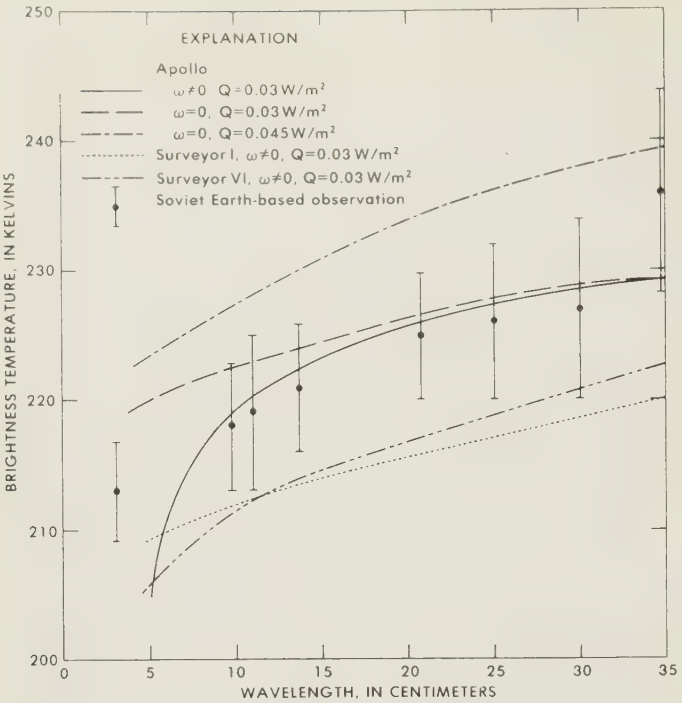

FIGURE 2.—Radiobrightness of the Apollo and Surveyor soils. The radiobrightness of the average Apollo soil ($\bar{\omega} \neq 0$), at wavelengths longer than 7 cm, agrees with the Soviet, Earth-based observations. The Rayleigh scattering model overestimates the darkening at wavelengths shorter than 7 cm. The spectral gradient of the Surveyor VI curve agrees with the observations but the temperatures are uniformly too cold. The approximation to Mie scattering overestimates scatter-induced darkening. The scatterer-free model for a heat flow of 0.045 W/m² has the correct spectral gradient but is uniformly 10 K too hot.

could be displaced upward 6 K by decreasing the effective relative permittivity from 3.0 to 2.3, the likely cause of the discrepancy is overestimation, at all wavelengths, of scattering albedo. The approximation of Mie scattering used in the computation would have this effect. Although the temperatures are low, the scattering increases the spectral gradient of radiobrightness in the 5- to 30-centimeter range of wavelengths to a gradient equivalent to greater than a 100-percent increase in heat flow for a scatterer-free Apollo model and equivalent to a 50-percent increase in heat flow for a scatterer-free Surveyor VI model. In the 10- to 30-centimeter range of wavelengths, the equivalents are a 70-percent increase for the Apollo model and a 20-percent increase for the Surveyor VI model. That is, the Apollo and the Surveyor VI scattering models have similar spectral gradients and, to the precision of the Rayleigh approximation, each is equivalent to something like a 50-percent increase in heat flow.

The spectral gradient of the Surveyor I scattering model is near that of the scatterer-free model of the same heat flow. The curve is simply displaced downward 10 K by the scattering. The difference in distribution of scatterers between the Surveyor I and Surveyor VI sites results in an increase in spectral gradient equivalent to a 50-percent increase in heat flow. Therefore, spectral gradients cannot be discounted by a systematic factor. Scattering causes an immutable uncertainty in the interpreted heat flow.

A polychromatic, microwave radiometer in lunar polar orbit cannot be justified as a heat-flow mapping instrument unless inaccuracies in interpreted heat flow of 0.015 W/m²—50 percent of the value measured at the Apollo 15 and 17 sites—are tolerable. A regional map, with this inaccuracy, of the Earth's heat flow would be of use because of the relatively great local variability of the Earth's heat flow. The Moon, however, lacks the recent volcanism and hydrothermal activity that are responsible for local anomalies on Earth. The objective of a lunar experiment would be to map regional heat-flow differences between near-side and far-side, pole and equator, and maria and highland. These differences may not be very much greater than 0.015 W/m². Unless the uncertainty caused by scattering can be reduced by, perhaps, mapping scattering cross sections with a polychromatic scatterometer in conjunction with the radiometer, the interpretation of lunar radiometric data may be unacceptably ambiguous.

REFERENCES CITED

Baldwin, J. E., 1961, Thermal radiation from the Moon and heat flow through the lunar surface: Royal Astron. Soc. Monthly Notices, v. 122, p. 513–622.

Bassett, H. L., and Shackelford, R. G., 1972, Dielectric properties of Apollo 14 lunar samples at microwave and millimeter wavelengths, *in* Proceedings of the third lunar science conference: Geochim. et Cosmochim. Acta, supp. 3, v. 3, p. 3157–3160.

Carrier, W. D., Mitchell, J. K., and Mahmood, Arshud, 1973, The relative density of lunar soil, *in* Proceedings of the fourth lunar science conference: Geochim. et Cosmochim. Acta, supp. 4, v. 3, p. 2403–2411.

England, A. W., 1975, Thermal microwave emission from a scattering layer: Jour. Geophys. Research, v. 80, p. 4484–96.

Gold, T., Bilson, E., and Yerbury, M., 1973, Grain size analysis and high frequency electrical properties of Apollo 15 and 16 samples, *in* Chamberlain, J. W., and Watkins, Carolyn, eds., Lunar Science IV: Houston, Lunar Science Institute, p. 293–295.

Hagfors, T., 1970, Remote probing of the moon by infrared and microwave emissions and by radar: Radio Science, v. 5, p. 189–227.

Keihm, S. J., and Langseth, M. G., Jr., 1975a, Microwave

emission spectrum of the Moon—Moon global heat flow and average depth of regolith: Science, v. 187, p. 64–66.
——1975b, Lunar microwave brightness temperature observations reevaluated in the light of Apollo Program findings: Icarus, v. 24, p. 211–230.
ach, R. L., and Watkins, J. S., 1973, The velocity structure of the lunar crust: The Moon, v. 7, p. 63–75.
tikov, V. D., 1965, Averaging effect on antenna radiation pattern in measurements of the radio emission of the Moon: Soviet Radiophysics, v. 8, p. 322–327.
ngseth, M. G., Jr., Clark, S. P., Jr., Chute, J. L., Jr., Keihm, S. J., and Wechsler, A. E., 1972, Heat-flow experiment, *in* Apollo 15 preliminary science report: U.S. Natl. Aeronautics and Space Adm. Spec. Pub. 289, sec. 11, 23 p.
ngseth, M. G., Keihm, S. J., and Chute, J. L., Jr., 1974, Heat-flow experiment, *in* Apollo 17 preliminary science report: U.S. Natl. Aeronautics and Space Adm. Spec. Pub. 330, sec. 9, 24 p.
nsky, J. L., 1966, Models of the lunar surface including temperature dependent thermal properties: Icarus, v. 5, p. 606–634.
hleman, D. O., 1972, Microwave emissions from the Moon, *in* Lucas, J. W., ed., Thermal characteristics of the Moon: Cambridge, Mass., Mass. Inst. Technology, Prog. in Astronautics and Aeronautics, v. 28, p. 51–81.
Salisbury, W. W., and Fernald, D. L., 1971, Subsurface temperature of the Moon: Jour. Astronautical Sci., v. 18, p. 236–243.
Shoemaker, E. M., and Morris, E. C., 1969, Size-frequency distributions of fragmental debris, *in* Surveyor program results: U.S. Natl. Aeronautics and Space Adm. Spec. Rept. 184, p. 82–96.
Stratton, J. A., 1941, Electromagnetic theory: New York, McGraw-Hill, 615 p.
Tikhonova, T. V., and Troitskii, V. S., 1969, Effect of heat from within the Moon on its radio emission for the case of lunar properties which vary with depths: Soviet Astronomy-AJ, v. 13, p. 120–128.
Troitskii, V. S., and Tikhonova, T. V., 1970, Thermal radiation from the Moon and the physical properties of its upper mantle: Radiofizika, v. 13, p. 1273–1311.
U.S. Goddard Space Flight Center, 1975, Lunar polar orbiter interim technical report X–703–75–141: p. 40–41. Available from Goddard Space Flight Center, Tech. Inf. Div., Code 250, Greenbelt, MD 20771.

Jour. Research U.S. Geol. Survey
Vol. 6, No. 4, July–Aug. 1978, p. 511–514

USE OF A REMOTE COMPUTER TERMINAL DURING FIELD CHECKING OF LANDSAT DIGITAL MAPS

By C. J. ROBINOVE and C. F. HUTCHINSON,
Reston, Va., Riverside, Calif.

Abstract.—Field checking of small-scale land classification ps made digitally from Landsat data is facilitated by use a remote portable teletypewriter terminal linked by tele- ne to the IDIMS (Interactive Digital Image Manipulation stem) at the EDC (EROS Data Center), Sioux Falls, Dak. When field checking of maps 20 miles northeast of ker, Calif., during the day showed that changes in classi- ation were needed, the terminal was used at night to nbine image statistical files, remap portions of images, and duce new alphanumeric maps for field checking during the t day. The alphanumeric maps can be used without serious ficulty in location in the field even though the scale is torted, and statistical files created during the field check be used for full image classification and map output at EDC. This process makes field checking faster than normal, vides interaction with the statistical data while in the d, and reduces to a minimum the number of trips needed work interactively with the IDIMS at the EDC, thus saving nificant amounts of time and money. The only significant blem is using telephone lines which at times create rious characters in the printout or prevent the line feed per advance) signal from reaching the terminal, thus rprinting lines which should be sequential. We recommend t maps for field checking be made with more spectral sses than are expected because in the field it is much easier group classes than to reclassify or separate classes when the remote terminal is available for display.

Preparation of small-scale maps from Landsat digi- data requires a sequence of steps consisting of ssification and subsequent field checking before a al map is produced. Reiteration of these steps re- ires several trips between the field location and the eractive computer system which can be expensive d time consuming. In order to shorten the process d reduce the cost, an experiment in the use of a mote computer terminal at the field location was nducted.

Acknowledgments.—The authors appreciate the aid the staff at the Data Analysis Laboratory at the DC (EROS Data Center), and particularly Charles Nelson, manager of the IDIMS (Interactive Digi- Image Manipulation System), for his help and tience in the conduct of this experiment.

INITIAL DIGITAL MAPPING TECHNIQUE

The mapping technique used with digital Landsat images is shown in the flow chart (fig. 1) and is described in more detail here. Facilities of the Data Analysis Laboratory of the EDC were used for Landsat image analysis. The two analysis systems utilized were the General Electric Image 100 driven by a DEC 11/35 and the Electromagnetic Systems Laboratory's IDIMS driven by a HP–3000. Results were recorded on the Optronics Film Recorder System. Figure 1 shows the steps in the analysis. The dashed line encloses the steps accomplished by use of a remote terminal.

The procedure involved analysis of a Landsat digital image on the Image 100 by selecting training sets representing known terrain units and classifying areas with similar radiance levels throughout the image. When a number of classes had been developed and the interpreters were satisfied that the resulting classified image was photointerpretively reasonable, that it included a sufficient number of classes, and that the classes covered over 90 percent of the selected subscene, the radiance means and covariance matrices for each class were recorded on magnetic tape.

The recorded statistical data were then used as input to the IDIMS which performed a maximum-likelihood classification of the image. The classified image was displayed on a color cathode ray tube and checked for accuracy and consistency by the interpreters. Grouping and separation of classes was then done by manipulation of the statistical files in the IDIMS until the interpreters were satisfied that the classified image represented the terrain conditions to the best of their knowledge and was ready for field checking.

The classified image was transferred to magnetic tape which was used to drive the Optronics film recorder to produce black-and-white film positives which were then combined in the photographic laboratory to produce a multicolor classified map which is suitable

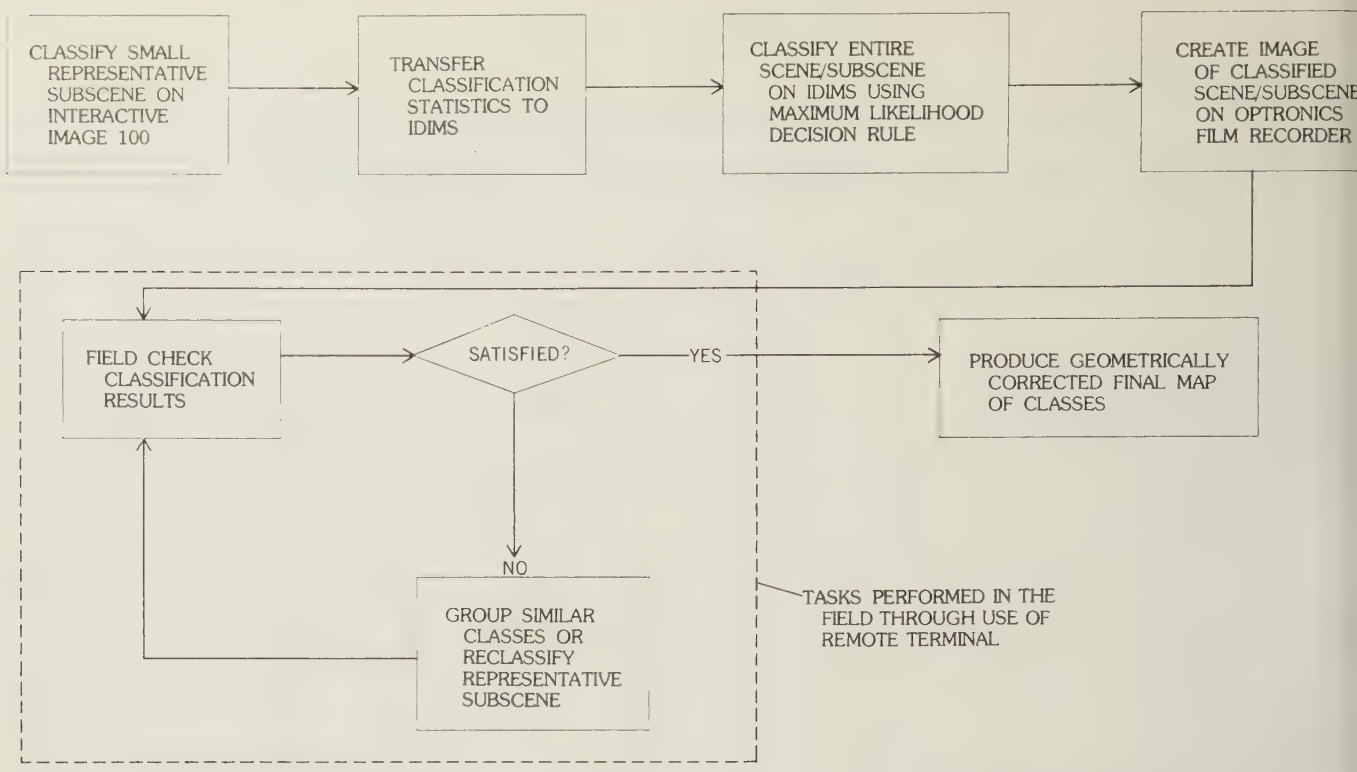
CLASSIFY SMALL REPRESENTATIVE SUBSCENE ON INTERACTIVE IMAGE 100
TRANSFER CLASSIFICATION STATISTICS TO IDIMS
CLASSIFY ENTIRE SCENE/SUBSCENE ON IDIMS USING MAXIMUM LIKELIHOOD DECISION RULE
CREATE IMAGE OF CLASSIFIED SCENE/SUBSCENE ON OPTRONICS FILM RECORDER
FIELD CHECK CLASSIFICATION RESULTS
SATISFIED?
YES
NO
PRODUCE GEOMETRICALLY CORRECTED FINAL MAP OF CLASSES
GROUP SIMILAR CLASSES OR RECLASSIFY REPRESENTATIVE SUBSCENE
TASKS PERFORMED IN THE FIELD THROUGH USE OF REMOTE TERMINAL

FIGURE 1.—Steps in production of a map from digital Landsat data. The reiteration of digital classification and field check is a necessary step in production of the final map and is shown within the dashed line.

for field checking. For this experiment, the field-check map was produced at a scale of 1:250 000 and was overlaid with the 1:250 000-scale topographic map in film positive form for ease of location. Figure 2*A* shows the portion of the Landsat scene used in this experiment. It has been enhanced by contrast stretching, haze removal, destriping, and edge enhancement to make it more readily interpretable to the eye than a normal photographic image made from the Landsat data. The raw Landsat data, in computer compatible tape format, were destriped and then were used for the initial anlysis. Figure 2*B* shows the classified image map which was used for field checking.

THE FIELD CHECKING EXPERIMENT

The area being mapped is a 7600 km^2 part of the eastern Mojave Desert east of Baker, Calif. The purpose is to map integrated terrain units consisting of various combinations of geomorphic units, soils, and vegetation which are usable for grazing land management.

Checking of the classification map was done in the field area about 20 miles northeast of Baker, Calif. Under normal circumstances, field checking of the map would result in changes such as grouping of some classes and separation of others because they a found to be only partially representative of the t rain units. The results of the field checking would n mally require a trip from Baker, Calif., to Sioux Fal S. Dak., to use the IDMS for grouping similar clas and reclassifying a small subscene to separate select classes. This process might need to be reiterated two three times before the map was considered satisfacto by the interpreters.

To eliminate repeated trips and to reduce cost remote computer terminal was used at the field site manipulate the statistics, reclassify the image, and p duce an alphanumeric map that was checked in t field. Computer operations were done at night and t map was taken into the field the next day and check A Texas Instruments Model 735 portable telety writer terminal was used in a motel room wh electrical power and a telephone were available. M of the functions of the IDIMS, with the exception the video display, can be operated from the termin

Image classification, statistical manipulation, grou ing of classes, and map printout were done with terminal. Figure 2*C* shows an alphanumeric print of an area that was field checked. Alphanumeric m symbols were selected for ease of visual discriminati No difficulty was encountered in locating the m

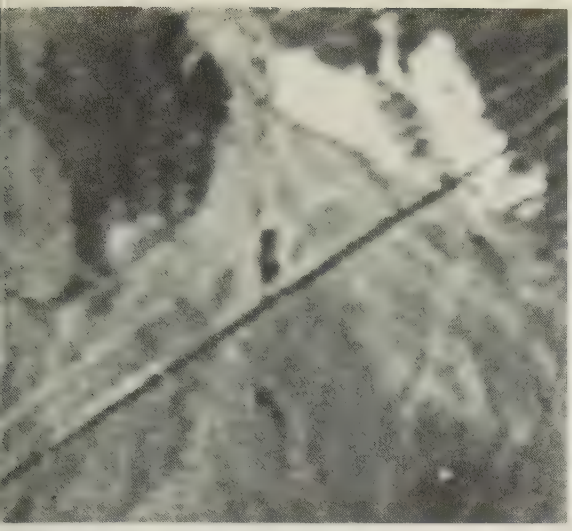

A

B

C

FIGURE 2.—Portion of Landsat image 1700–17422 and digital classification maps. The area shown is 74 km². *A*, Black-and-white print of color composite image which has been digitally enhanced for maximum interpretability. *B*, Digital classification map made by interactive use of the Image 100, classification by the IDIMS, and map production by the Optronics system. For field use, each class is shown in a separate color. *C*, Alphanumeric map produced on a computer terminal in the field and used for field checking of classification results.

ses in the field even though the scale of the map ifferent in the two directions because of the line character spacing of the terminal. The printout stricted to 64 pixels in the x-direction, but can be any length in the y-direction.[1] Small areas of 64x64 pixels (18 km²) were printed and checked, but the example shown in figure 2*C* samples and prints out every other pixel in every other line, thus allowing checking of a larger area (74 km² at one time.

After several iterations of classification and field checking, when the interpreters are satisfied with the results, the revised class statistics are used for classification of the full subscene and a map printout is made on the Optronics film recorder at the EDC and mailed to the interpreters. The final classification is geometrically corrected.

The only major problem encountered during the experiment involved the telephone lines. At times transmission was interrupted, which necessitated placing the call and logging on the computer again. Noisy telephone lines at times caused the terminal to print

[1] Vertical strips may be mosaiced together to produce any width desired, but this was judged somewhat impractical for field use.

spurious characters, and frequently the line feed signal was not received thus causing the terminal to overprint some lines. This is particularly troublesome when an alphanumeric map is being printed and requires re-running the mapping program until a satisfactory map is produced.

We recommend that the original computer-produced maps taken into the field contain more classes than are expected to be mapped. It is easier to use the remote terminal for grouping classes than for statistically separating them through reclassification when only the remote terminal rather than the interactive display is available.

FEASIBILITY AND EFFICIENCY

The use of the remote terminal to aid field checki of Landsat digital maps is quite feasible so long electric power and a telephone line are available a the problem of noisy telephone lines is not present.

Savings in time and cost can be significant. Repeat computer iterations and field check for the area und study near Baker, Calif., could require up to thr trips between Baker and Sioux Falls, S. Dak., at cost of up to $1000 for travel and expenses. Use the terminal at the field site eliminates this exper and considerably shortens the time required for t reiteration of computer classification and field chec ing.

Jour. Research U.S. Geol. Survey
Vol. 6, No. 4, July–Aug. 1978, p. 515–527

ACCURACY OF FLOOD MAPPING

By D. E. BURKHAM, Sacramento, Calif.

Abstract.—Information taken directly from published and unpublished reports was used to appraise the accuracy and limitations of the three general flood-mapping methods: detailed, historical, and physiographic. In the appraisal, the probable nationwide average standard error of estimate for depth and elevation in percentage of depth and in meters was determined for 100-year flood boundaries. Biases, users' errors, and certain time-variant errors were not considered. The probable standard error for the detailed method is 23 percent. Based on 3.9 m as the national average 100-yr depth, the probable standard error of estimate is 0.9 m. The detailed method is applicable to a wide range of hydraulic and topographic conditions; it is the only method tested that is directly applicable to floodways analysis. The method requires detailed data and time-consuming analyses, however, and it has only limited application for determining flood elevations for sheet flow and for flow in channels having readily movable boundaries. The probable standard error for the historical method is 23 percent. Based on the 3.9-m average 100-yr depth, the standard error is 0.9 m. The historical method is applicable to a wide range of hydraulic and topographic conditions if specific data are available. The method is not applicable to floodways analysis, and it has only limited application for flow in moveable-boundary channels. The standard error for the physiographic method is 27 percent. In meters, the error is 1.1. The physiographic method is simpler to apply than the other methods; however, it can be used only in natural channels having rigid boundaries. It is not applicable to sheet flow and to floodways analysis.

Mapping of flood plains has been greately accelerated during the past decade because flood-plain management has been recognized as a viable alternative to structural flood-control measures and because implementation of the National Flood Insurance Act of 1968 required information on the frequency of inundation to set flood insurance rates. Public Law 93–234, Flood Disaster Protection Act of 1973, requires the U.S. Geological Survey and other selected Federal agencies to "give the highest practical priority in allocation of manpower and other available resources" to assist the FIA (Federal Insurance Administration) and the HUD (U.S. Department of Housing and Urban Development) in identifying flood-prone areas. Present study guidelines require detailed and time-consuming analyses, which only a few Federal agencies and a very limited number of private engineering firms have the competence to perform. The detailed method presently being used has a broad application; it is being used, however, in areas where a simplified method might suffice. Since 1960, several simplified methods have been developed by the U.S. Geological Survey. These simplified approaches cannot be generally accepted as useful alternatives to the detailed method until the relative accuracies of the methods have been evaluated. An acceptable simplified approach that would have a broad application could alleviate manpower stresses.

This report describes and compares the probable national average standard errors of estimate for the different methods that have been used recently by the Geological Survey to define flood-boundary elevations for T-year discharges in natural channels. A T-year discharge is the discharge that will occur, on an average, once in T years—25 yr, 50 yr, and 100 yr. Unless otherwise stated, a T-year depth is the water-surface elevation or gage height for the T-year discharge minus the channel-bottom elevation or gage height (point of zero flow, elevation or gage height at which water ceases to move in the channel). In regard to the hydraulics of T-year discharges, natural channels (channels not significantly affected by manmade structures) are of two general types, rigid boundary and movable boundary. This paper is concerned primarily with the rigid-boundary type which is one that has a low probability of temporal change that would significantly affect the hydraulic characteristics of a T-year discharge.

Errors are discussed and brief descriptions are presented for three general classifications of methods: detailed, historical, and physiographic. Briefly, the detailed method involves the determination of a T-year water-surface profile by obtaining solutions to the dynamic equation for a T-year flood and the determination of flood boundaries by transferring elevations from the profile to a map. The historical method involves the adjustment of the profile for an experienced flood to obtain a T-year profile and the transferring of elevations from the profile to a map. The physiographic method involves the determination of T-year depths by use of a depth-frequency relation and the projection of the depths as elevations on a map.

The standard error of prediction, SE_p, for the different flood-mapping methods would be a better measure of error than the standard error of estimate, SE, but the writer concluded that only the effort required to approximate SE would be justified for this study. Both SE_p and SE can be used as a measure of the difference between estimated and true values of a characteristic; both are usually estimated on the basis of observed data. SE_p is the preferred value, however, because it better represents the total error; it represents both the bias error and the sampling error, whereas SE represents only the sampling error. The bias error is a time-invariant error caused by consistent overestimates or consistent underestimates of the true value of a parameter. For a regression equation, SE_p represents the error of points along the calculated regression line plus that of individual estimates around that line. SE represents only the error of individual estimates around the line, which is relatively simple to obtain. Because of the national scope of the study, and the complexity of the problem, it was necessary to deal with averages, lumped parameters, and reasonable speculations in order to approximate nationwide average standard errors for the different methods. Use of the standard error of prediction, therefore, was not justified.

The approach used in appraising the overall accuracy of a method requires that a standard error for each component (task, step, or part) of the method be computed, approximated, or assumed. Errors for the different components must be expressed in the same units to appraise the overall accuracy of the method and to compare the accuracy of one method with that of another. For this report, errors are given in meters and as a percentage of depth. For discussion purposes, errors also are given as a percentage of discharge in some instances. Errors for the different components are assumed to be independent. The numerical values given in this report are for 100-yr events unless stated otherwise.

Users' errors and certain time-variant errors, resulting from flood-boundary changes, are not considered in this report. A users' error develops when information on a flood-boundary map is incorrectly transferred to a point on the ground.

Acknowledgments.—The arrangement of this paper follows closely an outline suggested by R. W. Carter (written commun., 1972), and much of the information contained in the paper was taken directly from unpublished reports supplied by Carter and by other personnel in the Geological Survey districts. The writer greatly appreciates these contributions.

DETAILED METHOD

The detailed method of flood mapping consists three basic steps: (1) determining a T-year discharg (2) determining a water-surface profile for the T-ye discharge, and (3) developing a flood-boundary ma

100-Year Discharge

A 100-yr discharge determination for a reach interest is based on a flood-frequency analysis. If long-term record of discharge is available for a sit the flood-frequency analysis consists of the develo ment of a flood-frequency curve (U.S. Water R sources Council, 1976) from which the 100-yr di charge is obtained directly.

The standard error for a 100-yr discharge for gaged site depends on the type of assumed distrib tion (normal, lognormal, Gumbel, and log-Pears Type III), the error of the mean event, and the err in the slope of the frequency curve (Hardison, 1969 The standard error can be relatively large even thoug a long-term record is available. For example, assumin a lognormal distribution and a standard deviation 0.30 log units, the standard error of the 50-yr di charge determined from 25 yr of record is about 2 percent of the discharge (Hardison, 1969, fig. 3); th standard error for the 100-yr discharge probably woul be slightly larger.

Typically, streamflow records at a site of intere are not available, and flood-frequency information mu be transferred from gaged sites to the ungaged sit The transfer of 100-yr information from a gaged si to an ungaged site on another stream is usually do by regression of 100-yr floods on the physical an climatic characteristics of drainage basins.

The Geological Survey, in 1970, made studies b States to define regression equations for T-year di charges for ungaged streams. A characteristic regre sion equation has the following form:

$$Q_T = aA^bP^cS^d \ldots \quad (1$$

where

Q_T = T-year discharge,
A,P,S = parameters representing topographic or cl matic characteristics, and
a,b,c,d = regression coefficients.

The standard error of estimate for the equations fo the 50-yr flood in the different States ranged from 1 percent (of the discharge) in Georgia to 115 percen in Nebraska (fig. 1). Percentages quoted are co verted from errors in logarithmic units where ove estimation and underestimation, in percentage, a

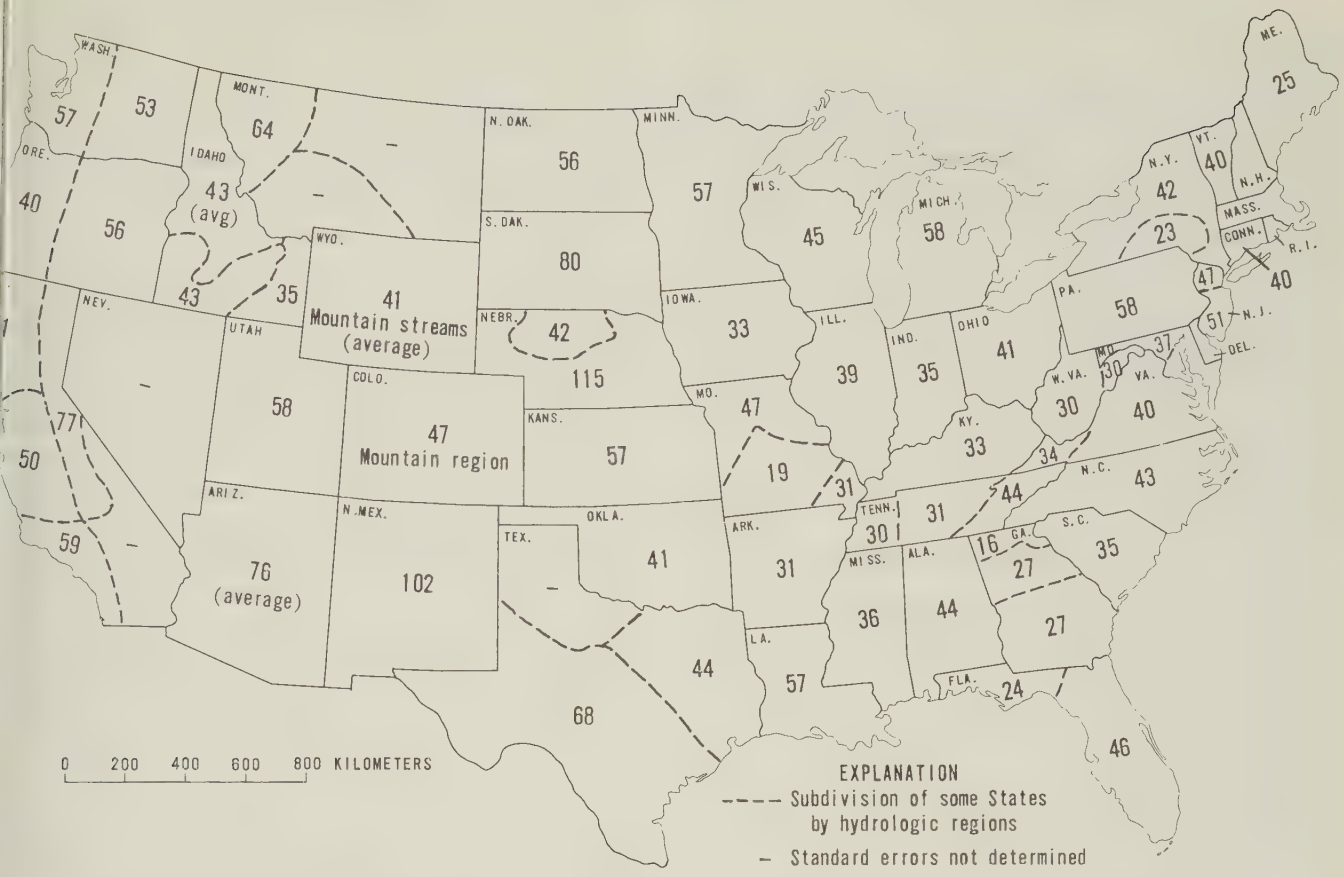

FIGURE 1.—Standard error by regression for 50-yr flood (modified from Benson and Carter, 1973, fig. 9).

eraged. The mean of the standard errors for the fferent States is 46 percent. According to R. W. rter (written commun., 1972), there is no evidence at other types of regional flood-frequency analysis uld yield errors of lower magnitude. The mean of ndard errors for the 100-yr discharge for the dif-ent States is assumed to be only insignificantly fferent from 46 percent. The method used to convert e standard error as a percentage of discharge to ndard error as a percentage of depth is presented the subsection "Errors in a Common Unit."

Water-Surface Profile

The detailed method of determining profiles for *T*-ar discharges involves basically the solution of the namic equation of gradually varied flow. There are ee broad classes of detailed methods (Chow, 1959): aphical-integration method, direct integration meth- and step method. The Geological Survey uses tep method (called the step-backwater method). A p method is characterized by dividing the channel o short reaches and carrying the computation step step from one end of a reach to the other.

The step-backwater method of determining surface profiles (Chow, 1959; Bailey and Ray, 1966) is designed for uniform flow in which the water-surface profile and energy gradient are parallel to the streambed, and the cross-sectional area, hydraulic radius, and depth remain constant through the reach. The method is assumed to be valid for a flow and a channel condition that prevail in rigid channels, if the energy losses are properly accounted for.

Data needed to determine a water-surface profile according to the detailed method can be classified as topographic and channel roughness. The topographic data—elevations and distances to common bases—may be obtained by a field survey or by a combination of a field survey and photogrammetry. Ground elevations and distances can be determined very accurately in field surveys; if desired, ground elevations can be determined without introducing significant errors.

A combination of field survey and photogrammetry is often used to develop contours on topographic maps; elevations and distances needed for the step-backwater computations can be scaled from these maps. The elevation obtained by this procedure is assumed to have a

standard error equal to one-fourth of the contour interval.

The Manning's n, which is used to represent channel roughness in computations to determine water-surface profiles, is a lumped parameter, and its value during flow in a natural channel depends on a number of time-variant and space-variant factors. Some of the factors that probably exert the greatest influence on the roughness coefficient are (1) flow-boundary roughness, (2) size and shape of stream channel and flood plain, (3) stream-channel irregularity and alinement, (4) vegetation, (5) obstructions, (6) flow depth and rate, (7) filling and scouring, (8) size and concentration of sediment in the flow, and (9) bed form. A high degree of uncertainty is often created in the selection of the proper Manning's n for a reach of interest.

Bailey and Ray (1966) conducted a study of 28 gaged sites to determine the accuracy of the step backwater procedure in duplicating stage-discharg relations in natural streams. These sites covered a wid range in hydraulic conditions that prevail at gagin stations. The stage-discharge relation was defined fo each site by current-meter measurements. Pertinen channel roughness and topographic data were ob tained for a long reach downstream from each gage site, and water-surface profiles for different dis charges were computed using the step-backwater pro cedure. Field surveys were used to obtain the topo graphic properties of the study stream. A compariso of the measured and computed discharge for all site is shown in figure 2. The standard error of the com puted discharge was + 19 percent and − 16 percen Bias in the results obtained using the method appar ently was insignificant.

Intuitively, it would appear that the 18 percen

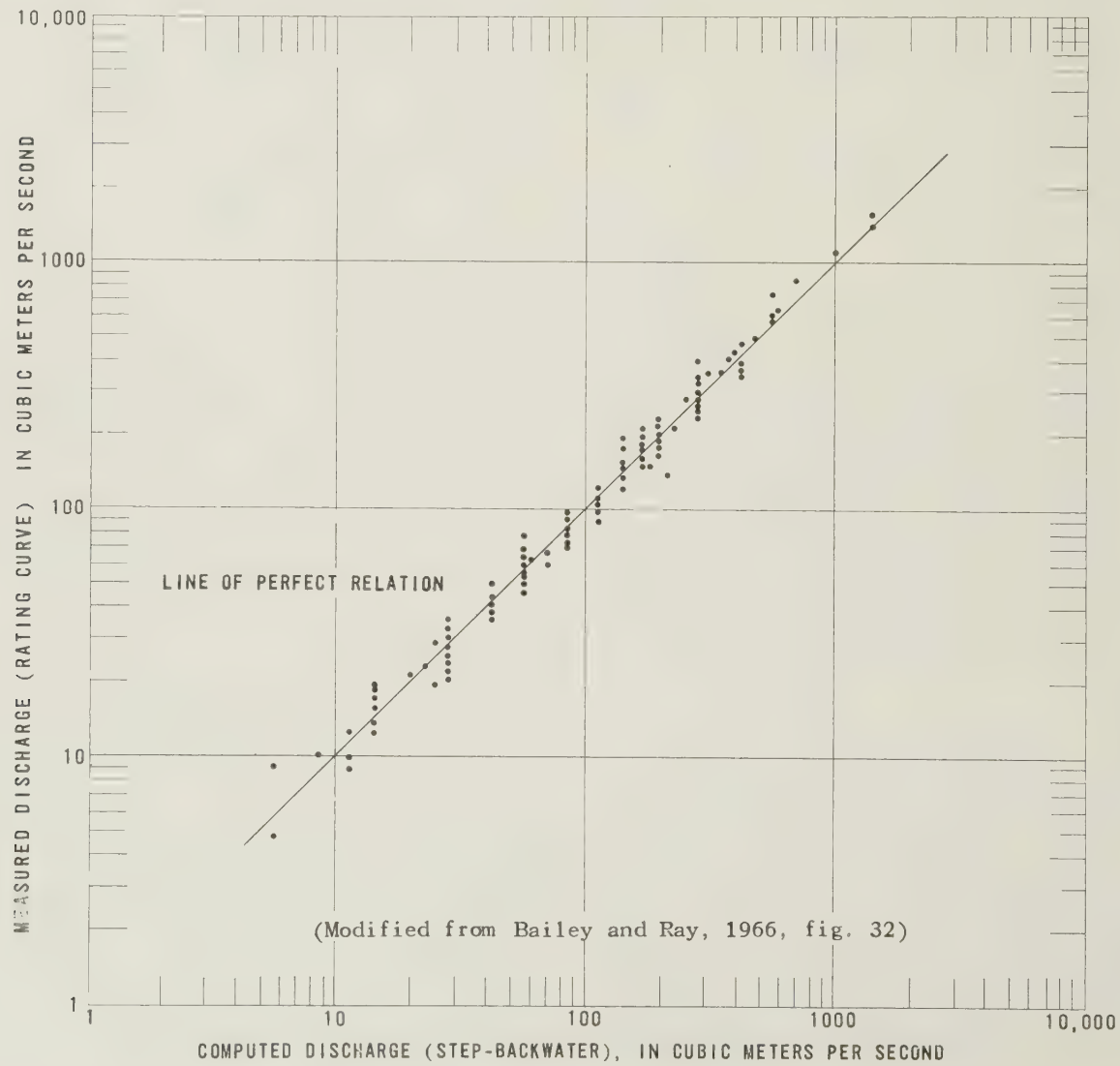

FIGURE 2.—Computed discharge compared with measured discharge.

ıean of + 19 and − 16 percent) standard error in- ɔduced in the water-surface profile would be too nservative when applied to a typical site for an IA study. This intuition is based on three criteria. ırst, gaging sites for which the step-backwater ethod was tested by Bailey and Ray (1966) were lected because of their favorable hydraulic charac- ristics, and therefore, these sites do not represent pical sites. Second, the typical user of the step- ackwater method for an FIA study probably does not ave the considerable "judgment and experience" presented by Bailey and Ray. Finally, for a typical IA study, the accuracy of the data used in the step- ackwater computations probably is not as good as at for data used by Bailey and Ray. In the absence results from a more representative test, however, a alue of 20 percent of the T-year discharge is assumed be a usable estimate of the standard error intro- uced in determining a water-surface profile. The ac- ptance of the 20 percent was based partly on the ct that there was a tendency towards a closer agree- ent between measured and computed discharge as e discharge increases (Bailey and Ray, 1966).

Flood-Boundary Map

The development of a flood-boundary map involves e transferring of elevations from a water-surface ofile to a map. The task is to define the intersection elevations with the ground surface. The elevations n be transferred directly during a field survey on e basis of a combination of a field survey and aerial otography or on the basis of elevation contours on a pographic map. As previously stated, ground eleva- ons can be determined very accurately by field sur- ys. If so desired, elevations from a water-surface ofile can be transferred to a map either by field rveys or by a combination of a field survey and use aerial photographs without introducing significant rors. The use of aerial photographs to transfer evations without introducing significant errors would quire that the boundary of the T-year flood be gged at selected sites along the flood plain before rial photographs are taken.

The accuracy of the contours must be considered in aluating errors in flood mapping when flood maps e developed on the basis of elevation contours. As eviously mentioned, the standard error of ground evations based on contours on topographic maps is sumed to be about one-fourth of the contour inter- l. Maps having contour intervals greater than about 5 m usually are not used to establish elevation-ground tersections; therefore, 0.4 m is assumed to be the andard error.

Errors in a Common Unit

Thus far in the report, errors in the 100-yr discharge and errors in the result of a step-backwater analysis are given as a percentage of discharge, and errors in elevations taken from topographic maps are given in meters. The desired units for the errors are depth in meters and percentage of depth.

The method used to convert the standard error in percentage of discharge to standard error in percentage of depth makes use of the slope of a depth-discharge relation for a typical natural channel. The relation between depth and discharge for relatively high flow rates can be represented by

$$\log d = \log c_1 + f \log Q \qquad (2)$$

in which

d = effective depth of water,

c_1 = a coefficient (equals the depth when Q equals 1),

f = slope of the stage discharge relation, and

Q = discharge.

Equation 2 is a straight line in the variables log d and log Q; therefore the slope of the line can be represented by

$$f = \frac{\log d_2 - \log d_1}{\log Q_2 - \log Q_1} , \qquad (3A)$$

or

$$f = \log \left(\frac{d_2}{d_1} \right) \Big/ \log \left(\frac{Q_2}{Q_1} \right) , \qquad (3B)$$

and therefore

$$\log \left(\frac{d_2}{d_1} \right) = f \log \left(\frac{Q_2}{Q_1} \right) . \qquad (3C)$$

Equation 3C can be used to approximate the ratio of estimated depth, d_e to true depth, d_t, if values for f and the ratio of estimated discharge, Q_e, to true discharge, Q_t, are available. Errors in percentage of depth then can be obtained using the following equation:

$$\text{Percent error} = 100 \left(\frac{d_e}{d_t} - 1 \right) . \qquad (4)$$

Errors in percentage of discharge previously given can be used in a transformed version of equation 4 to obtain the ratio Q_e/Q_t. An average value for f for a typical stream, however, must be obtained in order to use equation 3C.

An approximation of the average value for f for a

typical stream is obtained using data furnished by the district offices of the U.S. Geological Survey. Data that were readily available and pertinent to the evaluation of an average value for f consisted of depths and discharges for T-year events, depths and discharges for median flow rates (flow rates equaled or exceeded 50 percent of the time), and the gage heights for zero flows. These data were of a preliminary nature and, therefore, had to be scrutinized for errors and applicability before they could be used to determine values for f. The screening of the data was not based on a rigid set of criteria; therefore, the average value for f determined from the readily available data should be considered only as a reasonable approximation of the true mean.

Equation 3C was used to obtain values of f for 539 stage-discharge relations for selected sites in seven States (table 1). In the equation, the ratios d_{100}/d_{50} and Q_{100}/Q_{50}, in which the subscripts denote T-year events, were used to represent d_2/d_1 and Q_2/Q_1, respectively. For a few of the gaging sites, 50-yr depths and discharges were not readily available. For these sites the depths and discharges for flow rates equaled or exceeded 50 percent of the time were used instead of d_{50} and Q_{50}. The average of the computed values of f was 0.42 (table 1), which was used to represent f for a typical stream.

The computed standard error in d_{100} resulting from a standard error of 46 percent of the 100-yr discharge is 19 percent (of the depth). The 19 percent was obtained by using 1.46 for Q_c/Q_t and 0.42 for f in appropriate equations.

The computed standard error in d_{100} resulting from a standard error of 20 percent (of the discharge) in the water-surface profile is 8 percent (of the depth). The 8 percent was obtained by using 1.20 for Q_c/Q and 0.42 for f in appropriate equations.

A mean of the 100-yr depths for all natural stream in the United States that are subject to FIA studie was needed in order to change errors in meters t errors in percentages and to change errors in percent ages to errors in meters. In absence of a better esti mate, 3.9 m, the average of the 100-yr depths for 174 gaged sites for the 15 States shown in table 2, is used The coefficient of variability for the 100-yr depths a the 1742 sites is 52 percent.

The average standard error introduced is about 1 percent of the mean depth when elevations are trans ferred from water-surface profiles to flood maps o the basis of contours on topographic maps. The 1 percent is based on 3.9 m for mean depth and 0.4 m fo accuracy of the contours.

Overall Accuracy

The overall standard error for the detailed metho was obtained by use of the equation

$$SE = \sqrt{(SE_1)^2 + (SE_2)^2 + (SE_3)^2 \ldots (SE_n)^2} \qquad (5)$$

in which the subscripts represent components (o steps) and $(SE)^2$ represents variance. For the case i which no significant errors are introduced when eleva tions from a water-surface profile are transferred t a map, the probable overall average standard error fo flood-boundary elevations determined according to th detailed method is

$$(SE)_{D_1} = \sqrt{(19)^2+(8)^2} = 20.6 \text{ percent.}$$

When elevations from water-surface profiles are trans

TABLE 1.—*Statistics for the parameter* f *in the equation: log* d = *log* c_1 + f *log* Q
[See equation 2 for explanation of letter symbols]

State	Number of stations	Parameter f		
		Mean	Standard deviation	Variability index (percent)
Iowa	33	0.36	0.08	21
Maryland	40	.36	.07	19
Minnesota	81	.38	.10	26
New York	110	.46	.16	36
North Carolina	118	.45	.15	34
Ohio	68	.43	.12	27
Wisconsin	89	.39	.08	21
Weighted values	--	.42	.12	29

BLE 2.—*Summary of 100-yr depths* (d_{100}) *for gaging stations in the States given*

State	Number of stations	Mean of $\bar{d}_{100}$ (meters)	Standard deviation (meters)	Variability index (percent)
Basin size - 0 to 26 km²				
orado	10	0.72	0.39	54
rgia	--	--	--	--
inois	25	2.62	.88	34
a	19	2.50	1.08	43
sas	3	3.66	1.57	43
yland	14	[1]2.01	.96	48
sachusetts	14	[1]1.26	.70	56
nesota	15	[1]2.77	.73	26
souri	80	2.72	1.04	38
York	6	1.03	.31	30
th Carolina	8	[1]1.69	.76	45
o	3	[1]1.93	.44	23
ahoma	54	3.04	.95	32
nessee	28	[1]2.32	.90	39
consin	8	2.40	.89	37
Weighted values	--	2.47	.93	38
Basin size - 27 to 260 km²				
orado	116	1.21	.53	44
rgia	44	2.85	1.12	39
inois	73	3.45	1.44	42
a	37	3.84	1.41	37
sas	7	5.21	1.07	20
yland	33	[1]3.08	.94	30
sachusetts	17	[1]2.43	.99	41
nesota	13	[1]2.24	1.10	49
souri	10	4.57	1.05	23
York	40	2.35	.84	36
th Carolina	59	[1]3.47	1.77	51
o	30	[1]3.14	1.00	32
ahoma	34	4.39	1.48	34
nessee	34	[1]3.90	1.31	34
consin	22	2.27	1.08	47
Weighted values	--	2.88	1.18	41
Basin size - 261 to 1,300 km²				
lorado	66	2.26	1.32	58
orgia	62	4.42	2.00	45
linois	65	5.12	1.71	33
wa	33	4.69	1.55	33
nsas	12	7.13	1.99	28
ryland	8	[1]4.08	1.02	25
ssachusetts	14	[1]4.11	2.29	56
nnesota	23	[1]3.32	1.86	56
ssouri	32	6.52	2.04	31
w York	55	3.26	1.31	40

TABLE 2.—*Summary of 100-yr depths* (d_{100}) *for gaging stations in the States given*—Continued

State	Number of stations	Mean of $\bar{d}_{100}$ (meters)	Standard deviation (meters)	Variability index (percent)
Basin size - 261 to 1,300 km² --Continued				
North Carolina	48	[1]5.00	1.83	37
Ohio	53	[1]4.45	1.59	36
Oklahoma	13	7.65	1.97	26
Tennessee	10	[1]5.85	.92	16
Wisconsin	31	3.17	1.46	46
Weighted values	--	4.36	1.69	39
Basin size - greater than 1,300 km²				
Colorado	30	3.54	1.76	50
Georgia	41	6.98	2.58	37
Illinois	45	6.00	2.28	38
Iowa	36	5.46	1.50	28
Kansas	1	9.05	--	--
Maryland	1	[1]7.96	--	--
Massachusetts	--	--	--	--
Minnesota	33	[1]4.91	1.77	37
Missouri	41	8.78	1.90	22
New York	14	3.78	1.38	36
North Carolina	28	[1]6.61	2.75	42
Ohio	28	[1]5.94	1.93	32
Oklahoma	21	8.75	2.71	31
Tennessee	1	[1]12.34	--	--
Wisconsin	41	3.47	1.61	46
Weighted values	--	5.94	2.07	35
All sizes (km²)				
Colorado	222	1.83	1.34	73
Georgia	147	4.63	2.41	52
Illinois	208	4.18	1.92	46
Iowa	125	4.42	1.71	38
Kansas	23	6.19	2.10	34
Maryland	56	[1]3.05	1.31	43
Massachusetts	45	[1]2.59	1.83	71
Minnesota	84	[1]3.72	1.83	49
Missouri	163	5.12	2.99	58
New York	115	2.90	1.31	45
North Carolina	143	[1]4.48	2.41	54
Ohio	114	[1]4.48	1.92	43
Oklahoma	122	4.85	2.74	57
Tennessee	73	[1]3.69	1.89	52
Wisconsin	102	3.05	1.46	48
Weighted values	--	3.90	2.04	52

[1]The 100-year depth ($\bar{d}_{100}$) is the difference between the 100-year elevation and the elevation of median flows—50 percent duration.

erred to maps on the basis of contours, the probable verall average standard error is

$$(SE)_{D_2} = \sqrt{(19)^2 + (8)^2 + (10)^2} = 22.9 \text{ percent.}$$

he probable overall average standard errors in eters are 0.8 and 0.9, respectively. Unless otherwise ated, 23 percent and 0.9 m are used to represent $SE)_D$ in later discussions.

Limitations of the Method

The detailed method of flood mapping is applicable or a wide range of hydraulic and topographic conditions. Generally, the method can be used for those conditions where the conservation of mass and energy for gradually varied flow can be rationally described; therefore, it has only limited application for sheet flow and for flow in channels having readily movable boundaries.

HISTORICAL METHOD

The area inundated during a T-year discharge can be approximated from a record of a major flood if certain data are available. The required data include peak discharge of the flood and the elevation of high-water marks to a common datum. Aerial photographs

taken during or soon after the flood also represent useful information. To facilitate the approximation and discussion of the probable standard error in results obtained using this method, the components of the method are grouped into three tasks: (1) determining T-year discharge, (2) determining a water-surface profile for the T-year discharge, and (3) developing a flood-boundary map.

100-Year Discharge

The 100-yr discharge usually must be obtained by making a regional flood-frequency analysis. A standard error of 19 percent of the 100-yr depth has previously been computed for the 100-yr discharge.

Water-Surface Profile

The water-surface profile for a 100-yr flood can be approximated by the following steps: (1) develop a water-surface profile for the historical flood on the basis of high-water marks, (2) determine the frequency of the historical flood, (3) define the ratio of flood depths for various recurrence intervals, (4) on the basis of these ratios, determine the adjustment needed to correct the historical profile to obtain a 100-yr profile, and (5) add the adjustment to the profile obtained in step 1.

The water-surface profile for the historical flood can be readily determined if high-water marks are adequate. A 5-percent error is assumed for step 1.

Steps 2, 3, and 4 of the profile-development task involve the determination of adjustment to be added to the profile for the historical flood to obtain elevations for the 100-yr flood boundary. According to R. W. Carter (written commun, 1972), this adjustment normally would be less than about 0.6 m, which can be estimated using multiple correlation techniques and physiographic characteristics with a standard error of about 0.3 m. The 0.3 m would be about 8 percent of the estimated national average depth for the 100-yr flood. The basis for Carter's 0.6- and 0.3-m estimates is not known; however, in the absence of a better estimate the 8 percent is used for this study. Errors introduced in step 5 are assumed to be insignificant.

The probable national average standard error for the profile-development task is assumed to be 9 percent. This value was obtained by using 5 percent for step 1 and 8 percent for steps 2 to 4 in equation 5.

Flood-Boundary Map

Elevations usually are transferred from the 100-yr profile on the basis of contours on topographic maps and on the basis of aerial photographs when they are available. To be consistent with an assumed value fo a similar task for the detailed method, a 10-percen error is assumed for the historical method.

Overall Accuracy and Limitation

The probable overall standard error for the 100-y flood-boundary elevations determined according to th historical method is

$$(SE)_H = \sqrt{(19)^2 + (9)^2 + (10)^2}$$
$$= 23.3 \text{ percent.}$$

Unless otherwise stated, 23 percent is used to represen $(SE)_H$ in later discussions; the overall standard erro in meters is 0.9.

The historical method can be used for a wide rang of hydraulic and topographic conditions, if the neede data are available. Experience and judgment, howeve are required to obtain meaningful results, especiall when the adjustment of depth is greater than about 5 percent of the mean T-year depth for the reach of in terest. The method is not applicable to floodway analysis, and it has only limited application for flo in channels having readily movable boundaries.

PHYSIOGRAPHIC METHOD

The hydraulic and topographic properties of a rive reach are a function of the discharge of water an debris (Leopold and Maddock, 1953), which in tur is a function of the physical and climatic characteris tics of the drainage basin. These facts are the basi for the physiographic method of flood mapping. T facilitate the discussion of the method and the ap proximation of errors, the components of the physio graphic method are grouped into three tasks: (1) de termining T-year depths, (2) developing T-year floo profile, and (3) developing a flood-boundary map.

100-Year Depth

Two general procedures for making depth-frequenc analyses have been used recently by the Geologica Survey. These procedures are similar to the metho for regional flood-frequency analysis presented b Dalrymple (1960). For brevity in discussion, the tw procedures are called the index-flow method and th area-parameter method.

Index-flow method

The basic concepts for the index-flow method pre sented in this section are from a detailed description b Thomas (1964). As applied to hydrologic areas withi which the flood characteristics are comparable, th index-flow method involves four basic steps: (1) de

opment of flood-frequency curves and determina-
n of T-year discharges for selected gaging stations,
development of stage-discharge relations and de-
nination of T-year depths; (3) development of
phs showing the relation between the index flow
the T-year depths; Thomas (1964) used $Q_{2.33}$,
mean annual flood, as the index flow, and (4) de-
opment of graphs showing the relation between
an annual flood and drainage basin characteristics.

Thomas (1964) used streamflow records for 45 gag-
stations for his New Jersey study. For each gag-
g station, 1.5-, 2.33-, 5-, 10-, 15-, 25-, and 50-yr dis-
arges were determined from flood-frequency curves
1922–60. The flood-frequency curves were con-
ucted using methods outlined by Dalrymple
960). A depth for a T-year discharge was evaluated
subtracting a channel-bottom gage height from the
ge height for the T-year discharge. Thomas (1964)
veloped graphs showing relations between the in-
x flow (discharge) and the 1.5-, 2.33-, 5-, 10-, 15-,
-, and 50-yr depths for gaged sites in two different
gions—coastal plain and piedmont—in New Jersey.
e developed curves showing the average relation
tween size of basin and the mean annual flood for
ur areas having similar hydrologic characteristics.
applied to basins in New Jersey, the standard error
estimate for the index-flow method of determining
year depths is 21 percent (Thomas, 1964).

An index-flow method also was used to determine
year depths in Illinois; however, Q_2 was used to
present the index flow. Depth-frequency equations
re developed from regression analyses on data from
7 gaging sites. As applied to streams in Illinois, the
ndard error of estimate was 23 percent for the
dex-flow method (Winget, 1976).

The probable national average standard error of
imate for the index-flow method for determining
0-yr depths probably is significantly larger than the
erage of standard errors for New Jersey and Illi-
is. This premise is based on the following criteria:
) data used to develop and test pertinent equations
r New Jersey and Illinois were for gaging-station
es selected because of their favorable hydraulic
aracteristics and, therefore, the sites probably are
t typical, and (2) national average of the standard
ror, by regression for the 50-yr flood, is larger than
e average of standard errors by regression for New
rsey and Illinois (fig. 1).

A value of 25 percent is assumed to be a reasonable
imate for the probable national average standard
ror of estimate for the 100-yr depth determined
cording to the index-flow procedure.

Area-parameter method

The area-parameter method of determining T-year depths differs from the index-flow method in one general respect; the T-year depths are correlated directly with basin and climatic parameters. The resulting regression equation gives T-year depths directly.

The area-parameter method has been used since 1960 in 13 States to determine T-year depths. Comprehensive investigations to develop regression equations and determine the accuracy of these regression equations have been made in five of the States—Alabama, Colorado, Illinois, Kansas, and Oklahoma—listed in table 3. Reconnaissance-level investigations to develop relations between drainage area and T-year depths and to determine standard errors were made in the eight remaining States listed.

In Alabama, 100-yr depths for 129 gaged sites were regressed against 13 basin and climatic parameters (table 3). According to C. F. Hains (written commun., 1976), the 100-yr depths related principally to a 0.2 power of the drainage area. He combined the effects of the remaining significant parameters to obtain the following equation:

$$d_{100} = C_X A^{0.2} \qquad (6)$$

in which C_X is different for each of six hydrologic regions. The apparent standard error for the regression equation was 17 percent; however, this value has not been adjusted for degrees of freedom lost in outlining the hydrologic regions (C. F. Hains, written commun., 1976).

The comprehensive studies made in Colorado, Illinois, Kansas, and Oklahoma were similar in scope and procedure to that made in Alabama.

The average of the standard errors for regression equations developed as part of the comprehensive investigations is 23 percent, which was determined from the following values: 17 percent for Alabama, 27 percent for Colorado, 28 percent for Illinois, 19 percent for Kansas, and 24 percent for Oklahoma (table 3). Because of reasons previously described, the standard error of estimate probably should be larger than 23 percent; a value of 25 percent is used for this study.

The average of the standard errors for the eight drainage area-to-depth equations developed as part of the reconnaissance-level investigations is about 40 percent (table 3). The standard errors for the eight equations were not determined precisely; however, the 40 percent is assumed to be a reasonable approximation of the national average standard error of estimate for the reconnaissance-level investigations. This assumption is based partly on the summary of 100-yr depths for gaging-station sites (in 15 States) given in

TABLE 3.—*Summary of regression equations developed to estimate 100-yr depths* (d_{100}), *regions and States where the apply, and standard error of estimate for depths determined using the equations*

State[1]	Parameters tested for significance in regression analyses[2]	Equation	Region where equation applies	Standard error of estimate (percent)
Alabama	A, S, L, St, E, F, P, A_z, Lat, G, S_i, $I_{24,100}$, C_x	$d_{100} = C_x A^{0.2}$	State; C_x has been defined for six hydrologic regions within the State	17
Colorado	A, P, S_s, S_B	$d_{100} = 7.64\ S_s^{-0.517}$	Plains	21
		$d_{100} = .30\ A^{0.187} P^{0.059}$	Mountain	28
		$d_{100} = 3.13\ S_s^{-0.310}$	Northern plateau	22
		$d_{100} = .39\ A^{0.254}$	Southern plateau	36
Georgia	A	$d_{100} = .47 A^{0.50}$	1	50
		$d_{100} = .45 A^{0.42}$	2	46
		$d_{100} = .74 A^{0.33}$	3,4	50
		$d_{100} = 1.20 A^{0.25}$	5,6	46
Illinois	A, S	$d_{100} = 6.05\ A^{0.188} S^{0.997}$	State	28
Kansas	A, S, S_i	$d_{100} = 2.47\ A^{0.159}$	Glaciated basins	18
		$d_{100} = 1.70\ A^{0.236}$	Nonglaciated basins	19
Massachusetts	A	[3]$d_{100} = .57\ A^{0.233}$	State	40
Missouri	A	$d_{50} = 2.69 A^{0.130}$	Plains area	21
New York	A	$d_{100} = .82\ A^{0.20}$	State	38
North Carolina	A	[3]$d_{100} = .92\ A^{0.24}$	Mountains	38
		$d_{100} = 1.18\ A^{0.24}$	Piedmont province	28
		$d_{100} = .96\ A^{0.24}$	Coastal Plain	62
Oklahoma	A, I, RF	$d_{100} = .02\ A^{0.19} I^{1.06} RF$	State	24
Oregon	A	[3]$d_{50} = .80 A^{0.29}$	North and midcoast basins	22
		$d_{50} = .61 A^{0.30}$	South coast, Umpqua and Rogue basins	55
Tennessee	A	$d_{100} = 0.77\ A^{0.40}$	Knoxville vicinity	40
		$d_{100} = 1.42 A^{0.19}$	Chattanooga vicinity	50
		$d_{100} = 1.05\ A^{0.27}$	Northern highland rim	50
		$d_{100} = .74 A^{0.392}$	Central basin	40
		$d_{100} = 2.43 A^{0.15}$	West Tennessee	50
Wyoming	A	$d_{100} = .51\ A^{0.21}$	State	50

[1] Data taken from unpublished reports furnished by the Survey district for the indicated States. Questions concerning information contained in this report should be referred to the appropriate State.

[2] Explanation of symbols: A, Drainage area, in square kilometers; S, Main channel slope, in meters per kilometer; S_s, Slope of the streambed, in meters per kilometer; S_B, Slope of main channel, between two selected points, in meters per kilometer; L, Main channel length, in kilometers; St, Storage factor, in percent of drainage area in lakes and swamps; E, Average basin elevation, in meters; F, Forest factor, percentage of drainage area in forest; P, mean annual precipitation, in millimeters; A_z, Azimuth of the main channel, in degrees; Lat, Latitude of centroid of the basin, in degrees; G, Geologic storage factor; S_i, Soil infiltration factor; I, 2-year 24-hour rainfall, in millimeters; $I_{24,100}$, Rainfall intensity (24-hour, 100-year recurrence interval), in millimeters; C_x, RF, Regional factors.

[3] The 100-year depth (d_{100}) or 50-year depth is the difference between the 100-year elevation and the elevation of median flow—50 percent duration.

ble 2. The average of the weighted variability indices r basin sizes, 0 to 26 km², 27 to 260 km², 261 to 00 km², and greater than 1300 km², is 38 percent. ne 38 percent can be used as another reasonable ap- oximation of the national-average standard error of timate for the reconnaissance-level investigations.

Water-Surface Profile

A water-surface profile for the 100-yr flood can be veloped using two steps: (1) establish a channel- ttom profile based on a field survey, and (2) add 100- depths to the channel-bottom profile to obtain a 0-yr profile. As indicated previously, elevations and stances can be determined very accurately by field rvey; however, for practical purposes a maximum curacy usually is not obtained. A 5-percent error is sumed for step 1. The standard error introduced in ep 2 probably is insignificant.

Flood-Boundary Map

Elevations from the 100-yr profile can be trans- rred to a map on the basis of a field survey, on the sis of a combination of a field survey and use of rial photographs, or on the basis of elevation con- urs on a topographic map. As previously stated, e transfer of elevations can be accomplished without troducing significant errors if done by a field survey if done by the combination of field survey and aerial otography. An error of 10 percent is assumed when evations from a water-surface profile are transferred a map on the basis of contours on a topographic ap. The 10 percent is consistent with the assumed lue made for a similar task in the detailed method.

Overall Accuracy and Limitation

The probable overall standard errors of estimate for e physiographic method are computed for two levels investigation—comprehensive and reconnaissance. or the comprehensive level, the probable overall andard error for the 100-yr flood-boundary elevations

$$(SE)_{PC_1} = \sqrt{(25)^2 + (5)^2} = 25.5 \text{ percent (of depth)}$$

hen no significant errors are introduced in the devel- ment of a flood-boundary map, and

$$(SE)_{PC_2} = \sqrt{(25)^2 + (5)^2 + (10)^2} = 27.4 \text{ percent (of depth)}$$

hen the development of the flood-boundary map is sed on contours on a topographic map. For the re- nnaissance level, the probable overall standard error is

$$(SE)_{PR} = \sqrt{(40)^2 + (5)^2 + (10)^2} = 41.5 \text{ percent (of depth)}$$

when the development of the flood-boundary map is based on contours. In meters, the errors are 1.0, 1.1, and 1.6, respectively. Unless otherwise stated, 27 percent and 1.1 m are used to represent the overall average standard error, $(SE)_{PC}$, for a comprehensive investigation; 42 percent and 1.6 m are used to represent the probable overall standard error, $(SE)_{PR}$, for a reconnaissance-level investigation.

The physiographic method is applicable for natural channels having rigid boundaries. The method is not viable for studying the effects of local, onsite conditions, for determining the flood-boundary elevations for sheet flow, and for making floodways analyses.

SUMMARY AND CONCLUSIONS

Information taken directly from published and unpublished reports was used to appraise the accuracy of the different methods for flood-plain mapping that have been used by the U.S. Geological Survey at different places and times since 1960. The study was concerned with the national-average accuracy for the different methods. For brevity in determining and discussing accuracy, the methods scrutinized are classified as: detailed, historical, and physiographic (table 4). The elements (or tasks) of the three methods are as follows:

Detailed:

1. Determining the T-year discharge by regression equations.
2. Determining the water-surface profile for the T-year discharge; this requires detailed hydraulic and topographic information to be used in a step-backwater analysis which must be made for a reach of interest.
3. Developing a flood-boundary map; this requires the transferring of elevations from a profile to a map.

Historical:

1. Determining the T-year discharge by regression equations.
2. Determining the water-surface profile for the T-year discharge. This requires the development of a water-surface profile for a historical flood and the adjustment of the historical-flood profile to obtain a T-year profile.
3. Developing a flood-boundary map; this requires the transferring of elevations from a profile to a map.

TABLE 4.—*Probable nationwide average standard error for flood-boundary elevations for 100-yr floods, obtained according to the indicated methods and tasks*

Method	Task			Overall error	
	Determining 100-year discharge or 100-year depth	Determining 100-year profile	Transferring elevations from profile to map[1]		
	(Percent[2])	(Percent[2])	(Percent[2])	Percent[2]	Meters
Detailed	19	8	10	23	0.9
Historical	19	9	5	23	.9
Physiographic:					
Index-flow	[3]25	5	10	27	1.1
Area-parameter:					
Comprehensive	[3]25	5	10	27	1.1
Reconnaissance-level	[3]40	5	10	42	1.6

[1]Transferred on the basis of contours on topographic maps.
[2]Percent of 100-year depth.
[3]Represents standard error for the 100-year depth.

Physiographic:

1. Determining T-year depths; a regional depth-frequency analysis is required for this task.
2. Developing a T-year profile; this requires the development of a channel-bottom profile and the adjustment of the channel-bottom profile by adding T-year depths.
3. Developing flood-boundary maps.

The probable standard error of estimate, in percent of depth and in meters, was determined for 100-yr flood-boundary elevations (table 4). The depth is the difference in the water-surface elevation for the 100-yr discharge and the channel-bottom elevation. Users' errors, resulting when information on a map is incorrectly transferred to a point on the ground, and certain time-variant errors, resulting from flood-boundary changes, are not considered in this report.

The conclusions that are presented below are pertinent to a national average. The conclusions are as follows:

1. If all the possible viable methods of determining 100-yr flood-boundary elevations for natural streams had been tested for accuracy, the resulting nationwide standard errors of estimate probably would have ranged from 19 to 54 percent of the 100-yr depth. The 19 percent (of depth) represents the probable national-average standard error of estimate for regression equations developed to estimate 100-yr discharges (fig. 1). The 54 percent represents the probable standard error of estimate when 3.9 m, the average of 100-yr depths at 1752 streamflow-gaging stations, is used to represent the 100-yr depth. The 54 percent is obtained by using equation 4 in which 52 percent, the spatial coefficient of variation for 100-yr depths at the 1752 streamflow-gaging stations, is used to represent error for the 100-yr depth, 9 percent is used to represent the standard error in determining the 100-yr profile and 10 percent is used to represent the standard error in transferring elevations from a profile to a map.
2. The detailed method is applicable to a wide range of hydraulic and topographic conditions; it is the only method tested that is directly applicable to floodways analysis. Generally, the method can be used for conditions where the conservation of mass and energy for gradually varied flow can be rationally described. The method, therefore, has only limited application for sheet flow and for flow in channels having readily movable boundaries (sand channels). The probable standard

error of estimate for the 100-yr flood-boundary elevations is 23 percent. Based on 3.9 m as the national average 100-yr depth, the standard error of estimate is 0.9 m.

The historical method is applicable for a wide range of hydraulic and topographic conditions, if specific data are available. The specific data include peak discharge of the flood and the elevations of high-water marks referred to a common datum. Aerial photographs that show the areal extent of a historical flood of interest also provide useful information. The method has only limited application for flow in channels having readily movable boundaries (sand-channel streams). It is not applicable for floodways analysis. The probable standard error of estimate for the 100-yr flood-boundary elevations is 23 percent of the depth. Based on 3.9 m as the national average 100-yr depth, the standard error of estimate is 0.9 m.

The physiographic method is simpler to apply than the other methods. The application of the method is limited primarily to selected rural areas—areas not having a significant number of bridges, culverts, dams, dikes, canals and flumes—because it can be used only in natural channels (channels not significantly affected by manmade structures) having rigid boundaries (channels having a low probability of change that would significantly affect the hydraulic characteristics of a T-year discharge). The method is not viable for studying the effects of local, onsite conditions and for determining the flood-boundary elevations for sheet flow. For a comprehensive investigation, the probable standard error of estimate for the 100-yr flood-boundary elevation is 27 percent. The probable standard error of estimate is 42 percent if only a reconnaissance-level investigation is made (one in which size of basin is the only independent parameter used in a regression analysis). In meters, the errors would be 1.1 and 1.6, respectively.

5. The determination of the T-year discharge (or T-year depth for the physiographic method) introduces the largest component of error for the different methods; for the detailed method, the ratio of the standard error for the 100-yr discharge to the overall standard error is 0.83.
6. Investigations are needed to develop standard procedures for determining T-year discharges for ungaged streams more accurately. There is also a need for a feasible simplified method to determine T-year flood-boundary elevations in channels significantly affected by manmade structures, T-year flood-boundary elevations for sheet flow, T-year flood-boundary elevations for flow in channels having readily movable boundaries, and T-year flood elevations for floodways.

REFERENCES CITED

Bailey, J. F., and Ray, H. A., 1966, Definition of stage-discharge relation in natural channels by step-backwater analysis: U.S. Geol. Survey Water-Supply Paper 1869–A, 24 p.

Benson, M. S., and Carter, R. W., 1973, A national study of the streamflow data-collection program: U.S. Geol. Survey Water-Supply Paper 2028, 44 p.

Chow, Van Te, 1959, Open channel hydraulics: New York, McGraw-Hill Book Co., Inc., 680 p.

Dalrymple, Tate, 1960, Flood-frequency analyses: U.S. Geol. Survey Water-Supply Paper 1543–A, 80 p.

Hardison, C. H. 1969, Accuracy of streamflow characteristics, *in* Geological Survey research 1969: U.S. Geol. Survey Prof. Paper 650–D, p. D210–D214.

Leopold, L. B., and Maddock, T., Jr., 1953, The hydraulic geometry of stream channels and some physiographic implications: U.S. Geol. Survey Prof. Paper 252, 57 p.

Thomas, D. M., 1964, Flood-depth frequency in New Jersey: New Jersey Dept. Conserv. and Econ. Devel. Water Resources Circ. 14, 11 p.

U.S. Water Resources Council, 1976, Guidelines for determining flood flow frequency: U.S. Water Resources Council Hydrology Comm. Bull. 17, 26 p.

Winget, D. E., 1976, Index to water-resources data for Illinois: Champaign, Ill., U.S. Geol. Survey Water-Resources Inv. 76–87, 81 p.

Jour. Research U.S. Geol. Survey
Vol. 6, No. 4, July–Aug. 1978, p. 529–540

NATURAL RADIOACTIVITY IN GEOTHERMAL WATERS, ALHAMBRA HOT SPRINGS AND NEARBY AREAS, JEFFERSON COUNTY, MONTANA

By ROBERT B. LEONARD and VICTOR J. JANZER,
Helena, Mont., Denver, Colo.

Abstract.—Radioactive hot springs issue from a fault zone in crystalline rock of the Boulder batholith at Alhambra, Jefferson County, in southwestern Montana. The discharge contains high concentrations of radon, and the gross alpha activity and the concentration of adium-226 exceed maximum levels recommended by the Environmental Protection Agency for drinking water. Part of the discharge is diverted for space heating, bathing, and domestic use. The radioactive thermal waters at measured temperatures of about 60°C are of the sodium bicarbonate type and saturated with respect to calcium carbonate. Radium-226 in the rock and on fractured surfaces or coprecipitated with calcium carbonate probably is the principal source of radon that is dissolved in the thermal water and discharged with other gases from some wells and springs. Local surface water and shallow ground water are of the calcium bicarbonate type and exhibit low background activity. The temperature, percent sodium, and radioactivity of mixed waters adjacent to the fault zone increase with depth. Samples from most of the major hot springs in southwestern Montana have been analyzed for gross alpha and beta activity. The high level of radioactivity at Alhambra appears to be related to leaching of radioactive material from fractured siliceous veins by ascending thermal waters and is not a normal characteristic of hot springs issuing from fractured crystalline rock in Montana.

The purpose of this report is to describe anomalously high radioactivity in thermal waters in Alhambra Hot Springs located about 19 km southeast of Helena (fig. 1) and to suggest the relation of the hot springs to the local and regional geology and hydrology.

Several studies in the United States and elsewhere have described higher levels of radioactivity in thermal waters than in adjacent cooler ground water and surface water (Scott and Barker, 1962; O'Connell and Kaufmann, 1976). Radioactive decay may be a major source of the geothermal heat (Tilling and Gottfried, 1969; Blackwell and Robertson, 1973; Gabelman, 1976). Radiochemical studies by Wollenberg (1975), Stoker and Kruger (1975) and others suggest that radiochemical data can be a useful tool for the exploration and evaluation of geothermal resources. Moreover, the potentially deleterious effects of elevated levels of radioactivity on public health (U.S. Environmental Protection Agency, 1976) could impose severe restrictions on the development of geothermal resources. Data describing radioactivity of thermal waters are thus essential to an assessment of Montana's geothermal resources.

During a reconnaissance survey of local uraniferous deposits with a field-type Geiger counter, Thurlow and Reyner (1952) detected about twice the normal background levels of radioactivity at Alhambra Hot Springs and Boulder Hot Springs, about 30 km (kilometers) to the south (fig. 1). They reported that carbonate incrustations around the Alhambra springs registered more than 10 times normal radioactivity background and that radioactivity was detected with a scintillometer while traversing the area by automobile. During a reconnaissance by the U.S. Geological Survey in 1970, slightly higher than normal levels of radioactivity at Alhambra Hot Springs and normal background levels at Boulder Hot Springs were recorded with field equipment (E. C. Robertson, written commun., 1976). At both localities the thermal waters are used for space heating, bathing, and domestic purposes. Therefore, anomalously high levels of radioactivity could constitute potential hazards to health.

Acknowledgments.—The cooperation and assistance of local landowners, particularly Mrs. W. L. Bomparte, Mr. R. C. Butler, and Mr. W. W. Wall, and of Mr. W. J. Lindsay, a drilling contractor of Clancy, are sincerely appreciated. Mr. Larry Lloyd, health physicist of the MDHES (Montana Department of Health and Environmental Sciences), deserves special recognition for his continued advice, support, and release of unpublished data included in this report. His contributions to the investigation do not necessarily imply total agreement with the conclusions.

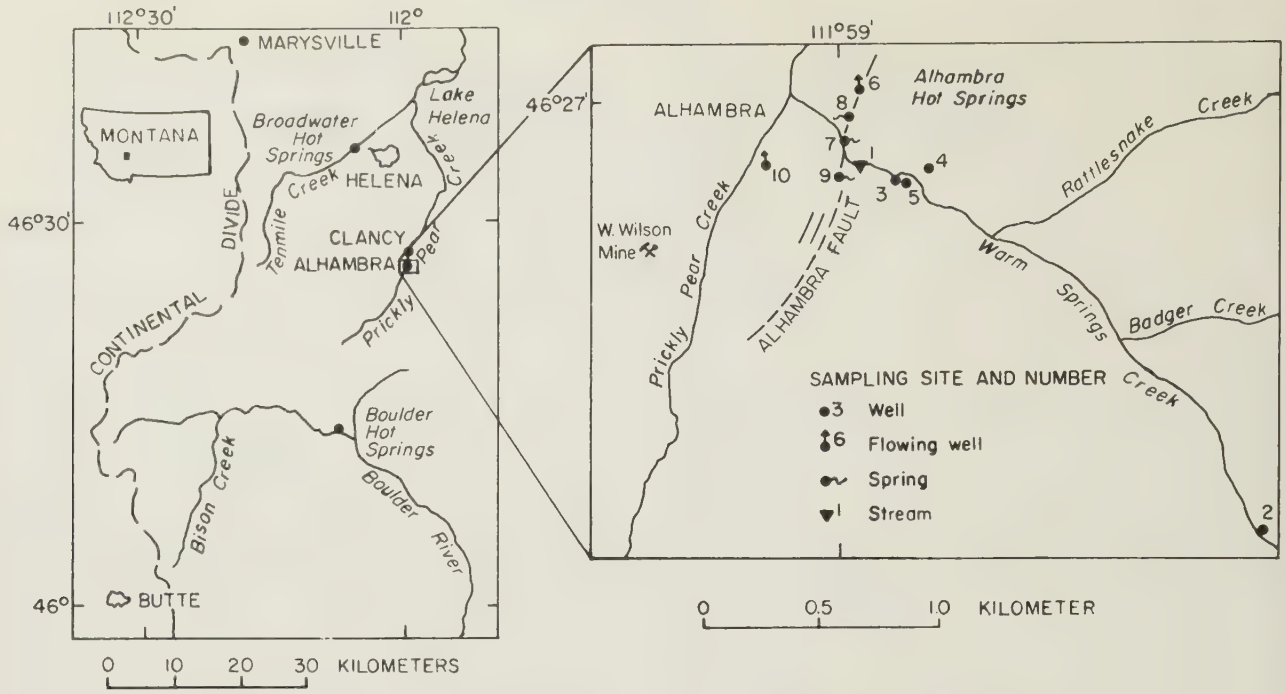

FIGURE 1.—Index map showing location of wells and springs in the Alhambra area.

GEOHYDROLOGIC SETTING

Three groups of hot springs, several zones of seepage, and a flowing hot-water well lie along a 0.5 km segment of the Alhambra fault (Smedes, 1966) in the valley of Warm Springs Creek near its mouth (fig. 1). Thermal waters issue from fractured quartz monzonite and alaskite or from the shallow overlying alluvium and colluvium at a combined rate of about 16 L/s (liters per second). Mean annual precipitation of about 500 mm (millimeters), chiefly in the form of snow in the Elkhorn Mountains to the east, sustains perennial streamflow and provides recharge to the fractured rock aquifers.

The hydrothermal system sustaining the Alhambra hot springs probably is confined to igneous intrusive and volcanic rock. Alhambra is located in the northeast part of the Boulder batholith, a composite pluton of Laramide (Late Cretaceous to early Tertiary) age that is composed primarily of quartz monzonite (Smedes, 1966; Knopf, 1963). The monzonite is typically sheeted and locally is crossed by pronounced systems of jointing. Dikes, plugs, and irregular masses of aplite, alaskite, and younger rhyolite (age 35.8±1.4 m.y., R. A. Chadwick, Montana State Univ., written commun., 1976) typically are shattered and sheared.

Nearly vertical silicified zones, locally called reefs, transect the quartz monzonite and the alaskite bodies. The reefs consist mainly of brecciated country rock containing many small discontinuous lenses of cryptocrystalline silica, some of which contains highly radioactive uranium minerals (Roberts and Gude, 1953). Although the reefs are resistant to erosion, forming prominent ridges and spurs, they have been faulted and somewhat brecciated before and after silicification that occurred soon after emplacement of the batholith (Pinckney, 1965).

Radioactivity in the batholith appears to be associated preferentially with siliceous rock. Samples of silicic Butte quartz monzonite and alaskites similar to the rock exposed near Alhambra Hot Springs contain 5.9 and 9.2 ppm (parts per million) uranium; 22.3 and 36.3 ppm thorium; and 3.6 and 4.5 percent potassium, respectively (Tilling and Gottfried, 1969, table 2). Average concentrations for the Boulder batholith are lower.

Near Alhambra, primary and secondary uranium minerals are concentrated in fissure fillings of microcrystalline quartz and chalcedony associated with siliceous reefs. Roberts and Gude (1953) reported that a sample of high grade ore from the abandoned W. Wilson mine, about 1 km southwest of the hot

prings, assayed 9.58 percent uranium. The main reef
h which the mine is located trends about N. 60° E.
Smedes, 1966). If continuous beneath alluvial and
olluvial deposits, the reef would intersect the Al-
ambra fault in the subsurface near the hot springs.

The crystalline rocks, including the reefs, presum-
bly are too old to represent sources of residual heat,
nd no firm evidence is available to support contact
f the thermal waters with younger hot rock. Radio-
ctive elements in the rocks of the Boulder batholith
re sufficiently abundant to produce a significant part
f the average measured heat flow of about 2 micro-
alories per square centimeter by radioactive decay
Blackwell and Robertson, 1973). However, decay of
adioactive elements in localized deposits probably is
negligible source of heat for the hot springs.

The mean annual air temperature at Alhambra is
bout 6°C. If geothermal gradients of 21°C/km
neasured in similar rock about 8 km to the southwest
Blackwell and Robertson, 1973) can be extrapolated
o Alhambra, the maximum temperature of 59.4°C
ecorded for the hot springs theoretically would be
xpected at a depth of 2.5 to 3 km. Evidence from a
eothermal test well at Marysville and the deep mines
t Butte (fig. 1) indicates that faults and fractures
imilar to those observed at Alhambra act as conduits
or deep circulation of meteoric waters through rock
hat normally is impermeable when intact.

METHODS OF INVESTIGATION

Samples for radiochemical analysis were collected
y the U.S. Geological Survey at hot spring 9, flowing
ot well 6, and Boulder Hot Springs (fig. 1) to sub-
tantiate the previously reported anomalies. Samples
vere also collected at Broadwater Hot Springs, about
.2 km west of Helena, because the springs represent
somewhat similar geohydrologic environment and
re under consideration for development as a source
f space heating and domestic water supply. Only the
amples from Alhambra showed a level of radioactivity
bove normal background. There, the gross alpha and
eta activity and the concentration of radium-226 ex-
eeded levels recommended for drinking water (U.S.
Environmental Protection Agency, 1976).

Larry Lloyd, of the MDHES, and the senior author
nade a reconnaissance survey during the summer of
976 by using an SPA3 scintillometer to localize the
ources of radioactivity at Alhambra. Observed levels
f radioactivity were 5 times normal background near
he hot springs and seeps and as much as 10 times
ormal background in travertine deposits around one
f the vents and in siliceous zones in adjacent frac-
tured crystalline rock. A similar scintillometer survey of the Broadwater Hot Springs failed to reveal abnormal levels of radioactivity. Analyses by MDHES for gross alpha and gross beta activity of selected water samples confirmed abnormal levels of radioactivity at the Alhambra Hot Springs and normal background levels at Boulder and Broadwater.

Additional samples for determination of dissolved uranium, radium-226, and radon by the National Water Quality Laboratory of the Geological Survey in Denver were then collected mainly at sites where the MDHES analyses showed abnormal levels of radioactivity. Some duplicate samples were also sent to MDHES for concurrent analysis.

SAMPLING PROCEDURES

At springs having multiple vents, the samples were obtained where the specific conductance, discharge, and temperature were highest. All the waters sampled were clear and virtually free of suspended matter.

Unfiltered samples for analysis by the Survey were collected in 4-L polyethylene bottles and acidified with reagent grade hydrochloric acid to a pH less than 1. Unfiltered samples for radiochemical analysis by the MDHES were collected in 1-L polyethylene bottles and acidified with reagent grade nitric acid to a pH of less than 1. The analyses for gross alpha and beta activity normally were completed within 1 week of collection.

Samples of thermal waters for determination of dissolved radon-222 were collected in 50 mL (milliliter) heavy-walled borosilicate glass collection tubes to which lengths of Tygon plastic tubing were attached. The lower (short) length of tubing was bent in the form of a U so that the open end was about 0.5 m above the sampler. When the desired sampling depth was reached, the trapped air was released through the longer length of tubing by opening a pinchcock at the surface. When a representative sample had been collected by alternately raising and lowering the sampler, the pinchcock was closed and the plastic tubes at each end were sealed for shipment. To minimize decay of the radon-222 (half-life, 3.823 days), the samples were shipped to the laboratory by priority mail for immediate processing.

Duplicate samples, filtered and unfiltered, normally were collected for chemical analysis by using methods approved by the Survey, with some modifications suggested for thermal-spring samples by Presser and Barnes (1974). Routine field measurements included water discharge by using a Hoff or pygmy current meter, temperature by using a maximum-reading

mercury thermometer and a thermistor-wheatstone bridge combination, pH by using a Sargent-Welch PBL pH meter, specific conductance by using a Yellow Springs Model 33 SCT meter, and alkalinity by titration. At several sites, samples of gas were collected in plastic and glass syringes. These samples were analyzed for nitrogen, oxygen plus argon, carbon dioxide, and methane by gas chromatography in the Survey laboratories in Menlo Park, Calif.

LABORATORY PROCEDURES

Detailed descriptions of the radiochemical procedures used by the Survey for water and sediment analysis are given by Thatcher, Janzer, and Edwards (1977). Determination of radon dissolved in water or mixed with gas or air is made by an alpha scintillation technique, which is similar to the technique for determining radium-226 using radon.

Determination of the gross alpha and gross beta-gamma radioactivity of a water sample is relatively simple and rapid. The results are useful as an indication of total sample radioactivity or as a screening technique. Analyses for dissolved uranium, radium-226, and radon-222 by the Survey were made only on those samples for which the gross alpha activity as determined by the MDHES was greater than 10 pCi/L (picocuries per liter).

LABORATORY RESULTS

The values of gross alpha and gross beta activity reported for duplicate samples by the Survey generally are much higher than corresponding values reported by the MDHES, particularly for samples containing high levels of gross alpha activity (table 1). Despite the apparent discrepancies, both laboratories verified anomalously high levels of radioactivity at the same sites, and the results varied somewhat proportionately from site to site. The results of recent proficiency tests conducted by EPA (Environmental Protection Agency) confirm the comparability of MDHES gross alpha data with reference standards distributed by EPA and suggest that the determinations of gross beta activity may be slightly lower than the actual values (Larry Lloyd, oral commun., 1977).

To be useful, comparative measurements of duplicate samples should be reported in the same units or be readily convertible to equivalent units. The Survey gross alpha measurements in water are reported in terms of micrograms per liter (μg/L); that is, mass units of equivalent natural uranium (Un) per liter, in preference to picocuries per liter, the activity units used by the MDHES and others. A conversion factor of 1 μg/L = 0.68 pCi/L is used to compare gross alpha determinations in this report.

A curie is the unit of radioactivity equivalent to 3.7×10^{10} disintegrations per second (becquerels). A picocurie (pCi), or 1×10^{-12} Ci, yields 2.22 distintegrations per minute and is one of the more common units used to describe the low level of radioactivity generally associated with environmental samples. Some confusion and uncertainty in reporting gross alpha measurements in water have resulted from the definition of a "special curie" for natural uranium and thorium, which was made by the National Committee of Radiation Protection (Ney, 1974; Hursch, 1974). Use of the "special curie" results in a conversion of mass to activity for natural uranium of 1 μg = 0.33 pCi. If the three isotopes U-238, U-235, and U-234 found in natural uranium in the proportions 99.28, 0.711, and 0.0006 percent, respectively (Edwards, 1968), occur in the same proportions in the standard isotope calibration solutions, the conversion 1 μg = 0.68 pCi is valid. Perhaps coincidentally, use of the "special curie" conversion factor of 0.33 would result in closer agreement between the results of the Survey and MDHES for high concentrations of gross alpha.

Natural uranium is commonly recommended and used as the gross alpha calibration isotope (American Public Health Association and others, 1976; American Society for Testing and Materials, 1976). Strontium-90 or cesium-137 is recommended as the gross beta calibration isotope. Natural uranium for alpha, and cesium-137 for beta reportedly are the calibration standards of reference for both laboratories. Therefore, the results should agree if the calibration solutions used are made from reliable standards preferably calibrated by or traceable to the National Bureau of Standards. Perhaps "natural" uranium salts used as standards for the gross alpha determinations should be tested to verify the coexistence of the isotopes in their natural abundance.

The maximum contaminant levels for public water supplies specified by the U.S. Environmental Protection Agency (1976) for gross alpha and gross beta radioactivity are 15 and 50 pCi/L, respectively. The 50 pCi/L level for gross beta applies if the average annual concentrations of tritium and strontium-90 are less than 20 000 and 8 pCi/L, respectively. Levels of these isotopes in the ground waters from the Alhambra area could reasonably be expected to be less than 500 and 0.1 pCi/L, respectively.

Gross alpha levels determined by the Survey ranged from 26 μg/L (18 pCi/L) in the sample from cold well 5 to 930 μg/L (630 pCi/L) from hot spring 9 (table 1). The corresponding determination by the

TABLE 1.—*Analyses of thermal and nonthermal waters*

Sample location number (fig.1)	Source	Location		Date of collection	Specific conductance (µmhos/cm) at 25°C	Temperature (°C)	Dissolved solids (sum of constituents) (mg/L)	Sodium-adsorption-ratio	Dissolved silica (SiO_2) (mg/L)	Gross alpha[1]		Dissolved natural uranium (µg/L)	Dissolved radium-226 (pCi/L)	Dissolved radon-222 (pCi/L)	Potassium-40 (pCi/L)	Gross beta[2]	
		Latitude	Longitude							USGS (µg/L)	MDHES (pCi/L)					USGS (pCi/L)	MDHES (pCi/L)
1	Warm Springs Creek.	46 26 51	111 58 48	6/29/76	-	-	-	-	1	-	5	-	-	-	-	-	2
				8/20/76	192	16.0	130	0.3	21	-	3	-	-	-	-	-	<3
2	Cold well---	46 25 54	111 57 15	8/20/76	384	10.0	251	1.0	14	-	12	-	-	-	-	-	10
3	Cold well---	46 26 49	111 58 44	6/29/76	295	8.9	227	1.0	24	-	3	-	-	-	-	-	6
				10/19/76	-	-	-	-	-	-	4	-	-	-	-	-	<6
4	Cold well---	46 26 52	111 58 36	6/29/76	410	16.1	334	1.7	29	-	11	-	-	-	-	-	18
				10/19/76	-	-	-	-	-	-	12	-	-	-	-	-	8
5	Cold well---	46 26 48	111 58 41	8/03/76	1,000	17.7	632	6.7	48	26	14	7.2	3.5	-	6.3	19	22
				10/13/76	-	-	-	-	-	-	6	-	-	-	-	-	10
6	Flowing hot well.	46 27 01	111 58 50	4/29/76	1,040	52.2	613	11	58	410	-	-	28	-	7.4	110	-
				6/29/76	1,080	54.0	-	-	61	240	112	.9	27	11,000[3]	7.1	69	56
				12/02/76	1,000	52.2	-	11	-	360	110	.8	28	24,000	7.2	90	70
7	Hot spring--	46 26 53	111 58 51	6/29/76	1,110	56.7	651	12	60	-	97	-	-	6,000	-	-	48
				10/19/76	-	-	-	-	-	-	70	-	-	-	-	-	54
8	Hot spring--	46 26 59	111 58 50	6/15/76	1,070	57.7	-	-	-	-	68	-	-	-	-	-	54
				6/29/76	827	59.4	909	12	67	290	94	.9	40	3,000	7.5	81	48
				10/19/76	-	-	-	-	-	-	81	-	-	-	-	-	43
9	Hot spring--	46 26 47	111 58 58	4/28/76	1,580	54.4	953	14	61	930	-	-	72	10,000	13	220	-
				6/15/76	1,600	55.6	-	-	-	-	153	-	-	-	-	-	131
				6/29/76	1,610	56.1	-	-	-	-	214	-	55-70	7,000[4]	-	-	100
				12/02/76	1,510	54.4	-	14	-	890	293	<.4	73	17,000	12	210	150
10	Flowing warm well.	46 26 52	111 59 14	7/10/76	1,680	27.0	1,060	15	67	-	77	-	-	-	-	-	59
				7/13/76	1,650	29.0	-	-	-	260	-	.5	27	-	15	81	-
				7/23/76	-	-	-	-	-	-	113	-	-	-	-	-	60
				10/19/76	-	-	-	-	-	-	121	-	-	-	-	-	53
				12/02/76	1,620	30.0	-	15	-	560	113	.8	37	37,000	15	130	77

[1]Theoretical conversion for natural uranium: 1µg/L = 0.68 pCi/L.
[2]As cesium-137.
[3]Corresponding gas sample 130,000 pCi/L.
[4]Corresponding gas sample 80,000 pCi/L.

MDHES for cold well 5 was 14 pCi/L; the maximum determined was 293 pCi/L (compared with 890 μg/L= 605 pCi/L reported by the Survey) for hot spring 9. Gross beta values ranged from 19 pCi/L in the sample from cold well 5 to 220 pCi/L (as cesium-137) from hot spring 9.

Although the MDHES analyses show lower levels of radioactivity than the Survey analyses for corresponding samples, both show that the samples of thermal water from wells and springs 6–10 exceed the maximum contaminant level for gross alpha and beta activity. According to the Survey analysis, gross alpha in the sample from cold well 5 exceeded the maximum contaminant level, but the MDHES determination was lower than the maximum contaminant level.

Radium-226 concentrations ranged from 3.5 pCi/L in cold well 5 to 73 pCi/L in hot spring 9. The drinking water regulations (U.S. Environmental Protection Agency, 1976) state that the maximum combined contaminant level for radium-226 plus radium-228 in community water systems is 5 pCi/L. With the exception of cold well 5, all the samples analyzed by the Survey contained concentrations of radium-226 alone exceeding the maximum contaminant level for radium.

None of the samples was analyzed for radium-228, a beta-emitting radium daughter resulting from the alpha decay of thorium-232. However, the predominance of thorium in the rocks suggests that radium-228 is present in the thermal waters. Activity ratios Ra-228/Ra-226 larger than unity have been reported from several surface- and ground-water sources in Colorado (Johnson, 1971); therefore, the concentration of radium in the waters may be significantly higher than reported.

Maximum concentration of radon-222 was 37 000 pCi/L in a water sample collected from flowing warm well 10. The reported levels probably are 5 to 10 percent lower than the true levels as a result of losses by diffusion of radon through the plastic tube closures. All-glass sampling tubes would have been preferable; however, these were not used because of their fragility, expense, and unavailability at the time of sample collection. Drinking water regulations of the U.S. Environmental Protection Agency (1976) do not specify a maximum contaminant level for radon.

The reported concentrations of potassium-40, a beta-emitter, and dissolved uranium are relatively insignificant in relation to public health. For example, the maximum concentration of potassium-40 was 15 pCi/L from flowing warm well 10. On the basis of an estimated potassium content of the human body of about 0.35 percent (Lange, 1969) and a specific activity of potassium-40 in natural potassium of abou 0.75 pCi/mg (picocurie of beta particles per milli gram), about 200 000 pCi of potassium-40 is presen in a human weighing 75 kg. Similarly, the reported concentrations of natural uranium, with the possible exception of the value of 7.2 μg/L for cold well 5 represent relatively insignificant contributions to the gross alpha content of the waters. The higher concentration of uranium in cold well 5 than in associated hot springs resembles similar occurrences in Nevada (Wollenberg, 1975).

SOURCES OF RADIOACTIVITY IN WATER

Either natural or manmade radioactivity, or both are found in varying concentrations in all precipitation and surface and ground waters. The natural radioactivity is caused by traces of (1) the long-lived parent members of three natural radioactive decay series—U-238 (uranium series), U-235 (actinium series), and Th-232 (thorium series) and their daughters (2) single long-lived radioactive elements, with potassium-40 being the most abundant, and (3) radionuclides such as tritium and carbon-14, which are produced by cosmic rays as well as by nuclear devices.

Uranium occurs in low concentrations in many natural waters; average seawater contains about 3 μg/L dissolved uranium (Gabelman, 1976). U-238 is the most abundant (99.28 percent) natural isotope of uranium. Its decay products, U-234, Th-230, Ra-226, Rn-222, Po-218, Po-214, and Po-210 decay by alpha emission. In terms of their activities (decay rates) U-238 and U-234 are about equally abundant in nature. The average activity ratio U-234/U-238 of about 1.4 in geothermal waters is suggested by a recent study in the western United States (O'Connell and Kaufmann, 1976). U-235 is much less abundant in nature (normally 0.7 percent of natural uranium) than U-238 and does not contribute significantly to the radioactivity of natural waters.

Although thorium is a major radioactive constituent of acid igneous rock, measured levels of thorium-232 greater than a few nanograms per liter (10^{-9} g/L) are rarely found in surface or ground waters. Thorium has been found in detectable concentrations in mine drainage from acid igneous rocks (V. J. Janzen, unpub. data, 1977), but because of the apparent immobility of the ions under normal conditions thorium generally is not a significant dissolved radioactive constituent of natural waters. However, the beta-emitting daughter radium-228 may, when combined with radium-226, occur at Alhambra at con

entrations approaching the maximum contaminant evel of 5 pCi/L established by the U.S. Environmental Protection Agency (1976).

RELATIONSHIP OF RADIOACTIVITY TO MAJOR DISSOLVED CONSTITUENTS

As water passes through the soil and rocks it dissolves varying quantities of the minerals, both radioactive and nonradioactive, with which it comes in contact. Therefore, the chemical composition of the water reflects the composition of the rocks as well as variations in temperature, pressure, and traveltime along its path in the subsurface.

All the waters sampled near Alhambra were of the calcium bicarbonate or sodium bicarbonate type. The water in general progresses from streamflow (No. 1) and shallow ground water (wells 2–5) of the calcium bicarbonate type to more highly radioactive thermal water (wells and springs 6–10) of the sodium bicarbonate type with increasing temperature, concentration of dissolved solids and silica, and sodium-adsorption-ratio (fig. 2, table 1). The sodium-adsorption-ratio (U.S. Salinity Laboratory Staff, 1954) is defined as

$$\frac{Na^{+}}{\sqrt{\frac{Ca^{2+} + Mg^{2+}}{2}}}$$

with all concentrations in milliequivalents per liter. It is normally used for describing the quality of irrigation waters but is convenient for describing differences in the cation distribution in thermal waters and, at Alhambra, for distinguishing thermal waters (high ratio) from the normal ground water (low ratio).

The relatively dilute calcium bicarbonate water from cold well 2 about 2.4 km upstream from the hot springs (fig. 1) is probably characteristic of the nonthermal shallow water in the fractured quartz monzonite. The radioactivity is near or below the level of detection, as it is in chemically similar waters from Warm Springs Creek and cold well 3 (table 1), respectively. Levels of radioactivity significantly higher than normal background, but far lower than in the thermal waters, were reported for selected samples of waters in wells penetrating similar aquifers several kilometers from the hot springs (Larry Lloyd, written commun., 1976).

The thermal waters from the Alhambra fault zone (Nos. 6–9, fig. 1) are remarkably similar chemically to the cooler, but slightly more mineralized, discharge of flowing warm well 10. Although less radioactive than the discharge from hot spring 9, which the well was meant to replace, the well water is too radioactive for domestic use. The similarities suggest a common source.

Discharges from cold wells 3–5 are mixtures of thermal and nonthermal waters. The temperature of the water in cold well 5 increased with depth. If the well were drilled deeper, the percentage of thermal water and the radioactivity in the discharge probably would be higher.

Calcium (in equivalent weights) is more abundant than sodium in most of the crystalline rock that underlies the Warm Springs watershed (Smedes, 1966); therefore, the predominance of calcium in the surface water and cool shallow ground water is not unexpected. The relatively low proportion of calcium and magnesium in the thermal waters, as indicated by the high sodium-adsorption-ratio (fig. 2), probably results mainly from the decreasing solubility of these carbonates and the increased solubility of sodium salts with increasing temperature. Despite the relatively low concentrations of calcium, solution-mineral equilibrium calculations (Mariner and others, 1976) show that hot spring 8 was saturated with calcium carbonate. Active deposition of calcium carbonate as radioactive travertine at the vent indicates saturation of hot spring 9 also.

According to Thurlow and Reyner (1952) a sample of the travertine or of a similar incrustation at a vent north of Warm Springs Creek contained 0.058 percent equivalent uranium but only 0.001 percent actual uranium and 10 times normal radioactive background. The high values of radioactivity in the discharge and in the travertine are consistent with Wollenberg's (1975) observation that high levels of radioactivity in Nevada thermal waters are commonly associated with calcium carbonate dominated, in contrast to silica dominated, hot springs. Most of the major hot springs in southwest Montana have been sampled by the Survey and analyzed for gross alpha and beta activity by MDHES. Besides Alhambra, only three other springs show high levels of radioactivity, and all three are actively depositing calcium carbonate; none of the three issues from fractured crystalline rock.

The relatively insignificant concentrations of dissolved uranium in the waters at Alhambra suggest that radium-226 and its short-lived alpha-emitting polonium daughters (Po-218 and Po-214) are the principal sources of the high alpha activity. High concentrations of radon-222 from several sources confirm the presence of its parent, radium-226, in the system (table 1).

High concentrations of radon are commonly found in water from fractured zones in crystalline rock.

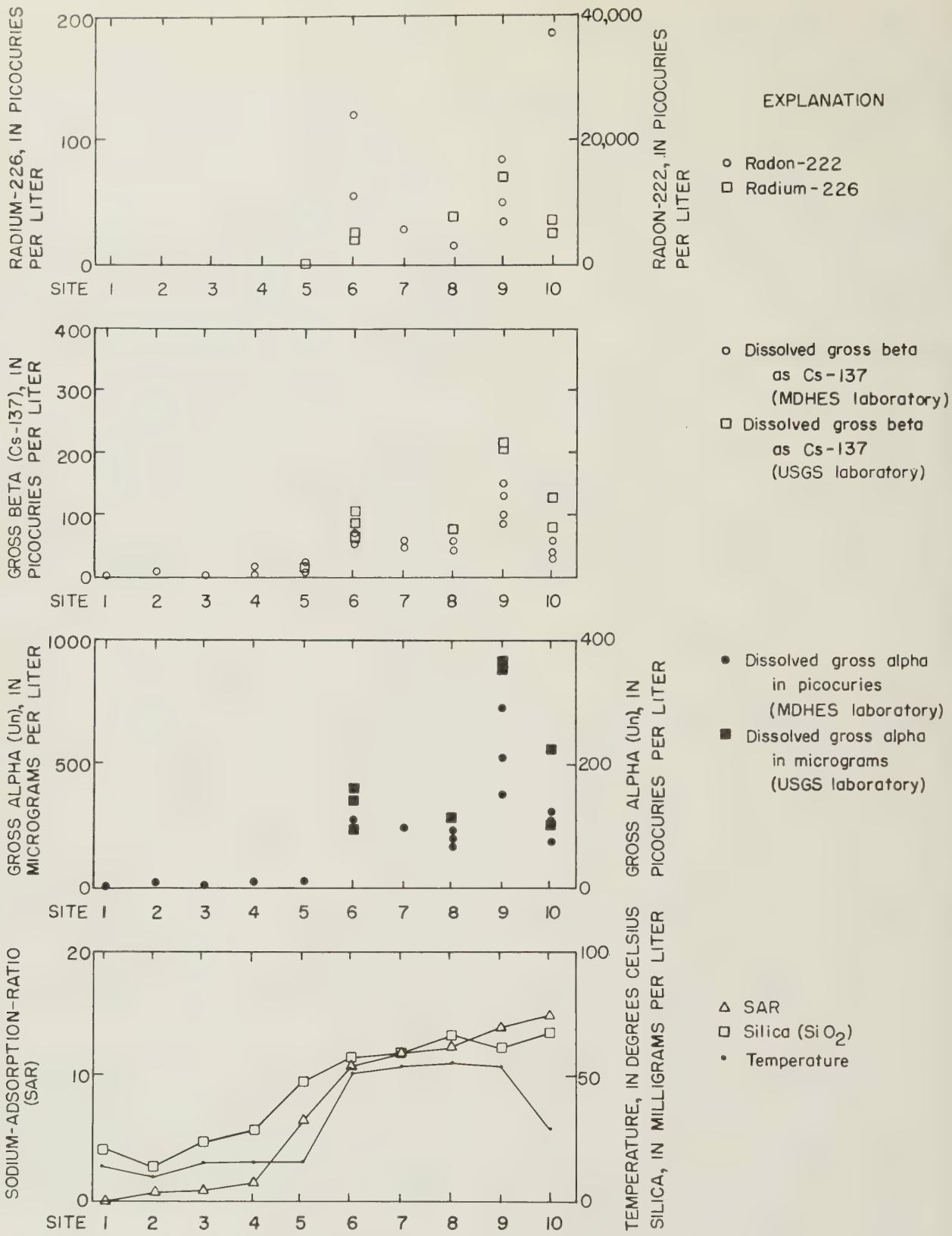

FIGURE 2.—Variations in radioactivity, sodium-adsorption-ratio, temperature, and concentration of silica in water samples.

he fracturing that accompanies seismic activity pre-mably increases the surface area of radioactive rock om which radon can be released and transferred to e water. Alhambra lies along the northern Inter-ountain Seismic Belt (Smith and Sbar, 1974) and subject to continuing seismic activity that may aintain open fractures in the rock. The epicenters three major earthquakes, one in 1925 and two in 35, lie within 32 km of Alhambra (Friedline and mith, 1974; Robertson and others, 1976).

Much higher concentrations of radon were found at e same sites in December 1976 than in April or ne 1976. The concentrations of radon were not pro-rtional to the concentrations of radium-226 in the mples nor were fluctuations in the two constituents rrelative (fig. 2). Radium-226 normally is not found water at the concentration required to produce e measured concentrations of radon; that is, in cess of several thousand picocuries per liter.

Although thorium isotopes are not generally signif-ant dissolved radioactive constituents of natural aters, they are formed in the dissolved state by the dioactive decay of the dissolved uranium isotopes -238 and U-234. Whereas the uranium tends to re-ain in solution as a stable carbonate complex, the orium isotopes plate out or are sorbed on rock rfaces. Concentrations of Th-234, U-234 (decay roduct of Th-234), and Th-230 are much higher on e surfaces of rock fractures that have been exposed percolating waters than in the bulk of the country ck (J. Rosholt, oral commun., 1977). Radium-226 sulting from the radioactive decay of the sorbed h-230 probably is the source of much of the dissolved don found in the thermal waters described in this udy.

Wollenberg (1975) and O'Connell and Kaufmann 976) suggest that radium-226, coprecipitated with lcium, can be a substantial secondary source of don. At least part of the radon at Alhambra prob-ly is a decay product of radium-226 in calcareous posits at depth.

No consistent relationship between the concentra-n of radon and the chemistry or temperature of the ater is apparent; however, the concentrations of ssolved radon in samples from flowing wells gen-ally were higher than in samples from the springs able 1, fig. 2). Spasmodic eruptions of gas from wing hot well 6, effervescent discharge from flowing arm well 10, and continuous gas bubbles in more tive hot springs denote supersaturation of the waters ith gas. A 60 mL syringe of gas from hot spring 9 ntained the equivalent of 80 000 pCi of radon-222 r liter of gas, and a similar sample from flowing hot well 6 contained 130 000 pCi/L. The activity of dissolved radon in corresponding water samples was 7000 and 11 000 pCi/L, respectively. Radon in the spring waters probably had more time to approach equilibrium with the atmosphere and to dissipate into the surrounding rock and soil at shallow depth than did radon in the more confined well waters.

Major components of the gas from the wells and springs are nitrogen (85–88 percent), oxygen and argon (4–6 percent), and carbon dioxide (8–9 percent). Whereas radon is a noble, nonreactive gas, reactions between carbon dioxide in solution and the rocks probably determine to a large extent the chemical properties of the thermal waters. Although the solubility of carbon dioxide in water varies inversely with temperature, it is retained in solution under hydrostatic head at depth where it can lower the pH of the water and react with the minerals in the rock to form soluble bicarbonates. Conversely, when carbon dioxide gas is liberated from ascending thermal waters as a result of the decline in hydrostatic pressure, the less soluble compounds, particularly calcium carbonate, can precipitate from a saturated solution to seal the conduits or to form travertine deposits at the surface. Precipitation of calcium would leave the waters relatively enriched with respect to the more soluble sodium bicarbonate.

Sodium (in equivalent weights) is more abundant than calcium in the silica-rich rocks associated locally with the hot springs and the radioactive anomalies. The high sodium and bicarbonate content of the thermal waters at Alhambra may result from the reaction:

$$CO_2 + Na \text{ silicate} + H_2O = HCO_3^- + Na^+ + H \text{ silicate}$$

which represents dissolution of sodium feldspar with the simultaneous conversion of carbon dioxide (CO_2) to bicarbonate (HCO_3^-), release of sodium ion (Na^+), and formation of clay. Calcium, potassium, silica (SiO_2), and soluble radioactive elements disseminated in the rock would be liberated concurrently. Sodium bicarbonate tends to inhibit precipitation of dissolved uranium (Barker and Robinson, 1963), thereby increasing its mobility.

Subsurface temperatures estimated from the concentrations of sodium, potassium, and calcium in the waters (Fournier and Truesdell, 1974) are about 157°C for hot spring 9 and 161°C for flowing warm well 10. The estimates are based on the assumptions that the ascending water had not interacted with the country rock after it left the geothermal reservoir, that it had not mixed with cooler shallow ground water, and that none of the three ions had precipitated enroute

to the point of discharge (Fournier and others, 1974). The difference of about 100°C between the estimated subsurface temperatures and measured surface temperatures suggests mixing. Precipitation of calcium, as almost certainly occurs at Alhambra, would lead to erroneously high temperature estimates, although the error probably is negligible.

The solubility of silica increases with temperature, and the solubility of amorphous silica is much greater than the solubility of primary quartz at the same temperatures. If the dissolved silica in the thermal waters is at equilibrium with primary quartz in the fractured crystalline rock aquifers, subsurface temperatures estimated from the concentrations of silica are about 111°C for hot spring 9 and 115°C for flowing warm well 10 (Fournier and Rowe, 1966). The estimated temperatures would be only about 82° and 87°C, respectively, if the equilibrium were with chalcedony (Fournier and Truesdell, 1974). If the water is cooled by mixing with shallow ground water, temperatures estimated using the cation and quartz geothermometers are nearly equal.

From his studies in Iceland, Arnorsson (1975) concluded that the silica concentration of hot springs associated with low-temperature reservoirs is controlled by the solubility of chalcedony if the reservoir temperature is less than 110°C, by quartz or chalcedony in the range from 110° to 180°C, and by quartz at temperatures greater than 180°C. The combined evidence indicates that the reservoir temperature for Alhambra Hot Springs is in the lowest range.

In several abandoned mines near Alhambra, secondary uranium minerals occur along fractures in veins of microcrystalline quartz or as disseminations in the monzonite wall rock "where they have clearly been deposited from circulating ground water" (Thurlow and Reyner, 1952, p. 18). Wright, Bieler, Shulhof, and Emerson (1954) state that the most recent of several varieties of chalcedony found in veinlets and enclosing breccia fragments are the most highly radioactive. However, they confirm the association of primary and secondary uranium minerals with chalcedonic gangue, which led Roberts and Gude (1953) to conclude that little or no migration of uranium has occurred since the primary uranium and chalcedony were deposited by ascending epithermal solutions. Current circulation of thermal water probably is dissolving the radioactive vein material and is unassociated with the primary emplacement and wallrock alteration that apparently took place before late Tertiary time.

The rough correlation between the concentration of silica and radioactivity (fig. 2), the absence of excessive radioactivity in hot springs from similar crysta line rock in Montana, and the local concentration radioactive minerals suggest that leaching of radioa tive material from fractured siliceous veins is t principal source of radioactivity in the thermal wate at Alhambra. If the radioactive elements were d rived from dissolution of chalcedonic vein deposi intercepted by the Alhambra fault or associated fra tures, at least part of the dissolved silica would derived from the same source. The silica geotherm meters then would confirm the association by Marine Presser, and Evans (1976) of Alhambra Hot Spring with reservoir temperatures less than 110°C.

CONCLUSIONS

1. High levels of radioactivity occur at Alhambr Hot Springs in the discharges from springs an flowing wells, in calcareous incrustations arou the springs, and in silicified zones and cha cedony veins in associated crystalline intrusiv rock. High levels of radioactivity are n characteristic of hot springs that issue fro fractured crystalline rock in Montana.
2. The thorium and uranium concentrations of t type of acid igneous rocks exposed near the h springs are higher than the average for t Boulder batholith. The predominance of thor um suggests that a toxic beta-emitting daughte radium-228, is present in the thermal water
3. Gross alpha and beta activities and the concentr tions of radium-226 in thermal waters fro springs and flowing wells exceed recommende maximum permissible levels of the U.S. Env ronmental Protection Agency (1976) for drin ing water. High concentrations of radon a dissolved in the water and mixed with oth gases at several sites.
4. In general, gross alpha and gross beta activiti determined by the Survey exceeded the valu reported for corresponding samples by t MDHES. Both laboratories verified anomalou ly high levels of radioactivity at the san sites, and the results were normally proportiona The discrepancies may be attributable to di ferences in calibration-isotope solutions an analytical procedures.
5. Fractures associated with the Alhambra fau appear to act as conduits for ascending therm waters that were heated by deep circulatio along a thermal gradient of about 21°C/km.
6. The chemical composition of the water rang from surface and shallow ground water of t calcium bicarbonate type to more highly radi

active thermal water of the sodium bicarbonate type with increasing temperature, concentrations of dissolved solids and silica, and sodium-adsorption-ratio.

7. Under atmospheric conditions some of the thermal waters are supersaturated with respect to calcium carbonate and carbon dioxide gas. Reactions of dissolved carbon dioxide with rocks in the subsurface probably have released the sodium and calcium ions and produced bicarbonate ion in the water.

8. Loss of carbon dioxide by ascending thermal waters caused deposition of radioactive travertine at the surface and probably in the subsurface.

9. Radium-226 is the source of radon-222 that is dissolved in the thermal water and discharged with other gases from several springs and wells. The radium-226 probably formed as a decay product of thorium-230 sorbed on fracture surfaces and coprecipitated with calcium carbonate.

10. Dissolution of radioactive chalcedony at depth probably accounts for most of the radioactivity and part of the dissolved silica in the thermal waters.

11. The reservoir temperature probably is less than 110°C, but could be as high as 160°C.

REFERENCES CITED

merican Public Health Association and others, 1976, Standard methods for the examination of water and wastewater [14th ed.]: New York, Am. Public Health Assoc., 1193 p.

merican Society for Testing and Materials, 1976, Annual book of ASTM standards, Part 31, Water: Philadelphia, Am. Soc. Testing Materials, 956 p.

rnorsson, Stefan, 1975, Application of the silica geothermometer in low temperature hydrothermal areas in Iceland: Am. Jour. Sci., v. 275, p. 763–784.

arker, F. B., and Robinson, B. P., 1963, Determination of beta activity in water: U.S. Geol. Survey Water-Supply Paper 1696–A, 32 p.

lackwell, D. D., and Robertson, E. C., 1973, Thermal studies of the Boulder batholith and vicinity, Montana: Soc. Econ. Geologists Guidebook, Butte Field Conf., p. D1–D8.

dwards, K. W., 1968, Isotopic analysis of uranium in natural waters by alpha spectrometry: U.S. Geol. Survey Water-Supply Paper 1696–F, 26 p.

ournier, R. O., and Rowe, J. J., 1966, Estimation of underground temperatures from the silica content of water from hot springs and wet steam wells: Am. Jour. Sci., v. 264, p. 685–697.

ournier, R. O., and Truesdell, A. H., 1974, Geochemical indicators of subsurface temperature—Part 2, Estimation of temperature and fraction of hot water mixed with cold water: U.S. Geol. Survey Jour. Research, v. 2, no. 3, p. 263–270.

Fournier, R. O., White, D. E., and Truesdell, A. H., 1974, Geochemical indicators of subsurface temperature—Part 1, Basic assumptions: U.S. Geol. Survey Jour. Research, v. 2, no. 3, p. 259–262.

Friedline, R. A., and Smith, R. B., 1974, Contemporary seismicity in the Helena, Montana region, *in* the Marysville, Montana, Geothermal Project Tech. Rept.: NSF–RANN Grant No. GI–389172, p. 75–94.

Gabelman, J. W., 1976, Expectations from uranium exploration: Am. Assoc. Petroleum Geologists Bull., v. 60, no. 11, p. 1993–2004.

Hursch, J. B., 1974, An argument against the use of the special curie for natural uranium and natural thorium: Health Physics, v. 27, p. 147–152.

Johnson, J. O., 1971, Determination of radium-228 in natural waters: U.S. Geol. Survey Water-Supply Paper 1696–G, p. 61–626.

Knopf, Adolph, 1963, Geology of the northern part of the Boulder batholith and adjacent areas, Montana: U.S. Geol. Survey Misc. Geol. Inv. Map I–381.

Lange, N. A., 1969, Handbook of chemistry: New York, McGraw-Hill Co., 2001 p.

Mariner, R. H., Presser, T. S., and Evans, W. C., 1976, Chemical characteristics of the major thermal springs of Montana: U.S. Geol. Survey Open-File Rept. 76–480, 31 p.

Ney, W. R., 1974, Specification of units for natural uranium and natural thorium; Statement of the National Council on Radiation Protection and Measurements: Health Physics, v. 27, p. 140.

O'Connell, M. F., and Kaufmann, R. F., 1976, Radioactivity associated with geothermal waters in the western United States: U.S. Environmental Protection Agency Office of Radiation Programs—LVF, ORP/LV–75–8A, 24 p.

Pinckney, D. M., 1965, Veins in the northern part of the Boulder batholith, Montana: Princeton Univ., Ph. D. dissert., 154 p.

Presser, T. S., and Barnes, Ivan, 1974, Special techniques for determining chemical properties of geothermal water: U.S. Geol. Survey Water-Resources Inv. 22–74, 11 p.

Roberts, W. A., and Gude, A. J., 1953, Uranium-bearing deposits west of Clancy, Jefferson County, Montana: U.S. Geol. Survey Bull. 988–F, p. 123–141.

Robertson, E. C., Fournier, R. O., and Strong, C. P., 1976, Hydrothermal activity in southwestern Montana: U.N. Symposium on The Development and Use of Geothermal Resources, 2d, Proc., v. 1, p. 553–561.

Scott, R. C., and Barker, F. B., 1962, Data on uranium and radium in ground water in the United States: U.S. Geol. Survey Prof. Paper 426, 115 p.

Smedes, H. W., 1966, Geology and igneous petrology of the northern Elkhorn Mountains, Jefferson and Broadwater Counties, Montana: U.S. Geol. Survey Prof. Paper 510, 116 p.

Smith, R. B., and Sbar, M. L., 1974, Contemporary tectonics and seismicity of the western United States with emphasis on the Intermountain Seismic Belt: Geol. Soc. America Bull., v. 85, no. 8, p. 1205–1218.

Stoker, A. K., and Kruger, P., 1975, Radon measurements in geothermal systems: Interdisciplinary research in engi-

neering and earth sciences: Stanford, Calif., Stanford Univ., Rept. SGP–TR–4, 116 p.

Thatcher, L. L., Janzer, V. J., and Edwards, K. W., 1977, Methods for determinations of radioactive substances in water and fluvial sediments: U.S. Geol. Survey Techniques Water-Resources Inv., book 5, chap. A5, 95 p.

Thurlow, E. E., and Reyner, M. L., 1952, Preliminary report on uranium-bearing deposits of the northern Boulder batholith region, Jefferson County, Montana: U.S. Atomic Energy Comm., 60 p.

Tilling, R. I., and Gottfried, David, 1969, Distribution of thorium, uranium, and potassium in igneous rocks of the Boulder batholith region, Montana, and its bearing on radiogenic heat production and heat flow: U.S. Geol. Survey Prof. Paper 614–E, 29 p.

U.S. Environmental Protection Agency, 1976, Interim pri mary drinking water regulations. Promulgation of regu lations on radionuclides: Federal Register, v. 41, no. 133 July 9, 1976, p. 28401–28409.

U.S. Salinity Laboratory Staff, 1954, Diagnosis and improve ment of saline and alkali soils: U.S. Dept. Agricultur Handb. 60, 160 p.

Wollenberg, H. A., 1975, Radioactivity of geothermal systems U.S. Energy Research and Devel. Adm. Rept. LBL 3232, 27 p.

Wright, H. D., Bieler, B. H., Shulhof, W. P., and Emerson D. O., 1954, Mineralogy of uranium-bearing deposits i the Boulder batholith, Montana: U.S. Atomic Energ Comm. Ann. Rept. RME–3095, Apr. 1, 1954, 80 p.

Jour. Research U.S. Geol. Survey
Vol. 6, No. 4, July–Aug. 1978, p. 541–545

DEFINITION OF REGIONAL RELATIONSHIPS BETWEEN DISSOLVED SOLIDS AND SPECIFIC CONDUCTANCE, SUSQUEHANNA RIVER BASIN, PENNSYLVANIA AND NEW YORK

By DAVID J. LYSTROM, FRANK A. RINELLA, and
WILLIAM D. KNOX, Portland, Oreg.

bstract.—This report presents statistical tests for assess- the accuracy and validity of two regional models of the tionship between dissolved-solids concentration and spe- conductance. These models are used to estimate dissolved- ds concentrations based on specific-conductance measure- nts. The two regional models are compared with station dels for 27 stream sites in the Susquehanna River basin. average standard errors of estimate of two regional dels, when used to estimate dissolved-solids concentrations the 27 stream sites, are 10.7 and 10.6 percent. In compari- , the station models have average standard errors of 9.0 9.3 percent, respectively. Results of the statistical tests icate that in the Susquehanna River basin the regional dels can be used to estimate dissolved-solids concentrations n specific-conductance data for sites for which chemical lyses are not available.

Specific conductance is often used as an indicator of tain aspects of water quality (Steele and Matalas, 74; Singh and Kalra, 1975). The major dissolved rganic constituents in water can be related to spe- c conductance by use of linear regression. (See for mple, Steele, 1968, 1972, 1976; Hawkinson and ele, 1975; Blakey and others, 1972.) During com- ation of water-quality data for a regional study of eam water in the Susquehanna River basin in Penn- vania and New York, it was found that dissolved- ids concentrations can be estimated from specific ductance with acceptable accuracy by using re- ssion relationships. This report presents two site- cific regression relationships (station models) for h of the 27 stream sites and two regional regression tionships (regional models). Regional models apply ll streams in the Susquehanna River basin. Criteria established for statistical tests used to determine he regional models are significantly different from tion models. The accuracy of each model is sum- rized to indicate expected errors.

Although the method was developed for use with ilable data, experience with it has shown that re- nal or station models would also be useful in the design of data-collection networks. Specific conductance is considerably less costly to obtain than the corresponding dissolved-solids concentration. This statistical method provides an effective means of evaluating the trade-off of reduced costs versus loss of accuracy in estimating dissolved solids indirectly from specific conductance rather than determining it directly from field samples by laboratory analysis.

BASIN SETTING

The Susquehanna River empties into the Chesapeake Bay and drains the largest basin (71 250 km²) along the east coast of the United States. About three-quarters of the basin is in Pennsylvania and one-quarter in New York. The Susquehanna River basin spans four physiographic provinces (see fig. 1), the (1) Appalachian Plateaus, (2) Valley and Ridge, (3) Blue Ridge, and (4) Piedmont provinces (Fenneman, 1928). The northeast part of the Appalachian Plateaus is characterized by well-rounded hills and flat valleys resulting from continental glaciation. The unglaciated southwest part of the Appalachian Plateaus is characterized by flat-topped mountains having deeply incised stream valleys. The Valley and Ridge province is characterized by steep parallel mountains and ridges separated by valleys. Only a very small part of the mountainous Blue Ridge province lies within the Susquehanna River basin. The Piedmont province contains terrain that is gently rolling to hilly.

The climate in the Susquehanna River basin is moderate. Average annual precipitation ranges from 810 mm in the northwestern part of the basin to 1120 mm in the southern and east-central parts, with a basin average of approximately 1020 mm. About 50 percent of the precipitation over the Susquehanna River basin appears in the stream as runoff. Large losses occur during the hot summer months due to evaporation and transpiration.

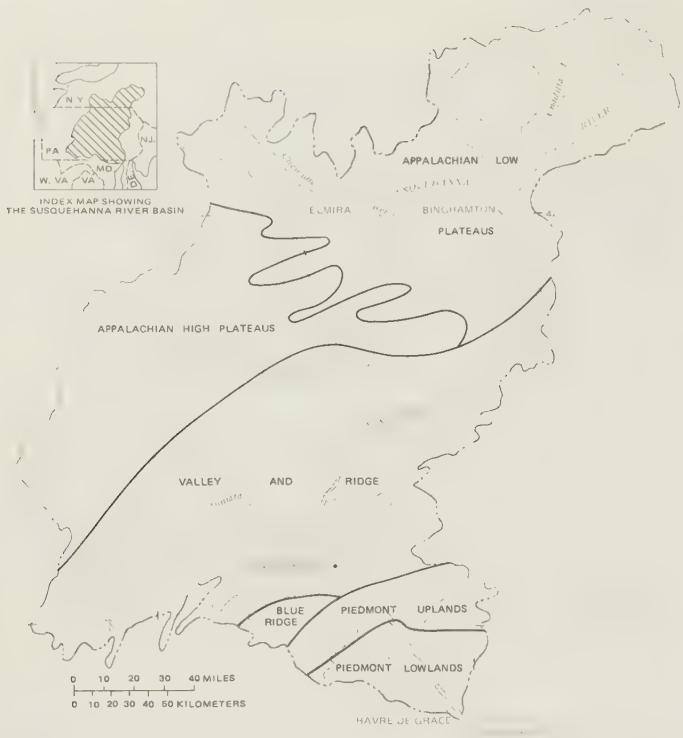

FIGURE 1.—Physiographic provinces of the Susquehanna River basin (Fenneman, 1928).

The chemical character of tributaries of the Susquehanna basin is influenced by three major factors: (1) streamflow, (2) geology and ground water, and (3) land-use practices.

The highest dissolved-solids concentrations occur during periods of base flow due to the effects of ground-water inflow, evaporation, and coal-mine drainage. As streamflow increases, the dissolved-solids concentration is lowered by dilution from direct runoff (Anderson, 1963). Stream water quality is influenced by the wide variety of geologic formations. The geology of the basin is characterized predominantly by sandstone and shale, glacial outwash, limestone and dolomite, coal, and some metamorphic rock. Streams receiving water drained from the coal fields in the eastern and western parts of the basin have low pH and high concentrations of iron, sulfate and free sulfuric acid. Farm cultivation, urbanization, and industrialization in the Susquehanna River basin also influence the chemical character and quality of the surface water.

APPROACH

The approach used in this study is intended to establish the accuracy and utility of site-specific and regional relationships between dissolved solids a specific conductance. Analysis of variance is used determine the significance of differences between t types of linear-regression relationships (models) a between regional and site-specific (station) models

Station models

Plots of available dissolved-solids concentrati versus specific conductance for 27 stream stations (

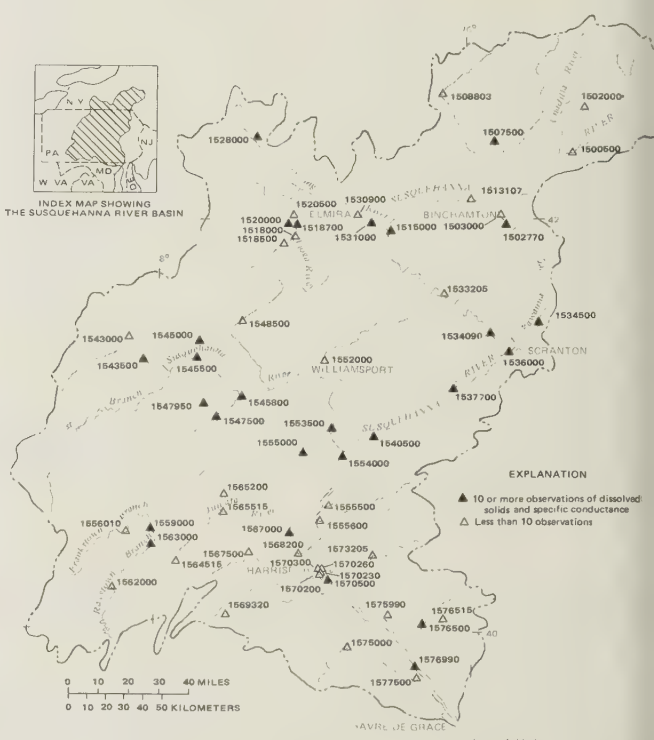

FIGURE 2.—Location of stream-sampling sites for which d solved-solids concentration and corresponding value specific conductance are available.

locations in figure 2) in the Susquehanna River bas show that linear-regression models fit the data ve well. Correlation coefficients of these relationshi commonly exceed 0.97, and data points are random distributed about the regression line. Station mod are based on a minimum of 10 data points duri water years 1965–76. This period was selected as o in which land use was relatively stable. Figure represents a typical station plot for the Lackawan River at Old Forge, Pa.

The two linear models shown in figure 3 are defin by the following linear regression equations:

$$Y = a + b\,X \qquad (1)$$

$$Y = (\overline{Y}/\overline{X})X \qquad (2)$$

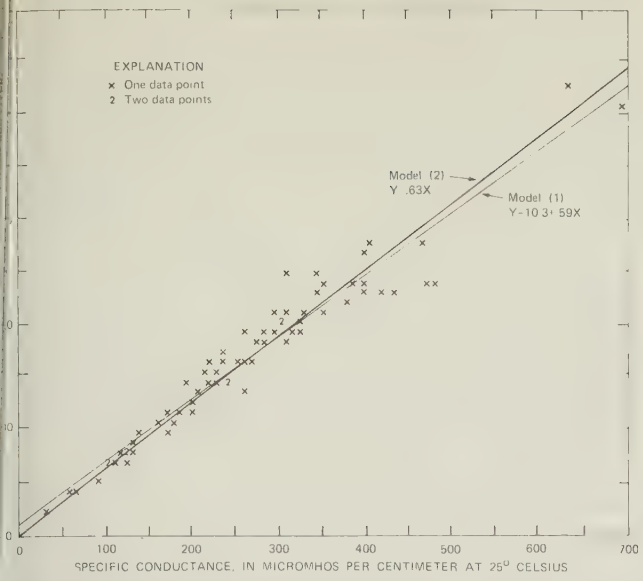

GURE 3.—Station plot of dissolved-solids concentration versus specific conductance for water years 1965–76, Lackawanna River at Old Forge, Pa. (1 micromho = 1 microsiemens.)

here Y represents dissolved-solids concentrations, X specific conductance, a and b are least squares linear gression constants, $\overline{Y}$ is the mean dissolved-solids ncentration, and $\overline{X}$ is the mean specific conductance. he basic difference between these two models is that odel 2 has a Y intercept of zero. Theoretically, the term in model 1 will approach zero as specific conctance approaches zero. However, the ranges of ecific conductance in streams rarely approach zero. herefore, the a term is included in model 1 to provide regression line that will fit the upper ranges of a nlinear relationship more accurately. (See Steele, 71).

A standard analysis-of-variance test (Mendenhall, 71) was used for each station to determine if the o models are statistically different. In this test the riance, V_1, of the data about model 1 is divided by e variance, V_2, about model 2. Variance is defined by

$$V_1 = \sum_{1}^{N} \frac{(Y_o - Y_c)^2}{N - 2} \tag{3}$$

d

$$V_2 = \sum_{1}^{N} \frac{(Y_o - Y_c)^2}{N - 1} \tag{4}$$

ere Y_o is the observed dissolved-solids concentran, Y_c is the corresponding dissolved-solids concentration computed by model 1 or 2, and N is the number of data points. The ratio of variances is compared to values in a standard F distribution (Afifi and Azen, 1972, app. II, table 6) for a specified percentile of significance. The results of the analysis-of-variance test (Anova) for all 27 stations indicate that there is no difference between models 1 and 2 at the 95-percent level of significance. The results of the Anova test also indicate that the constant a in model 1 does not differ significantly from zero. The average standard errors of estimate for all 27 stations are 9.0 and 9.3 percent for models 1 and 2, respectively. Both models therefore produce statistically similar results.

Regional models

Two regional models for the Susquehanna River basin were developed from 1441 paired values of dissolved-solids concentration and specific conductance for 59 stations (locations shown in fig 2) during water years 1965–76. These data are plotted in figure 4.

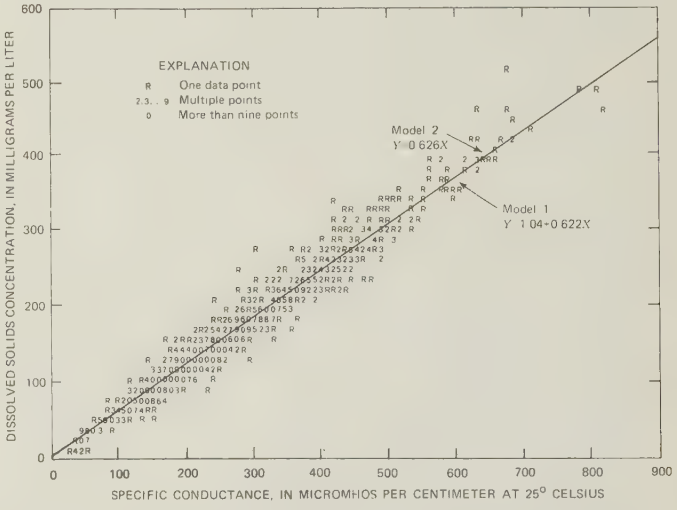

FIGURE 4.—Regional plot of dissolved-solids concentration versus specific conductance for water years 1965–76, Susquehanna River basin (1 micromho = 1 microsiemens.)

Fitting model 1 to the regional data by least-squares regression results in the equation

$$Y = 1.04 + 0.622X, \tag{5}$$

and fitting model 2 to the same data results in the equation

$$Y = 0.626X, \tag{6}$$

where Y is dissolved-solids concentration and X is specific conductance. The standard error of estimate of

both equations 5 and 6 is ±16.6 mg/L or ±10.5 percent of the mean dissolved-solids concentration.

As shown in figure 4, equations 5 and 6 are nearly equivalent. The analysis of variance of the pooled data about equations 5 and 6 indicates that there is no significant difference at the 95-percent level. Although either equation could be used, equation 6 is more easily computed.

REGIONAL MODELS COMPARED WITH STATION MODELS

The regional models are intended to estimate dissolved-solids concentration from specific conductance at stream sites where dissolved-solids data are not available. It is therefore desirable to assess the accuracy of the regional models (eqs 5 or 6) compared with station models.

The Anova test was applied for each of 27 sets of station data to evaluate whether the regional models differ significantly from the station models. It was found, using model 1, that five station models were different from the regional model at the 95-percent level of significance. A similar test for model 2 r vealed four significant differences among the 27 se of data. These results indicate that about 17 perce of the station models differ significantly from t regional models. If all data were drawn hypothetical from the same population, only 5 percent of the st tion models would be expected to be different from t regional model at the 95-percent level of significanc

The Anova test implies that errors resulting fro use of a regional model at some stations would be si nificantly greater than the errors resulting from t station models. To evaluate these errors, table 1 lis the standard errors of estimate of the station mode and the standard errors of estimate resulting fro applying two regional models (eqs 5 and 6) at eac station. The standard errors for the station mode and regional models are comparable. The average standard errors of estimate for station models 1 or is only about 1.5 percent lower than the average f the regional models. Differences between the statio and regional models that are significant at the 9 percent level are footnoted in table 1.

TABLE 1.—*Regression constants and standard errors of estimate for station and regional models*

Station number	Station name	Number of data points	Range of observed specific conductance[1]		Model 1 $Y = a + bX$				Model 2 $Y = (\bar{Y}/\bar{X})X$		
					Station model		Standard error of estimate in percent of mean dissolved solids		Station model	Standard error of estimate in percent of mea dissolved solids	
			Min	Max	a	b	Station model	Regional model[2]	$\bar{X}/\bar{Y}$	Station model	Regiona model[3]
1502770	Susquehanna River near Great Bend, N.Y.	34	71	214	11.3	.49	9.2	[4]16.1	.56	9.5	[4]15.6
1507500	Genegantslet Creek at Smithville Flats, N.Y.	29	45	101	15.0	.42	9.4	11.6	.65	11.7	11.9
1515050	Susquehanna River at Sayre, Pa.	18	82	266	- 3.3	.59	11.6	15.1	.58	11.3	14.4
1518700	Tioga River at Tioga Junction, Pa.	10	98	395	- 6.1	.67	7.1	8.0	.64	6.9	7.4
1520000	Cowanesque River near Lawrenceville, Pa.	19	120	834	15.5	.54	5.6	[4]13.3	.58	6.8	[4]13.4
1528000	Fivemile Creek near Kanona, N.Y.	38	116	362	7.3	.57	6.1	[4] 8.5	.60	6.2	[4] 8.5
1531000	Chemung River at Chemung, N.Y.	21	117	427	- 1.9	.62	8.6	8.9	.61	8.4	8.7
1534090	Susquehanna River at Falls, Pa.	14	99	334	10.2	.53	9.5	13.8	.59	10.0	13.3
1534500	Lackawanna River at Archbald, Pa.	51	164	691	-11.6	.72	7.7	[4]12.5	.68	7.9	[4]12.1
1536000	Lackawanna Tiver at Old Forge, Pa.	68	33	695	10.3	.59	11.1	11.3	.63	11.4	11.3
1537700	Susquehanna River near Hunlock Creek, Pa.	71	100	625	- 5.2	.65	12.6	12.8	.64	12.6	12.7
1540500	Susquehanna River at Danville, Pa.	125	110	821	-15.8	.71	10.4	[4]12.7	.65	11.2	12.5
1543500	Sinnemahoning Creek at Sinnemahoning, Pa.	47	68	506	7.7	.57	11.0	12.3	.61	11.4	12.3
1545500	West Branch Susquehanna River at Renovo, Pa.	45	193	676	- 7.1	.63	6.0	6.5	.61	6.1	6.5
1545600	Young Woman's Creek near Renovo, Pa.	89	25	56	15.8	.31	18.7	20.9	.69	20.2	22.0
1545800	West Branch Susquehanna River at Lock Haven, Pa.	72	149	914	- 3.4	.63	5.4	5.6	.62	5.5	5.6
1547500	Bald Eagle Creek at Blanchard, Pa.	29	142	396	16.8	.56	8.2	8.5	.62	8.3	8.4
1547950	Beech Creek at Monument, Pa.	44	123	519	- 6.5	.65	8.1	8.4	.62	8.2	8.2
1553500	West Branch Susquehanna River at Lewisburg, Pa.	71	99	523	1.0	.65	12.6	13.4	.65	12.6	13.3
1554000	Susquehanna River at Sunbury, Pa.	60	80	457	- 4.4	.65	13.8	13.9	.63	13.7	13.7
1555000	Penns Creek at Penns Creek, Pa.	27	122	233	14.2	.52	6.8	8.5	.60	7.0	8.3
1559000	Juniata River at Huntingdon, Pa.	56	177	563	9.4	.58	5.1	6.2	.61	5.3	6.3
1563000	Raystown Branch Juniata River near Huntingdon, Pa.	48	119	357	5.5	.61	6.9	7.0	.63	6.9	6.9
1567000	Juniata River at Newport, Pa.	65	135	606	13.6	.58	7.2	7.8	.62	7.7	7.8
1570500	Susquehanna River at Harrisburg, Pa.	119	115	460	- 1.6	.63	11.5	11.5	.62	11.4	11.5
1576500	Conestoga River at Lancaster, Pa.	50	305	478	33.9	.54	5.4	5.6	.62	5.5	5.6
1576990	Susquehanna River at Holtwood, Pa.	13	160	498	- 4.4	.65	8.4	8.7	.63	8.1	8.3
Averages values		----	----	----	-----	-----	9.0	10.7	.62	9.3	10.6

[1] Microsiemens per centimeter at 25°C.
[2] $Y=1.04+0.622X$ (eq 5).
[3] $Y=0.626X$ (eq 6).
[4] Regional model significantly different from station model at the 95-percent level.

should be noted that the errors resulting from onal models may produce a bias. That is, a re-al model may tend to overestimate or underesti-e the concentration of dissolved solids for a spe- site. The occurrence of bias is more likely at sites re a regional model differs significantly from a ion model.

CONCLUSIONS

he results of the Anova tests and a comparison of dard errors in table 1 indicate that station models nd 2 will yield comparable results for the Susque-na River basin. Regional models defined by equa-s 5 and 6 can also be considered equivalent to n other.

t was also found by use of the Anova test that the rs resulting from use of the regional models were ificantly greater than for station models for about ercent of the stations. It is therefore recommended t station models should be used where adequate a are available. The accuracy of station models be judged from computation of standard errors of mate as shown in table 1.

t places where specific conductance has been mea-d but dissolved-solids data are not available, the onal models (eqs 5 or 6) can be used to estimate olved-solids concentration from specific conduc-ce. The magnitude of errors shown in table 1 for regional models was found acceptable for estimat- dissolved solids in a regional water-quality anal-.

DISCUSSION

he results of this study are applicable primarily he Susquehanna River basin and possibly to simi- adjacent stream basins. The methodology, however, be applied to any river basin or study region.

tation models (model 1) shown in table 1, were l to estimate additional dissolved-solids concentra-s for 14 stream stations in a regional water-quality y of the Susquehanna River basin. The regional el (eq 5) was used for an additional 10 stations. se estimates of dissolved-solids values were essen- to provide adequate data for relating the occur-ce of dissolved solids to land use and other physical racteristics of drainage basins.

The computer program used in this study to plot data and to compute the regression constants, standard errors of estimates, and ratios of variance is available in Fortran IV language adapted to a CDC 6600 computer system. The data input to the program is a magnetic tape compiled from the U.S. Geological Survey's water-quality computer files and retrieval system (Wanda C. Meeks, written commun., 1974).

REFERENCES CITED

Afifi, A. A., and Azen, S. P., 1972, Statistical analysis: A computer oriented approach: New York, Academic Press, Inc., 366 p.

Anderson, P. W., 1963, Variations in the chemical character of the Susquehanna River at Harrisburg, Pennsylvania: U.S. Geol. Survey Water-Supply Paper 1779–B, 17 p.

Blakey, J. F., Hawkinson, R. O., and Steele, T. D., 1972, An evaluation of water-quality records for Texas streams: U.S. Geol. Survey open-file rept. 54 p.

Fenneman, N. M., 1928, Physiographic divisions of the United States [3d ed.]: Assoc. Am. Geographers Annals, v. 18, no. 4, p. 261–353.

Hawkinson, R. O., and Steele, T. D., 1975, Regression analysis and regionalization of water-quality characteristics of major streams in the United States [abs.]: Internat. Assoc. Geochem. and Cosmochem.–Internat. Assoc. Hydrol. Sci., International Symposium on the geochemistry of natural waters, Burlington, Ontario, Canada, 1975, p. 25.

Mendenhall, William, 1971, Introduction to probability and statistics: Belmont, Calif., Duxbury Press, 466 p.

Singh, Teja, and Kalra, Y.P., 1975, Specific conductance methods for in situ estimation of total dissolved solids: Am. Water Works Assoc. Jour., v. 67, no. 1, p. 99–100.

Steele, T. D., 1968, Digital-computer applications in chemical-quality studies of surface water in a small watershed *in* The use of analog and digital computers in hydrology, volume 1 *of* Proceedings of the IASH–UNESCO Symposium at Tucson, Ariz., in December 1968: Internat. Assoc. Sci. Hydrology Pub. 80, p. 203–214.

——— 1971, A study of the chemical quality of streamflow in Arkansas: U.S. Geol. Survey open-file rept., 40 p.

——— 1972, The SYSLAB system for data analysis of historical water-quality records: U.S. Dept. Commerce, Natl. Tech. Inf. Service, PB–222 777, 41 p.

——— 1976, A bivariate-regression model for estimating chemical composition of streamflow or ground water: Internat. Assoc. Hydrol. Sci. Bull., v. 11, no. 1, p. 149–161.

Steele, T. D., and Matalas, N. C., 1974, Principal-component analysis of stream-flow chemical quality data *in* Mathematical models on hydrology, volume 1 *of* Proceedings of the Symposium at Warsaw in July 1971: Internat. Assoc. Hydrol. Sci. Pub. 100, p. 355–363.

Jour. Research U.S. Geol. Survey
Vol. 6, No. 4, July–Aug. 1978, p. 547–552

PRELIMINARY EVALUATION OF THE FLOATING DOME METHOD OF MEASURING REAERATION RATES

By DOYLE W. STEPHENS, NSTL Station, Miss.

stract.—The floating dome method of measuring reaera- rates was evaluated using a modified tracer technique a disturbed equilibrium technique. The lack of agreement een results of the floating dome method and the other ods was attributed to limitations in instrument accuracy ified by physical relationships of the dome to the water nn rather than conceptual errors in the dome method. In niques where polarographic oxygen probes are used to tor the oxygen content within the dome atmosphere, the of volume of the dome to volume of the water column r the dome must be kept below 0.02 to minimize instru- error to less than 10 percent of the predicted oxygen sport. The combination of instrument limitations, coupled environmental limitations caused by wind and the green- e effects, severely restrict application of the floating e method.

opeland and Duffer (1964) introduced the float- dome method of measuring gaseous diffusion rates vater as an improvement of the gasometric tent nique developed and used in England (Gameson Barrett, 1958). The dome method consists of float- a rigid dome enclosure on the water surface to te a small area through which gaseous exchange the atmosphere in the dome occurs. The oxygen ent of the vapor phase in the dome and in the water nonitored over a suitable time period, and the de- se in oxygen content of the vapor phase in the e is related to the increase in oxygen content of water to provide an estimate of the reaeration rate. water must be undersaturated with oxygen at the ation of the measurement period and must not ex- saturation during the measurement interval. The hod assumes that the gas-transfer coefficient within enclosure is equivalent to the transfer coefficient he open water. This assumption has been reported d only for still or gently circulating waters (Welch,). Furthermore, Gameson and Barrett (1958) re- ed that the tent enclosure causes underestimations eaeration rates when waves approaching a height cm are present. Owens (1965) stated that despite restriction of turbulence within the enclosure, com- ative experiments using enclosures and other nods yield similar results, but no specific references were cited. Sugiura and others (1963) found that the reaeration rate is primarily determined by turbulence in the water, not the air phase; hence, the dome should not influence the estimate. Conversely, Zogorski and Faust (1973) believed the dome distorts the gas-transfer rate by interfering with wind and wave action beneath it.

There are several other environmental limitations to the use of the dome method. The greenhouse effect was recognized by Copeland and Duffer (1964) in their original paper, and several attempts to use the dome on a windswept estuary failed owing to dome movement across the water surface (R. L. Cory, oral commun., 1976).

Hall (1971) introduced a modification of the dome procedure based on the measurement of the diffusion of gaseous oxygen into a floating dome filled with nitrogen. This technique has been used successfully by researchers at the Chesapeake Biological Laboratory in Maryland (W. R. Boynton and W. M. Kemp, written commun., 1977).

The floating dome method of Copeland and Duffer (1964) has been cited numerous times in the literature as a direct method of measuring reaeration rates in natural waters, but it has been actually employed in only a few instances (Duffer and Dorris, 1966; Hannan and Dorris, 1970). Juliano (1969) attempted to use the dome to measure reaeration in an estuary but found that the available instrumentation was not suited to monitoring oxygen charges within the dome. Hannan and Dorris (1970) reported that the dome method yielded results comparable with those calculated using the equation of Odum and Hoskin (1958). Aside from occasional comparisons of the dome method with predictive equations, there has been little evaluation of the dome method due to the lack of suitable comparative techniques of measuring reaeration rates. With the advent of tracer methodology (Tsivoglou and others, 1965; Rathbun and others, 1975), it has become possible to evaluate older methods of measuring reaeration coefficients.

METHODS

A modification (Rathbun and others, 1975) of the radioactive tracer technique of Tsivoglou and others (1965; 1968) was used to measure the reaeration coefficient in a continuously mixed tank while simultaneously measuring the reaeration coefficient using both the floating dome (Copeland and Duffer, 1964) and the disturbed equilibrium methods (Gameson and Truesdale, 1959). The tracer technique is based on the observation that the ratio of the rate coefficient of a gas desorbing from water under mixed conditions to the rate coefficient for oxygen being absorbed by the same water is a constant, regardless of mixing conditions. The procedure consists of dissolving a quantity of tracer gas into the water and measuring its desorption with time. The desorption coefficient of the tracer gas is then converted to a reaeration coefficient by means of a constant determined from laboratory experimentation. The modified tracer technique uses ethylene and propane as the tracer gases in place of the more hazardous krypton-85. The disturbed equilibrium method (Gameson and Truesdale, 1959) consists of reducing the dissolved-oxygen content of the water to a level below saturation and monitoring the oxygen recovery of the water.

Four experiments were conducted utilizing two different dome designs and two different test tanks. Two experiments were run in the laboratory, and two outdoors. Tap water was used in all experiments.

The two experiments run in the laboratory, Lab. 1 and Lab. 2, March 23 and 31, 1976, respectively, used a fiberglass tank with a diameter of 0.75 m and a water depth of 0.31 m. The plexiglass dome used in these experiments was rectangular with a pitched roof and a volume of 32.52 L and covered a surface area of 0.121 m^2. It was supported by a 0.06-m-wide wood frame around the base. A wire support held a dissolved-oxygen probe (Yellow Springs Instrument Co., Model 54) and a temperature probe (Enviro-Labs, Model IS–102) in the air space within the dome. A second pair of oxygen and temperature probes were placed in the water below the dome. The output signals from the oxygen and temperature probes were multiplexed (EnviroLabs, Model SC 210–2) and punched at 30-minute intervals onto a 16-channel paper tape using an analog-digital recorder (Fischer and Porter Co., type 1542). The probe used to measure oxygen within the dome was calibrated in fresh air to an arbitrary midscale value representing 100-percent saturation. Subsequent readings were related to this value. The oxygen probe used in the water was calibrated using micro-Winkler titrations of the tank water (Carpenter, 1965; Carritt and Carpenter, 1966). Oxyg saturation values were calculated according to We (1970) and corrected for barometric pressure.

The procedure for initiating an experiment consis of stripping the oxygen from the tank water us nitrogen gas and a porous diffuser until the dissolv oxygen content of the water was about 48 perc saturation. The dome, containing its sensors, was th floated on the water surface, and the subsurface oxyg and temperature sensors were added. Water satura with ethylene and propane was added to give init concentrations of approximately 10 micrograms liter in the tank. A laboratory stirring impeller si ated 0.14 m below the water surface and running 1900 revolutions per minute was then started and until completion of the experiment.

Two experiments were run outdoors, Outdoor 1 July 8 and Outdoor 2 on November 11, 1976, in an o stainless-steel tank measuring 6.1 m long, 1.2 m wi and 1.8 m deep. The experiments were conducted w a water depth of about 1 m. A high-velocity pump v employed at one end of the tank to provide const circulation. A plastic tarpaulin shielded the part the tank where the dome and instrumentation w located. The instrumentation and procedures for large-tank experiments were similar to those used the small-tank experiments. The dome used in large tank consisted of the bottom part of a se hemispherical plastic dessicator (Nalge Co.) moun on a polyfoam frame. The dome had a radius of 0.1 and a volume of 4.96 L and covered an area of 0.053 m

Water samples were collected at 30-minute interv for ethylene and propane analysis and samples micro-Winkler determinations of oxygen were usua taken every hour. Micro-Winkler titrations were u as a comparative backup for the oxygen probe. Wa samples for hydrocarbon analysis were either sipho from the tanks allowing the sample bottle to fl once or collected using a self-flushing submersi sampler. Analysis for dissolved hydrocarbons done using a gas chromatograph with a flame ioni tion detector in conjunction with a stripping cham and cold trap apparatus (Shultz and others, 197 The desorption coefficient for each of the hydrocar gases was calculated using the equation

$$K_H = \frac{\log_e (C_I/C_F)}{\Delta T},$$

where K_H is the desorption coefficient in recipr hours;

C_F is the final concentration of the hyd carbon gas;

C_I is the initial concentration of the hydrocarbon gas; and

ΔT is the time period in hours.

practice, the log (base e) of the individual hydrocon concentrations is plotted with time, and a least-res fit is made through these points. The slope of line is the desorption coefficient, K_H. The desorpcoefficient for each hydrocarbon gas is then red to the reaeration coefficient, K_2, for oxygen by

$$K_2 = \frac{K_H}{1/R}, \quad (2)$$

re R is the ratio of the laboratory determined detion coefficient of the hydrocarbon gas to the abtion coefficient for oxygen as determined in stirred calibration studies (R. E. Rathburn, oral com., 1977). Oxygen diffusion rates were calculated g R values of 1.15 for the ratio K_O:K_E and 1.39 the ratio K_O:K_P, where K_E is the desorption coient for ethylene, K_P is the desorption coefficient propane, and K_O is the absorption coefficient for gen. The calculation of gas-transfer coefficients sured by the floating dome method was, according Slack and others (1973), adapted from Copeland Duffer (1964).

he reaeration coefficient, in reciprocal hours, was verted to a gas-transfer rate using the following ation:

$$k = K_2 \ (C_S - C), \quad (3)$$

re k is the gas-transfer rate in grams per cubic meter per hour at a 100-percent saturation deficit;

K_2 is the reaeration coefficient, in reciprocal hours, calculated from hydrocarbon data;

C_S is the average 100-percent saturation, in grams per cubic meter, possible during the experiment for water temperature encountered; and

C is set at zero to reflect a 100-percent saturation deficit.

eaeration coefficients for the disturbed equilibrium hod were calculated using the equation

$$K_2 = \frac{\log_e \frac{C_{s,I} - C_I}{C_{s,F} - C_F}}{\Delta T}, \quad (4)$$

re K_2 is the reaeration coefficient in reciprocal hours;

$C_{s,F}$ is the final dissolved-oxygen saturation value;

$C_{s,I}$ is the initial dissolved-oxygen saturation value;

C_F is the final dissolved-oxygen concentration;

C_I is the initial dissolved-oxygen concentration; and

ΔT is the time period in hours.

The reaeration coefficient was then converted to a gas-transfer rate using equation 3.

RESULTS

Oxygen diffusion rates, in the two experimental tanks, measured using the floating dome method, the disturbed equilibrium method, and the hydrocarbon tracer method are presented in table 1. Predicted oxygen diffusion rates using the hydrocarbon tracer method are a maximum of 10 percent greater than the rate predicted by the disturbed equilibrium method for the Lab. 2 experiment. Rates predicted for the Outdoor 1 experiment using the hydrocarbon tracers range from 3 percent greater to 25 percent less than the rate predicted by the disturbed equilibrium method. There is less agreement between the hydrocarbon method and the disturbed equilibrium method for the remainder of the experiments. This variation is probably due to the lack of sampling for hydrocarbons and micro-Winkler titrations during nighttime periods. Most experiments were initiated in late morning and terminated early the next morning. This resulted in a reduced number of samples representing terminal hours of the experiment. Any analytical errors on these sam-

TABLE 1.—*Summary of oxygen diffusion rates predicted by the hydrocarbon tracer method, disturbed equilibrium method, and floating dome method*

Experiment	Time interval (h)	Predicted oxygen diffusion rate, in grams per cubic meter per hour, at a 100-percent saturation deficit			
		Hydrocarbon tracer method		Disturbed equilibrium method	Floating dome method
		Propane	Ethylene		
Dome volume, 32.52 L					
Lab. 1	Initial 6	(1)	(1)	1.14	5.05
	Total 19	(1)	(1)	1.48	5.30
Lab. 2	Initial 6	1.07	1.09	1.10	7.16
	Total 21.5	1.04	1.13	1.03	4.46
Dome volume, 4.96 L					
Outdoor 1	Initial 5	0.60	0.82	1.11	1.33
	Total 20	.59	.81	.79	.36
Outdoor 2	Initial 5	1.64	2.82	2.07	1.64
	Initial 8	---	---	1.73	1.37
Outdoor 2	Total 23.5	1.85	2.52	0.68	(2)

[1] Not used.
[2] Dome returned to a 100-percent saturation value 10 hours after experiment initiated.

ples would then assume greater significance in the calculation of reaeration rates.

There was poor agreement between oxygen diffusion rates measured using the floating dome method and the other methods for the first two experiments. In both of these experiments, a large-volume dome (32.52 L) was used over a small volume of water (49.6 L). With this condition, small errors in the determination of oxygen within the dome are translated into large errors in the predicted reaeration rate. A smaller dome (4.96 L) used over 49.8 L of water in the next series of experiments provided results more comparable with the range observed using the disturbed equilibrium and tracer methods (table 1).

Inherent in the dome method is the need to accurately measure the decrease in gaseous oxygen content within the dome atmosphere while simultaneously measuring the increase in dissolved oxygen within the water. Measured changes in the percent oxygen content in the dome atmosphere are used to calculate the total quantity of oxygen which diffused from the dome atmosphere into the water column. The problems in applying the dome method then involve accurately measuring the oxygen content within the dome atmosphere and minimizing the effect of instrument error in the calculation of the observed oxygen transported from the dome.

There are three sources of error in the use of a polarographic oxygen meter: Instrument component limitations, such as nonlinearity; oxygen sensor limitations, such as nonlinearity and membrane differences; and environmental variables, such as barometric pressure and relative humidity.

The manufacturer (Yellow Springs Instrument Co.) states that for the Model 54 system with all errors additive, the maximum error at 20°C would be ±0.59 ppm (parts per million) when using the meter scale of 0 to 10. The probability of all errors being additive is small; hence, the error accumulation is believed to be one-half of the maximum. The errors for the 0 to 20 scale would be about double those at the 0 to 10 scale.

There is little the user can do to eliminate errors due to instrument component limitations and limitations of the oxygen sensor. If care is given to the calibration and the use of the system, errors due to altitude, barometric pressure, and relative humidity can be eliminated and, according to the manufacturer, maximum error becomes ±0.32 ppm when using the meter scale of 0 to 10.

The effects of errors due to maximum instrument tolerances of ±0.3 and ±0.6 ppm were calculated using a hypothetical model based on previous experiments with the reaeration methods investigated. Model conditions consisted of a final oxygen saturation of 8.24 mg/L (milligrams per liter) at 25°C, initial dissolved oxygen deficit of 4.24 mg/L, barometric pressure of 101.3 kP2, and a water column volume of 50 L below the dome. Under these conditions, 162 milliliters of oxygen must be transported into the 50-L water column before saturation at 8.24 mg/L is reached. Calculations based on the two domes used in this study (volumes of 4.96 and 32.52 L) were included (table 2). It is evident that estimates made using a small-volume dome on deep water will be less affected by instrument errors than those using a large dome on shallow water. In general, the ratio of total dome volume to volume of the water column below the dome must be less than 0.021 if the maximum instrument error is to be less than 10 percent of the observed oxygen change within the dome atmosphere. The application of this principle to use of a dome containing 32.52 L, like the large dome used in this study, under conditions of the model indicated that the water depth below the dome be a minimum of 11 m.

Comparison of mean rates for oxygen diffusion measured using the hydrocarbon tracer and the disturbed equilibrium methods with those measured using the dome (table 3) illustrates the considerable overestimation of rates by the dome for Lab. 1 and Lab. 2 experiments and the first part of Outdoor 1. The two outdoor experiments were run using a dome with a volume of 4.96 L which reduced the effect of the maximum meter error and partially improved the agreement between

TABLE 2.—*Relationship of dome size and water column volume to observed changes in oxygen meter readings for model conditions*

Area of dome (m^2)	Total dome volume (L)	Ratio of volumes—dome to water column	Water depth to satisfy model condition (m)	Observed change in oxygen meter to satisfy model conditions (ppm)	Error as percentage of observed change, assuming meter error of—	
					0.3 ppm	0.6 ppm
Circular:						
0.020	1.072	0.0214	2.49	7.2	4	8
.031	2.094	.0419	1.59	3.7	8	16
.053	4.96	.0992	.94	1.6	19	38
Rectanguar:						
0.121	32.52	.6504	.41	.24	125	250

TABLE 3.—*Comparison of mean oxygen diffusion rates measured using ethylene and propane tracer gases and the disturbed equilibrium method with diffusion rates measured using the floating dome method*

Experiment	Mean for tracers and disturbed equilibrium, in $(g/m^3)/h$	Range	Dome-measured rates, in $(g/m^3)/h$	Dome rate as the percentage of mean
Lab. 1 ----	1.14	--------	5.05	443
	1.48	--------	5.30	358
Lab. 2 ----	1.09	1.07–1.10	7.16	657
	1.07	1.03–1.13	4.46	417
Outdoor 1 _	.84	0.6 –1.11	1.33	158
	.73	.59–0.81	.36	49
Outdoor 2 _	2.18	1.64–2.82	1.64	75
	1.73	--------	1.37	79

the dome-measured reaeration rates and those of the hydrocarbon tracer and the disturbed equilibrium methods.

An attempt was made to calculate reaeration coefficients (K_2 of eqs 2 and 3) on an hourly basis from results of both domes. The large dome predicted a total transport of oxygen in excess of that necessary to saturate the water for the initial hour of the two laboratory experiments. Prediction of hourly rate coefficients gave more reasonable results when the 4.96 L dome was used.

Relative humidity and temperature were noted to have considerable influence on the oxygen meter and the probe performance. The probe used within the dome atmosphere was air calibrated at ambient relative humidity to a midscale value of 10 (0–20 scale) and was then placed inside the dome where the humidity reached 100 percent. As the probe was designed to be calibrated and operated at 100-percent humidity, any departure from that value results in an error in measurement. The manufacturer states that calibration at 50-percent relative humidity results in 0.12 ppm error at 20°C and 0.27 ppm error at 30°C. Observation indicates that this error is a negative error resulting in an underestimation of oxygen content within the dome atmosphere.

Although the probes are temperature compensated, it was observed that a 1.2°C rise in temperature of the dome atmosphere resulted in a 0.5- to 2.5-percent decrease in the apparent oxygen content of the dome as indicated on the oxygen meter. Conversely, a decrease in temperature within the dome atmosphere would result in an increase in the apparent oxygen content of the dome as indicated on the meter. This problem was overcome for Outdoor 2 by directing the output from the small submersible pump, which circulated water over the underwater probe membrane, to the dome surface, which maintained it at near water temperature. The laboratory experiments did not exhibit dome temperature fluctuations greater than 1°C. This would result in a maximum overestimation of 4–18 percent in the oxygen diffusion rate. During the Outdoor 1 experiment, the dome atmosphere experienced a 6.2° C rise in temperature in the initial 4 hours of the experiment. This could introduce a 32- to 160-percent overestimation of oxygen diffusion rates. Correcting the dome-estimated value for Outdoor 1 in table 1 by the maximum overestimation would place it at 1.01 $(g/m^3)/h$, which is within the range of 0.60–1.11 $(g/m^3)/h$ as obtained by the other methods. The atmosphere in the water-cooled dome used in Outdoor 2 experienced a 2.3°C rise in temperature in the initial 5 hours. The corresponding increase in water temperature was 1.8°C. This could result in a 17- to 83-percent overestimation of oxygen diffusion rates. However, the dome-predicted rates for the experiment are underestimated with respect to the other methods by about 75 percent. If decreases in dome temperature are assumed to have the inverse effect as increased temperature, then the possible underestimation error resulting from the nighttime observed 2.6°C drop in dome temperature could be as high as 80 percent. Apparently, underestimation errors resulting from the cooler nighttime temperatures of November more than compensated for the overestimation caused by the warm afternoon temperatures.

CONCLUSIONS

Preliminary evaluation of the floating dome method of measuring oxygen reaeration rates using a modified tracer technique and a disturbed equilibrium method demonstrated a variety of practical problems in the application of the dome method.

In theory, the dome method should produce realistic estimates under some environmental conditions. In practice, the limitations imposed by instrumental accuracy necessitate use of small-volume domes on deep water such that the ratio of dome volume to water column volume is less than 0.02. Additionally, the dome atmosphere must be maintained near the oxygen probe calibration temperature, and probe calibration must be done at 100-percent relative humidity.

The use of alternative methods to polarographic measurement of gaseous oxygen within the dome may solve many of the operational problems experienced in this evaluation. Gas chromatography has been successfully used to measure both gaseous and dissolved oxygen (Weiss and others, 1972; Park and Catalfomo, 1964), but it is difficult to apply to remote field situations. The manometric technique of Scholander (1942) was also used by Copeland and Duffer (1964), and its

low cost and portability may lend it to field use (see Scholander and others, 1955).

Several environmental factors have been reported to limit application of the dome method. The dome must be used at night to avoid the greenhouse effect, or water cooling of the dome must be used to reduce internal heating. Wind and waves tend to move the dome around, factors which preclude its use on large open waters. Additionally, the water upon which the dome rests must be well mixed, and any oxygen demand (respiration) or oxygen production (photosynthesis) must be known.

The floating dome method for measuring oxygen diffusion rates has potential, but the use of current polarographic oxygen monitoring systems severely limits its application. Most of the environmental limitations may be circumvented by proper experimental design and equipment construction. Further work is needed in the application of alternative methods for the determination of gaseous oxygen within the dome, particularly the Scholander (1955) method. If its reported accuracy for oxygen analysis (± 0.2 percent) can be obtained in the field and precise determinations made of dissolved oxygen using micro-Winkler titrations (± 0.07 mg/L O_2) or polarographic techniques (± 0.2 mg/L O_2), then the floating dome method could provide a usable field tool.

REFERENCES CITED

Carpenter, J. H., 1965, Chesapeake Bay Institute technique for the Winkler dissolved oxygen method: Limnology and Oceanography, v. 10, no. 1, p. 141–143.

Carritt, D. W., and Carpenter, J. H., 1966, Comparison and evaluation of currently employed modifications of the Winkler method for determining dissolved oxygen in seawater: Marine Research Jour., v. 24, p. 286–318.

Copeland, B. J., and Duffer, W. R., 1964, Use of a clear plastic dome to measure gaseous diffusion rates in natural waters: Limnology and Oceanography, v. 9, no. 4, p. 494–499.

Duffer, W. R., and Dorris, T. C., 1966, Primary productivity in a southern great plains stream: Limnology and Oceanography, v. 11, no. 2, p. 143–151.

Gameson, A. L. H., and Barrett, M. J., 1958, Oxidation, reaeration, and mixing in the Thames estuary, *in* Oxygen relationships in streams: U.S. Dept. Commerce, Natl. Tech. Inf. Service, PB–214 898, p. 63–93.

Gameson, A. L. H., and Truesdale, G. A., 1959, Some oxygen studies in streams: Inst. Water Engineers Jour., v. 13, no. 2, p. 175–187.

Hall, C. A., 1971, Migration and metabolism in a stream ecosystem: Chapel Hill, North Carolina Univ., Dept. Zoology and Dept. Environmental Sci., and Eng., rept. 49, 243 p.

Hannan, H. H., and Dorris, T. C., 1970, Succession of a macrophyte community in a constant temperature river: Limnology and Oceanography, v. 15, no. 3, p. 442–453.

Juliano, D. W., 1969, Reaeration measurements in an estuary Am. Soc. Civil Engineers Jour., v. 95, no. SA–6, p. 1165 1178.

Odum, H. T., and Hoskin, C. M., 1958, Comparative studie on the metabolism of marine waters: Texas Univ. Inst Marine Sci. Pub., v. 5, p. 16–46.

Owens, Morlais, 1965, Some factors involved in the use o dissolved-oxygen distribution in streams to determin productivity, *in* Goldman, C. R., ed., Primary productivity in aquatic environments: Berkeley, California Univ Press, p. 209–224.

Park, Kilho, and Catalfomo, Magdalena, 1964, Gas chromato graphic determination of dissolved oxygen in sea wate using argon as carrier gas: Deep-Sea Research, v. 11, p 917–920.

Rathbun, R. E., Shultz, D. J., and Stephens, D. W., 1975 Preliminary experiments with a modified tracer tech nique for measuring stream reaeration coefficients: U.S Geol. Survey Open-File Rept. 75–256, 39 p.

Scholander, P. F., 1942, Analyzer for quick estimation o respiratory gases: Jour. Biological Chemistry, v. 146, p 159–162.

Scholander, P. F., Van Dam, L., Claff, C. Lloyd, and Kan wisher, J. W., 1955, Micro gasometric determination o dissolved oxygen and nitrogen: Woods Hole Biologica Bull., v. 109, p. 328–334.

Shultz, D. J., Pankow, J. F., Tai, D. Y., Stephens, D. W. an Rathbun, R. E., 1976, Determination, storage, and pres ervation of low molecular weight hydrocarbon gases i aqueous solution: U.S. Geol. Survey Jour. Research, v. 4 no. 2, p. 247–251.

Slack, K. V., Averett, R. C., Greeson, P. E., and Lipscomb R. G., 1973, Methods for collection and analysis o aquatic biological and microbiological samples: U.S. Geol Survey Techniques Water-Resources Inv., book 5, chap A–4, 165 p.

Sugiura, Y., Ibert, E. R., and Hood, D. W., 1963, Mass trans fer of carbon dioxide across sea surfaces: Marine Re search Jour., v. 21, no. 1, p. 11–24.

Tsivoglou, E. C., Cohen, J. B., Shearer, S. D., and Godsil, P J., 1968, Tracer measurement of stream reaeration, pt 2, Field studies: Water Pollution Control Federatio Jour., v. 40, no. 2, p. 285–305.

Tsivoglou, E. C., O'Connell, R. L., Walter, C. M., Godsil, P J., and Logson, G. S., 1965, Tracer measurements of at mospheric reaeration, pt. 1, Laboratory studies: Wate Pollution Control Federation Jour., v. 37, no. 10, p. 1343 1362.

Weiss, R. F., 1970, The solubility of nitrogen, oxygen, an argon in water and seawater: Deep-Sea Research, v. 1 p. 721–735.

Weiss, R. F., Bucher, P., Oeschger, H., and Craig, H., 1972 Compositional variations of gases in temperate glaciers Earth and Planetary Sci. Letters, v. 16, p. 178–184.

Welch, H. E., 1968, Use of modified diurnal curves for th measurement of metabolism in standing water: Limno ogy and Oceanography, v. 13, no. 4, p. 679–687.

Zogorski, J. S., and Faust, S. D., 1973, Atmospheric reaera tion capacity of streams, pt. 1, Critical review of method available to measure and to calculate the atmospheri reaeration rate constant: Environmental Letters, v. 4 no. 1, p. 35–39.

CHANGE OF ADDRESS FORM

NAME—FIRST, LAST

COMPANY NAME OR ADDITIONAL ADDRESS LINE

STREET ADDRESS

CITY | STATE | ZIP CODE

PLEASE PRINT OR TYPE

(or) COUNTRY

Mail this form to:

NEW ADDRESS
Journal of Research of the
U.S. Geological Survey
Superintendent of Documents
Government Printing Office SSOM
Washington, DC 20402

Attach last subscription label here.

(please detach here)

SUBSCRIPTION ORDER FORM

SUBSCRIPTION ORDER FORM

Enter my subscription to "Journal of Research of the U.S. Geological Survey" at $18.90 (domestic) or $23.65 (foreign). Domestic remittance should be made by money order or check. Foreign remittance should be made by international money order, draft on an American bank, or UNESCO coupons.

NAME—FIRST, LAST

COMPANY NAME OR ADDITIONAL ADDRESS LINE

STREET ADDRESS

CITY | STATE | ZIP CODE

PLEASE PRINT OR TYPE

(or) COUNTRY

☐ Remittance Enclosed (Make checks payable to Superintendent of Documents)

☐ Charge to my deposit Account No.....

MAIL ORDER FORMS TO:
Superintendent of Documents
Government Printing Office
Washington, DC 20402

ANNOUNCEMENT

DIRECT-MAIL SALES OF USGS OPEN-FILE REPORTS By the U.S. Geological Survey

Purpose of Program

- To furnish microfiche or paper-duplicate copies of open-file reports from a single, centrally located facility.
- To provide faster order-filling service to the public for copies of open-file reports.
- To increase the availability of earth-science information to the scientific community.

Order USGS Open-File Reports From:

Open-File Services Section, Branch of Distribution, U.S. Geological Survey, Box 25425, Federal Center, Denver, CO 80225. (Telephone: 303-234-5888.)

Price information will be published in the monthly listing "New Publications of the Geological Survey."

This facility will stock open-file reports only. Please do not mix orders for open-file reports with orders for any other USGS products. Checks or money orders, in exact amount for open-file reports ordered, should be made payable to U.S. Geological Survey. Prepayment is required.

Order by series and number (such as Open-File Report 77-123) and complete title.

Inquiries concerning this new program should be sent to the address given above.

☆U.S.GOVERNMENT PRINTING OFFICE: 1978--261-198/10

RECENT PUBLICATIONS OF THE U.S. GEOLOGICAL SURVEY

The following books may be ordered from the Branch of Distribution, U.S. Geological Survey, 1200 South Eads Street, Arlington, VA 22202 (an authorized agent of the Superintendent of Documents, Government Printing Office). Prepayment is required. Remittances should be sent by check or money order payable to U.S. Geological Survey. Give series designation and number, such as Bulletin 1368–A, and the full title. Prices of Government publications are subject to change. Increases in costs make it necessary for the Superintendent of Documents to increase the selling prices of many publications offered. As it is not feasible for the Superintendent of Documents to correct the prices manually in all the previous announcements and publications stocked, the prices charged on your order may differ from the prices printed in the announcements and publications.

In addition to the publications mentioned below, other professional papers, water-supply papers, bulletins, circulars, single copies of the periodical "Earthquake Information Bulletin," maps, and items of general interest, such as leaflets, pamphlets, and booklets, are available at the above address. All new Survey publications are listed in a free monthly catalog, "New Publications of the Geological Survey"; to subscribe, send name and address to U.S. Geological Survey, 329 National Center, Reston, VA 22092. (Some reports that are now out of print at the Superintendent of Documents can also be obtained at the Branch of Distribution address.)

Professional Papers

P 521–A. Regional hydrogeology of the Navajo and Hopi Indian reservations, Arizona, New Mexico, and Utah, by M. E. Cooley, J. W. Harshbarger, J. P. Akers, and W. F. Hardt, *with a section on* Vegetation, by O. N. Hicks. 1969. p. A1–A61, 12 maps in separate pocket. $7.

P 712–D. Hydrologic processes and radionuclide distribution in a cavity and chimney produced by the Cannikin nuclear explosion, Amchitka Island, Alaska, by H. C. Claassen. 1978. p. D1–D28; plate in pocket. $2.50.

P 798–C. Geology and geochemistry of the West Ore Body and associated skarns, Copper Canyon porphyry copper deposits, Lander County, Nevada, by T. G. Theodore and D. W. Blake, *with a section on* Electron microprobe analyses of andradite and diopside, by N. G. Banks. 1978. p. C1–C85. $3.25.

P 813–D. Summary appraisals of the Nation's ground-water resources—Rio Grande region, by S. W. West and W. L. Broadhurst. 1975. p. D1–D39. $1.25 (Reprint.)

P 864–B. Joint systems in the Watchung Basalt flows, New Jersey, by G. T. Faust. 1978. p. B1–B46. $2.30.

P 964. A land use and land cover classification system for use with remote sensor data, by J. R. Anderson, E. E. Hardy, J. T. Roach, and R. E. Witmer. 1976. 28 p. 75c. (Reprint.)

P 997. Paleogene floras from the Gulf of Alaska region, by J. A. Wolfe. 1977 (1978). 108 p., 30 plates. $3.75.

P 1008. Large landslides, composed of megabreccia, interbedded in Miocene basin deposits, southeastern Arizona, by M. H. Krieger. 1977 (1978). 25 p.; plates in pocket. $2.75.

P 1012. Hydrogeology of the karst of Puerto Rico, by E. V. Giusti. 1978. 68 p.; plates in pocket. $2.10.

P 1019. Climatography of the Front Range Urban Corridor and vicinity, Colorado, by W. R. Hansen, John Chronic, and John Matelock. 59 p. $2.75.

P 1025. Stratigraphy and microfaunas of the Oquirrh Group in the southern East Tintic Mountains, Utah, by H. T. Morris, R. C. Douglass, and R. W. Kopf. 1977 (1978). 22 p.; 3 plates; 1 plate in pocket. $2.10.

P 1028. Studies related to the Charleston, South Carolina, earthquake of 1886—a preliminary report, edited by D. W. Rankin, 1977 (1978). 204 p. Chapters A–O. $4.75.

P 1030. Erosion and sediment yields in the Transverse Ranges, southern California, by K. M. Scott and R. P. Williams. 1978. 38 p. $1.70.

P 1031. Medicine Lodge thrust system, east-central Idaho and southwest Montana, by E. T. Ruppel. 1978. 23 p. $1.30.

P 1044–B. Use of temperature surveys at a depth of 1 meter in geothermal exploration in Nevada, by G. H. Olmsted. 1977 (1978). p. B1–B25. $1.40.

Bulletins

B 1434. Geology and mineral deposits of the Needle Mountains district, southwestern Colorado, by L. J. Schmitt and W. H. Raymond. 1977 (1978). 40 p.; plate in pocket. $1.

B 1435–A. Changes in stratigraphic nomenclature by the U.S. Geological Survey, 1976, by N. F. Sohl and W. B. Wright. 1977 (1978). p. A1–A151. $2.75.

B 1435–C. The Pliocene Conant Creek Tuff in the northern part of the Teton Range and Jackson Hole, Wyoming, by R. L. Christiansen and J. D. Love. 1978. p. C1–C9. 90c.

Water-Supply Papers

W 1663–I. Relation of bulk precipitation and evapotranspiration to water quality and water resources, St. Thomas, Virgin Islands, by D. G. Jordan and D. W. Fisher. 1977 (1978). p. I1–I30. $1.40.

W 2042. Mean annual runoff in the Upper Ohio River basin. 1941–70, and its historical variation, by R. M. Beall. 1978. 32 p.; plates in pocket. $2.

W 2050. Application of digital profile modeling techniques to ground-water solute transport at Barstow, California, by S. G. Robson. 1978. 28 p.; plate in pocket. $1.90. (Supersedes Open-File Report 77–276.)

Techniques of Water-Resources Investigations

TWI 3–A6. General procedure for gaging streams, by R. W. Carter and Jacob Davidian. 1968. 13 p. $1. (Reprint.)

TWI 3–A7. Stage measurement at gaging stations, by T. J. Buchanan and W. P. Somers. 1968. 28 p. $1.40. (Reprint.)

U.S. GOVERNMENT
PRINTING OFFICE
PUBLIC DOCUMENTS DEPARTMENT
WASHINGTON, D C 20402
OFFICIAL BUSINESS
PENALTY FOR PRIVATE USE $300

FOURTH-CLASS MAI
POSTAGE & FEES PA
USGS
PERMIT No. G23